IL
NUOVO CIMENTO
ORGANO DELLA SOCIETÀ ITALIANA DI FISICA
SOTTO GLI AUSPICI DEL CONSIGLIO NAZIONALE DELLE RICERCHE

VOL. XVI, N. 4 *Serie decima* 16 Maggio 1960

Diffraction of a Plane Electromagnetic Wave by Cylinders with Anisotropic Conductivity (*).

R. E. KELLY (**) and A. RUSSEK
The University of Connecticut - Storrs, Conn.

(ricevuto il 16 Novembre 1959)

Summary. — The diffraction of a plane electromagnetic wave at an arbitrary angle of incidence on isotropic and hollow anisotropically conducting cylinders of infinite length is investigated. The anisotropically conducting cylinders considered are *a*) a cylinder which conducts in the axial direction only and *b*) a cylinder which conducts in the θ-direction only (such as a tightly wound helix). The diffracted fields are determined by meeting the appropriate boundary conditions on the cylindrical surfaces. Expressions are also given for the induced surface currents and the cross-sections; plots of the latter and of the angular distribution of diffracted energy are presented. A discussion of the physical mechanism whereby anisotropic conductivity effects differ from those of isotropic conductivity is also included. It is found that the axially conducting cylinder is transparent to an incident TE wave whereas the TM polarization results in a field identical to that of an isotropic cylinder. The θ-conducting cylinders produce diffracted fields which do not preserve the polarization of the incident wave. For increasing ratio of radius to wave length, the cross-sections increase to a point at which they begin to oscillate and finally approach constant values.

(*) Based in part on a thesis submitted by R. E. KELLY in partial fulfilment of the requirement for the Ph. D. degree at the University of Connecticut.

(**) Now at the University of Mississippi, University, Miss.

1. – Introduction.

The diffraction of electromagnetic waves by perfect conductors has long received considerable attention in the literature; exact solutions have been worked out for many geometries and approximate solutions for many more. Only recently, however, has any attention been devoted to diffraction effects caused by anisotropically conducting surfaces, such as screens made up of fine, closely spaced parallel wires, all insulated from each other. Such a surface has, of course, the property that current flow in it is restricted to a single direction, and it will henceforth be termed « unidirectionally conducting ». It is hoped that no confusion will result from this usage of the word « unidirectional » as contrasted to the other usage applied to, say, a diode in a circuit.

Diffraction problems involving unidirectionally conducting surfaces were first attempted by TORALDO DI FRANCIA [1], who solved approximately the problem of diffraction of a plane wave by a small circular disc with unidirectional conductivity. He found that the electromagnetic cross-section for such a disc is zero for that component of the incident electric vector polarized perpendicularly to the direction of conductivity and equal to that of an isotropically conducting disc for that component of $\boldsymbol{E}$ parallel to the direction of conductivity. This result may not seem surprising at first glance; it is, however, when it is realized that the isotropically conducting disc has currents both parallel to and perpendicular to the incident electric field direction. Further work on diffraction by unidirectional conductors was done by KARP [2], who obtained closed form expressions for the diffraction of a plane wave by a semi-infinite screen which is conducting along a direction making an arbitrary angle with the edge. RADLOW [3] has solved the problem of a dipole field incident on the same diffracting geometry. Finally, TORALDO DI FRANCIA [4] has discussed Babinet's principle for diffraction by a plane screen with unidirectional conductivity.

The entire subject of diffraction by unidirectional conductors is clearly of potential value in microwave physics. Such conductors can easily be made by embedding fine wires in a non-conducting plastic, and offer an additional degree of freedom in design problems. (A unidirectionally conducting plane, for example, reflects one polarization and transmits the other; hence it can be used as a microwave polarizer.) However, before this potential can be realized, an intuitive understanding must be gained of the kinds of diffraction

(1) G. TORALDO DI FRANCIA: *Nuovo Cimento*, **3**, 1276 (1956).

(2) S. N. KARP: N.Y.U. Institute of Mathematical Sciences, Division of Electromagnetic Research, Report no. EM-108 (1957).

(3) J. RADLOW: *Quart. Appl. Math.*, **17**, 113 (1959).

(4) G. TORALDO DI FRANCIA: *Nuovo Cimento*, **9**, 309 (1958).

effects one can expect from various geometries. Until now, only plane geometry has been considered, with edge effects taken into account. The purpose of the present work is to begin to extend the understanding of diffraction produced by unidirectionally conducting surfaces to effects produced by non-planar surfaces.

Specifically, the problems here solved are the diffraction of plane electromagnetic waves of arbitrary polarization at an arbitrary angle of incidence by *a*) a cylinder which conducts only in a direction parallel to the axis and *b*) a cylinder which conducts only circumferentially, such as a tightly wound helix. In addition, the diffraction of the same incident field produced by an ordinary (isotropically conducting) cylinder is also obtained, so that the *difference* in diffraction effects between anisotropic and isotropic cylinders can be studied in detail. Cylindrical geometry was chosen, in this work, because of the importance of the cylinder in antennas, transmission lines and diffraction gratings. Not inconsequential in the choice was the fact that rigorous solutions for the field components can be obtained in this case.

At this point, it may be well to point out that although diffraction of a plane wave perpendicularly incident on an ordinary cylinder is well known, very little consideration has been given to the case of oblique incidence. VAN DE HULST [5] and WAIT [6] have brief accounts of the problem at oblique incidence without a consideration of surface currents, cross-sections and angular distribution of diffracted energy. Since these effects are all considered here, it appears that a contribution is also being made to the subject of diffraction by ordinary cylinders.

Section 2 first gives a brief review of the boundary conditions that apply on the surface of a unidirectional conductor. Following this, exact solutions for the diffracted field components are obtained by applying the appropriate boundary conditions for incident fields which are plane waves at arbitrary angle of incidence. Two polarizations, transverse electric (in which the electric vector of the incident plane wave is perpendicular to the cylinder axis), and transverse magnetic, are considered for each of three types of cylinders: isotropic, paraxially conducting and circumferentially conducting. Hence six distinct cases are considered in all.

In Section 3, the surface currents induced on the cylinders are obtained from the field components. Following that, the far fields are obtained and the cross-section per unit length of cylinder is then computed for each case. Numerical calculations have been performed and are presented to illustrate the changes in diffraction effects consequent on the substitution of anisotropic for isotropic cylinders.

---

(5) H. C. VAN DE HULST: *Light Scattering by Small Particles* (New York, 1957).
(6) J. R. WAIT: *Cand. Journ. Phys.*, **33**, 189 (1955).

2. – The diffracted fields.

2·1. *Boundary conditions.* – Inasmuch as the diffracted field is determined by forcing it, acting together with the incident field, to satisfy the appropriate boundary conditions, it is useful to review these conditions.

For a perfect isotropic conductor, it is well known that the conditions are determined by the fact that a perfect conductor is unable to sustain an electric field. Consequently the tangential components of $\boldsymbol{E}$ must vanish at the surface. From this and Maxwell's equations, it follows that the normal component of $\boldsymbol{H}$ must vanish at the surface also. The normal component of $\boldsymbol{E}$ and tangential components of $\boldsymbol{H}$ are unrestricted at the surface. Since these fields must all vanish immediately within the conductor, the discontinuities in these components are accounted for by surface charge and current distributions.

The boundary conditions that apply on unidirectionally conducting surfaces differ from the above in that the surface is perfectly able to sustain a tangential electric field *perpendicular* to the direction of conductivity. This component can freely pass through the surface. The conditions are listed below.

a) The tangential component of $\boldsymbol{E}$ *parallel* to the direction of conductivity vanishes at the surface.

b) The tangential component of $\boldsymbol{E}$ *perpendicular* to the direction of conductivity is merely required to be continuous across the surface.

c) The normal component of $\boldsymbol{E}$ is unrestricted at the surface. Any discontinuity in this component is accounted for by surface charge.

d) The tangential component of $\boldsymbol{H}$ *parallel* to the direction of conductivity is only required to be continuous across the surface.

e) The tangential component of $\boldsymbol{H}$ *perpendicular* to the direction of conductivity is unrestricted at the surface. Any discontinuity in this component is accounted for by surface current.

f) The normal component of $\boldsymbol{H}$ is only required to be continuous across the surface. This is not an independent condition, but follows from Maxwell's equation $\nabla \times \boldsymbol{E} = -\mu \dot{\boldsymbol{H}}/c$ and the conditions on the tangential components of $\boldsymbol{E}$.

2·2. *Geometry and notation.* – The geometry is illustrated in Fig. 1. The cylinder, of radius R, has as axis the z-axis. The orientation of the x-axis is chosen so that the propagation vector $\boldsymbol{k}$ of the incident plane wave is in the x-z plane. The acute angle between this vector and the x-axis is denoted by γ.

For brevity in notation, the x-component of $\boldsymbol{k}$ will be designated by K and the z-component by L:

$$\boldsymbol{k} = \boldsymbol{i}K + \boldsymbol{k}L \,. \tag{1}$$

The solutions for the field components are obtained in cylindrical co-ordinates ϱ, θ, and z defined, in the usual way, by

$$x = \varrho \cos\theta \,, \quad y = \varrho \sin\theta \,, \quad z = z \,. \tag{2}$$

The diffracted electric and magnetic fields are denoted by $\boldsymbol{e}$ and $\boldsymbol{h}$ respectively, and the incident fields by $\boldsymbol{E}^i$ and $\boldsymbol{H}^i$. The total fields are, by definition, the vector sum of the two in each case

$$\boldsymbol{E} = \boldsymbol{E}^i + \boldsymbol{e} \,, \quad \boldsymbol{H} = \boldsymbol{H}^i + \boldsymbol{h} \,. \tag{3}$$

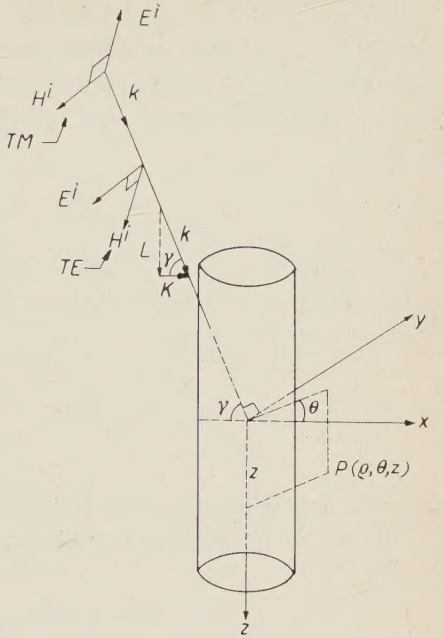

Fig. 1. – Geometry and notation. The electric and magnetic field of the incident plane wave are shown for the two polarizations considered.

It is also convenient to introduce the following functions, which will considerably abbreviate the expressions for the fields obtained below:

$$J_n^{\pm}(x) = J_{n-1}(x) \pm J_{n+1}(x) \,, \tag{4a}$$

$$H_n^{\pm}(x) = H_{n-1}(x) \pm H_{n+1}(x) \,, \tag{4b}$$

$$G_n = H_n^-(KR)J_n^-(KR) + H_n^+(KR)J_n^+(KR)\sin^2\gamma \,, \tag{4c}$$

$$A = \tfrac{1}{2}E_0 \exp\left[i(Lz - \omega t)\right] , \tag{4d}$$

where J_n is a Bessel function of order n, H_n is a Hankel function of the first kind and order n and E_0 is the magnitude of the incident electric field.

2·3. *The mathematical solution.* – In each of the six cases below for which solutions are obtained for the field components, the incident plane wave is first expanded in terms of Bessel functions

$$\boldsymbol{E}^i = \boldsymbol{E}_0 \exp\left[i(\boldsymbol{k}\cdot\boldsymbol{r} - \omega t)\right] = 2A\,\frac{\boldsymbol{E}_0}{E_0}\sum_{n=0}^{\infty}\varepsilon_n i^n J_n(K\varrho)\cos n\theta \,, \tag{5a}$$

$$\boldsymbol{H}^i = \frac{\boldsymbol{k}\times\boldsymbol{E}_0}{k}\exp\left[i(\boldsymbol{k}\cdot\boldsymbol{r} - \omega t)\right] = 2A\,\frac{\boldsymbol{k}\times\boldsymbol{E}_0}{kE_0}\sum_{n=0}^{\infty}\varepsilon_n i^n J_n(K\varrho)\cos n\theta \,, \tag{5b}$$

where $\varepsilon_0 = 1$ and all $\varepsilon_n = 2$ for $n > 0$. The diffracted fields are most conveniently obtained from a combination of electric and magnetic Hertzian vectors, of which only the z-components are required in this problem. Denoting, then, these components by Π^e and Π^m respectively, the diffracted fields are given by [7]

$$(6)\qquad \begin{cases} e_\varrho = \dfrac{\partial^2 \Pi^e}{\partial \varrho \partial z} - \dfrac{1}{c\varrho}\dfrac{\partial \dot{\Pi}^m}{\partial \theta} & h^\varrho = \dfrac{1}{c\varrho}\dfrac{\partial \dot{\Pi}^e}{\partial \theta} + \dfrac{\partial^2 \Pi^m}{\partial \varrho \partial z}, \\ e_\theta = \dfrac{1}{\varrho}\dfrac{\partial^2 \Pi^e}{\partial \theta \partial z} + \dfrac{1}{c}\dfrac{\partial \dot{\Pi}^m}{\partial \varrho}, & h_\theta = -\dfrac{1}{c}\dfrac{\partial \dot{\Pi}^e}{\partial \varrho} + \dfrac{1}{\varrho}\dfrac{\partial^2 \Pi^m}{\partial \theta \partial z}, \\ e_z = \dfrac{\partial^2 \Pi^e}{\partial z^2} - \dfrac{1}{c^2}\ddot{\Pi}^e, & h_z = \dfrac{\partial^2 \Pi^m}{\partial z^2} - \dfrac{1}{c^2}\ddot{\Pi}^m, \end{cases}$$

where a dot denotes partial differentiation with respect to time. In order that the fields (6) be solutions of Maxwell's equations, Π^e and Π^m must be of the form

$$(7)\qquad \begin{cases} \Pi^e = \exp\left[i(Lz - \omega t)\right] \sum_{n=0}^{\infty} Z_n(K\varrho)\left[a_n \sin n\theta + b_n \cos n\theta\right] \\ \Pi^m = \exp\left[i(Lz - \omega t)\right] \sum_{n=0}^{\infty} Z_n(K\varrho)\left[\alpha_n \sin n\theta + \beta_n \cos n\theta\right], \end{cases}$$

where Z_n denotes a Bessel or Hankel function and a_n, b_n, α_n, β_n, are arbitrary constants which are determined from the boundary conditions. In all cases, outside the cylinder, Z_n will be a Hankel function of the first kind (representing outward travelling waves). In those cases for which fields exist inside the cylinder, Z_n will be a Bessel function for the interior fields. These choices are determined by the boundary conditions that the diffracted fields shall only be outgoing at infinity and that the fields shall be non-singular on the axis.

Expressions for the diffracted fields in the six cases considered are listed below. For the sake of brevity, the algebra by which the coefficients a_n, b_n, α_n, β_n are obtained by applying the boundary conditions on the surface of the cylinder will be omitted. The specific boundary conditions which apply at the cylinder (obtained from the general considerations of Section 2·1) will be given for each type of cylinder, along with the solutions obtained. That these solutions satisfy the appropriate boundary conditions can be readily verified by the direct substitution $\varrho = R$.

---

[7] See, for example, J. A. STRATTON: *Electromagnetic Theory* (New York, 1941).

Only the electric fields are presented. The magnetic fields are obtained from these in the usual manner by Maxwell's equation

$$\boldsymbol{h} = (ik)^{-1}\nabla\times\boldsymbol{e}\,, \tag{8}$$

where μ has been set equal to unity.

2·3.1. Isotropically conducting cylinder. – The boundary conditions imposed at $\varrho = R$ (not all of which are independent) are, in this case

$$e_z(R) + E_z^i(R) = 0\,, \tag{9a}$$

$$e_\theta(R) + E_\theta^i(R) = 0 \tag{9b}$$

$$h_\varrho(R) + H_\varrho^i(R) = 0\,, \tag{9c}$$

and there will be no fields within the cylinder.

a) Incident electric field is parallel to the y-axis (TE)

$$e_\varrho = \sum_{n=0}^{\infty} U_n H_n^+(K\varrho)\sin n\theta \tag{10a}$$

$$e_\theta = \sum_{n=0}^{\infty} U_n H_n^-(K\varrho)\cos n\theta \tag{10b}$$

$$e_z = 0\,, \tag{10c}$$

where

$$U_n = A\varepsilon_n i^{n+1} J_n^-(KR)/H_n^-(KR)\,. \tag{10d}$$

b) Incident magnetic field is parallel to the y-axis (TM)

$$e_\varrho = -\sin\gamma \sum_{n=0}^{\infty} V_n H_n^-(K\varrho)\cos n\theta \tag{11a}$$

$$e_\theta = \sin\gamma \sum_{n=0}^{\infty} V_n H_n^+(K\varrho)\sin n\theta \tag{11b}$$

$$e_z = 2i\cos\gamma \sum_{n=0}^{\infty} V_n H_n(K\varrho)\cos n\theta\,, \tag{11c}$$

where

$$V_n = A\varepsilon_n i^{n+1} J_n(KR)/H_n(KR)\,. \tag{11d}$$

2·3.2. Cylinder conducting in z-direction only. – In this case there will, in general, be fields within the cylinder. Therefore, some of the boundary conditions imposed at $\varrho = R$ relate the external to the internal fields. Denoting by $R+$ and $R-$, field points immediately outside and immediately inside the cylinder, the boundary conditions are:

$$e_z(R+) + E_z^i(R+) = E_z(R-) = 0 \tag{12a}$$

$$e_\theta(R+) + E_\theta^i(R+) = E_\theta(R-) \tag{12b}$$

$$h_z(R+) + H_z^i(R+) = H_z(R-) . \tag{12c}$$

Note that within the cylinder, the field components are not decomposed into incident and diffracted parts.

a) Incident electric field is parallel to the y-axis (TE)

$$\boldsymbol{E} = \boldsymbol{E}^i \qquad \text{for} \quad \varrho < R \tag{13}$$

$$\boldsymbol{e} = 0 \qquad \text{for} \quad \varrho > R . \tag{14}$$

Thus, this type of cylinder is completely transparent to an incident TE wave.

b) Incident magnetic field is parallel to the y-axis (TM)

$$\boldsymbol{E} = 0 \qquad \text{for} \quad \varrho < R \tag{15}$$

$$e_\varrho = -\sin\gamma \sum_{n=0}^{\infty} V_n H_n^-(K\varrho) \cos n\theta \qquad \text{for} \quad \varrho > R \tag{16a}$$

$$e_\theta = \sin\gamma \sum_{n=0}^{\infty} V_n H_n^+(K\varrho) \sin n\theta \qquad \text{for} \quad \varrho > R \tag{16b}$$

$$e_z = 2i \cos\gamma \sum_{n=0}^{\infty} V_n H_n(K\varrho) \cos n\theta \qquad \text{for} \quad \varrho > R . \tag{16c}$$

These fields are identical to those specified by eqs. (11), produced when the same incident polarization is diffracted by an ordinary cylinder.

2·3.3. Cylinder conducting in θ-direction only. – In this case too, there will also, in general, be fields within the cylinder. The boundary conditions are:

$$e_z(R+) + E_z^i(R+) = E_z(R-) \tag{17a}$$

$$e_\theta(R+) + E_\theta^i(R+) = E_\theta(R-) = 0 \tag{17b}$$

$$h_\theta(R+) + H_\theta^i(R+) = H_\theta(R-) . \tag{17c}$$

a) Incident electric field is parallel to the y-axis (TE).

For $\varrho < R$:

$$E_\varrho = A \sin^2\gamma \sum_{n=0}^{\infty} \varepsilon_n i^{n+1} \frac{H_n^+(KR)}{G_n} \cdot [J_n^-(KR)\, J_n^-(K\varrho) - J_n^+(KR) J_n^+(K\varrho)] \sin n\theta\,, \tag{18a}$$

$$E_\theta = A \sin^2\gamma \sum_{n=0}^{\infty} \varepsilon_n i^{n+1} \frac{H_n^+(KR)}{G_n} \cdot [J_n^-(KR) J_n^+(K\varrho) - J_n^+(KR) J_n^-(K\varrho)] \cos n\theta\,, \tag{18b}$$

$$E_z = 2A \sin\gamma \cos\gamma \sum_{n=0}^{\infty} \varepsilon_n i^n \frac{H_n^+(KR) J_n^-(KR)}{G_n} J_n(K\varrho) \sin n\theta\,. \tag{18c}$$

For $\varrho > R$:

$$e_\varrho = A \sum_{n=0}^{\infty} \varepsilon_n i^{n+1} \frac{J_n^-(KR)}{G_n} \cdot [J_n^-(KR) H_n^+(K\varrho) + J_n^+(KR) H_n^-(K\varrho) \sin^2\gamma] \sin n\theta\,, \tag{19a}$$

$$e_\theta = A \sum_{n=0}^{\infty} \varepsilon_n i^{n+1} \frac{J_n^-(KR)}{G_n} \cdot [J_n^-(KR) H_n^-(K\varrho) + J_n^+(KR) H_n^+(K\varrho) \sin^2\gamma] \cos\theta\,, \tag{19b}$$

$$e_z = 2A \sin\gamma \cos\gamma \sum_{n=0}^{\infty} \varepsilon_n i^n \frac{J_n^+(KR) J_n^-(KR)}{G_n} H_n(K\varrho) \sin n\theta\,. \tag{19c}$$

b) Incident magnetic field is parallel to the y-axis (TM).

For $\varrho < R$:

$$E_\varrho = A \sin\gamma \sum_{n=0}^{\infty} \varepsilon_n i^{n+1} \frac{H_n^-(KR)}{G_n} \cdot [J_n^-(KR) J_n^-(K\varrho) - J_n^+(KR) J_n^+(K\varrho)] \cos n\theta\,, \tag{20a}$$

$$E_\theta = A \sin\gamma \sum_{n=0}^{\infty} \varepsilon_n i^{n+1} \frac{H_n^-(KR)}{G_n} \cdot [J_n^+(KR) J_n^-(K\varrho) - J_n^-(KR) J_n^+(K\varrho)] \sin n\theta\,, \tag{20b}$$

$$E_z = 2A \cos\gamma \sum_{n=0}^{\infty} \varepsilon_n i^n \frac{H_n^-(KR) J_n^-(KR)}{G_n} J_n(K\varrho) \cos n\theta\,. \tag{20c}$$

For $\varrho > R$:

$$(21a) \qquad e_\varrho = -A \sin\gamma \sum_{n=0}^{\infty} \varepsilon_n i^{n+1} \frac{J_n^+(KR)}{G_n} \cdot \cdot [J_n^-(KR) H_n^+(K\varrho) + J_n^+(KR) H_n^-(K\varrho) \sin^2\gamma] \cos n\theta ,$$

$$(21b) \qquad e_\theta = A \sin\gamma \sum_{n=0}^{\infty} \varepsilon_n i^{n+1} \frac{J_n^+(KR)}{G_n} \cdot \cdot [J_n^-(KR) H_n^-(K\varrho) + J_n^+(KR) H_n^+(K\varrho) \sin^2\gamma] \sin n\theta ,$$

$$(21c) \qquad e_z = -2A \sin^2\gamma \cos\gamma \sum_{n=0}^{\infty} \varepsilon_n i^{n+} \frac{[J_n^+(KR)]^2}{G_n} H_n(K\varrho) \cos n\theta .$$

3. – Surface currents, far fields and cross-sections.

3·1. *Surface currents.* – A study of the surface currents induced on the cylinder in the various cases yields valuable physical insight on the manner in which anisotropic conductivity affects the diffraction properties. For this reason, the surface currents will be listed and discussed. It may be worthwhile to point out, parenthetically, that the surface charge densities were also obtained, in each case, from the fields, although they will not be presented here. The surface charge and current distributions were then tested to make sure that they satisfied the equation of continuity. This constitutes an independent check on the computations by which the fields were determined from the boundary conditions.

Now σ, the surface current per unit length induced on the cylinder, is found from the discontinuity in the tangential component of the total magnetic field across the surface,

$$(22a) \qquad \sigma_z = (c/4\pi)[h_\theta(R+) + H_\theta^i(R+) - H_\theta(R-)]$$

$$(22b) \qquad \sigma_\theta = -(c/4\pi)[h_z(R+) + H_z^i(R+) - H_z(R-)] .$$

Note that the particular form in which eqs. (22) are written was chosen because each of the fields derived in the previous section is expressed in terms of an incident and a diffracted part outside the cylinder, whereas only the total field component is given inside the cylinder. The surface currents, obtained in this manner, are listed below.

1a) Isotropic cylinder, incident TE wave

$$(23a) \qquad \sigma_\theta = -\frac{2cA}{\pi^2 kR} \sum_{n=0}^{\infty} \frac{\varepsilon_n i^{n+1}}{H_n^-(KR)} \cos n\theta ,$$

$$(23b) \qquad \sigma_z = \frac{2cA}{(\pi kR)^2} \frac{\sin\gamma}{\cos^2\gamma} \sum_{n=0}^{\infty} \frac{n\varepsilon_n i^{n+1}}{H_n^-(KR)} \sin n\theta .$$

1*b*) Isotropic cylinder, incident TM wave

$$\sigma_\theta = 0 \tag{24a}$$

$$\sigma_z = \frac{cA}{\pi^2 kR \cos\gamma} \sum_{n=0}^{\infty} \frac{\varepsilon_n i^n}{H_n(KR)} \cos n\theta \,. \tag{24b}$$

2*a*) z-conducting cylinder, incident TE wave

$$\sigma_\theta = 0 \tag{25a}$$

$$\sigma_z = 0 \,. \tag{25b}$$

2*b*) z-conducting cylinder, incident TM wave

$$\sigma_\theta = 0 \tag{26a}$$

$$\sigma_z = \frac{cA}{\pi^2 kR \cos\gamma} \sum_{n=0}^{\infty} \frac{\varepsilon_n i^n}{H_n(KR)} \cos n\theta \,. \tag{26b}$$

3*a*) θ-conducting cylinder, incident TE wave

$$\sigma_\theta = -\frac{2cA}{\pi^2 kR} \sum_{n=0}^{\infty} \varepsilon_n i^{n+1} \frac{J_n^-(KR)}{G_n} \cos n\theta \,, \tag{27a}$$

$$\sigma_z = 0 \,. \tag{27b}$$

3*b*) θ-conducting cylinder, incident TM wave

$$\sigma_\theta = \frac{2cA \sin\gamma}{\pi^2 kR} \sum_{n=0}^{\infty} \varepsilon_n i^{n+1} \frac{J_n^+(KR)}{G_n} \sin n\theta \,. \tag{28a}$$

$$\sigma_z = 0 \,. \tag{28b}$$

The various functions employed in eqs. (23)–(28) are defined in eqs. (4).

Some intuitively plausible general « rules » and considerations for plane waves striking anisotropically conducting surfaces are illustrated by these results. (It should be emphasized that these are *not* theorems with the proofs omitted, but rather intuitively justified speculations based upon the results obtained to date. If these speculations are correct, they should, of course, be rigorously provable. They are included here because it is just such stimulation that warrants the consideration of special cases, such as plane, half-plane and cylindrical geometry.)

1) If, at the surface, the incident electric field is *everywhere parallel* to the direction of conductivity (the entire electric field, not just the tangential

component), then the diffracted field will be exactly the same as for an isotropic conductor. Note, however, that at an edge, an « isotropic » conductor is really anisotropic, since it can conduct in one direction only, along the edge. Therefore, for example, an anisotropically conducting half-plane with the incident electric field parallel to the direction of conductivity should not, in general, yield the same diffracted field as an ordinary half-plane.

2) If, at the surface, the incident electric field is everywhere perpendicular to the direction of conductivity, no currents at all can be induced and the object will be perfectly transparent, producing no diffracted fields.

3) If, at the surface, the angle between the incident electric field and the direction of conductivity varies from point to point, then the variation in induced current from point to point leads to surface charge concentrations which will, in general, be different from that required to cancel off the component of electric field normal to the surface. These charge concentrations will therefore give rise to a component of electric field perpendicular to the direction of conductivity. (Nothing, of course, can give rise to electric fields at the surface parallel to the direction of conductivity.) These fields could not be produced by the isotropic conductor which could sustain currents that would cancel them off. In this way, anisotropic conductors can generate a diffracted field that is, in part, characteristic of the polarization opposite to that of the incident wave.

Speculation 1 can be intuitively justified as follows. If the incident electric field has no normal component, it does not attempt to induce any surface charge. If, further, it is everywhere parallel to the direction of conductivity at the surface, is does not attempt to induce any current in a direction in which the surface cannot conduct. Consequently, the induced surface currents and, therefore, the diffracted fields should be exactly the same as for an isotropic conductor. This case is illustrated by comparing the current densities of the isotropic and z-conducting cylinders for a TM plane wave at normal incidence (case 1b) and 2b) for $\gamma = 0$). They are, as predicted, identical.

The intuitive justification of speculation 2 is that an incident field which only attempts to move a charge in a direction in which that charge can not move will induce no surface currents, and hence, no surface charge as well. This is illustrated by the z-conducting cylinder for a TE wave at any angle of incidence and for a θ-conducting cylinder for a TM wave at normal incidence.

Speculation 3 is rather vague, and is therefore best approached by the consideration of a special case. It will be observed from eq. (23b) that for a TE wave incident obliquely on an isotropic cylinder, σ_z does not vanish, even though the incident electric field does not have any z-component. The reason for this is that current flow in the θ-direction tends to cause a surface charge

distribution, as illustrated in Fig. 2, which exceeds that necessary to account for the normal component of $\boldsymbol{E}^i$. As a result, this charge build-up tends to create a tangential electric field parallel to the z-axis. In an ordinary cylinder this is impossible and such a secondary field is prevented by appropriate currents in the z-direction. However, the θ-conducting cylinder can sustain this electric field and has therefore created a diffracted z-component of electric field. This field is actually radiated, as can be seen in the next section. On the other hand, the currents that flow in the z-direction of the ordinary cylinder do not radiate, since the total current in the z-direction (σ_z integrated over θ) is equal to zero.

Fig. 2. – Charge distribution on cylinder.

3·2. *The asymptotic fields.* – The determination of the asymptotic diffracted field components (far fields) is made by using the approximate forms taken by the Hankel functions when $K\varrho \gg 1$.

$$H_n(K\varrho) \simeq (2/\pi K\varrho)^{\frac{1}{2}} \exp\left[i\left(K\varrho - \frac{\pi}{4} - \frac{n\pi}{2}\right)\right], \tag{29}$$

from which

$$H_n^+(K\varrho) \simeq 0 \tag{30a}$$

$$H_n^-(K\varrho) \simeq 2iH_n(K\varrho)\,. \tag{30b}$$

The substitution is straightforward, and the results are listed below.

1a) Isotropic cylinder, TE wave incident

$$e_\varrho \simeq 0 \tag{31a}$$

$$e_\theta \simeq -2(2/\pi K\varrho)^{\frac{1}{2}} \exp\left[i\left(K\varrho - \frac{\pi}{4}\right)\right] \sum_{n=0}^{\infty} i^{-n-1} U_n \cos n\theta\,, \tag{31b}$$

$$e_z \simeq 0\,. \tag{31c}$$

1*b*) Isotropic cylinder, TM wave incident

$$e_\varrho \simeq 2(2/\pi K\varrho)^{\frac{1}{2}} \exp\left[i\left(K\varrho - \frac{\pi}{4}\right)\right] \sin\gamma \sum_{n=0}^{\infty} i^{-n-1} V_n \cos n\theta \,, \tag{32a}$$

$$e_\theta \simeq 0 \,, \tag{32b}$$

$$e_z \simeq -2(2/\pi K\varrho)^{\frac{1}{2}} \exp\left[i\left(K\varrho - \frac{\pi}{4}\right)\right] \cos\gamma \sum_{n=0}^{\infty} i^{-n-1} V_n \cos n\theta \,. \tag{32c}$$

2*a*) z-conducting cylinder, TE wave incident

$$e_\varrho = e_\theta = e_z = 0 \,. \tag{33}$$

2*b*) z-conducting cylinder, TM wave incident.
The fields are the same as those for the isotropic cylinder, eqs. (32).

3*a*) θ-conducting cylinder, TE wave incident

$$e_\varrho \simeq -2(2/\pi K\varrho)^{\frac{1}{2}} \exp\left[i\left(K\varrho - \frac{\pi}{4}\right)\right] \sin^2\gamma A \sum_{n=0}^{\infty} \frac{\varepsilon_n}{G_n} J_n^+(KR) J_n^-(KR) \sin n\theta \,, \tag{34a}$$

$$e_\theta \simeq -2(2/\pi K\varrho)^{\frac{1}{2}} \exp\left[i\left(K\varrho - \frac{\pi}{4}\right)\right] A \sum_{n=0}^{\infty} \frac{\varepsilon_n}{G_n} [J_n^-(KR)]^2 \cos n\theta \,, \tag{34b}$$

$$e_z \simeq 2(2/\pi K\varrho)^{\frac{1}{2}} \exp\left[i\left(K\varrho - \frac{\pi}{4}\right)\right] \cdot \cos\gamma \sin\gamma A \sum_{n=0}^{\infty} \frac{\varepsilon_n}{G_n} J_n^+(KR) J_n^-(KR) \sin n\theta \,. \tag{34c}$$

3*b*) θ-conducting cylinder, TM wave incident

$$e_\varrho \simeq 2(2/\pi K\varrho)^{\frac{1}{2}} \exp\left[i\left(K\varrho - \frac{\pi}{4}\right)\right] \sin^3\gamma A \sum_{n=0}^{\infty} \frac{\varepsilon_n}{G_n} [J_n^+(KR)]^2 \cos n\theta \,. \tag{35a}$$

$$e_\theta \simeq -2(2/\pi K\varrho)^{\frac{1}{2}} \exp\left[i\left(K\varrho - \frac{\pi}{4}\right)\right] \sin\gamma A \sum_{n=0}^{\infty} \frac{\varepsilon_n}{G_n} J_n^+(KR) J_n^-(KR) \sin n\theta \,. \tag{35b}$$

$$e_z \simeq -2(2/\pi K\varrho)^{\frac{1}{2}} \exp\left[i\left(K\varrho - \frac{\pi}{4}\right)\right] \sin^2\gamma \cos\gamma A \sum_{n=0}^{\infty} \frac{\varepsilon_n}{G_n} [J_n^+(KR)]^2 \cos n\theta \,. \tag{35c}$$

3·3. *The scattering cross-section and angular distribution of diffracted energy.* – The scattering diameter D, which is commonly called the cross-section per unit length of cylinder, is given by

$$D = (8\pi/cE_0^2 \cos\gamma) \int_0^{2\pi} S_\varrho \varrho \, \mathrm{d}\theta \,, \tag{36}$$

where S_ϱ is the time average of the ϱ-component of the Poynting vector for the diffracted field,

$$S_\varrho = (c/8\pi)\,\mathrm{Re}\,(e_\theta \bar{h}_z - e_z \bar{h}_\theta)\,. \tag{37}$$

Here, $\bar{h}_z$ and $\bar{h}_\theta$ denote the complex conjugates of h_z and h_θ. The scattering diameter (multiplied by a unit length of cylinder) defines an area which, by definition, intercepts as much incident energy per unit time as is found radiated away (per unit length along the z-axis) by the diffracted field. The substitutions and integrations are straightforward and yield:

$$D_{\mathrm{TE,iso}} = \frac{4}{K}\sum_{n=0}^{\infty}\varepsilon_n\left|\frac{J_n^-(KR)}{H_n^-(KR)}\right|^2, \tag{38a}$$

$$D_{\mathrm{TM,iso}} = \frac{4}{K}\sum_{n=0}^{\infty}\varepsilon_n\left|\frac{J_n(KR)}{H_n(KR)}\right|^2, \tag{38b}$$

$$D_{\mathrm{TE},z\text{-con}} = 0 \tag{38c}$$

$$D_{\mathrm{TM},z\text{-con}} = D_{\mathrm{TM,iso}} \tag{38d}$$

$$D_{\mathrm{TE},\theta\text{-con}} = \frac{4}{K}\sum_{n=0}^{\infty}\varepsilon_n\left|\frac{J_n^-(KR)}{G_n}\right|^2\left[(J_n^-(KR))^2 + (J_n^+(KR))^2\sin^2\gamma\right], \tag{38e}$$

$$D_{\mathrm{TM},\theta\text{-con}} = \frac{4\sin^2\gamma}{K}\sum_{n=0}^{\infty}\varepsilon_n\left|\frac{J_n^+(KR)}{G_n}\right|^2\left[(J_n^-(KR))^2 + (J_n^+(KR))^2\sin^2\gamma\right]. \tag{38f}$$

The angular distribution, $D(\theta)$, is a measure of the amount of diffracted energy per unit cylinder length propagated away from the cylinder in the angular region from θ to $\theta+\mathrm{d}\theta$ for unit intensity of the incident wave and is given by

$$D(\theta) = (E_0^2\cos\gamma)^{-1}\,\mathrm{Re}\,(e_\theta \bar{h}_z - e_z \bar{h}_\theta)\,. \tag{39}$$

The integral of $D(\theta)$ over a large cylindrical surface will result in the cross-section, D.

4. – Numerical computations and results.

In order to gain further insight into the kind of diffraction phenomena produced by anisotropic conductors, some numerical computations were performed on the results of the previous two sections.

The most important special case to be considered is that of normal incidence. At normal incidence, each of the anisotropically conducting cylinders is completely transparent to one of the polarizations and behaves exactly the

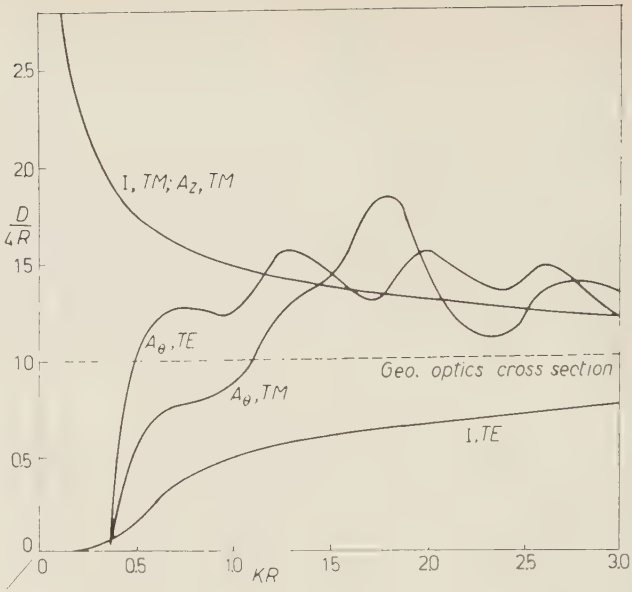

Fig. 3. – The scattering diameters. Here, the scattering diameter divided by $4R$ is plotted as a function of KR with the angle of incidence γ held fixed at 45°. The curves are labeled as follows: I stands for isotropic; A_θ stands for θ-conducting; A_z stands for z-conducting; TE for transverse electric and TM for transverse magnetic.

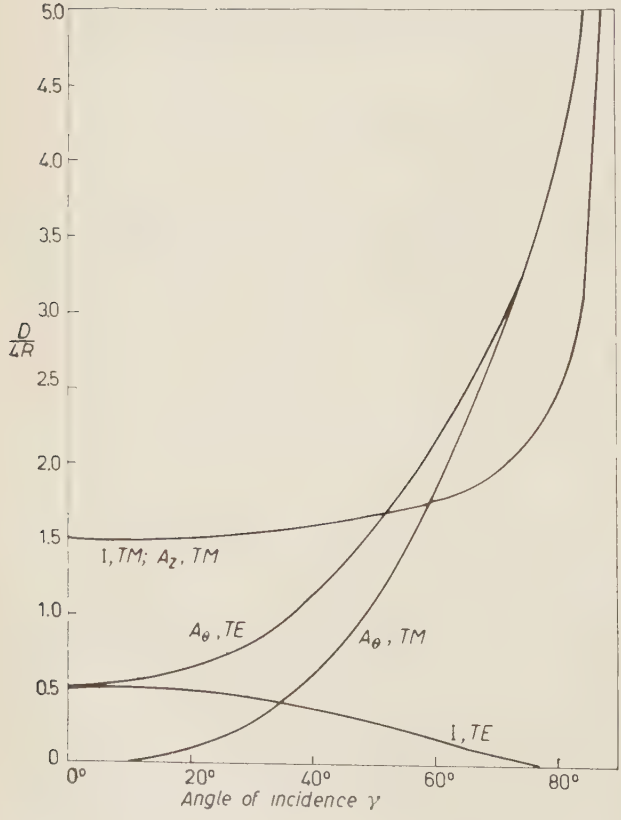

Fig. 4. – The scattering diameters. Here, the scattering diameter divided by $4R$ is plotted as a function of angle of incidence γ with KR held fixed at 1.0. The curves are labeled as follows: I stands for isotropic; A_θ stands for θ-conducting; A_z stands for z-conducting; TE for transverse electric and TM for transverse magnetic.

same as the isotropic cylinder for the other polarization, as exhibited in Table I. No numerical computations are presented for this case, inasmuch as they can be found elsewhere.

TABLE I. – *Comparison of field quantities at normal incidence.*

Transverse electric incident wave	Transverse magnetic incident wave
$\boldsymbol{e}_{z\text{-con}} = 0$	$\boldsymbol{e}_{z\text{-con}} = \boldsymbol{e}_{\text{iso}}$
$\boldsymbol{e}_{\theta\text{-con}} = \boldsymbol{e}_{\text{iso}}$	$\boldsymbol{e}_{\theta\text{-con}} = 0$

The results at normal incidence merely verify what one would have expected all along. The really interesting behavior occurs at oblique incidence, as is illustrated in Figs. 3, 4 and 5.

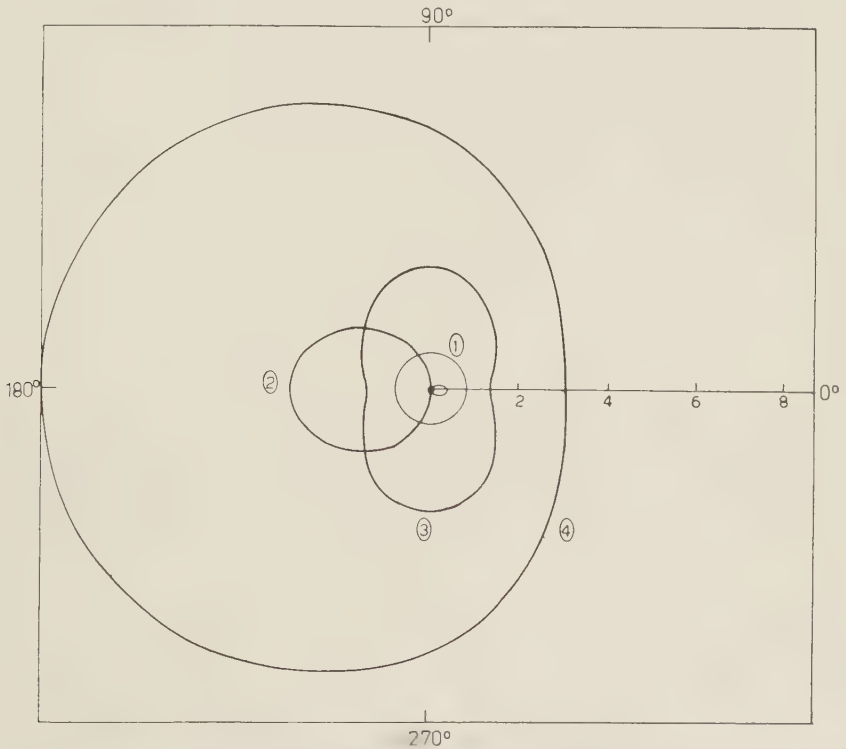

Fig. 5. – The angular distribution of diffracted energy for the case in which $\gamma = 45°$ and $KR = 0.1$. Curve 1 is a polar plot of $(4R)^{-1}D(\theta)$ for the TM polarization for either an isotropic or a z-conducting cylinder. Curves 2, 3 and 4 represent plots of the quantity $10^4(4R)^{-1}D(\theta)$ for TE, isotropic, for TM, θ-conducting and for TE, θ-conducting, respectively.

Fig. 3 shows the effective scattering diameter D at 45° angle of incidence. This is, in all ways, a typical angle of incidence. It will be observed, there, that the scattering diameter of a z-conducting cylinder for a TM incident wave is exactly the same as for an isotropic cylinder excited by this polarization. Thus it can be seen that only the z-component of the incident field is effective in producting a radiative diffracted field for the isotropic cylinder. Of greater potential interest is the behavior of the θ-conducting cylinder which, for both polarizations, exhibits resonance phenomena nearly charcteristic of a circle of radius R superimposed on a basic variation. When $KR \gg 1$, the cross-section for the TE polarization approaches $4R$, which is identical to the isotropic cylinder for both polarizations; the cross-section for an incident TM wave tends to zero as $KR \to \infty$.

Fig. 4 shows the dependence of the scattering diameter on angle of incidence γ for fixed value of $KR = 1.0$. It can be seen there that the θ conducting cylinder presents a bigger effective diameter to the incident wave, at large angle of incidence, than does the isotropic cylinder.

Fig. 5 presents the various angular distributions of diffracted energy for a very small cylinder, $KR = 0.1$, at 45° incidence.

* * *

The authors would like to thank Dr. EDGAR EVERHART for his helpful critical comments.

RIASSUNTO (*)

Si studia la diffrazione di un'onda elettromagnetica piana incidente con un angolo arbitrario su cilindri isotropici e cavi, anisotropicamente conduttori, di lunghezza infinita. I cilindri anisotropicamente conduttori considerati sono: *a*) un cilindro conduttore solo in direzione assiale e *b*) un cilindro conduttore solo nella direzione θ (come un'elica strettamente avvolta). I campi diffratti vengono determinati introducendo le opportune condizioni ai limiti sulle superfici cilindriche. Si danno anche le espressioni per le correnti superficiali indotte e le sezioni trasversali; si danno anche dei diagrammi di queste ultime e della distribuzione angolare dell'energia diffratta. Si include anche una discussione del meccanismo fisico per cui gli effetti della conduttività anisotropica differiscono da quelli della conduttività isotropica. Si trova che il cilindro assialmente conduttore è trasparente per un'onda TE incidente, mentre la polarizzazione produce un campo identico a quello del cilindro isotropico. I cilindri conduttori secondo θ producono campi diffratti che non conservano la polarizzazione dell'onda incidente. Per un rapporto crescente fra il raggio e la lunghezza d'onda, le sezioni trasversali aumentano sino ad un punto in cui cominciano ad oscillare ed infine si avvicinano a dei valori costanti.

(*) *Traduzione a cura della Redazione.*

Lifetimes, Branching Ratios, and Asymmetries in Σ-Hyperon Decays (*).

S. C. Freden, H. N. Kornblum and R. S. White

Lawrence Radiation Laboratory - Livermore - Cal.

(ricevuto il 25 Novembre 1959)

Summary. — Σ-hyperons produced by the capture of K^--mesons in nuclear emulsion have been studied. The mean lifetime of the Σ^+-hyperons which decay via the proton and π^+-meson modes has been measured. For the proton mode using 117 decays at rest and in flight we find $\bar{\tau}_{\Sigma^+\to p(all)} = (8.5^{+1.4}_{-1.1})\cdot 10^{-11}$ s. Using the 49 decays in flight only and the method of Maximum Likelihood, $\bar{\tau}_{\Sigma^+\to p(flight)} = (9.5^{+18.7}_{-3.8})\cdot 10^{-11}$ s. For these decays the calculated lifetime is strongly dependent upon the measured Σ-hyperons energies. Both statistical and systematic errors tend to lower the measured lifetime. The lifetime calculated from 37 Σ^+ decays in flight into π^+ mesons is $\bar{\tau}_{\Sigma^+\to\pi^+(flight)} = (6.0^{+6.8}_{-2.0})\cdot 10^{-11}$ s and is essentially unchanged when a cut-off of $5\cdot 10^{-11}$ s is used. No evidence exists for a short-lived component. The following branching ratios have been found:

$$\frac{\Sigma^+\to p+\pi^0}{\Sigma^+\to n+\pi^+} = 1.00 \pm 0.09 \qquad \text{and} \qquad \frac{\Sigma^+\to p+\gamma}{\text{all } \Sigma^+} < 0.75\% .$$

The values for the asymmetry parameters have been measured. When combined with previous data they are found to be $\alpha^0 P = -0.03 \pm 0.14$, $\alpha^+ \bar{P} = 0.03 \pm 0.16$ and $\alpha^- \bar{P} = -0.14 \pm 0.75$. The superscripts refer to the charges of the decay π-mesons.

1. – Introduction.

The lifetimes, non-leptonic branching ratios, and up-down asymmetries in the decays of the Σ-hyperons have been investigated. The Σ-hyperons were produced by the capture of negative K-mesons which came to rest in

(*) This work was performed under auspices of the U. S. Atomic Energy Commission.

nuclear emulsion. Only those K^--meson captures which yielded two prongs, a Σ-hyperon and a π-meson, were picked for analysis for the following reasons:

1) The fraction of Σ-hyperons in those events is about four times as high as in the multiply pronged events. Thus considerably fewer heavy tracks must be scrutinized to pick out the Σ-hyperons. This reduces the chance of missing a Σ decay into a π-meson and also that of confusing a proton scatter with a Σ decay into a proton.

2) These two pronged events are the only type suited for studying the up-down asymmetry in the Σ-hyperon decay.

3) The charged π-meson partner helps determine the charge and energy of the Σ-hyperon.

2. – Lifetimes.

Several groups of emulsion workers have reported lifetimes for Σ-hyperons which decayed into charged π-mesons that are shorter than those obtained for Σ^+-hyperons that decay into protons in emulsion and for all decay modes in bubble chambers ([1,2]). In this section it will be shown that these low measured values of the lifetimes may be attributed to statistical and systematic errors in the determination of the Σ-hyperon energies.

Only Σ^+-hyperons were picked for detailed lifetime analysis. This was done because the Σ^+-hyperons which decayed into protons provide information which may be used to determine the energies of those Σ^+-hyperons which decayed into π^+-mesons. Such a comparison is not available in the case of decaying Σ^--hyperons.

2·1. $\Sigma^+ \to p + \pi^0$. – A total of 117 Σ^+ decays into protons have been observed from two-pronged $\Sigma^+\pi^-$ stars from K^- captures at rest. Of these, 49 were decays in flight. In 113 of these cases the decay proton came to rest in the stack and the Σ^+-hyperon energy was determined from the energy and angle of the decay proton. In the four remaining cases the ranges of the decay protons were determined from ionization measurements ([3]). Fig. 1 is a plot of the range distribution of the decay protons from the 117 events. The shaded areas are those cases for which the Σ^+-hyperon decayed at rest.

([1]) S. C. FREDEN, F. C. GILBERT and R. S. WHITE: *Bull. Am. Phys. Soc.*, **3**, 25 (1958).

([2]) D. A. GLASER, M. M. L. GOOD and D. R. O. MORRISON: *Proceedings of the 1958 Annual International Conference on High Energy Physics at CERN* (Geneva, 1958), p. 271.

([3]) P. H. FOWLER and D. H. PERKINS: *Phil. Mag.*, **46**, 587 (1955).

Fig. 2*a* is a plot of the energy distribution of these Σ^+-hyperons at the K^- capture point. Again, the shaded areas represent Σ^+ hyperons which decayed at rest. An event marked with a « *P* » is a K^- capture at rest on a free proton.

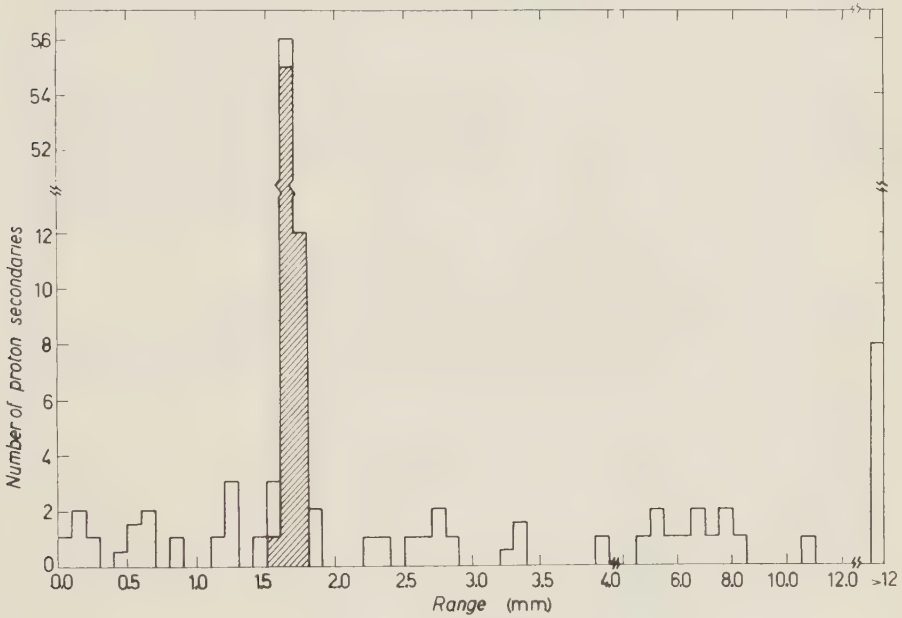

Fig. 1. – Plot of the range distribution of the proton secondaries from the decays $\Sigma^+ \to p + \pi^0$. The shaded area represents decays at rest.

The lifetime for all the $\Sigma^+ \to p$ decays was then calculated from the expression

$$\bar{\tau} = \frac{1}{n_F}\left[\sum_{i=1}^{n_F} t_i + \sum_{j=1}^{n_R} T_j\right], \tag{1}$$

in which t_i is the time to decay for decays in flight and T_j is the moderation time for those which decay at rest; n_F is the number of decays in flight and n_R the number of decays at rest. The lifetime thus obtained is

$$\bar{\tau}_{\Sigma \to p(all)} = (8.5^{+1.4}_{-1.1}) \cdot 10^{-11} \text{ s},$$

which is in excellent agreement with the mean value of $(8.4^{+0.7}_{-0.6}) \cdot 10^{-11}$ s obtained from Σ^+ decays into protons in flight and at rest in emulsions and all Σ^+ decays in bubble chambers ([2]).

The lifetime may also be calculated using only the decays in flight by the method of Maximum Likelihood (4). The best estimate of the mean lifetime is obtained as the maximum of the expression

$$P(\tau) = \prod_{i=1}^{n} \frac{1}{\tau} \frac{\exp[-t_i/\tau]}{1-\exp[-T_i/\tau]}\,, \tag{2}$$

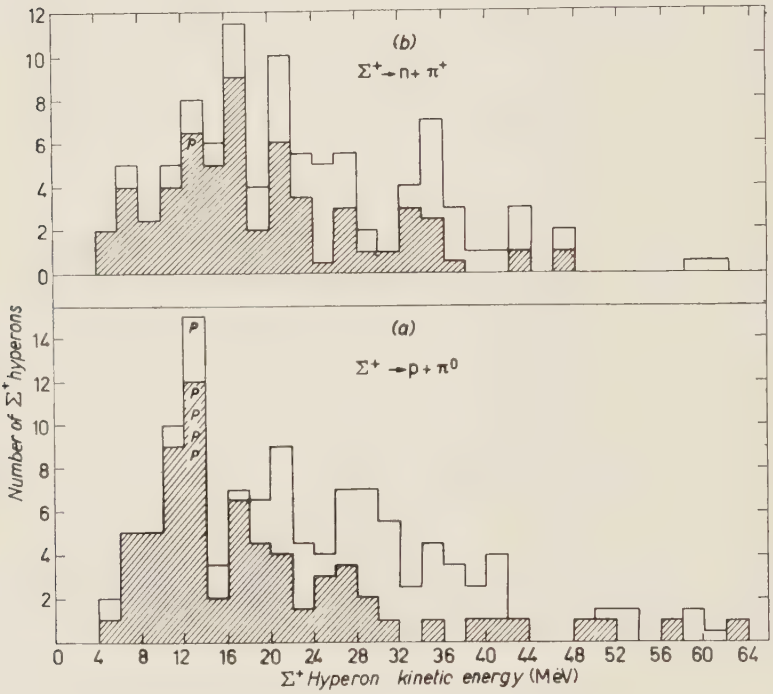

Fig. 2. – Plot of the energy distribution of the Σ^+-hyperons. Curve (*a*) is for the decay mode $\Sigma^+ \to p + \pi^0$. Curve (*b*) is for $\Sigma^+ \to n + \pi^+$. The shaded areas represent decays at rest. Events marked with a « *P* » are K^- captures on free protons.

plotted as a function of τ. T_i is the potential time. Alternately, the lifetime may be obtained as the solution of the expression

$$\frac{\partial}{\partial \tau} \log P(\tau) = \sum_{i=1}^{n} \frac{t_i}{\tau} - 1 + \frac{T_i}{\tau} \frac{\exp[-T_i/\tau]}{(1-\exp[T_i/\tau])} = 0\,. \tag{3}$$

(4) M. S. BARTLETT: *Phil. Mag.*, **44**, 249 (1953); E. AMALDI: *Suppl. Nuovo Cimento*, **2**, 253 (1955); C. FRANZINETTI and G. MORPURGO: *Suppl. Nuovo Cimento*, **6**, 577 (1957); M. F. KAPLON, A. C. MELISSINOS and T. YAMANOUCHI: NYO-2621 (unpublished).

The statistical errors on the value of $\bar{\tau}$ obtained from eq. (2) or (3) are estimated from the expression

$$S(\tau) = \frac{\sum_{i=1}^{n}\left[\frac{t_i}{\tau} - 1 + \frac{T_i}{\tau}\frac{\exp[-T_i/\tau]}{(1-\exp[-T_i/\tau])}\right]}{\left\{\sum_{i=1}^{n}\left[1 - \frac{T_i^2}{\tau^2}\frac{\exp[-T_i/\tau]}{(1-\exp[-T_i/\tau])^2}\right]\right\}^{\frac{1}{2}}}, \tag{4}$$

which is asymptotically normal with zero mean and unit variance. Equation (4) plotted as a function of $1/\tau$ is nearly linear in the vicinity of $\bar{\tau}$, making graphical interpolation easy. The lifetime thus obtained for the 49 Σ^+ decays in flight into protons is

$$\bar{\tau}_{\Sigma^+\to p(\text{flight})} = (9.5^{+18.7}_{-3.8})\cdot 10^{-11}\ \text{s}\,,$$

which is in good agreement with the accepted lifetime of the Σ^+-hyperon. Fig. 3 curve (*a*) is a plot of eq. (4) for these 49 events.

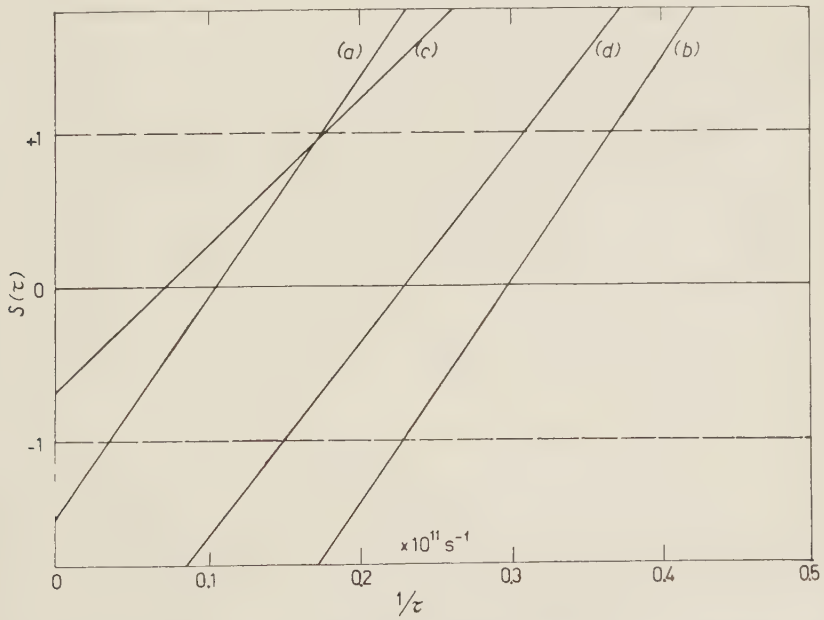

Fig. 3. – Plot of $S(\tau)$ from eq. (4) versus $1/\tau$. Curve (*a*) is the unaltered data. Curves (*b*) and (*c*) are for the $+20\%$ and -20% cases respectively. Curve (*d*) is for the $\pm 20\%$ case.

The lifetime obtained using decays in flight and at rest (eq. (1)) is determined primarily by the proper times of those hyperons that come to rest. These can be accurately determined from the hyperon ranges. The calculated

lifetime is insensitive to the energies of the hyperons that decay in flight. However, exactly the opposite is true when the lifetime is obtained only from the decays in flight by the method of Maximum Likelihood. This is the situation for the Σ^+-hyperons that decay into π^+-mesons. The energies of those Σ^+-hyperons that decay into π^--mesons are determined primarily by ionization measurements on the Σ^+-hyperon tracks. It is therefore important to investigate the effects on the measured $\bar{\tau}$ of statistical and systematic errors in the determination of the Σ^+-hyperon energies. It is evident from eq. (2) for the situation where $T_i > \tau$ that the weighting factors $1 - \exp[-T_i/\tau]$ approach unity and the lifetime is primarily determined by the decay times t_i. These are relatively insensitive to the Σ-hyperon energies. For the situation under investigation, however, the $T_i \lesssim \tau$ and the calculated lifetime is strongly dependent upon the weighting factors and therefore upon the energies of the Σ^+-hyperons.

The effects of systematic errors were investigated first. We added 20% to the energy of each of the 49 Σ^+-hyperons that decayed in flight into a proton and then subtracted 20% from each of their energies. The 20% figure was chosen because we find experimentally that ionization measurements, especially in the region under investigation ($10 \lesssim g^* \lesssim 20$; *i.e.*, 40 MeV $\gtrsim T_\Sigma \gtrsim$ $\gtrsim$ 10 MeV), are subject to systematic and statistical errors of about 10%. At 20 MeV, an error of 10% in the measured ionization of a Σ-hyperon causes an error in its energy of 20%. When the energies were reduced by 20%, only 32 Σ^+ decays in flight remained. The new T_i and t_i were then calculated for each event and eq. (4) was plotted for the two new sets of values. These are shown in Fig. 3 curves (*b*) and (*c*) for the $+20\%$ and -20% cases, respectively. The mean lifetimes and their errors for these cases are:

$$\bar{\tau}_{+20\%} = (3.3^{+0.7}_{-0.4}) \cdot 10^{-11} \text{ s},$$

$$\bar{\tau}_{-20\%} = (13.7^{+\infty}_{-8.1}) \cdot 10^{-11} \text{ s}.$$

It should be noted that the systematic error of $+20\%$ reduced the apparent lifetime by a factor of almost 3 and reduced the standard error by a factor of 10 at the lower end and a factor of 27 at the upper end.

The effects of statistical errors were handled in a similar fashion. Half of the Σ^+-hyperons were chosen at random and their energies were increased by 20%; the other half had their energies decreased by 20%. Forty Σ^+-hyperon decays in flight remained. Equation (4) was then plotted for these events and is shown in Fig. 3 curve (*d*). The lifetime obtained is

$$\bar{\tau}_{\pm 20\%} = (4.3^{+2.3}_{-1.1}) \cdot 10^{-11} \text{ s},$$

which is almost two standard deviations away from the accepted lifetime of the Σ^+-hyperon. To show that no systematic errors were introduced by this division, the halves were interchanged. The results were unchanged.

The data of Figs. 4 and 5 are used to help determine the energies of those Σ^+-hyperons that decay into π^+-mesons and to select events for the asymmetry calculation in Section 5. In Fig. 4 are plotted the true angles between the Σ^+-hyperons and their π^--meson partners, $\theta_{\pi\Sigma\pi}$, as a function of the sum of the kinetic energies of the two particles, $T_\pi + T_\Sigma$. This is done for the 47 events where the π^- partners stopped in the stacks. The close grouping of events

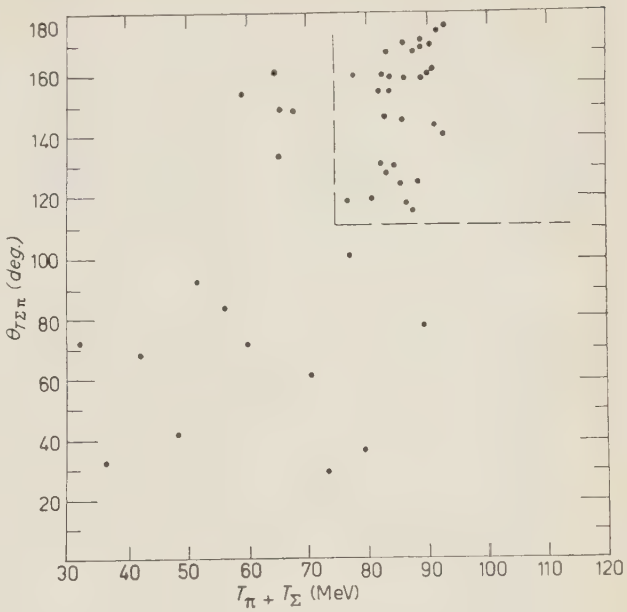

Fig. 4. – Plot of the true angle between the Σ^+-hyperon and its π^--meson partner versus the sum of their kinetic energies.

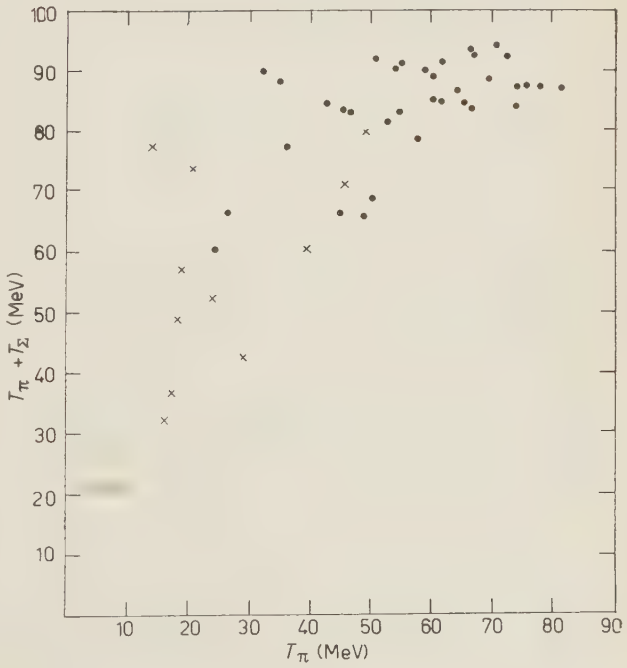

Fig. 5. – Plot of the sum of the kinetic energies of the Σ^+-hyperon and its π^--meson partner versus the kinetic energy of the π^--meson partner. The dots represent those events for which the true angle between the hyperon and the π-meson partner is greater than 110°. The crosses are those events for which the true angle is equal to or less than 110°.

for $\theta_{\tau\Sigma\pi} > 110°$ and $T_\pi + T_\Sigma > 75$ MeV is evidence that these events represent cases where the Σ^+-hyperon and its π^--meson partner escaped from the nucleus without interacting with other nucleons. Sixty-six (± 12) percent of the two-pronged $\Sigma^+\pi^-$ events fall into this category. Fig. 5 presents the same events as Fig. 4 with $T_\pi + T_\Sigma$ plotted against T_π. The dots are those events for which $\theta_{\tau\Sigma\pi} > 110°$ and the crosses are those events for which $\theta_{\tau\Sigma\pi} \leqslant 110°$. For those events having $\theta_{\tau\Sigma\pi} > 110°$ and $T_\pi \geqslant 55$ MeV, the grouping around $T_\pi + T_\Sigma - 87.0$ MeV is quite marked. In fact the standard deviation on $T_\pi + T_\Sigma$ for any one event in that category is only ± 4 MeV, or 20% for a 20 MeV Σ-hyperon. This fact will be used to help determine the energies of those Σ^+-hyperons that decay into π^+-mesons.

2·2. $\Sigma^+ \to n + \pi^+$. – Although the energies of the Σ^+-hyperons that decay into protons are very accurately determined from the kinematics of the decays, the energies of those Σ^+-hyperons that decay into π^+-mesons cannot be accurately determined for several reasons:

1) The energies of the π^+-meson secondaries are generally very insensitive to the Σ^+-hyperon energies. For example, at 90 degrees in the laboratory system, the energy of the π^+ secondary from the decay of a 20 MeV Σ^+-hyperon is 88 MeV, while at 30 MeV the π^+-meson energy is 87 MeV. Thus, even if a π^+-meson secondary stops in the stack the range straggling ($\approx 2\%$ in energy) causes a considerable error in the inferred Σ^+-hyperon energy.

2) Most of the π^+ secondaries do not stop in the stacks. Thus their energies are less reliably determined from ionization measurements than from range.

3) Since these Σ^+-hyperons have a mean energy of about 20 MeV, the ionizations of their tracks are near saturation ($g^* \approx 15$), making the determination of the hyperon energies by this method subject to large statistical and systematic errors.

In spite of these difficulties the lifetime for the Σ^+-hyperons that decayed into π^+-mesons was measured by the Maximum Likelihood method. The $\Sigma^\pm$-hyperons that decayed into $\pi^\pm$-mesons were separated according to charge in the following way:

1) $\Sigma^+ \to \pi^+$ at rest. The ionization and the scattering indicated that the hyperon decayed at rest, or the π^+ secondary came to rest and the kinematics were consistent with a decay at rest. These events were not used in the lifetime calculation but were used to determine the up-down asymmetry.

2) $\Sigma^+ \to \pi^+$ in flight. The π^+ secondary came to rest and the kinematics were consistent with a decay in flight or the ionization and scattering indicated a decay in flight and the π^- partner ended or disappeared in flight.

3) $\Sigma^- \to \pi^-$ in flight. The π^- secondary came to rest or disappeared in flight or the π^+ partner ended. Five identified π^--mesons and no π^+-mesons disappeared in flight, so this criterion is considered reliable to determine the charge of a π^--meson.

From a total of 144 $\Sigma^\pm$ decays into π^+ mesons, we identified 58 Σ^+ decays at rest, 37 Σ^+ decays in flight, and 17 Σ^- decays in flight. The remaining 32 $\Sigma^\pm$-hyperons could not be identified with respect to charge and were not used in the analyses. These methods of identification may slightly bias the energy distribution of the identified Σ^+-hyperons but should not affect the calculated lifetime.

The energy of each of the Σ^+-hyperons that decayed in flight into a π^+-meson was determined by one of three methods.

1) Kinematics of the decay were used if the energy of the π^+-meson secondary could be determined accurately from its range of from an ionization measurement near the end of its range and the decay angle was such that the statistical uncertainty in its range could cause only a small error in the calculated Σ^+-hyperon energy.

2) Ionization was used if the dip angle, θ_{V_Σ}, of the hyperon track was less than 45° in the unprocessed emulsion and 1) above did not apply.

3) The fact that $T_\pi + T_\Sigma = 87 \pm 4$ MeV if $\theta_{\pi\Sigma\pi} > 110°$ and $T_\pi > 55$ MeV was used if the π^- partner came to rest and 1) or 2) above did not apply or if the hyperon track was too short to give reasonable statistics for the ionization measurement.

The energy distribution of all the Σ^+-hyperons that decayed into π^+-mesons is shown in Fig. 2*b*. The shaded events again represent decays at rest. The energy distributions for the two decay modes are statistically the same in spite of the method of determining the charge of the Σ^+-hyperons that decayed into π^+-mesons. Also, the mean energies for the two cases are the same, 23 MeV. More pertinent to the lifetime calculation is the fact that for only the decays in flight the energy distributions are again statistically the same, as are the mean energies, 28 MeV.

The lifetime for the 37 decays in flight is

$$\bar{\tau}_{\Sigma^+ \to \pi^+ (\text{flight})} = (6.0^{+6.8}_{-2.0}) \cdot 10^{-11} \text{ s} .$$

This is in agreement with the accepted lifetime of the Σ^+-hyperon.

To eliminate decays at rest we applied a cut-off, $T_i - t_i = 5 \cdot 10^{-11}$ s, to the data. This eliminated all decays of Σ^+-hyperons with energies less than about 24 MeV at the decay point. It should be noted that if two Σ^+-hyperon decay rates exist the lifetime obtained using the cut-off data would be biased toward the shorter lifetime. When the cut-off was applied to the Σ^+ decays into π^+-mesons, only ten events remained. The lifetime for these events is

$$\bar{\tau}_{\Sigma^+ \to \pi^+ (\text{c.o.})} = (6.8^{+\infty}_{-4.2}) \cdot 10^{-11} \text{ s} ,$$

which is the same as the value for all Σ^+ decays in flight into π^+-mesons. This is additional evidence *against* the existence of a short-lived component.

Again it should be emphasized that although the systematic errors in the determination of the energies of the Σ^+-hyperons that decay into π^+-mesons appear to be negligible, the statistical errors will tend to give a low value for the mean lifetime. Therefore, the lifetimes calculated in this section for the Σ^+ decays into π^+-mesons probably represent lower limits to the actual Σ^+ lifetime. This consideration makes a short-lived component even less likely.

3. – The branching ratio $(\Sigma^+ \to p + \pi^0)/(\Sigma^+ \to n + \pi^+)$.

As mentioned above, 117 Σ^+-hyperon decays into protons have been observed from two-pronged $\Sigma^+\pi^-$ events. The probability of finding all Σ^+ decays from such events is taken to be 100%. The total number of Σ^+ decays into π^+-mesons can be obtained in the following way. Fifty-eight such decays were observed at rest. An additional 37 Σ^+ and 17 Σ^- decays were identified out of a total of 86 Σ^+ decays in flight into π^+-mesons. Charge was determined either from the charge of the secondary π-meson or from that of the π-meson partner. Since the energy distributions of the π-meson partners are very similar for Σ^+ and Σ^- production in nuclei, no bias is introduced in determining the charge of a Σ-hyperon by this method. The bias introduced in the charge determination by looking at the decay π-mesons is negligible because the energy difference between the π^- and π^+-mesons is small (≈ 5 MeV) and only about 20% of the charges were determined by this method.

The observed ratio of Σ^+ decays in flight into π^+-mesons to Σ^- decays in flight is $37/17 = 2.18^{+0.97}_{-0.61}$. Therefore the number of Σ^+ decays in flight into π^+-mesons out of the 32 $\Sigma^\pm \to \pi^\pm$ decays whose charges were not identified is 22 ± 3, giving a total of 117 Σ^+ decays into π^+-mesons. The branching ratio is then

$$\frac{\Sigma^+ \to p + \pi^0}{\Sigma^+ \to n + \pi^+} = \frac{117}{117} = 1.00 \pm 0.09 .$$

This value is in agreement with the $|\Delta I| = \frac{1}{2}$ selection rule ([5]) and with the experimental results of other workers ([6]).

4. – The decay mode $\Sigma^+ \to p + \gamma$.

We can put an upper limit on the possible decay mode $\Sigma^+ \to p + \gamma$ from the data of Fig. 1. For such a decay at rest the proton will have an energy of 26.5 MeV and a range of 3.0 mm in emulsion. There is no such candidate where 68 $\Sigma^+ \to p + \pi^0$ decays at rest were observed. Thus, $(\Sigma^+ \to p + \gamma)/(\Sigma^+ \to p + \pi^0) < 1.5\ \%$. In Section 3 we showed that $(\Sigma^+ \to p + \pi^0)/(\Sigma^+ \to n + \pi^+) = 1$. Therefore,

$$\frac{\Sigma^+ \to p + \gamma}{\text{all } \Sigma^+ \text{ decays}} < 0.75\ \% .$$

The theoretical predictions for the branching ratio $(\Sigma^+ \to p + \gamma)/(\Sigma^+ \to p + \pi^0)$ vary from about 10^{-2} to 10^{-4}, so that the data presented here are not inconsistent with the theory ([7]). Considerably more data must be accumulated to determine the branching ratio accurately.

5. – Up-down asymmetries.

Since the now famous paper of LEE and YANG ([8]) experimenters have been looking for evidence of non-conservation of parity in weak interactions. Conclusive evidence has been found for parity non-conservation in β-decay ([9]), π decay, and μ decay ([10]). The asymmetry in the decay of the Λ^0-hyperon

---

([5]) M. GELL-MANN and A. H. ROSENFELD: *Ann. Rev. Nucl. Sci.*, Vol. 7 (Palo Alto, 1957), p. 407.

([6]) G. A. SNOW: *Proceedings of the Seventh Annual Rochester Conference* (New York, 1957), p. VIII-14. M. KOCH, M. NIKOLIĆ, M. SCHNEEBERGER and H. WINZELER: private communication.

([7]) R. F. BEHRENDS: *Phys. Rev.*, **111**, 1691 (1958); P. PRAKASH and A. H. ZIMERMAN: *Nuovo Cimento*, **11**, 869 (1959).

([8]) T. D. LEE and C. N. YANG: *Phys. Rev.*, **104**, 254 (1956).

([9]) C. S. WU, E. AMBLER, R. W. HAYWARD, D. D. HOPPES and R. P. HUDSON: *Phys. Rev.*, **105**, 1413 (1957).

([10]) R. L. GARWIN, L. M. LEDERMAN and M. WEINRICH: *Phys. Rev.*, **105**, 1415 (1957); J. FRIEDMAN and V. TELEGDI: *Phys. Rev.*, **105**, 1681 (1957); C. S. WU: *Proceedings of the Seventh Annual Rochester Conference* (New York, 1957), p. VII-20.

is also now well established ([11,12]). However, the question of parity violation in the decays of the Σ-hyperons produced by K⁻-mesons is inconclusive ([12]). Recent experimental work at Berkeley with π^+-produced Σ^+-hyperons shows parity violation in the proton decay mode of the Σ^+-hyperons ([13]).

Various emulsion groups have looked for « up-down » asymmetries in the decays of the charged Σ-hyperons produced by the capture of K⁻-mesons in emulsion. Because of the Fermi momentum of the capturing nucleon the produced Σ-hyperon and π-meson are not colinear and therefore define a plane. As is customary we define the normal to this production plane as $p_\Sigma \times p_{\pi_{\text{partner}}}$ and take $\xi \equiv (p_\Sigma \times p_{\pi_{\text{partner}}}) \cdot P_{\pi_{\text{secondary}}} > 0$ to mean « up ».

For hyperon spin $\frac{1}{2}$ and K-meson spin 0 the decay angular distribution has the form

$$W(\xi)\,\mathrm{d}\xi \sim (1 + \alpha \overline{P} \xi)\,\mathrm{d}\xi\,, \tag{5}$$

where $\overline{P}$ is the polarization averaged over the production angles. Integrating over ξ we get

$$\alpha \overline{P} = \frac{N_{\text{up}} - N_{\text{down}}}{\frac{1}{2}(N_{\text{up}} + N_{\text{down}})}\,. \tag{6}$$

A result different from zero for $\alpha\overline{P}$ indicates non-conservation of parity in the decay; however, a zero result may be due to parity conservation or to the lack of polarization of the decaying particles.

Table I lists the data of this experiment separately and combined with previous emulsion results ([12]).

If an asymmetry exists in any of the decay modes it would be more prominent in events where the Σ-hyperon and the π-meson partner escape from the capturing nucleus without being scattered. From Fig. 4 the tight grouping of events for $T_\pi + T_\Sigma > 75$ MeV and $\theta_{\pi\Sigma\pi} > 110°$ indicates that most of these are examples where the Σ^--hyperon and the π^--meson partner were unscattered in escaping from the nucleus. Column 5 of Table I gives the up-down ratio for these selected events and column 6 gives the value of $\alpha\overline{P}$ for them.

([11]) E. Eisler, R. Plano, A. Prodel, N. Samios, M. Schwartz, J. Steinberger, P. Bassi, V. Borelli, G. Puppi, H. Tanaka, P. Woloschek, U. Zoboli, M. Conversi, P. Franzini, I. Mannelli, R. Santangelo and V. Silvestrini: *Phys. Rev.*, **108**, 1353 (1957).

([12]) D. A. Glaser: *Proceedings of the 1958 Annual International Conference on High Energy Physics at CERN* (Geneva, 1958), p. 267.

([13]) R. L. Cool, B. Cork, J. W. Cronin and W. A. Wenzel: *Phys. Rev.*, **114**, 912 (1959).

TABLE I. – *Up-down asymmetries in the decays of Σ-hyperons.*

Decay mode	N_{up}/N_{down} This exper.	N_{up}/N_{down} Combined	$\alpha\overline{P}$	N_{up}/N_{down} selected	$\alpha\overline{P}$ selected
$\Sigma^+ \to p + \pi^0$	56/56	199.5/205.5	0.03 ± 0.14	38/36	0.05 ± 0.32
$\Sigma^+ \to n + \pi^+$	45/49	148/144	$+0.03 \pm 0.16$	33/39	-0.17 ± 0.33
$\Sigma^- \to n + \pi^-$	$6\frac{1}{2}/7\frac{1}{2}$		-0.14 ± 0.75		

The results indicate that $\alpha\overline{P}$ is not statistically different from zero for any of the decay modes. The work of COOL *et al.* shows an asymmetry in the proton decay mode of $\alpha^0\overline{P} = 0.70 \pm 0.30$ for Σ^--hyperons produced by interaction of 1.0 GeV π^+ mesons with protons [13]. The most logical way to explain the discrepancy between this work and theirs is that the Σ-hyperons produced by K^- captures at rest in emulsion are unpolarized.

6. – Conclusions.

1) From 117 Σ^+ decays in flight and at rest into protons the calculated mean lifetime is $\overline{\tau}_{\Sigma^+ \to p(all)} = (8.5^{+1.4}_{-1.1}) \cdot 10^{-11}$ s. This is in excellent agreement with the accepted lifetime, $\overline{\tau} = (8.4^{+0.7}_{-0.6}) \cdot 10^{-11}$ s, obtained from emulsions and bubble chambers. Using the 49 decays in flight only and the method of Maximum Likelihood the measured lifetime is

$$\overline{\tau}_{\Sigma^+ \to p(flight)} = (9.5^{+18.7}_{-3.8}) \cdot 10^{-11} \text{ s} .$$

2) Systematic and statistical errors in the determination of the hyperon energies were found to change significantly the lifetime calculated from the decays in flight only. A systematic change of $+20\%$ in the energies of the 49 Σ^+-hyperons that decayed in flight into protons yielded the lifetime $\overline{\tau}_{+20\%} = (3.3^{+0.7}_{-0.4}) \cdot 10^{-11}$ s. For a -20% systematic error the lifetime is $\overline{\tau}_{-20\%} = (13.7^{+\infty}_{-8.1}) \cdot 10^{-11}$ s. A $+20\%$ error applied to half of the events and -20% to the other half to simulate statistical errors gives a lifetime $\overline{\tau}_{\pm 20\%} = (4.3^{+2.3}_{-1.1}) \cdot 10^{-11}$ s.

3) The lifetime obtained from 37 Σ^+ decays in flight into π^+-mesons is $\overline{\tau}_{\Sigma^+ \to \pi^+(flight)} = (6.0^{+6.8}_{-2.0}) \cdot 10^{-11}$ s. Using a cut-off of $5 \cdot 10^{-11}$ s the lifetime becomes $\overline{\tau}_{\Sigma^+ \to \pi^+(c.o.)} = (6.8^{+\infty}_{-4.2}) \cdot 10^{-11}$ s. These values are evidence against a short-lived component for the Σ^+-hyperon.

4) The branching ratio $(\Sigma^+ \to p + \pi^0)/(\Sigma^+ \to n + \pi^+) = 1.00 \pm 0.09$, which is in agreement with the $|\Delta I| = \frac{1}{2}$ selection rule and with the results of other workers.

5) No Σ^+ decay via the mode $\Sigma^+ \to p + \gamma$ was observed in 68 $\Sigma^+ \to p + \pi^0$ decays at rest. Thus we place an upper limit on the branching ratio $(\Sigma^+ \to p + \gamma)/(\text{all } \Sigma^+) < 0.75\ \%$.

6) No up-down asymmetries were observed. Combining our data with the previous results yields the following values for the asymmetry parameters: $\alpha^0 \overline{P} = -0.03 \pm 0.14$, $\alpha^+ \overline{P} = 0.03 \pm 0.16$, $\alpha^- \overline{P} = -0.14 \pm 0.75$. The superscripts refer to the charges of the decay π-mesons.

* * *

We wish to thank Dr. HARRY HECKMAN for setting up the separated K^--meson beam. We appreciate the co-operation of Dr. E. J. LOFGREN and the Bevatron crew. Our thanks go to Mrs. BARBARA ALLEN, Miss PATRICIA BANKS, Mrs. IRENE BROWN, Mrs. LOIS BUTTON, Miss CLAUDIA CRANE, Mrs. THEODORA HILLIARD, Mrs. MARGARET JEPSON, Mrs. BEVERLY LAGISS, Mrs. EMILY MUSKOPF, Mrs. MARTHA SINGLETON, Mrs. CLARICE SISEMORE, Mrs. NANCY STRATTON, Mrs. SOPHIE WARD, and Mrs. ELIZABETH WILSON for locating the events and for taking measurements.

RIASSUNTO (*)

Si sono studiati gli iperoni Σ prodotti dalla cattura di mesoni K^- nelle emulsioni nucleari. È stata misurata la vita media degli iperoni Σ^- che decadono in protoni o mesoni π^+. Per i decadimenti in protoni usando 117 decadimenti a riposo ed in volo, troviamo $\overline{\tau}_{\Sigma^+ \to p(\text{tutti})} = 8.5^{+1.4}_{-1.1} \cdot 10^{-11}$ s. Usando solo i 49 decadimenti in volo ed il metodo di massima probabilità, $\overline{\tau}_{\Sigma^+ \to p(\text{in volo})} = 9.5^{+18.7}_{-3.8} \cdot 10^{-11}$ s. Per questi decadimenti la vita calcolata dipende fortemente dalle energie misurate degli iperoni Σ. Gli errori sia statistici che sistematici tendono ad abbassare la vita media misurata. La vita media calcolata da 37 decadimenti in volo a mesoni π^+ è $\overline{\tau}_{\Sigma^+ \to \pi^+(\text{in volo})} = 6.0^{+6.8}_{-2.0} \cdot 10^{-11}$ s e non cambia sensibilmente se si usa un cut-off di $5 \cdot 10^{-11}$ s. Non si hanno prove di un componente a vita breve. Si sono trovati i seguenti rapporti di branching:

$$\frac{\Sigma^+ \to p + \pi^0}{\Sigma^+ \to n + \pi^+} = 1.00 \pm 0.09 \quad \text{e} \quad \frac{\Sigma^+ \to p + \gamma}{\text{tutti i } \Sigma^+} < 0.75\% .$$

Si sono misurati i valori dei parametri di asimmetria. In combinazione con i dati precedenti si trova che sono $\alpha^0 \overline{P} = -0.03 \pm 0.14$, $\alpha^+ \overline{P} = 0.03 \pm 0.16$ e $\alpha^- \overline{P} = -0.14 \pm 0.75$. Gli indici superiori si riferiscono alle cariche dei mesoni π di decadimento.

(*) *Traduzione a cura della Redazione.*

On the Grain Density in Ilford G-5 Emulsion of Singly Charged Relativistic Particles.

B. Jongejans

Natuurkundig Laboratorium, Universiteit van Amsterdam - Amsterdam

(ricevuto il 29 Dicembre 1959)

Summary. — The grain density in nuclear emulsion has been determined as a function of the value of $(\gamma - 1)$ of the particle producing the track. Values of the parameter $(\gamma - 1)$ between 0.8 and 10^3 were taken into consideration. The nummer of blobs per unit length has been directly determined. Transformation of blob density into grain density has been carried out. Care has been taken to relate all determinations to each other, a constant scale of reference being found in pions of momentum between 5.2 and 5.7 GeV/c. The results are in agreement with the theory given by Sternheimer. The value (501 ± 8) eV was used for the ionization potential of AgBr in the present work. This value was taken from Barkas. The cut-off energy consequently determined is 100 keV. It is shown that the results are not very sensitive to this last value.

1. – Introduction.

The theory of the energy loss of charged particles in matter has been initiated by Bohr [1], and extended later on by others. The density effect has been first calculated by Fermi [2], and later on *e.g.* by Sternheimer [3] and Budini *et al.* [4]. The subject was thoroughly reviewed by Price [5] to whom we refer for literature prior to 1955.

From the publications on this subject that have appeared after this year

---

[1] N. Bohr: *Phil. Mag.*, **25**, 10 (1913).

[2] E. Fermi: *Phys. Rev.*, **57**, 485 (1940).

[3] R. M. Sternheimer: *a*) *Phys. Rev.*, **88**, 851 (1952); *b*) **89**, 1148 (1953); *c*) **91**, 256 (1953); *d*) **93**, 351 (1953); *e*) **93**, 1434 (1953); *f*) **103**, 511 (1956).

[4] P. Budini: *Nuovo Cimento*, **10**, 236 (1953); P. Budini and L. Taffara: *Nuovo Cimento*, **4**, 23 (1956).

[5] B. T. Price: *Rep. Prog. in Phys.*, **18**, 52 (1955).

we quote SHAPIRO ([6]), KEPLER *et al.* ([7]), ALEXANDER *et al.* ([8]), LANOU *et al.* ([9]).

Increasing interest in, and more ready availability of high energy particles made the question of the restricted energy loss (energy losses smaller than T_0 per incidental collision) in the relativistic region appear worth-while another investigation.

The theories currently employed, require at least two not precisely known quantities, the mean ionization potential I and the cut-off energy T_0.

In producing curves from these theories for numerical data one is faced with a lack of unanimity regarding these constants. This is easily understood because these constants have only a limited influence on the restricted energy loss and the role of one can be partly fulfilled by the other. The mean ionization potential I in nuclear emulsion was recently accurately determined by BARKAS ([10]) from range determinations. His value for I is used. The theoretical predictions and the experimental verifications ([5]) show that the variation in average restricted energy loss in nuclear emulsion does not exceed 15% when $\gamma > 2.5$ ($\gamma^2 = 1/(1-\beta^2)$, where β is the velocity of the traversing particle that produces a track in the emulsion).

Therefore it has been tried to obtain an accuracy of 1% in each determination of the relative energy loss (the quotient of two energy losses).

Tests of the human factor involved in the measurements revealed that a higher accuracy seems unattainable. Beside this, economy of manpower begins to play a role when more is required from the method of counting blobs with the human eye. The results reported here comprise 2-person-years of work for the gathering of raw data alone. It was assumed in conformity with the theoretical expectation that restricted energy loss of singly charged particles only depends on the velocity of the traversing particle. This assumption is in accordance with our experimental findings.

2. – Theory.

2·1. *Adopted formulas.* – For the average rate of restricted energy loss of singly charged particles in emulsion we adopted the following formula as given by STERNHEIMER ([3c]).

$$(1) \qquad \frac{1}{\varrho}\left(\frac{\partial E}{\partial x}\right)_{T_0} = \frac{2\pi n_0 e^4}{\varrho m \beta^2 c^2}\left[\ln \frac{2mc^2 \cdot T_0 \cdot \beta^2}{I^2(1-\beta^2)} - \beta^2 - \delta(\beta)\right].$$

([6]) M. M. SHAPIRO: *Hand. d. Phys.*, **45**, 342 (1958).

([7]) R. G. KEPLER, C. A. D'ANDLAU, W. B. FRETTER and L. F. HANSEN: *Nuovo Cimento*, **70**, 71 (1958).

([8]) G. ALEXANDER and R. H. W. JOHNSTON: *Nuovo Cimento*, **5**, 363 (1957).

([9]) R. E. LANOU and H. L. KRAYBILL: *Phys. Rev.*, **113**, 657 (1959).

([10]) W. H. BARKAS: *Nuovo Cimento*, **8**, 201 (1958).

The left hand side is the average rate of energy loss per g cm^{-2} whereby the individual energy loss does not exceed in any act the amount T_0. As we have to compare energy losses relative to the energy loss of a particle with known β, we are not interested in the constant $2\pi n_0 e^4/\varrho mc^2$.

In this investigation this particle was a pion of momentum between 5.2 and 5.7 GeV/c, taken from a beam and referred to as beam pion.

The remaining entities are: mc^2 the rest mass energy of the electron, I the mean ionization potential for AgBr taken as (501 ± 8) eV according to BARKAS ([10]) and $\delta(\beta)$ a correction coming from the so called density effect.

The quantity $\delta(\beta)$ is defined by ([3f]):

$$\delta(\beta) = \sum_i \left\{ f_i \ln\left(\frac{l_i^2 + l^2}{l_i^2}\right)\right\} - l^2(1-\beta^2)\,, \tag{2}$$

l is found from:

$$\frac{1}{\beta^2} - 1 = \sum_i \frac{f_i}{\bar{\nu}_i^2 + l^2}\,, \tag{3}$$

where

$$\bar{\nu}_i = \frac{\nu_i}{(ne^2/\pi m)^{\frac{1}{2}}}\,, \tag{4}$$

$$l_i = (\bar{\nu}_i^2 + f_i)^{\frac{1}{2}}\,, \tag{5}$$

The denominator of (4) is the plasma frequency ν_p of the medium. The energies $h\nu_i$ are determined in the following manner. A mean ionization value I_m is defined by:

$$I_m = h\nu_p \prod_i l_i^{f_i}\,. \tag{6}$$

As a first approximation for $h\nu_i$ is taken the ionization energy of the i-th shell, for f_i is taken the occupation number of the i-th shell divided by the atomic number Z. This value of I_m is compared with the experimental determined value I from range measurements. In this first approximation these two values are not equal. As a second approximation the frequencies ν_i are all multiplied by a constant factor so as to make I_m and I equal. It is argued by STERNHEIMER that the best values ν_i to be inserted in (2) to (5) are those that make I_m and I equal.

The development of the term $\delta(\beta)$ has been greatly simplified by the analytical approximation given by STERNHEIMER ([3a,3f]). These expressions are accurate up to the order that is met in experimental situations.

According to STERNHEIMER ([3a,3f]), formula (1) can be written:

$$(7a)\quad \frac{1}{\varrho}\left[\frac{\partial E}{\partial x}\right]_{T_0} = \frac{A}{\beta^2}\left[B + 0.69 - \beta^2 - C + \ln T_0\,(\mathrm{MeV}) - a\left(X_1 - {}^{10}\log\frac{\beta}{\sqrt{1-\beta^2}}\right)^m\right],$$

if

$$X_0 < {}^{10}\log\frac{\beta}{\sqrt{1-\beta^2}} < X_1;$$

$$(7b)\quad \frac{1}{\varrho}\left[\frac{\partial E}{\partial x}\right]_{T_0} = \frac{A}{\beta^2}\left[B + 0.69 - \beta^2 - C + \ln T_0\,(\mathrm{MeV})\right],$$

if

$${}^{10}\log\frac{\beta}{\sqrt{1-\beta^2}} > X_1;$$

$$(7c)\quad \frac{1}{\varrho}\left[\frac{\partial E}{\partial x}\right]_{T_0} = \frac{A}{\beta^2}\left[B + 0.69 - \beta^2 + \ln T_0\,(\mathrm{MeV}) + 4.606\left({}^{10}\log\frac{\beta}{\sqrt{1-\beta^2}}\right)\right],$$

if

$${}^{10}\log\frac{\beta}{\sqrt{1-\beta^2}} < X_0\ .$$

The values of the constants are seen from Table I.

TABLE 1. – *Constants for formula* (7).

	A	B	$-C$	a	X_1	m	X_0
$(I/Z)_{AgBr}$ = 9.2 eV	0.066 8	15.1	5.14	0.160	3	3.18	0.10
$(I/Z)_{AgBr}$ = 14.0 eV	0.067 1	14.25	5.95	0.023 5	4	4.03	0.30

Two series of constants are given, relying on two experimental sources. Apart from A, the constant are dimensionless, A in units MeV/gcm^{-2}. A is not of direct interest for blob counting.

We took $(I/Z)_{AgBr} = (12.1 \pm 0.2)$ eV and applied an interpolation between the results of (7) for the upper row constants and the lower row constants. For T_0 several values were inserted as will be clear from the following.

2·2. *Discussion of the formulas.* – The average rate of restricted energy loss discussed in the preceding chapter must be connected to an observable quantity. In our opinion the best suited one for emulsion is the grain density.

Most authors assume a linear relationship between grain density and average rate of restricted energy loss.

In absence of a rigorous treatment we also adopt the linear relationship between grain density and average rate of restricted energy loss. We then have for the grain density g:

$$g = Q \frac{2\pi n_0 e^4}{mc^2\beta^2}\left[\ln \frac{2mc^2 \cdot T_0 \cdot \beta^2}{I^2(1-\beta^2)} - \beta^2 - \delta(\beta)\right]. \tag{8}$$

The factor Q varies with what is commonly called the degree of development. We investigated how far our experimental results come up to conclusions from (8).

We have the feeling that a theoretical justification of the linear relationship is lacking a detailed understanding of the various processes involved. Too many unknown features play a role in the different steps leading to grain formation.

Some calculations have been performed *e.g.* by BETHE ([11]) who computed how the total energy loss is made up between the different modes of excitation. These calculations however cannot be easily extended to the process of grain formation. Recently the problem has also been formulated by BARKAS ([12]) who suggests to introduce a relative efficiency for energy utilization.

Our results in emulsion can be represented by the curve (8), using three constants I, Q and T_0.

One usually gets rid of Q by taking only relative grain densities g^*, *i.e.* the quotient of two grain densities. The question arises how T_0 and I determine the shape of the curve. When $\delta(\beta)$ can be neglected, *i.e.* in the low energy side of the « trough » only the constant $\ln (T_0/I^2)$ matters; when β is exactly 1 the behaviour of $\delta(\beta)$ is such, that I is eliminated from the factor between square brackets of (8), but T_0 is not. In principle one has a method to determine T_0 and I independently from ionization measurements. One has to analyse the low energy side of the « trough » and to measure the plateau value, or in other words the position of the minimum and the depth of the « trough » determine T_0 and I. In practice however g^* from (8) varies not more than a few percent if one chooses pairs T_0 and I from reasonable intervals, T_0 (2 keV $\div$ 100 keV) ([5,8]) and I (377 eV $\div$ 574 eV) ([3d,3f]) for AgBr. On the other hand the experimental accuracy will scarcely be better than one percent and therefore a large spread in the actual values of T_0 and I can be expected.

Measurements of range also yields values of the mean ionization potential I.

([11]) H. BETHE: *Handbuch der Physik Quantentheorie*, (Berlin, 1933), pag. 519.
([12]) W. H. BARKAS: UCRL - 4687.

It was thought of help to fix one of the constants in this way, the more as I is used in computing $\delta(\beta)$. Unfortunately there exists an uncertainty as to the exact value of I.

We took the data of BARKAS [10].

It was decided to compare the results with the average restricted energy loss in AgBr only, a convention usually adopted. We expect that the influence of gelatine upon the experimental results can be neglected at present.

It was found *e.g.* that the experimental points could also be fitted by a curve pertaining to constants from the nuclear emulsion ($I = 331$ eV) and this certainly means an overestimate of the influence of the gelatine.

The constant T_0 appearing from our measurements (100 keV) differs from what was formerly expected ($(2 \div 5)$ keV) [5]. This last energy corresponds to a range of a δ-ray about equal to the silverhalide crystal (*) size. No explanation is given.

3. – Experiment.

3·1. *Technique.* – Details of the experimental conditions at exposure have been published before [13]. The stack (AF stack) consisted of 80 pellicles G-5 emulsion ($20 \times 20 \times 4.8$) cm^3.

Inspection of Fig. 13 of reference [5] shows that great experimental care has to be taken to assure reproducible and physically significant results. We shall now pay some attention to this matter.

The tracks essential to the research reported here consist of:

1) Pions, secondaries of beam pions, stopping in the emulsion, $1.8 < \gamma < 2.5$.

2) Secondary pions from interactions induced by pions of 3), $\gamma \approx 3.5$.

3) Pion tracks $36.8 < \gamma < 41.6$.

4) Electron pairs, $65 < \gamma < 1100$.

This assembly of tracks might not have all advantages one could desire, it certainly has the physical important benefit of being created nearly at one instant (exposure time 7 hours).

Fading is not expected because the stack has been developed directly after

(*) We want to make a distinction between the undeveloped silverhalide crystals with mean diameter 0.30 μm and a visible grain of 0.60 μm. For the first we use the word crystal, for the latter grain.

[13] D. J. HOLTHUIZEN and B. JONGEJANS: *Suppl. Nuovo Cimento*, **14**, 429 (1959).

the Bevatron exposure at Berkeley, at any rate it would equally effect all tracks. All measurements of blob counts were performed with a magnification of 6×100. The identification of the pions of group 3 required careful selection because of the electron pairs, which were nearly parallel to them.

A casual misinterpretation of a muon as pion would not give a momentum change of influence. Electrons quickly loose their energy due to radiation losses in traversing emulsion. The procedure adopted was to follow a presumed beam pion over 4 cm; if the track had not suffered a deviation larger than 1 degree or had formed an obvious interaction of the expected energy, the track was assumed to be a beam pion. The pions of group 2 were identified by the combination of $p\beta$ and b (blob density) measured on them. The measurements did not allow another choice than a pion if we exclude that muons are created in the primary interaction.

The identification of the electrons was performed by tracing them through the emulsion till they could not be followed further due to their excessive scattering and low ionization. The identity of the pions of group 1 was seen from their decay.

Besides blob counting and identifying, energy measurements had to be performed. The energy of the beam pions was known from the conditions at exposure. The calculations were confirmed by relative scattering measurements on a Koristka MS 2 microscope using cell sizes of 500, 1000 and 1500 μm. (See also FOWLER *et al.* [14]), the beam described by them was also used in our experiment). The scattering measurements on the secondary pions (group 2) and the electrons (group 4) are described in detail in Section 3·2. The energy of the secondary pions (group 1) has been determined from range measurements. The range-energy curve of BARKAS *et al.* [15]) has been used, no correction for density was applied. The over-all-density of the emulsion was determined after the exposure and found to be (3.83 ± 0.03) g cm^{-3}. The error results from the determination of the volume of the stack. The uncertainty from this source was thought less than the straggling error. The treatment of the data from this source is outlined in Section 3·3.

The problem of uniform development of different sites in one plate, and of different plates among each other, was faced by mapping the tracks of interest in regions of (1×1) cm^2 per plate. The quotient of the grain density of the tracks and the grain density of beam pions in the same region of one square centimeter is reported. Every blob density of the beam pions used for

([14]) W. B. FOWLER, W. M. POWELL and J. I. SHONLE: *Nuovo Cimento*, **11**, 428 (1959).

([15]) W. H. BARKAS, P. H. BARRETT, P. CUËR, H. HECKMAN, F. M. SMITH and H. K. TICHO: *Nuovo Cimento*, **8**, 185 (1958).

reference was determined with a statistical accuracy coming from 10^4 blobs. The variation found in the different plates is shown in Fig. 1.

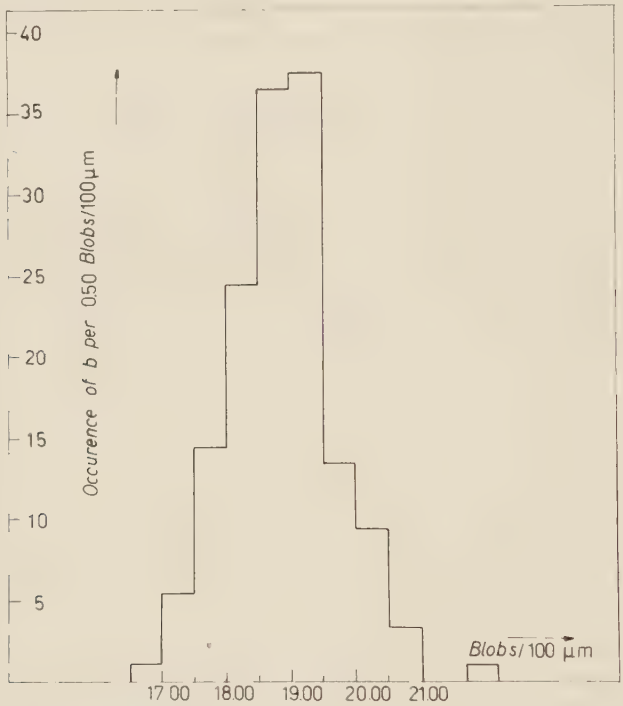

Fig. 1. – Fluctuation of b in AF Stack. Histogram of occurrence of blob density (b=number of blobs per 100 μm) of beam pions in different regions of plates. Each entry pertaining to this experiment was measured with an accuracy coming from 10^4 blobs. Some earlier data of preliminary measurements of b relying on $2 \cdot 10^3$ blobs are also included. The observed spread reflects influence of observer, statistics and regionally unequal development.

3·2. *Energy determination by scattering.* – The usual procedure, selecting two appropriate cell sizes, was followed. Noise elimination was performed; the variation of the scattering constant with cell size was taken into account. To the value of $p\beta c$ obtained in this way an error was assigned following Di Corato *et al.* ([16]). The ratio of D_{2n}/D_{ι} was always larger than 2. The scattering constants, $K(s, \beta)$ slowly varying with cell size and velocity β, are taken from Voyvodic ([17]). To be sure that the absolute values given there apply

([16]) M. Di Corato, B. Locatelli and D. Hirschberg: *Suppl. Nuovo Cimento*, **4**, 448 (1956).

([17]) L. Voyvodic: *Prog. in Cosmic Ray Phys.*, **2**, 219 a.f. (1954).

to our circumstances, an independent check was made. To this end was determined the multiple Coulomb scattering of positive ions stopping in the emulsion. These measurements were performed at a range between 2.5 and 10 cm. These measurements yielded a scattering constant for the specific combination of β and cell size s. With our method two scattering constants belonging to two values of s are needed to obtain $p\beta c$. From standard theory it can be easily derived that

$$(9) \qquad D^2_{\exp}(s_1, \beta) - D^2_{\exp}(s_2, \beta) = \frac{(100\times 2\pi)^2}{(360)^2}\left(\frac{1}{p\beta c}\right)^2 [K^2(s_1, \beta)s_1^3 - K^2(s_2, \beta)s_2^3] ,$$

where $p\beta c$ is in MeV, $D_{\exp}(s_1, \beta)$ the mean of the experimental observed second differences in μm, s is the cell size in units of 100 μm and $K(s_1, \beta)$ is the scattering constant in MeV·degree/$\sqrt{100}$ μm.

As a first approximation we assumed the variation of K being given by the curve of reference [17]. Thus we expressed $K(s_2, \beta)$ in terms of $K(s_1, \beta)$ and have then a one to one correspondence between K and $p\beta c$. The results of the calibration are given in Table II.

TABLE 2. – *Calibration of the scattering constant.*

s →	50 μm	100 μm	200 μm
$\frac{K(s, 0.72)\text{measured}}{K(s, 0.72)\text{theor.}}$	1.033 ± 0.027	1.018 ± 0.037	0.989 ± 0.052

The value of 0.72 for β has to be understood as the mean of the sample of pions. We concluded that our experiment guaranteed the use of the theoretical curves (*).

When the determination of the multiple Coulomb scattering of the electrons was completed they were grouped in samples each containing approximately 10^4 blobs. In this way the horizontal lines in Fig. 4*a* for the electron data $\gamma > 65$ have to be understood. They are not indicative for the error in electron momentum ($\approx 15\%$) but stand for the range of admitted momenta. Theory predicts and experiment shows that this is useful in our case.

The errors in the pion momenta (group 2) come from scattering statistics: 15%. The multiple Coulomb scattering of the pions was determined twice to eliminate gross errors and this was also the case with some of the electrons. Of those electrons of high energy that were traced some centimeters the scattering data were combined to prove their mutual correctness.

(*) Our thanks are due to D. J. HOLTHUIZEN who guided and largely performed the calibration of the scattering constant.

All data were compatible with an absorption length $L = 3$ cm from

$$E_x = E_0 \exp[-x/L], \tag{10}$$

where E_x is the energy of the electron having traversed x cm emulsion and E_0 the initial energy of the electron.

3·3. *The reduction of data depending on the range.* – Two pions were selected for the purpose of having points on the low energy side of the « trough ». Of one the blob density was counted between 15 and 10 cm range, while the other was investigated between 23 and 10 cm range. This last pion crossed the stack diagonally. The ranges were measured along straights of the track. A correction was applied for the non-visibility of the pion track in the surface and bottom layers. This correction was found by comparing steeply dipping black tracks with the pion track. These pion tracks largely determine the value of T_0 as can be seen from Fig. 4*a*.

We used the data of ALEXANDER *et al.* [8] to relate the grain density g_i of the pion with range R_i to the grain density that would correspond to a range of 12.5 cm if 10 cm $< R_i <$ 15 cm or to a range of 19 cm if 15 cm $< R_i <$ $<$ 23 cm.

In short this method amounts to averaging the data taking into account the slightly non-linear relationship between grain density and range in this region. For the error in the range due to straggling we took 2.6 % [18] and assigned this value to the resulting point.

3·4. *Conversion of blobs to grains.* – For the conversion of blobs to grains, measurements of the distribution of gaps in tracks had to be performed. These data were analysed using:

$$P(z) = C \exp[-z/w]\,\mathrm{d}z\,, \tag{11}$$

$P(z)$ the probability of occurrence of a gap with length between z and $z+\mathrm{d}z$, w is the mean gap length and C a normalization constant.

From (11) it is easily seen that

$$w = w_l - l \tag{12}$$

and

$$X_l/X_0 = \left(\frac{l}{w} + 1\right) \exp[-l/w]\,. \tag{13}$$

where w_l is the mean length of the gaps with length larger than l and X_l is the total gap length of gaps larger than l. From the measured gap length distri-

[18] W. H. BARKAS and D. M. YOUNG: UCRL - 2579.

bution of a specific track, w has been deduced in three ways using (11)–(13).

From w we calculated g, the grain density, employing

$$g = \frac{l}{w + \alpha}, \tag{14}$$

where α stands for a quantity directly related to the diameter of the AgBr crystal. For α we took the mean diameter of the crystals 0.30 μm. The same track that was used in gap length measurements yielded a value for b, the blob density, that is related to the other quantities by

$$b = g \exp\left[\frac{-(a - \alpha + \varepsilon_0)}{w}\right], \tag{15}$$

where a is the grain diameter and ε_0 is a correction for the limited resolution of the optical apparatus. This procedure is essentially the same as that of ALEXANDER *et al.* (8). Other calculation schemes have been proposed, their results are however practically equal in the region where they are used here. We want to emphasize that the relative blob density (the quotient of two blob densities) does not coincide with the relative grain density (the quotient of two grain densities) as is seen from the preceding formulas. This fact has not always been taken into account. The difference between the relative blob density and relative grain density was always below 2%. The value for $(a - \alpha + \varepsilon_0)$ was (0.50 ± 0.10) μm, the uncertainty in this constant gave rise to a variation in relative grain density of at most 0.2%.

3·5. *Gradient of development.* – To determine this effect each plate was divided in 9 sections parallel to the glass. Each section was approximately

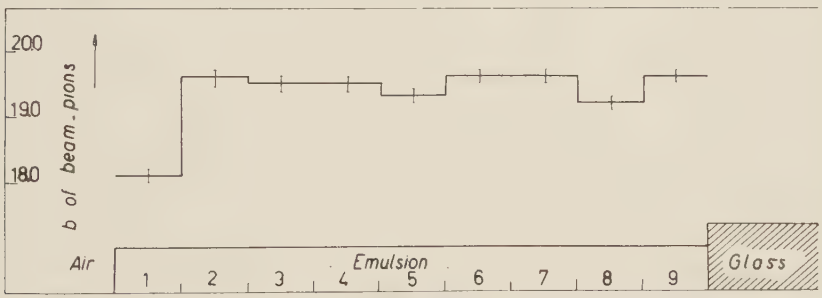

Fig. 2. – Gradient of development in AF Stack. Measured blob density b (number of blobs per 100 μm) as a function of depth in emulsion. The emulsion was divided in 9 equisized layers. No absolute dimensions are given on the abscissa because the thickness of the emulsion varied 5÷10% over long periods of time even though the room where our plates are stored and used was controlled as to humidity and temperature. The vertical lines indicate an estimated error from statistics; in each group between $2 \cdot 10^4$ and $4 \cdot 10^4$ blobs were counted.

30 μm thick. From some plates chosen at random the blob density of the beam pions in every section was determined. The results averaged per section are shown in Fig. 2 and warrant the conclusion of constant development with depth, except for the section closest to air.

The measurements were therefore restricted to the eight levels 2 to 9, that were considered to be uniform. Only in one case this restriction was lifted, but there the measurements were calibrated with beam pions that were also entirely confined to section 1.

3·6. *Prevention of errors.* – With this we have in mind errors that can arise from wrong reading, counting and/or calculating. To minimize effects of this kind all measurements were done twice. During the second run the results of the first run were concealed for the observer.

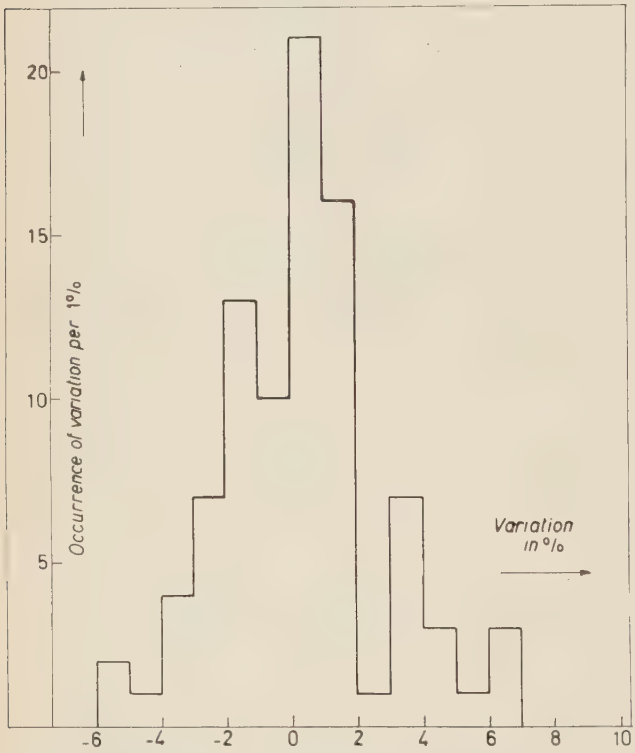

Fig. 3. – Histogram of occurrence of deviations in relative grain density. The difference between the second and first determination is given. The deviation is positive when the second determination yields a higher value than the first one.

For the final results the mean of both runs has been taken, unless one run showed an obvious mistake, in which case it was ignored. This method of repeating allowed us to have an idea about the dependence of the results on different persons performing the measurements and on one person acting at different times. Our findings can be summarized as follows:

a) Direct readings of blob density for one person from time to time can vary by a few percent. In one instance a specific trend of 3% was noticed in the decision of one person.

b) The spread in the relative grain densities when the measurements were done twice is shown in Fig. 3. From this figure one sees that it will be hard to obtain results in grain counting substantially better than 1%. No significant difference was observed for the combinations AA, BB or BA, therefore all pairs of data are given in one figure. It has to be understood that AA means person A redetermining a relative grain count that had been previously done by person A.

3·7. *Assignment of errors.* – The uncertainties in the energy values have been explained already. The error in the relative grain density requires special attention.

It is natural to assume that a statistical error is present. As a first approximation we took for the value of the statistical error (SE) ([19]):

$$SE = \frac{75}{\sqrt{N_b}}\,\% \,. \tag{16}$$

It must be kept in mind that this relation is phenomenological and may require adaption for every special case.

Since for every energy group the grain density of the reference point was measured from more blobs than the grain density of the group of tracks, we can take for N_b the total number of blobs of the tracks determining the point, in order to compute the SE in $\bar{g}^*$.

Secondly, since every point in Fig. 4*a* was made up of measurements on n tracks or part of tracks (n varied between 3 and 16) we were in the position to calculate the spread in the measurements. From the different determination we calculated the standard deviation (SD) from the mean given by:

$$SD = \left(\sum_{i=1}^{n} \frac{(g_i^* - \bar{g}^*)^2}{n(n-1)} \right)^{\frac{1}{2}}. \tag{17}$$

The value of $\bar{g}^*$ is the mean value of g_i^* inserted in Fig. 4*a*, g_i^* is the value as deduced from one of the n determinations. The results are compared in Table III.

As was shown in Section 3·6, the determination of g and consequently of g^* is also influenced by a personal factor. When the measurements were concluded it was decided to attempt a qualitative estimate for the value of the error in g^*.

([19]) M. Teucher: *Ergebnisse der Exakten Naturwissenschaften*, **28**, 407 (1955).

TABLE 3. – *Statistical error and Standard deviation for the various energies.*

$1/(\sqrt{1-\beta^2})-1$	Stat. Error (%)	Stand. Deviat. (%)
0.81	0.5	0.8
1.10	0.6	0.6
2.04	1.0	1.6
3.26	0.8	1.0
40	—	— (*)
65 ÷ 100	0.9	1.1
100 ÷ 150	0.7	0.8
150 ÷ 200	0.9	1.9
200 ÷ 300	0.6	1.0
350 ÷ 500	0.8	1.8
600 ÷ 850	1.0	1.0
850 ÷ 1100	0.6	1.5

(*) Normalization point.
The standard deviation is drawn in fig. 4.

To this end it was assumed that the electron data ($\gamma - 1 > 65$) belonged to one specific value of g^*. From these electrons those measurements were selected that came from electron tracks with a length $0.8 < l < 1.2$ cm, corresponding with a number of blobs $1700 < N_b < 2200$. From this sample we analysed the variance σ_{g^*} (*). Two samples were obtained, one from the first run and one from the second run. Each sample contained 26 units. We assumed the following relation

$$(\sigma_{g^*})^2 = \sigma_{\text{obs}}^2 + \sigma_{\text{stat}}^2 , \tag{18}$$

where σ_{obs} stands for the variance due to the imperfect counting procedure; for σ_{g^*} we obtained 3%, σ_{stat} could be deduced in comparing data from the first and second run, $\sigma_{\text{obs}} = 1.6\%$.

When it is assumed in analogy with (16) $\sigma_{\text{stat}} = (a/\sqrt{N_b})\%$ we find for $a \approx 120$, since the mean of N_b for the sample is 1970. Fluctuations in the values of σ may be expected because only three determinations were available. Nevertheless they may be of help in estimating errors in blob counting on an accuracy level of a few percent. The errors may be summarized as follows: when we count on a track 2000 blobs, and these are compared with another 10^4 blobs of reference tracks, we are still left with a probability $\frac{1}{3}$, of classifying the track of interest with a g^* differing 3% from its true value.

(*) Our thanks are due to Mr. J. TH. RUNNENBURG (Mathematisch Centrum Amsterdam) for discussion on this subject.

4. – Results.

The result of the work described above, after having made the appropriate corrections is best summarized in Fig. 4*a*. The three curves represent formula (8) with T_0 20, 100 and 500 keV respectively. The abscissa is expressed in $(1/\sqrt{1-\beta^2})-1$, the kinetic energy of the traversing particle divided by its restmass energy. All curves are normalized at the point of the beam pions. This fact clearly brings out the variations in the different curves. To obtain an objective choice for the best value of T_0, the method of the least squares was applied. The best fit yielded $T_0 = 100$ keV.

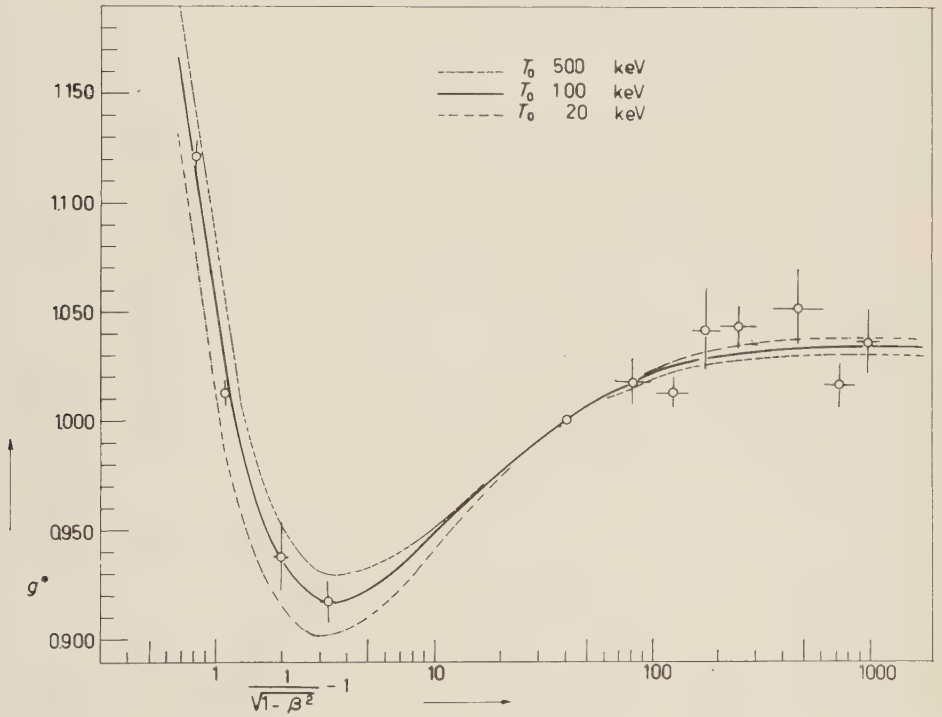

Fig. 4*a*. – Relative grain density versus kinetic energy divided by rest mass energy. The errors in energy loss are standard deviations taken from Table II. The horizontal bars are explained in the text. Three curves are drawn to show variation of theory with the parameter T_0. All curves are normalized at the calibration point of the beam pions.

In order to agree with the convention of ALEXANDER *et al.* [8], the best curve is redrawn in Fig. 4*b*, the lowest value of the « trough » being normalized to 1.

The variation of

$$\sum [g^*_{\text{exp}} - g^*_{\text{theor}\,T_0}(I = 501 \text{ eV})]^2 , \tag{19}$$

with T_0 can be seen in Fig. 5. The sum is meant over the experimental points.

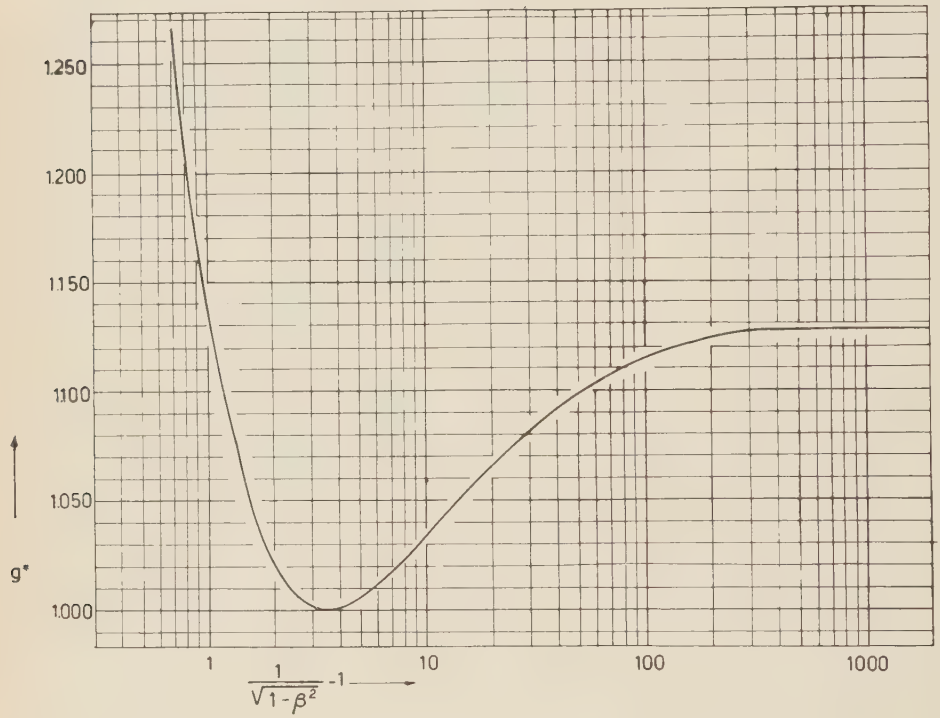

Fig. 4*b*. – Relative grain density versus kinetic energy divided by rest mass energy. Only the curve best fitting our experimental results is shown. It represents formula (8) with $I = (501 \pm 8)$ eV and $T = 100$ keV. In order to join previous publications the curve is normalized at 1.000 for the minimum value.

The value $T = 100$ keV is not critical, we have the feeling that 40 keV would be too low, 200 keV too high. Beside the theoretical curves for $I_{\text{AgBr}} = 501$ eV, which we prefer to others, we also drew curves for $I_{\text{AgBr}} = 377$ eV ($I/Z = 9.2$ eV) ([3a]) and $I_{\text{AgBr}} = 574$ eV ($I/Z = 14.0$ eV) ([3f]). From these curves we also made a least squares adjustment to our experimental points. The relevant values of (19) are also shown in Fig. 5. It is easily understood from inspection of this figure, why widely varying values for T_0 are found in

the literature. The discussion of energy loss data does not depend critically upon either T_0 or I. A maladjustment of one parameter can be partly compensated by the other.

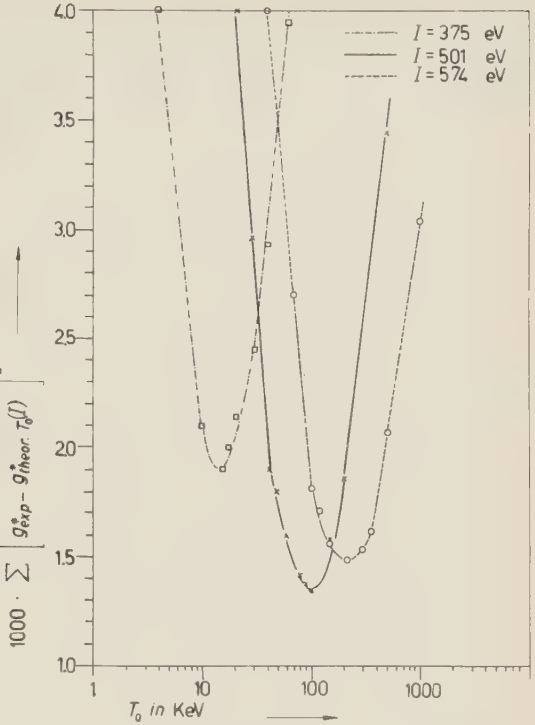

Fig. 5. – The value of $\sum [g^*_{\text{exp}} - g^*_{\text{th. or } T_0}(I)]^2$ for three values of I and as function of T_0. The sum is extended over all measured points. The ordinate is dimensionless since g^* is a number.

4·1. *Discussion of the results.* – The agreement between theory and experiment is reasonable. The value of $T = 100$ keV differs somewhat from those of ALEXANDER *et al.* [5] and other authors [20,21], possible reasons have been mentioned.

It seems that a remarkable agreement exists about the ratio plateau to minimum; we find

$$\frac{g_{\text{plateau}}}{g_{\text{minimum}}} = 1.129 \pm 0.010 .$$

This value can be compared *e.g.* with 1.133 ± 0.008 of ALEXANDER *et al.* [5] and 1.14 ± 0.03 of STILLER *et al.* [20].

FLEMING *et al.* [22] find for $b_{\text{plateau}}/b_{\text{minimum}} = 1.13$ which we interpret as $g_{\text{plateau}}/g_{\text{minimum}} = 1.14$ with an error estimated as 1%. From MICHAELIS *et al.* [23] we deduced $g_{\text{plateau}}/g_{\text{minimum}} = 1.097 \pm 0.010$ making a correction from blobs to

[20] B. STILLER and M. M. SHAPIRO: *Phys. Rev.*, **92**, 735 (1953).
[21] L. JAUNEAU and J. TREMBLEY: *Suppl. Nuovo Cimento*, **1**, 230 (1955).
[22] J. R. FLEMING and J. J. LORD: *Phys. Rev.*, **92**, 511 (1953).
[23] R. P. MICHAELIS and C. E. VIOLET: *Phys. Rev.*, **90**, 723 (1953).

grains. Former measurements gave somewhat lower values for the plateau/minimum ratio. To base the discussion on a same footing we compare in Table IV the different values of T_0 which we deduced from $g_{\text{plateau}}/g_{\text{minimum}}$ and relying on $I = 501$ eV.

TABLE 4. – *Comparison of some values of T_0 as explained in the text.*

Author	$g_{\text{pl}}/g_{\text{min}}$	T_0(keV)
ALEXANDER *et al* [8]	1.133 ± 0.008	70
STILLER *et al* [20]	1.14 ± 0.03	40
FLEMING *et al* [22]	1.14 ± 0.01	40
MICHAELIS *et al* [23]	1.097 ± 0.010	500
Present work	1.128 ± 0.010	100

Of course it has to be kept in mind that this ratio reflects only one aspect of the « trough » and that a detailed analysis requires more data.

As a further conclusion from our work we want to mention the persisting rise of energy loss for γ higher than 40. This is an essential feature of the theory taking into account several dispersion frequencies. The assignment of only one characteristic frequency to the electrons of the medium would give a quicker rise to the plateau value.

It is hoped that the curve given in Fig. 4*b* will be of future use. A word of warning may be added. The experimental precautions needed to observe the small differences of energy loss reported in G-5 emulsion may be very time consuming.

* * *

This work is part of the research program of the Institution for Fundamental Research of Matter (F.O.M.) financially supported by the Netherlands Organization for Pure Scientific Research (Z.W.O.). The author is indebted to Dr. E. J. LOFGREN and the Bevatron crew for the facilities provided at the Bevatron.

It is a pleasure to thank Prof. Dr. G. W. RATHENAU for his constant interest and encouragement and the creation of a beneficial atmosphere. Thanks are due to Mr. A. G. TENNER and Mr. F. ARTMANN for helpful criticism and to Mr. D. J. HOLTHUIZEN with whom the salient features of this work were discussed in detail.

The work heavily leaned on the basic measurements performed by Mrs. A. REUS and Mrs. E. G. KOEK-TIPPMANN. The collaboration of the other scan-

ners of the Amsterdam Emulsion Group is appreciated. Mr. T. J. VAN DER LINDE performed the greater part of the computations, the calculational aid of Mr. A. D. SASTRADIWIRIA is gratefully acknowledged.

RIASSUNTO (*)

Si è determinata la densità dei grani nella emulsione nucleare come funzione del valore del $(\gamma - 1)$ della particella che genera la traccia. Si sono presi in considerazione valori del parametro $(\gamma - 1)$ fra 0.8 e 10^3. Il numero di blobs per unità di lunghezza è stato determinato direttamente. Si è eseguito il passaggio dalla densità dei blobs alla densità dei grani. Si è avuto cura di confrontare tutte le determinazioni fra di loro per mezzo di una scala costante di riferimento formata dai pioni di impulso compreso fra 5.2 e 5.7 GeV/c. I risultati concordano con la teoria formulata da Sternheimer. Nel presente lavoro per il potenziale di ionizzazione dell'AgBr si è usato il valore (501 ± 8) eV. Questo valore è stato preso dai lavori di BARKAS. L'energia di taglio determinata in conseguenza è 100 keV. Si dimostra che i risultati non risentono molto delle variazioni di questa ultima quantità.

(*) *Traduzione a cura della Redazione.*

The Energy Spectrum of Nuclei with Charge $Z \geqslant 6$ in the Primary Cosmic Radiation.

S. Biswas (*), P. J. Lavakare (**), K. A. Neelakantan and P. G. Shukla

Tata Institute of Fundamental Research - Bombay

(ricevuto il 4 Gennaio 1960)

Summary. — The « knock-on electron » technique has been employed to determine the energy spectrum of nuclei with charge $Z \geqslant 6$ in the primary cosmic radiation. In this technique the energy per nucleon of a heavy primary cosmic ray nucleus is determined by measuring the angles of emission and the energies of electrons which the nucleus « knocks on » in elastic collisions along its path in traversing nuclear emulsion. Since the energies of the knock-on electrons are relatively small (< 100 MeV in this experiment), they can be measured with precision by the method of multiple Coulomb scattering. The conditions for reliable estimation of primary energy have been determined and the reliability of the method verified by comparison with results obtained by other methods. The charges and energies of the particles have been determined in the following two ways: (i) for particles which are arrested in the emulsion, from measurements of range and δ-ray density; (ii) for particles which do not stop, from measurements of δ-ray density and of the energies and the angles of emission of the fast knock-on electrons; in the few cases where the particle slowed down in traversing the stack, the variation of δ-ray density along the track was determined. Measurements were made on 291 tracks obtained in a stack flown from Iowa, ($\lambda = 53°$ N), at 113 000 *ft.* for four hours on March 13, 1956. 206 of these tracks were due to particles with charge $Z \geqslant 6$. The exponent of the integral energy spectrum of the medium ($6 \leqslant Z \leqslant 9$) group of nuclei has been obtained as 1.65 ± 0.27 in the energy range 0.23 to 9 GeV/nucleon and that of the heavy ($Z \geqslant 10$) group of nuclei as 1.82 ± 0.59 in the energy interval 0.41 to 9 GeV/nucleon. The exponent for the S-group of nuclei ($Z \geqslant 6$) is then 1.78 ± 0.24. The geomagnetic cut-off energy at $\lambda = 54.5°$ N has been estimated to be 230 MeV/nucleon. The values of the flux of M and H-nuclei were found to be 10.7 ± 1.0 and 5.3 ± 0.7 particles/m² s sr, respectively (on March 13, 1956). A comparison of these values with those obtained in other experiments shows that a Forbush type of decrease had taken place in the intensity of the heavy nuclei, similar to that observed by McDonald in the α-particle flux on the same flight; neutron monitors on ground had also recorded a Forbush decrease at the same time.

(*) Now at the University of Minnesota, U.S.A.

(**) Now at the University of Rochester, U.S.A.

1. – Introduction.

In this paper we describe an experiment which we have carried out in this laboratory to determine the energy spectra of the medium ($6 \leqslant Z \leqslant 9$) and heavy ($Z \geqslant 10$) groups of nuclei of the primary cosmic radiation. For this we have used a technique different from those hitherto employed in this type of work. We have determined the energies of the heavy primary nuclei by the «knock-on electron» method, which may be described briefly in the following terms. In traversing nuclear emulsions, these nuclei make elastic collisions with the electrons of the medium. The energies of these knock-on electrons are relatively small and may, therefore, be determined with precision by the method of multiple Coulomb scattering. The energy per nucleon of the primary particle can then be evaluated from a knowledge of the angles of emission and the energies of the knock-on electrons. The knock-on electron method has been employed in the past for other types of experiments, for example, to determine the masses of mesons photographed in Wilson chambers (LEPRINCE-RINGUET *et al.* [1,2]), to measure the cross-section for the production of fast knock-on electrons by μ-mesons in nuclear emulsions (KANNANGARA *et al.* [3]) and in attempts to determine the masses of minimum ionizing particles in nuclear emulsions (CAMERINI and FOWLER [4] and DE MARCO *et al* [5]).

In this investigation, we have established the conditions under which the primary energy can be estimated reliably by this technique. It is shown that the estimate of primary energy determined under these conditions agrees well with those obtained by other established methods. The frequency of knock-on electrons for primary particles of charge $Z < 2$ is too small to permit systematic measurements of energies, whereas for primary particles of charge $Z \geqslant 5$ the frequency if sufficient for systematic measurements. Therefore, the method is of particular value in determinations of the energies, and thereby the energy spectra, of heavy nuclei with charge $Z \geqslant 6$ in the primary cosmic radiation.

The energy spectra of these nuclei, ($Z \geqslant 6$), have been measured by the nuclear emulsion technique alone. The methods used so far are based on measurements of ionization-residual range, ionization-multiple scattering and the study of nuclear interactions which lead to the breakup of the primary nuclei into α-particle fragments. Measurements of ionization and of range can be used to determine the charge and energy of the particle accurately.

---

(1) L. LEPRINCE-RINGUET, S. GORODETZKY, E. NAGEOTTE and R. RICHARD-FOY: *Phys. Rev.*, **59**, 460 (1941); *Journ. Phys. et Rad.*, **2**, 63 (1941).

(2) L. LEPRINCE-RINGUET and M. LHÉRITIER: *Compt. Rend.*, **219**, 618 (1944); *Journ. Phys. et Rad.*, **7**, 65 (1946).

(3) M. L. T. KANANGARA and M. ZIVKOVIC: *Phil. Mag.*, **44**, 797 (1953).

(4) U. CAMERINI and P. H. FOWLER: unpublished.

(5) A. DE MARCO, A. MILONE and M. REINHARZ: *Nuovo Cimento*, **1**, 1041 (1955).

However, this is applicable only over a small region in the low energy end of the spectrum (KAPLON *et al.* [6]). For measurements of multiple Coulomb scattering, very flat tracks are necessary to overcome the effect of spurious scattering (BISWAS *et al.* [7,8]). This technique has been used by FOWLER and WADDINGTON [9] for α-particles in the energy range (1.8 ÷ 3.0) GeV/nucleon. The flux of nuclei of $Z > 6$ is smaller by a factor of about ten and, therefore, emulsion stacks used so far have been usually too small to accumulate enough tracks of sufficient length for the determination of the energy spectrum by this technique. When a heavy nucleus breaks up into three or more α-particles (and other fragments), a measurement of the average opening angle of the α-particles, or of the relative scattering between the α-particles, provides a method for estimating the primary energy [6]. This method is, in general, applicable only to nuclei of energy ≥ 3 GeV/nucleon. Also, these measurements can be made only on a small fraction of the primary particles since the process is rather infrequent. (About 25% of the interactions of the heavy ($Z \geq 10$) group of nuclei and about 5% of that of the medium ($6 \leq Z \leq 9$) group of nuclei lead to three or more fragments of $Z \geq 2$).

An indirect method has also been used to determine the energy spectra of primary heavy nuclei. In this, the magnetic field of the earth, which causes different cut-off rigidities to exist at different latitudes, has been used as an energy selector. In order to determine the energy spectra from measurements of the vertical flux at different latitudes, vertical cut-off energies given by the dipole approximation of the earth's magnetic field have been used. Since it has been shown [10-13] that the dipole approximation is seriously in error, the above method, as employed, is fraught with difficulties. Moreover, the variation of the flux of α-particles and heavy nuclei with solar activity [14-17] introduces additional difficulties.

[6] M. F. KAPLON, B. PETERS, H. L. REYNOLDS and D. M. RITSON: *Phys. Rev.*, **85**, 295 (1952).

[7] S. BISWAS, B. PETERS and RAMA: *Proc. Ind. Acad. Sci.*, A **41**, 154 (1955).

[8] S. BISWAS, N. DURGA PRASAD and S. MITRA: *Proc. Ind. Acad. Sci.*, A **46**, 167 (1957).

[9] P. H. FOWLER and C. J. WADDINGTON: *Phil. Mag.*, **1**, 637 (1956).

[10] J. A. SIMPSON, K. B. FENTON, J. KATZMAN and D. C. ROSE: *Phys. Rev.*, **102**, 1648 (1956).

[11] C. J. WADDINGTON: *Nuovo Cimento*, **3**, 930 (1956).

[12] P. ROTHWELL: *Phil. Mag.*, **3**, 961 (1958).

[13] P. ROTHWELL and J. J. QUENBY: *Suppl. Nuovo Cimento*, **8**, 249 (1958).

[14] F. B. MCDONALD: *Phys. Rev.*, **107**, 1386 (1957).

[15] P. S. FREIER, E. P. NEY and C. J. WADDINGTON: *Phys. Rev.*, **114**, 365 (1959).

[16] P. S. FREIER, E. P. NEY and C. J. WADDINGTON: *Phys. Rev.*, **113**, 921 (1959).

[17] S. BISWAS, P. J. LAVAKARE, K. A. NEELAKANTAN and P. G. SHUKLA: *Phys. Rev.* (in course of publication).

At the time this experiment was started last year, there was no direct determination of the energy spectrum of the M-group and there were only two experiments each on the energy spectra of the H and the S-group ([6,18,19]). Furthermore, there were considerations put forward by SINGER ([20]), on the basis of flux measurements at different geomagnetic latitudes, that the different components of the primary cosmic radiation may have different energy spectra. This obviously has an important bearing on the question of the origin and propagation of cosmic radiation. It was, therefore, considered worth-while to make a direct measurement of the energy spectra of the M and H-groups of nuclei using the same method in both cases. We used the ionization-range method for slow particles and the knock-on electron method for the faster ones. From these measurements we have obtained the energy spectra of M-nuclei and H-nuclei in the energy range 0.23 to 9 GeV/nucleon. This range of energy is considerably greater than any over which measurements have been reported hitherto; the spectrum starts right at the geomagnetic cut-off value and there is a factor of 40 between the lowest and highest energy points.

2. – Determination of primary energy by the « knock-on electron » method.

2·1. *Method.* – The energy per nucleon of the primary heavy nucleus can be determined from measurements of the angle of emission and the energy of the knock-on electron by using the relation:

$$\gamma_e - 1 = \frac{2(\gamma_p^2 - 1)}{1 + \gamma_p^2 \operatorname{tg}^2 \omega}, \tag{1}$$

or

$$\gamma_p = \left[\frac{\gamma_e + 1}{2 - (\gamma_e - 1)\operatorname{tg}^2 \omega}\right]^{\frac{1}{2}},$$

where γ_p = *total* energy per nucleon of the primary nucleus *in units of nucleon rest mass*, γ_e = *total* energy of the knock-on electron *in units of electron rest mass* and ω = angle of emission of the knock-on electron with respect to the direction of the primary particle. (The rest mass of the electron is neglected compared to that of the nucleon in the above.)

([18]) C. J. WADDINGTON: *Nuovo Cimento*, **5**, 737 (1957).

([19]) R. CESTER, A. DEBENEDETTI, C. M. GARELLI, B. QUASSIATI, L. TALLONE and M. VIGONE: *Nuovo Cimento*, **7**, 371 (1958).

([20]) S. F. SINGER: *Progress in Elementary Particles and Cosmic Ray Physics*, vol. **4** (Amsterdam, 1958).

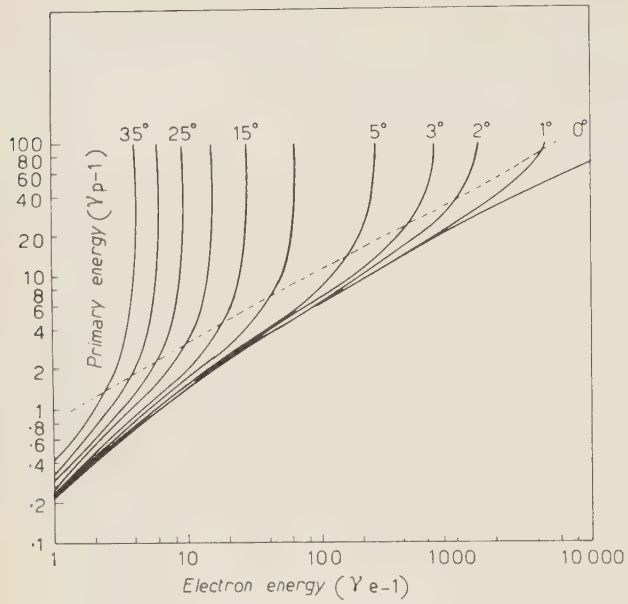

Fig. 1. – Relation between the energy of the primary particle, $(\gamma_p - 1)$, and the energy of the knock-on electron, $(\gamma_e - 1)$, for various angles of emission (ω). The dotted line represents the limit of significant measurement of the primary energy as considered by us. $(\gamma_p - 1)$ = kinetic energy per nucleon of the primary nucleus in units of nucleon rest mass. $(\gamma_e - 1)$ = kinetic energy of the electron in units of electron rest mass.

Relation (1) is shown in Fig. 1, on a log-log plot. It may be seen that, for a given angle ω, the energy of the electron increases almost linearly with increase in the primary energy up to a certain point; beyond this its energy is more or less insensitive to the primary energy. Thus, for a given angle ω, measurements of the energy of the electron can yield a reliable estimate of the primary energy up to a certain point; beyond this, a small error in the determination of the energy of the electron will cause a very large error in the estimate of the primary energy so as to render the information almost useless. The limit of significant measurement as considered by us is shown by the dotted line in Fig. 1, which corresponds to a slope of 1.5. For reliable estimation of the primary energy the measured value of the energy of the electron should lie below the dotted line. Clearly, for each value of the primary energy there is a « maximum useful » angle. A plot of the « maximum useful » angle (ω_{max}) of the knock-electron *vs.* primary energy is shown in Fig. 2.

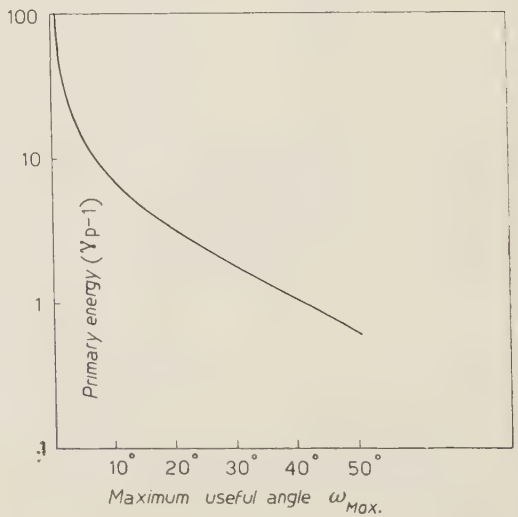

Fig. 2. – The maximum useful angle of the knock-on electron (ω_{max}) as a function of primary energy, $(\gamma_p - 1)$.

2·2. *Calculation of error on the primary energy.* – The error on the primary energy, γ_p, can be obtained from the relation

$$(2) \qquad \frac{\delta\gamma_p}{\gamma_p} = \sqrt{f_1^2\left(\frac{\delta\gamma_e}{\gamma_e}\right)^2 + f_2^2\left(\frac{\delta\omega}{\omega}\right)^2},$$

where

$$f_1 = \left(\frac{\partial\gamma_p}{\partial\gamma_e}\right)\frac{\gamma_e}{\gamma_p} \quad \text{and} \quad f_2 = \left(\frac{\partial\gamma_p}{\partial\omega}\right)\frac{\omega}{\gamma_p}.$$

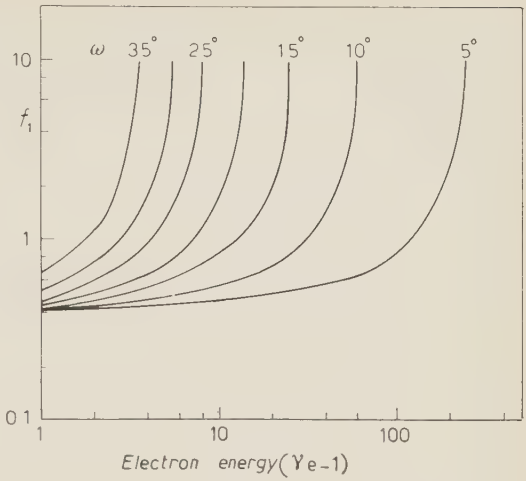

Fig. 3*a*. – The function f_1 used for the calculation of errors on the primary energy, plotted against electron energy, $(\gamma_e - 1)$, for different values of the angle ω.

The functions f_1 and f_2 are plotted against $(\gamma_e - 1)$ for different values of the angle ω in Figs. 3*a* and 3*b*; measurements of the energy of the electron and its angle of emission were made under optimum conditions such that the error on each is minimum. These conditions, as well as the details concerning f_1 and f_2 and the calculation of error on the primary energy, are given in Appendix I.

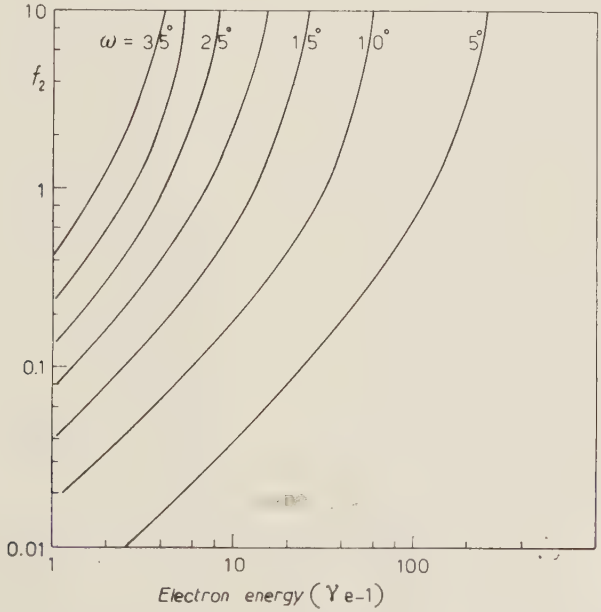

Fig. 3*b*. – The function f_2 used for the calculation of errors on the primary energy, plotted against electron energy, $(\gamma_e - 1)$, for different values of the angle ω.

2·3. *Frequency of useful knock-on electrons.* – The number of electrons of kinetic energy between W and $W+\mathrm{d}W$, which are elastically scattered by a primary nucleus of charge Ze and velocity βc, is given by the transcribed Mott formula ([21]):

$$(3) \qquad \mathrm{d}N(W\,\mathrm{d}W) = \frac{2\pi n Z^2 e^4}{m_e^2 \beta^2 c^2} \cdot \frac{\mathrm{d}W}{W^2} \cdot \left[1 - \frac{1-\beta^2}{2}\left(\frac{W}{m_e c^2}\right) + \frac{Z\pi\beta}{137}\left(\frac{1}{2\beta^2}\cdot\frac{W}{m_e c^2}\right)^{\frac{1}{2}}\left\{1 - \frac{1}{2}\,\frac{1-\beta^2}{\beta^2}\left(\frac{W}{m_e c^2}\right)\right\}\right],$$

where n is the number of electrons per cm³ of the medium.

The number of knock-on electrons with energy between $(\gamma_e - 1)_{\min} m_e c^2$ and $(\gamma_e - 1)_{\max} m_e c^2$ is obtained from the above relation. (For a given primary energy γ_p, the energies of the electrons emitted at the maximum useful angle $\omega_{\max}$ (as given in Fig. 2) and at an angle $\omega = 0$ are $(\gamma_e - 1)_{\min}$ and $(\gamma_e - 1)_{\max}$ respectively.) The first term of (3) gives:

$$(4) \qquad N = \frac{KZ^2}{\beta^2} \cdot \frac{\frac{1}{2}\,\mathrm{tg}^2\,\omega_{\max}}{1 - 1/\gamma_p^2},$$

where the value of the constant K is 0.521/cm for Ilford G-5 emulsion. Higher order terms are important for primary energies above 1 GeV/nucleon and have been taken into account. In Fig. 4 is plotted the frequency of useful knock-on electrons with angles of emission up to $\omega_{\max}$, as a function of the primary energy for various nuclei; these values have been calculated using equation (3).

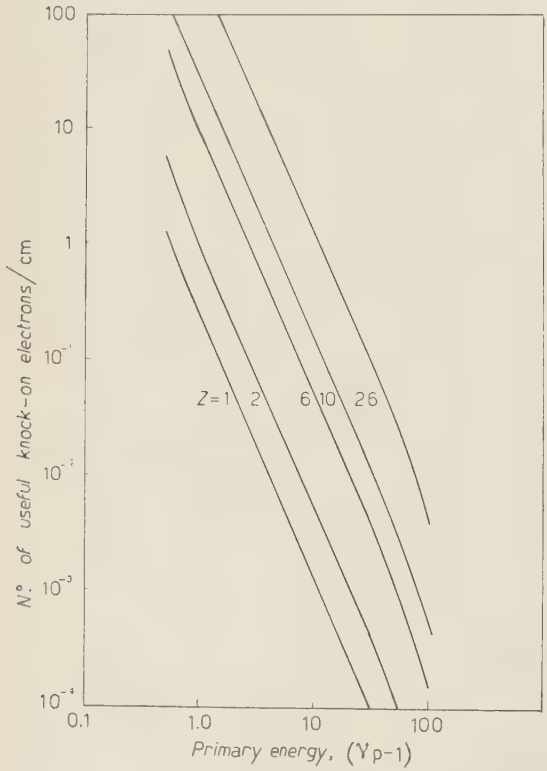

Fig. 4. – The frequency of useful knock-on electrons as a function of the primary energy for various nuclei.

The frequency of knock-on electrons increases rapidly with

([21]) H. L. Bradt and B. Peters: *Phys. Rev.*, **74**, 1828 (1948).

increasing charge of the primary nuclei. In a stack where an average track length of (10 ÷ 15) cm is available, the frequency is adequate for energy measurements to be carried out on almost all particles of charge $Z \geq 6$, which do not interact and which are not brought to rest. The upper limit for measurement of energy is pushed up with increasing average track length. However, since the interaction mean free paths in emulsion for M-nuclei and H-nuclei are ~ 13 cm and ~ 10 cm respectively, a stack in which the average track length is greater than these does not help much in pushing up the upper limit.

It may be noted that Fig. 4 showd the *theoretical* number of useful knock-on electrons. The actual number will be less because some of the knock-on electrons will not be suitable for measurements owing to unfavourable geometry.

2·4. *Verification of the results of the knock-on electron method.* – The reliability of the knock-on electron method for determination of the primary energy has been verified as follows:

a) Determination of the energy of a primary particle from several knock-on electrons which it gives rise to: A few tracks with sufficiently long lengths in the stack, and due to nuclei with charge $Z \geq 6$, were scanned for several knock-on electrons and the primary energy was calculated from measurements on each of these. Some examples are shown in Table I(*a*). It can be seen that the various determinations agree among

TABLE I *a*. – *Comparison of the various estimates of primary energy obtained from measurements on several knock-on electrons.*

Track no.	Angle of emission of the electron (ω^0)	Energy of the electron ($\gamma_e - 1$)	Primary energy γ_p
H 29	5.9 ±0.9	108.5 ±8.8	11.5 ±2.8
	6.6 ±0.6	84.0 ±6.9	9.9 ±1.5
	9.0 ±0.3	58.3 ±8.6	10.6 ±1.1
	16.7 ±0.8	20.3 ±2.0	11.3 ±4.4
H 17	7.9 ±0.5	39.0 ±2.3	5.7 ±0.4
	10.5 ±0.4	32.5 ±2.2	6.3 ±0.6
	15.0 ±0.5	22.7 ±2.9	8.2 ±3.0
	22.4 ±1.9	12.0 ±1.3	> 6
H 921	17.1 ±7.2	3.75 ±0.75	1.87 ±0.28
	20.5 ±4.9	1.78 ±0.36	1.47 ±0.15
	26.3 ±2.7	2.20 ±0.57	1.70 ±0.30
	27.1 ±2.7	2.40 ±0.46	1.79 ±0.27

$\gamma_e - 1$: kinetic energy of the electron in units of electron rest mass.
γ_p: total energy per nucleon of the primary nucleus in units of nucleon rest mass.

themselves within the errors of measurements. It can also be seen that, on the average, the error increases with the increase in the angle of emission of the knock-on electron.

b) Comparison of the estimates of primary energy as obtained from knock-on electrons and from multiple scattering measurements: We selected all tracks of length $\geqslant 2$ cm per emulsion, for which the primary energy as determined from at least two suitable knock-on electrons was less than ~ 1 GeV/nucleon; such a selection was made to minimize the effects of spurious scattering present in nuclear emulsions ([7,8]). Direct scattering measurements were made on these tracks using cell sizes 0.5, 1 or 2 mm so that the ratio of signal to spurious scattering was more than ~ 2. The value of the scattering constant used was that calculated by FITCHEL and FRIEDLANDER ([22]) for heavy nuclei. The results shown in Table I(*b*) indicate good agreement between the two methods.

TBLE I*b*. – *Comparison of the estimates of primary energy obtained from knock-on electrons and direct scattering measurements.*

Track no.	Primary energy, γ_p		
	From knock-on electrons		From direct scattering measurements
	individual values	weighted mean	
H 242	1.95 ± 0.35 2.53 ± 0.50	2.14 ± 0.27	1.88 ± 0.13
H 735	1.39 ± 0.11 1.39 ± 0.11	1.39 ± 0.08	1.41 ± 0.05
H 785	1.76 ± 0.29 1.53 ± 0.18	1.68 ± 0.15	1.60 ± 0.05
H 894	1.80 ± 0.26 1.63 ± 0.17	1.69 ± 0.14	1.79 ± 0.12
H 909	3.22 ± 1.23 1.75 ± 0.20	1.78 ± 0.20	1.97 ± 0.14

c) Comparison of the estimates of the energies of protons of ~ 3 GeV as obtained from knock-on electrons and from relative scattering measurements: We obtained knock-on electrons emit-

([22]) C. FICHTEL and M. W. FRIEDLANDER: *Nuovo Cimento*, **10**, 1032 (1958).

ted at angles $\leqslant 19°$ on tracks of ~ 3 GeV protons recorded in an emulsion exposed in the Brookhaven cosmotron beam. The energies of the protons as measured by the knock-on electron method and by relative scattering ([8]) are shown in Table I(*c*). It is seen that there is good agreement between the results obtained by the two methods.

TABLE I *c*. – *Comparison of the estimates of the energy of protons (of* ~ 3 GeV) *from measurements on knock-on electrons and from relative scattering measurements.*

Knock-on electron no.	Angle of emission of the electron (ω^0)	Energy of the electron $\gamma_e - 1$	Primary energy, γ_p		
			from knock-on electrons		from relative scattering
			individual values	weighted mean	
1	6.0 ± 1.0	16.8 ± 4.2	3.23 ± 0.43		
2	14.2 ± 0.8	10.9 ± 1.8	3.26 ± 0.46	3.21 ± 0.26	3.53 ± 0.21
3	16.6 ± 1.4	9.4 ± 1.8	3.12 ± 0.61		
4	19.2 ± 1.9	8.0 ± 2.0	3.10 ± 0.82		

These results indicate that a reliable determination of the primary energy can be made in the energy region 0.3 to 10 GeV/nucleon by the knock-on electron method when electrons which satisfy the conditions given in Sect. 2·1 are selected.

2·5. *Sources of uncertainty.* – The sources of uncertainty which may lead to wrong values of the primary energy are enumerated below:

a) Large angle elastic scattering of the electron within ~ 10 μm of its origin.

b) Large loss of energy by the electron in bremsstrahlung processes within ~ 10 μm of its origin.

c) Accidental background electron originating from the track.

d) Energy loss of the electron by ionization.

e) Scattering of the electron in the same atom from which it originates.

f) Change in the direction of the electron due to its orbital motion in the atom.

Most of these have been discussed earlier by DE MARCO *et al.* ([5]).

The effect of uncertainties arising from *d*), *e*) and *f*) can be shown to be very small and, hence, the uncertainty in the results mainly arises from *a*), *b*)

and *c*). In the present experiment the uncertainty due to *a*), *b*) and *c*) taken together has been evaluated from a statistical analysis of the measurements on about 500 knock-on electrons and is given in Appendix II. It was found that $\sim 10\%$ of the knock-on electrons gave wrong values of the primary energy. This uncertainty was overcome by measuring two or more knock-on electrons on each heavy primary track.

3. – Experimental procedure for measurements on heavy primary tracks.

3·1. *The emulsion stack and exposure.* – An emulsion stack consisting of 30 Ilford G-5 stripped emulsions, each of dimensions 15 cm × 15 cm × 0.06 cm was flown from Iowa (geomagnetic latitude $\lambda = 53°$ N) on 13th March, 1956; it floated at an altitude of 113 000 ft (6.1 g/cm² of residual air) for 4 hours and 40 minutes. The emulsion surfaces were flown vertical and the packing used was mainly bakelite of thickness 0.3 g/cm². The flight curve is shown in Fig. 5.

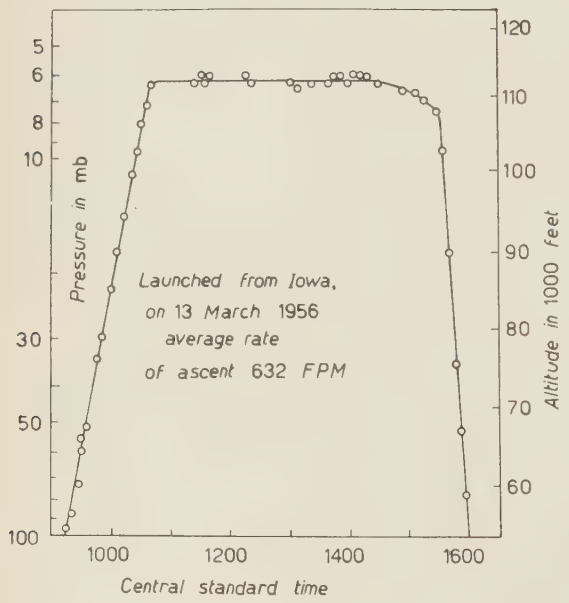

Fig. 5. – Time-altitude curve for the balloon flight.

3·2. *Procedure of selection of tracks.* – The two outside emulsions were scanned for heavy primary tracks which satisfied the following criteria:

a) Ionization greater than that of a relativistic Be nucleus.

b) Projected track lenght > 1.8 mm/plate.

c) Zenith angle $< 60°$.

Tracks satisfying these conditions were followed through successive emulsions to see whether the particles producing them came to rest, interacted or passed out of the stack. (1 cm from each of the vertical processed edges and 5 cm from the lower horizontal processed edge were left out of the scanning area.)

Only tracks satisfying the following criteria were selected for charge and energy determinations:

a') δ-ray density in the first emulsion $\geqslant 2.8/100$ μm. (Our values of δ-ray density for tracks of relativistic boron and carbon nuclei are 2.4 and 3.2/100 μm, respectively.)

b') Projected length in the first emulsion $\geqslant 2$ mm.

c') Zenith angle $\leqslant 45°$.

d') Track length before interaction, if the particle interacted in flight, $\geqslant 4$ cm.

e') Length in the stack $\geqslant 4$ cm, if the particle passed out of the stack.

f') Length in the stack $\geqslant 5$ mm, if the particle came to rest.

In an area of 223.4 cm², 280 tracks were found to satisfy the above selection criteria.

Some additional area was scanned for nuclei of $Z \geqslant 10$. The scanning criteria were the same as before except that the ionization in the first emulsion had to be equal to or greater than that of a relativistic fluorine nucleus and the projected length in the first plate $\geqslant 1.5$ mm. Out of 21 tracks obtained, 11 were found to be due to nuclei of $Z \geqslant 10$. Only these 11 tracks were included in the analysis.

The scanning efficiency was determined by a second observer who rescanned 135 cm² of the same area using the same conditions, *viz.* *a*), *b*) and *c*); the scanning efficiency for tracks satisfying a') b') and c') was found to be 95%.

3·3. *Measurements of charge and of energy.* – Charge and energy determinations were carried out by one of the following methods: *a*) for particles which were brought to rest in the emulsion, measurements were made of range and of δ-ray density; *b*) for particles which did not stop in the stack but showed a large visible change in ionization, the variation of δ-ray density along the track was measured; *c*) for the remaining tracks, the δ-ray density was measured and the energy per nucleon determined by the knock-on electron method.

All δ-ray density measurements were made by one observer. For tracks with δ-ray density less than 6/100 μm, the standard convention of counting all δ-rays with four or more grains was used. For tracks of higher δ-ray density, a « long range » convention was used. These conventions as well as the procedure used for obtaining a calibration curve of δ-ray density *vs.* charge are given in Appendix III.

a) Charge and energy determination for particles stopping in the stack: Measurements of δ-ray density and of range were made to determine the charge and energy of particles stopping in the stack. Curves

of range *vs.* kinetic energy were plotted for the most abundant isotope of each charge Z from 2 to 26. These curves were calculated from the range-energy relation for protons in G-5 emulsion as given by BARKAS [23]. Curves of δ-ray density (N_δ) *vs.* kinetic energy were also plotted for various values of charge Z, using the relation $N_\delta = aZ^2/\beta^2 + b$; the values of a and b were obtained from δ-ray density calibration curves (Appendix III). From these two sets of curves a plot of $N_\delta/100$ μm *vs.* range (g/cm²) for different charges was obtained. Two sets of curves were obtained corresponding to the two conventions employed for counting of δ-rays. These sets of curves were used for the determination of the charge and energy of stopping particles.

b) Charge and energy determinations from variations of δ-ray density along the track: A small fraction of the primary particles which passed through the stack, or interacted after traversing 4 cm, showed a large visible change (more than 30 to 40 %) in δ-ray density between the two extremities of the track. In these cases, it was found that the knock-on electrons emitted were of such low energy that, even if their tracks were flat at the beginning, they became steep after a short distance (~ 70 μm), because of the very high multiple scattering, and were thus unsuitable for measurements. For such particles the variation of δ-ray density along the track was used to determine the charge and energy.

c) Charge and energy determinations by measurements on knock-on electrons: The energy per nucleon of heavy primary nuclei passing through the stack or interacting in the stack after a length of 4 cm was obtained from measurements on knock-on electrons as discussed in Sect. 2. These heavy primary tracks were scanned under a magnification of 100×15 for tracks of knock-on electrons. A track at minimum ionization originating from the primary track was accepted as due to a knock-on electron after it was carefully checked by two observers. The general procedure was to scan the entire track length and note down all tracks of knock-on electrons with angles of emission $< 30°$. For acceptance, a knock-on electron track had to satisfy the following conditions: *a*) dip angle less than 20°, and *b*) the length of the electron track had to be such that at least about $(10 \div 15)$ independent cells were available for multiple scattering measurements. (When an electron suffered a large angle scattering, the measurement of multiple scattering was generally confined to the length up to that point; if it was found that there was no significant loss of energy of the electron at the point of large angle scattering, the track-length beyond this was also used for measurements.) On each track at least two knock-on electrons (within the useful angle) were

[23] W. H. BARKAS: *Nuovo Cimento*, **8**, 201 (1958).

measured, and from each of these the primary energy γ_p was evaluated. These two values of the primary energy had to be consistent with each other within two standard deviations; details of this are discussed in Appendix II. If the two values were inconsistent, measurements were made on a third « useful » knock-on electron and the value of the primary energy was again calculated. It was found that this value of γ_p was in agreement with that obtained from either the first or the second knock-on electron. The final value of the primary energy was obtained from the weighted mean of the two estimated values which were consistent with each other.

For primary energies less than ~ 5 GeV/nucleon it was possible to obtain on each track at least two knock-on electrons within the useful angle since the mean available track length in the stack is ~ 10 cm. For primary particles of energy between ~ 5 to 10 GeV/nucleon, two knock-on electrons were obtained on some tracks, while for others only one knock-on electron was available within the useful angle. In these cases, the second knock-on electron track outside the useful angle was measured but yielded a value of primary energy with large errors. This value had to be consistent with that obtained from the first knock-on electron. For particles with energy above 10 GeV/nucleon, both knock-on electrons gave only lower limits to the value of primary energy; these were got from the lower limits for the angles of emission and the energies of the electrons.

The charge of each primary nucleus was obtained from the sets of curves of $N_\delta/100\ \mu$m *vs.* kinetic energy per nucleon for various charge values.

The number of particles analysed by the above three methods is given below:

(*a*)	$N_\delta/100\ \mu$m and residual range	78 particles
(*b*)	Variation of $N_\delta/100\ \mu$m along the track	15 particles
(*c*)	Knock-on electrons and $N_\delta/100\ \mu$m	198 particles
	Total	291 particles

3·4. *Energy of particles at the top of the atmosphere.* – From the measured energy of the particle inside the stack, its energy at the entrance point was obtained using the range-energy relation in emulsion. Next, using the range-energy relation in air, the energy of each particle at the top of the atmosphere was obtained from the amount of air (and packing material) traversed by it before entering the stack; (since the amount of packing material was small and it was-composed of light material—mainly bakelite—it was directly added to the amount of air traversed by the particle). In extrapolating the energy of particle to the top of the atmosphere it was assumed that no loss of charge occured in the air above the stack. This condition is satisfied by the majority of particles of charge $Z \geqslant 6$, since the stack was exposed at very high altitude.

4. – Results and discussion.

4·1. *Charge spectrum.* – Measurements of charge and of energy were made on 291 tracks which satisfied the selection criteria given in Section 3·2. The charge spectrum of these particles is shown in Fig. 6. 136 and 70 of the above

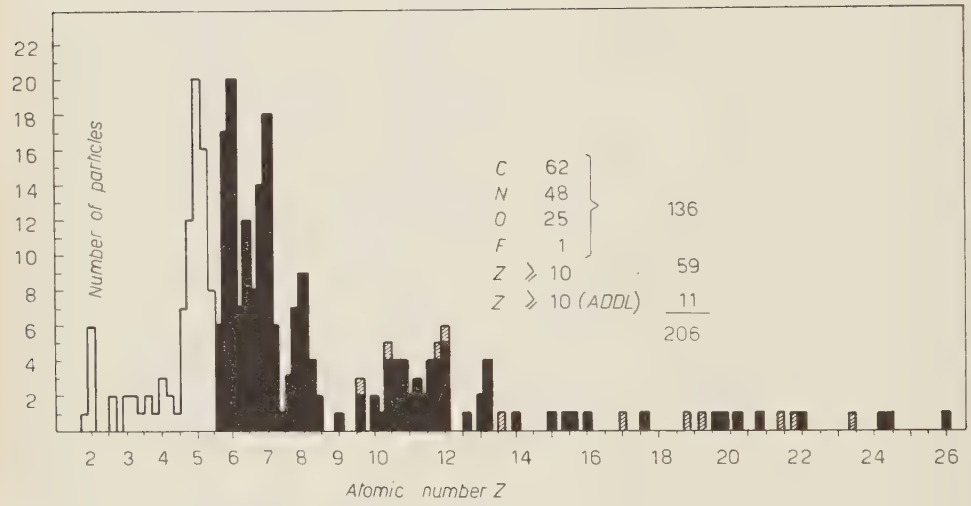

Fig. 6. – The charge spectrum of heavy nuclei at flight altitude. The shaded part represents the eleven additional tracks with charge $Z \geqslant 10$ (mentioned in Sect. 3·2).

particles were identified as belonging to the medium and heavy group of nuclei respectively; the charge resolution obtained is good enough to reliably group them in this manner.

4·2. *Energy spectra.* – The number of particles of the M and H groups observed in the various energy intervals is shown in Table II. In addition, 11 particles of the H-group were observed in the energy interval 0.28 to 0.41 GeV/nucleon. These are not included in the Table, since particles of *high* atomic number in this group will not be observed in this energy interval owing to absorption in the overlying matter. (At the flight altitude, the minimum energy required by a nucleus with charge $Z = 26$ to penetrate the overlying matter is 410 MeV/nucleon and that required by a nucleus with charge $Z = 8$ is 230 MeV/nucleon.) The observed numbers shown in Table II were then corrected to take into account those particles which interacted in the stack before traversing 4 cm. For this correction, each track was assigned a weight $\exp[R/\lambda]$; in this, R is the actual (measured) range in the stack for

stopping particles of range $R < 4$ cm and $R = 4$ cm for all the remaining tracks; λ is the interaction mean free path in emulsion of the group to which the particle belongs. The numbers were then corrected for particles which traversed the stack during the ascent of the balloon. The corrected numbers are also shown in the Table.

TABLE II. – *Energy distribution of M and H nuclei.*

Kinetic energy interval (GeV/nucleon)		0.23 ÷ ÷0.41	0.41 ÷ ÷0.70	0.70 ÷ ÷0.83	0.83 ÷ ÷0.99	0.99 ÷ ÷1.34	1.34 ÷ ÷2.11	2.11 ÷ ÷3.30	3.3 ÷ ÷5.0	5.0 ÷ ÷9.0	⩾9.0
No. of particles observed	M	20	20	17	15	21	19	10	5	7	2
	H		13	9	13	5	4	9	4	1	1
No. of particles corrected for interactions	M	24.2	26.6	22.8	20.1	28.2	25.5	13.4	6.7	9.4	2.7
	H		18.1	13.7	19.7	7.6	6.1	13.7	6.1	1.5	1.5
No. of particles corrected for interactions and ascent	M	22.9	23.1	21.6	19.0	26.1	23.1	12.1	6.0	8.5	2.7
	H		15.8	12.6	19.2	7.3	5.4	12.2	5.4	1.5	1.5

The integral energy spectrum can be represented by the relation:

$$N(\geqslant E) = \frac{C}{(1+E)^m}, \tag{5}$$

where N = the number of particles above an energy E, E – the kinetic energy expressed in GeV/nucleon, and C – a constant. The best value of the exponent « m » and its error, *in an integral plot*, cannot be calculated directly by the usual statistical methods, since the various points on such a plot are strongly correlated. Hence, to obtain the best value of « m » and its error we have used the *differential energy spectrum*. In Fig. 7, is shown the differential energy spectrum of the M-group of nuclei for the energy interval 0.23 to 9 GeV/nucleon and of the H-group of nuclei for the energy interval 0.41 to 9 GeV/nucleon. A « least square fit » to this data gives the exponent $(m+1)$ as 2.65 ± 0.27 for M-nuclei and 2.82 ± 0.59 for H-nuclei. The errors quoted are *standard deviations* on the least square fit lines. *We have taken the value of « m » and its error in the integral plot to be the same as that obtained from the differential spectrum.* The values of the exponent « m » of the integral energy spectra of M and H groups (Fig. 8) are thus 1.65 ± 0.27 and 1.82 ± 0.59 respectively.

It can be shown in the following way that the above values of « m » and its error give a correct representation of the integral energy spectra. One can fit a line directly to the integral energy spectrum considering only two flux values with reasonable statistics and having a minimum correlation. If we adopt this procedure, then the values of « m » in the integral energy spectra of M and H nuclei are obtained as 1.72 ± 0.26 and 1.74 ± 0.48 respectively. (For M-nuclei the flux values for energies >0.23 GeV/nucleon and >5.0 GeV/nucleon, and for H-nuclei the flux values for energies >0.41 GeV/nucleon and 2.11 GeV/nucleon were used.) The errors quoted are the extreme limits of the slope. These values of « m » and their errors are consistent with the values 1.65 ± 0.27 and 1.82 ± 0.59 obtained from the differential spectra.

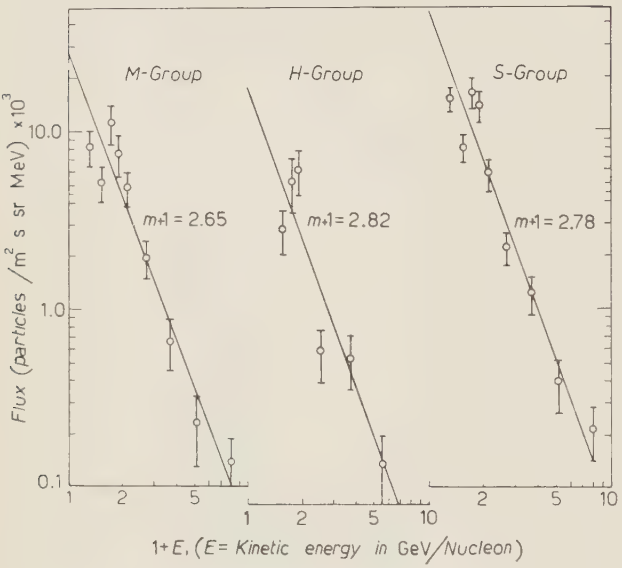

Fig. 7. – Differential energy spectra of M-nuclei ($6 \leqslant Z \leqslant 9$), H-nuclei ($Z \geqslant 10$) and S-nuclei ($Z \geqslant 6$).

The results indicate that, within experimental errors, the M and H groups of nuclei have the same exponent. Therefore, we have combined the data of the M and H groups

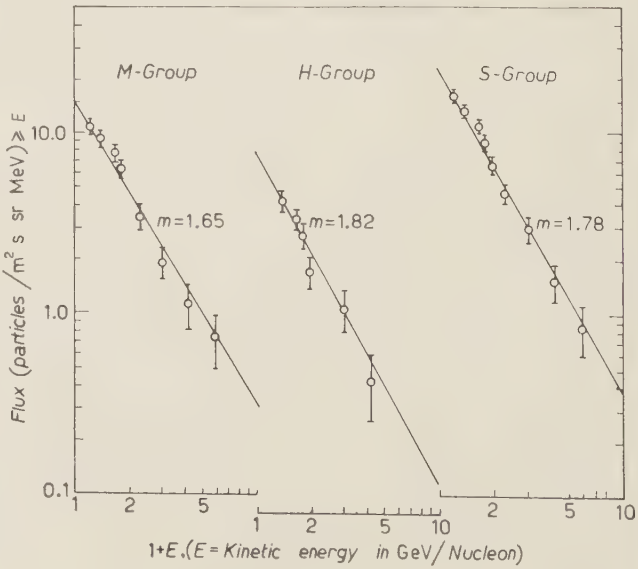

Fig. 8. – Integral energy spectra of M-nuclei, H-nuclei and S-nuclei.

and obtained the exponent « m » for S-nuclei ($Z \geqslant 6$) as 1.78 ± 0.24, over the energy range 0.23 to 9 GeV/nucleon. (The number of H-nuclei in the energy interval 0.23 to 0.41 GeV/nucleon was obtained by assuming that the slope of the integral spectrum of H-nuclei between 0.23 to 0.41 GeV/nucleon is the same as that between 0.41 and 9 GeV/nucleon.) The differential and integral energy spectra of S-nuclei are also shown in Figs. 7 and 8 respectively.

The values of the exponent « m » of the integral energy spectra of α-particles, M-nuclei and H-nuclei obtained by various investigators by direct energy determinations are summarized in Table III. In most of the previous exper-

TABLE III. – *Results of various direct determinations of the integral energy spectra of nuclei of charge* $Z \geqslant 2$.

Authors	Ref.	Method	Kinetic energy (GeV/nucleon)	Exponent « m » of the integral energy spectra of various charge groups			
				α	M	H	S
APLON *et al.*	(6)	Opening angle of α-fragments and relative scattering	3.0 ÷20.0			1.35 ± 0.15 (77)	
OWLER and ADDINGTON	(9)	Multiple scattering	1.8 ÷3.0	1.50 ± 0.18 (139)			
ADDINGTON	(18)	Multiple scattering	1.8 ÷3.0	1.70 ± 0.20 (150)			1.20 ± 0.30 (52)
CDONALD	(24)	Čerenkov-scintillation counter telescope	0.28 ÷0.88	1.40 ± 0.20 (~ 500)			
STER *et al.*	(19)	Interactions and the opening angles of α-fragments	1.5 ÷3.0			$1.50^{+0.30}_{-0.20}$	$1.54^{+0.16}_{-0.13}$ (275)
IN *et al.*	(25)	Interactions, opening angles of α-fragments and relative scattering	7.0 ÷100		1.57 ± 0.20	1.62 ± 0.20	1.60 ± 0.15 (115)
esent ork (*)	—	Knock-on electrons, range-ionisation	0.23 ÷9.00		1.65 ± 0.27 (136)	1.82 ± 0.59 (70)	1.78 ± 0.24 (206)

(*) Errors quoted are standard deviations on the « least square fit » lines to the differential spectra. For most of the other experiments the procedure used for assigning errors is not stated.

Numbers shown in brackets indicate the total number of tracks used.

(24) F. B. MCDONALD: *Phys. Rev.*, **104**, 1723 (1956).

(25) P. L. JAIN, E. LOHRMANN and M. W. TEUCHER: *Phys. Rev.*, **115**, 654 (1959).

iments, the procedure used for assigning errors is not clearly stated. In the case of M and H nuclei especially, the errors quoted appear to be underestimated when one considers the number of tracks on which the values are based and the uncertainties existent in the energy determinations. The emulsion stack used in the present experiment was exposed on the same flight (flight 5) on which McDONALD [14] measured the energy spectrum of α-particles in the energy region 0.3 to 0.9 GeV/nucleon, using a Čerenkov-scintillator counter telescope. The exponent « m », as calculated by us from his data, is 1.5 for α-particles and is consistent, within experimental errors, with the values for M and H nuclei obtained in this experiment. The results in Table III are consistent with the assumption that the various chemical elements in the primary cosmic radiation have the same value for the exponent « m ». However the error on « m » in all of the experiments carried out so far on the M and H nuclei are too large to reveal any small scale differences in the spectra as suggested by SINGER [20]. There is thus a distinct need for experiment of greatly increased accuracy.

4·3. *Geomagnetic cut-off energy.* – The lowest energy particle of the M-group observed in this experiment was a carbon nucleus of energy 230 MeV/nucleon. At the flight altitude (6.1 g/cm² of air) the « air cut-off » for a carbon nucleus *i.e.* the minimum energy required to penetrate the overlying air (+ small packing material, ~ 2 g/cm²) and a length of 5 mm in emulsion, is 200 MeV/nucleon. Between 230 MeV/nucleon and 260 MeV/nucleon, 5 carbon nuclei were detected but none were found with energies between 200 MeV/nucleon and 230 MeV/nucleon. The energies of almost all of the particles in the low energy end of the spectrum were determined from measurements of the residual range and consequently are very accurate. Therefore, 230 MeV/nucleon represents the geomagnetic cut-off energy obtained in this experiment. This is in agreement with the value (220 $\pm$ 30) MeV/nucleon estimated by McDONALD [14] for α-particles in his experiment on the same flight. At ceiling, the balloon drifted from 53.5° to 54.5° N geomagnetic latitude (Fig. 4-*b*), ref [26]), flight no. 5). The cut-off should, therefore, correspond to the highest geomagnetic latitude reached *i.e.* $\lambda \sim 54.5°$ N. The measured cut-off energy is in disagreement with the value of ~ 400 MeV/nucleon predicted from a simple dipole approximation of the earth's magnetic field. QUENBY and WEBBER [27] have calculated the cut-off energies at various latitudes using additional non-dipole terms to describe the earth's magnetic field. Their value for the geomagnetic cut-off at $\lambda = 53.5°$ N is 255 MeV/nucleon and at $\lambda = 54.5°$ N is 175 MeV/nucleon. These

[26] F. B. McDONALD and W. R. WEBBER: *Phys. Rev.*, **115**, 194 (1959).
[27] J. J. QUENBY and W. R. WEBBER: *Phil. Mag.*, **4**, 90 (1959).

values are not in disagreement with our measured value of 230 MeV/nucleon. Due to the close proximity of the values « air cut-off », 200 MeV, and the lowest energy we have measured, 230 MeV, and the possibility that the integral energy spectrum bends over at low energies, we cannot exclude the possibility that the cut-off at $\lambda = 54.5°$ N is as low as 175 MeV/nucleon, as predicted by QUENBY and WEBBER.

4·4. *Flux values at the top of the atmosphere.* – The values of the flux M, H and S nuclei at the top of the atmosphere, obtained by using the diffusion equation given by NOON and KAPLON [28], are shown in Table IV. As can be seen from this table, the extrapolated flux data are not very sensitive to the values used for the absorption mean free paths (Λ) in air for M and H nuclei; this is so because the extrapolation is only over a small thickness of overlying air (6.1 g of air). A comparison of these values with those obtained by other investigators on other occasions shows that *a Forbush type of decrease had occurred in the intensity of heavy nuclei* ($Z \geqslant 6$) *of the primary radiation, at the time this stack was exposed at high altitude* [17]; *a similar type of*

TABLE IV. – *Flux values of M, H and S-nuclei at the top of the atmosphere.*

	Extrapolation to the top of the atmosphere carried out assuming	
	$\Lambda_M = 33$ g/cm^2; $\Lambda_H = 29$ g/cm^2 [25]	$\Lambda_M = 26$ g/cm^2; $\Lambda_H = 41$ g/cm^2 [29,30]
	(particles/m^2 s sr)	(particles/m^2 s sr)
J_M^0 ($\geqslant 230$ MeV/nucleon)	9.7 ± 0.9	10.7 ± 1.0
J_H^0 ($\geqslant 230$ MeV/nucleon)	5.8 ± 0.7	5.3 ± 0.7
J_S^0 ($\geqslant 230$ MeV/nucleon)	15.5 ± 1.1	16.0 ± 1.1

The above flux values are based on the number of particles observed in an area of 158.7 cm^2 in the central region of the emulsion plate, since conditions (d') and (e') mentioned in Sect. 3·2 had to be satisfied. This area contained 109 particles of the M-group and 55 particles of the H-group.

[28] J. H. NOON and M. F. KAPLON: *Phys. Rev.*, **97**, 769 (1955).

[29] R. E. DANIELSON, P. S. FREIER, J. E. NAUGLE and E. P. NEY: *Phys. Rev.*, **103**, 1075 (1956).

[30] M. V. K. APPA RAO, S. BISWAS, R. R. DANIEL, K. A. NEELAKANTAN and B. PETERS: *Phys. Rev.*, **110**, 751 (1958).

decrease in the flux of α-particles was observed by McDonald using a counter telescope carried on the same flight as the present stack; neutron monitors at $\lambda = 56°$ N *had also shown a large Forbush decrease at the same time.*

It thus appears that modulation mechanisms which cause short term intensity variation affect sometimes the heavy primary nuclei of the cosmic radiation.

5. – Summary.

i) The energy spectrum of nuclei with charge $Z \geqslant 6$ in the primary cosmic radiation has been determined by employing a technique different from those previously used in this type of work. In this technique, the energies (per nucleon) of heavy primary cosmic ray nuclei have been determined by measuring the angles of emission and the energies of « knock-on electrons » which they produce by elastic collisions in traversing nuclear emulsions. The conditions necessary for a reliable determination of the primary energy by the « knock-on electron technique » have been established; and it is shown that the energy evaluated under these conditions agrees well with that determined by other methods. This technique is of value in determining the energies of heavy nuclei with energies up to about 10 GeV/nucleon.

ii) The exponent of the integral energy spectrum of the M-group of nuclei has been obtained as 1.65 ± 0.27, in the energy range 0.23 to 9 GeV/nucleon, and of the H-group of nuclei as 1.82 ± 0.59, in the energy range 0.41 to 9 GeV/nucleon. Since the various points (denoting flux values) on the integral plot of the energy spectrum are not independent, we have used the differential plot to obtain the best value of the exponent and its error; it is shown that this procedure gives a correct representation of the integral energy spectrum and its error. Within the experimental errors, both charge groups appear to have the same exponent for the integral energy spectrum. Hence the data for H and M nuclei have been combined and the exponent of S-nuclei ($Z \geqslant 6$) obtained as 1.78 ± 0.24. The exponent of the integral energy spectrum of α-particles recorded by a counter telescope on the same flight is 1.5; this was deduced by us from the data obtained by McDonald [14]. These observations are consistent, within experimental errors, with the assumption that the various chemical elements in the primary cosmic radiation have the same value for the exponents of their integral energy spectra. However, the errors on the exponent, in all of the experiments in which direct determinations of the integral energy spectra of M and H nuclei have been made, are too large to reveal any differences in the spectra of the various chemical elements as suggested by Singer [20]. There is thus a need for further experiments of increased accuracy to resolve this controversy.

iii) The geomagnetic cut-off energy at $\lambda = 54.5^\circ$ N has been obtained as 230 MeV/nucleon. This value is in agreement with that estimated by McDONALD ([14]) for α-particles in his experiment on the same flight. This is inconsistent with the value expected from a simple dipole approximation of the earth's magnetic field; but it is consistent with the value predicted by QUENBY and WEBBER ([27]).

iv) The flux values of M and H groups of nuclei, extrapolated to the top of the atmosphere, are (10.7 ± 1.0) and (5.3 ± 0.7) particles/m^2 s sr respectively. These values were obtained using absorption mean free paths in air as directly measured by DANIELSON ([29]) at $\lambda = 10^\circ$ N and used in an earlier experiment by APPA RAO *et al.* ([30]). Because of the high altitude attained by the balloon, the (extrapolated) flux values are not very sensitive to the values of the absorption mean free paths used. From a comparison of these flux values with those obtained by other investigators on other occasions, we have shown that a Forbush type of decrease had taken place in the intensity of heavy nuclei ($Z \geqslant 6$) of the primary radiation at the time this stack was exposed ([17]).

* * *

We wish to thank Professor B. PETERS for useful suggestions during the early part of this work. We are particularly thankful to Professor M. G. K. MENON for valuable discussions and for going through the paper in great detail. We are grateful to Dr. R. R. DANIEL for his critical comments which have been of great value. We are indebted to Dr. F. B. McDONALD and the U.S Office of Naval Research for having carried the emulsion stack on their balloon flight and to Dr. YASH PAL for having made the necessary arrangements for exposure. It is a pleasure to record the help of Mrs. T. M. UPADHYAY, Mrs. T. N. R. RAO, Miss F. BULSARA and Miss S. JOSHI in scanning the emulsions.

APPENDIX I

Calculation of the error on primary energy: conditions for minimum error.

AI.1. *Error on the energy of the electron.* – The relative error on the energy of the electron was calculated from the relation:

$$\frac{\delta(\gamma_e - 1)}{\gamma_e - 1} \simeq \frac{\delta \Delta}{\Delta} = \frac{0.78}{\sqrt{n}} \left(1 + \frac{2\varepsilon^2}{\Delta^2} + \frac{2\varepsilon^4}{\Delta^4}\right)^{\frac{1}{2}}, \tag{6}$$

where Δ = true scattering sagitta,
n = number of independent cells used in the scattering measurements,
ε = total noise.

Cell sizes of 10, 20, 40, 60 and 80 μm were used for multiple scattering measurements on the electron tracks. Reading noise was determined by taking readings at each ordinate twice, as given by BISWAS *et al.* (7). Grain noise was obtained from the reading noise and reading plus grain noise as measured on tracks of high energy particles at minimum ionization; the grain noise (0.09 μm) was added quadratically to the reading noise obtained for each knock-on electron. (The reading plus grain noise cannot be obtained for slow knock-on electron tracks by repeating readings at a « displaced » set of grains (7) because of the high multiple scattering on these tracks.) This method of obtaining ε was checked by determining ε directly on fast knock-on electrons. (The stage noise is negligible for the small cell lengths used in this experiment.) It was found that reading noise varied from track to track depending on the energy of the particle; measurements were, therefore, made separately for each track. Wherever possible, the cell size was chosen to minimize the error on the electron energy; however, for very low energy particles, cell sizes less than 10 μm are not practicable. The error on electron energy was calculated from the relation (6).

The scattering constant for electrons of energy (2.5÷200) MeV has been experimentally determined (HISDAL (31); HEYMANN and WILLIAMS (32); VIOLET (33)) and is in agreement with that given by Molière's theory. There is some disagreement (31,32) at an electron energy of ~1 MeV which may be due to experimental biases. We have used the scattering constant as given by Molière (for a $4\bar{D}$ cut-off), taking into account the variation of K with cell size as given by VIOLET (33).

A1.2. *Error in the angle of emission.* – The true angle of emission, ω, of the knock-on electron was obtained using the following relation:

(7) $$\cos\omega = \cos\theta\cos\varphi\cos\varphi_0 \pm \sin\varphi\sin\varphi_0 .$$

θ = the projected angle (on the plane of the emulsion) between the tracks of the electron and of the primary particle, φ = dip angle made by the electron track and φ_0 = dip angle made by the primary track. The projected angle θ was measured with an eyepiece micrometer. When a certain length l of the electron track is used to determine the best fit of the hair line, the error $\delta\theta$ is given by DE MARCO *et al.* (5) as:

(8) $$\delta\theta = \sqrt{\left(\frac{K}{l^{\frac{3}{2}}}\right)^2 + \left(\bar{\alpha}\sqrt{\frac{l}{300}}\right)^2}.$$

The first term arises from the setting error. The constant K was experimentally determined as $K = 25°$. The second term arises from the scattering of

(31) E. HISDAL: *Phil. Mag.*, **43**, 790 (1952).
(32) F. F. HEYMANN and W. F. WILLIAMS: *Phil. Mag.*, **1**, 212 (1956).
(33) C. E. VIOLET: *Phys. Rev.*, **104**, 1454 (1956).

the track in the length l. The error $\delta\theta$ is minimum when $\partial(\delta\theta)/\partial l = 0$, and the optimum length is given by:

$$l_{\text{opt}} = 5.5 \left(\frac{K}{\bar{\alpha}}\right)^{\frac{1}{2}}. \tag{9}$$

In our measurements the length l was taken close to the optimum and $\delta\theta$ was calculated from the relation (8).

When a length L is used for a measurement of the dip angle φ, the error $\delta\varphi$ is given by:

$$\delta\varphi = \left| \frac{2(\delta Z)^2 S}{L^2} + \varrho^2 \left\{ \left(\frac{\delta S}{S}\right)^2 + \left(\frac{\delta L}{L}\right)^2 \right\} + \left(\frac{\bar{\alpha}^2}{300} L\right) \right|^{\frac{1}{2}}, \tag{10}$$

where δZ = error in reading the depth scale (~ 0.5 μm),
S = shrinkage of emulsion and
ϱ = tg φ. We have taken $\delta S/S = 5\%$ and $\delta L = 1$ μm.

The error $\delta\varphi$ is minimum when $\partial(\delta\varphi)/\partial L = 0$ and the optimum value of L is given by:

$$L_{\text{opt}} = 8.43 \left\{ \frac{\varrho^2(\delta L)^2 + 2S^2(\delta Z)^2}{\bar{\alpha}^2} \right\}^{\frac{1}{3}}. \tag{11}$$

The dip angle φ was measured using a length L close to the optimum value and the error $\delta\varphi$ was calculated from eq. (10).

The error on the true angle ω was calculated from the relation

$$(\delta\omega)^2 = \frac{(\theta \cdot \delta\theta)^2 + (\varphi \pm \varphi_0)^2 [(\delta\varphi)^2 + (\delta\varphi_0)^2]}{\omega^2}. \tag{12}$$

(In deriving this relation the approximation $\measuredangle = \text{tg} \measuredangle = \sin \measuredangle$ has been used Since the angles considered here are usually less than 25°, the error involved is small.) The angle φ_0 was obtained from the total length of the primary track in an emulsion, projected on the plane of the emulsion, and assuming that the emulsion thickness = 600 μm. The error $\delta\varphi_0/\varphi_0$ was taken as 5% which is the average uncertainty in the emulsion thickness.

AI.3. *Error on primary energy.* – As given in Sect. 2·2, the error on the primary energy can be obtained from the relation:

$$\frac{\delta\gamma_{\text{p}}}{\gamma_{\text{p}}} = \sqrt{f_1^2 \left(\frac{\delta\gamma_{\text{e}}}{\gamma_{\text{e}}}\right)^2 + f_2^2 \left(\frac{\delta\omega}{\omega}\right)^2}, \tag{2}$$

where

$$f_1 = \frac{\partial\gamma_{\text{p}}}{\partial\gamma_{\text{e}}} \cdot \frac{\gamma_{\text{e}}}{\gamma_{\text{p}}} = \frac{\gamma_{\text{e}}}{2(\gamma_{\text{e}} + 1)} + \frac{\gamma_{\text{e}} \cdot \gamma_{\text{p}}^2 \,\text{tg}^2\,\omega}{2(\gamma_{\text{e}} + 1)}, \tag{2a}$$

and

$$f_2 = \frac{\partial \gamma_p}{\partial \omega} \cdot \frac{\omega}{\gamma_p} = \frac{(\gamma_e - 1)\gamma_p^2 (\operatorname{tg} \omega \sec^2 \omega)\, \omega}{\gamma_e + 1} . \tag{2b}$$

In Figs. 3*a* and 3*b* the functions f_1 and f_2 have been plotted against $(\gamma_e - 1)$ for different values of ω.

On each heavy primary track at least two knock-on electron were measured. The error on each of the γ_p values was obtained by using the above relations and the error on the weighted mean of the γ_p values evaluated. The distribution of errors on the weighted mean γ_p values of all the primary tracks of $Z \geqslant 6$ is shown in Fig. 9.

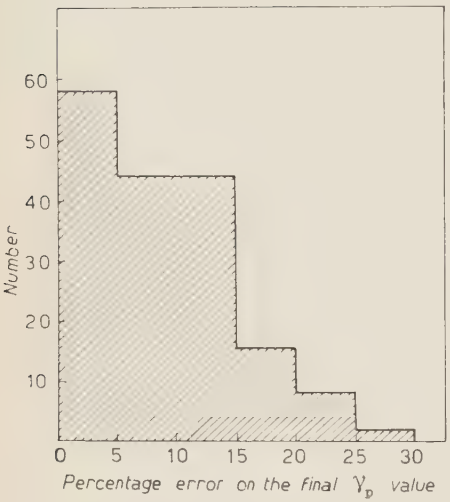

Fig. 9. – The distribution of percentage errors on the weighted mean values of primary energy γ_p obtained from knock-on electron.

Appendix II

Statistical analysis of the errors on the primary energies as obtained by the knock-on electron method.

In this experiment measurements have been made on a total of about 500 knock-on electrons produced by heavy primary nuclei. On each primary track at least two useful knock-on electron tracks were measured. If the values of γ_p obtained from these two were not consistent with each other (within two standard deviations), then a third knock-on track was measured. For the purpose of this analysis, of the pair of values which were consistent with each other, the one with the smallest error was considered as the best estimate of γ_p; we then classified the number of cases in which the second value — and the third whenever done — was consistent with the best estimate within one, two or more than two standard deviations.

These numbers are compared with those expected for a normal distribution in Table V. It may be seen that the number of pairs which agree with each other within one and two standard deviations is about that expected for a normal distribution. This indicates that the calculated errors on the primary energy γ_p are approximately right. In the fourth column of Table V is listed the number of pairs of values which differ by $\geqslant 2$ standard deviations; in this column the observed number (31) is greatly in excess of the number

expected (12) for a normal distribution. This gives the number of occasions when a measurement gives a wrong value of the primary energy. In addition, there is a separate group of 31 electrons which lie within the useful angle but

TABLE V. – *Statistical analysis of errors on the primary energies.*

	$\pm 1\sigma$	$\pm 2\sigma$	$> 2\sigma$
Observed number	151	56	31
Expected number for a normal distribution	162	64	12

Number of cases in which measurements on a pair of knock-on electron tracks (on a heavy primary track) yield two values of the primary energy γ_p consistent within ± 1, ± 2 and > 2 standard deviations.

in which the electron gives an indeterminate value of primary energy and this value is in disagreement with that obtained from another useful electron. Thus, out of a total of about 500 knock-on electrons, ~ 50 electrons *i.e.* 10 % of the total give wrong values of the primary energy. We attribute this to the uncertainties arising from sources (*a*), (*b*) and (*c*), discussed in Sect. 2·5.

APPENDIX III

δ-ray density measurements and charge calibration.

For tracks with high δ-ray density ($> 6/100$ μm) a « long range » convention was used. According to this convention, all δ-rays were counted which projected outside two parallel straight lines 2.5 μm away on either side of the primary track. In our measurements, the mean consistency of counting of δ-rays was 6.3 % for the standard convention and 9.5 % for the long range convention. For stopping particles δ-rays were counted on segments of the track close to the point of entry of the particle. An average length of 4 to 5 mm of a heavy primary track was used for δ-ray counting.

The charge calibration curve for the standard convention of δ-ray counting was obtained by using relativistic α-particles and « charge indicating interactions » of relativistic particles of charge 5, 6, 7 and 8. The relation between δ-ray density per 100 μm (N_δ) and the atomic number Z, up to $Z = 8$, can be represented by $N_\delta = aZ^2 + b$ where $a = 0.077$ and $b = 0.47$. In a similar manner the calibration curve was obtained for the « long range » convention and gives values $a = 0.0435$ and $b = 0.045$. This calibration curve was extrapolated to $Z > 8$ and was checked by a charge indicating interaction of a

relativistic particle with $Z = 13$. In the absence of calibration events above $Z = 13$ this calibration curve could be in error by one or two units of charge in the region of atomic number $Z \sim 20$.

RIASSUNTO (*)

La tecnica degli « elettroni d'urto » è stata impiegata per determinare lo spettro dell'energia dei nuclei con carica $Z \geqslant 6$ nella radiazione cosmica primaria. In questa tecnica l'energia per nucleone di un nucleo pesante di raggi cosmici primari si determina misurando gli angoli di emissione e le energie degli elettroni che il nucleo « colpisce » nelle collisioni elastiche lungo il suo cammino attraverso l'emulsione nucleare. Poichè le energie degli elettroni d'urto sono relativamente piccole (< 100 MeV in questo esperimento), possono essere misurate con precisione col metodo dello scattering multiplo di Coulomb. Si sono determinate le condizioni per una attendibile valutazione dell'energia primaria e si è verificata l'attendibilità del metodo per confronto con i risultati ottenuti con altri metodi. Le cariche e le energie delle particelle sono state determinate in due modi: 1) per le particelle che si arrestano nell'emulsione con misure del percorso e della densità dei raggi δ; 2) per le particelle che non vi si fermano, misurando la densità dei raggi δ e le energie e gli angoli di emissione degli elettroni d'urto veloci; nei pochi casi in cui le particelle rallentavano nell'attraversare lo stack, si è determinata la variazione della densità dei raggi δ lungo la traiettoria. Si fecero misurazioni su 291 tracce ottenute in uno stack di emulsioni lanciato dallo Iowa, ($\lambda = 53°$ N) a 113 000 ft. per quattro ore il 13 Marzo 1956. 206 di queste tracce erano dovute a particelle con carica $Z \geqslant 6$. L'esponente dello spettro integrale dell'energia del gruppo medio ($6 \leqslant Z \leqslant 9$) di nuclei si è determinato in 1.65 ± 0.27 nel campo di energie fra 0.23 e 9 GeV/nucleone e quello del gruppo pesante ($Z \geqslant 10$) di nuclei in 1.82 ± 0.59 nell'intervallo di energie fra 0.41 e 9 GeV/nucleone. L'esponente del gruppo S ($Z \geqslant 6$) di nuclei è quindi 1.78 ± 0.24. L'energia di cut-off geomagnetico a $\lambda = 54.5°$ N si è stimata in 230 MeV/nucleone. Si è trovato che i valori del flusso di nuclei M ed H sono (10.7 ± 1.0) e (5.3 ± 0.7) particelle/m^2 s sr, rispettivamente (13 Marzo 1956). Un confronto di questi valori con quelli ottenuti in altre prove mostra che ha avuto luogo un decremento di tipo Forbush nell'intensità dei nuclei pesanti, analogo a quello osservato da McDonald nel flusso di particelle α nello stesso volo; nella stessa epoca, rivelatori di neutroni a terra hanno pure registrato un decremento di Forbush.

(*) *Traduzione a cura della Redazione.*

On a Convergent Non-local Field Theory. - I.

E. Arnous (*)

Centre National de Recherche Scientifique - Paris

W. Heitler

Institut für Theoretische Physik, Universität - Zürich

Y. Takahashi (*)

Dublin Institute for Advanced Studies

(ricevuto il 20 Gennaio 1960)

Summary. — A non-local field theory is developed (and formulated in interaction representation) with the view of obtaining a converging theory. At least one special type of form factor is known for which this theory *converges throughout*, but in this and the following paper the form factor is not specified (it may even be a q-number). The view is taken that convergence should take precedence over exact Lorentz-invariance, because present knowledge does not necessarily exclude a violation of Lorentz-invariance *inside the source*. It is shown that the total charge is the same as in local theory and is conserved, provided only that the form factor commutes with the field operators. The invariance against groups of transformations is discussed in a general way and for the special case of Lorentz-transformations. It is shown that the Schrödinger equation can always be formulated in an invariant manner, but that this does not imply the invariance of the S-matrix. The conditions for the invariance of the S-matrix are derived. The theory contains the local theory as a special case.

Introduction.

A few years ago a considerable amount of work has been done on non-local field theories, with the view of obtaining a convergent theory (1). However,

(*) Temporarily at the University of Zürich.

(1) Compare for instance: Ch. Møller and P. Kristensen: *Kgl. Dan. Vid. Selsk.*, **27**, no. 7 (1952); C. Bloch: *Kgl. Dan. Vid. Selsk.*, **27**, no. 8 (1952); G. Wataghin: *Nuovo Cimento*, **5**, 689 (1957), and numerous other papers.

while strict Lorentz-invariance was demanded, it turned out that the divergences reappear in higher approximations. Also gauge invariance was violated. The attempts have, therefore, been abandoned again. The divergences can be traced to the very Lorentz-invariance which is maintained throughout. On the other hand, it cannot be denied that field theories must be finite and a certain amount of pressure is exerted by experimental facts indicating something like a *finite size* of the elementary particles (2). A finite size may be expressed by some non-local features in the interaction between the particles. It therefore, seemed to us advisable to resume the work, making convergence the prime and overruling demand. A formulation of a theory on a different basis with a specified form factor has recently been suggested by us (3), which is a generalization of the extended source model, and has turned out to be convergent throughout (4). Thus, at any rate, convergent non-local field theories *can* be formulated. In view of what is said above it is hardly surprising, however, to find that this particular theory is not strictly Lorentz-invariant. Lorentz-invariance is violated *inside* the source, and this exhibits itself in non-invariant radiative corrections. The form factor itself is invariant and therefore the first order of perturbation theory is also invariant, although, of course, some departure from the local theory is predicted. The difficulty

(2) The following facts can be quoted in this connexion: (i) the $\pi^{\pm}$-π^0 mass difference which is probably mainly an electromagnetic self-energy; (ii) the proton-neutron mass difference which is probably a mixed electromagnetic-mesonic self-energy, order e^2f^2, e^2f^4 ... (cfr. R. P. FEYNMANN and G. SPEISMANN: *Phys, Rev.*, **94**, 500 (1954), and L. O'RAIFEARTAIGH, B. SREDNIAWA and CH. TERREAUX: *Nuovo Cimento*, **14**, 376 (1959)). Perhaps similar considerations obtain for the K^0-K^+ mass difference. (iii) The π-nucleon scattering. While perturbation theory based on the first order gave on the whole the correct gross behaviour of the cross section (W. HEITLER and H. W. PENG: *Proc. Cam. Phil. Soc.*, **38**, 296 (1942)), the quantitative improvement (G. F. CHEW: *Phys. Rev.*, **94**, 1748, 1755 (1954)), due to the inclusion of higher orders on grounds of the non-relativistic extended source model is very considerable. The same applies to the photo-meson production. It may be remarked that in these calculations the *non-renormalizable* p.v. coupling is used which, for *second order processes* is not the non-relativistic limit of the p.s. coupling (contrary to numerous statements made in the literature). Thus the use of a finite size model is imperative. (iv) Although the finite size of the charge and of the magnetic moment distribution of the nucleons is primarily an effect of meson theory (compare M. SLOTNICK and W. HEITLER: *Phys. Rev.*, **75**, 1645 (1949)) a quantitative investigation indicates a finite size of the nucleon itself. (L. K. PANDIT: *Helv. Phys. Acta*, **31**, 379 (1958); *Nuovo Cimento*, **10**, 534 (1958)). All these effects lead to a size of the elementary particles of the order $\hbar/Mc$, M = nucleon mass, for all interactions.

(3) E. ARNOUS and W. HEITLER: *Nuovo Cimento*, **11**, 443 (1959), cfr. also Part II, Sect. **6**. In the first paper the C, P, T invariance and causality are also discussed.

(4) For details see part II, Sect. **6** and a special paper by L. O'RAIFEARTAIGH: to be published.

—if not the impossibility—to reconcile convergence and exact Lorentz-invariance within a non-local framework suggests a critical examination of the experimental evidence of Lorentz-invariance inside the finite size of a particle. For example, if we sacrifice Lorentz-invariance in this sense, it will turn out that the self-mass of a particle, about 3% of the rest mass for the electron, would not be strictly invariant, and Einstein's formula for the mass-velocity relation would not be quite exact. Present evidence in this respect is rather wanting ([5]). A certain measure of velocity dependence of the self-mass would hardly contradict the present data. More accurate measurements, especially at higher energies ($> mc^2$) are most desirable. For the special form factor mentioned above the self mass would decrease as soon as the momentum $p > mc$ and tend to zero for $p \gg mc$ ([4]). In this case the theoretical mass would be measurable.

A more severe test of strict Lorentz-invariance can be seen in the anomalous magnetic moment of theel ectron and in the Lamb-shift. As is well known, local quantum-electrodynamics yields the correct results only when Lorentz- and gauge-invariance are used as *explicite* and additional demands in the evaluation. However, these effects are somewhat indirect and it is very difficult to be sure that no less restrictive demands could lead to results which agree with the data within their accuracy. On the other hand these effects will be a severe test on any theory differing from the local one.

The purpose of this work (parts I and II) is not so much to suggest a definite theory with a specified form factor but rather to discuss, in a manner as general as possible, a non-local theory of which it is known that it embodies within its framework the possibility of convergence. In view of what was said above it seemed advisable not to exclude, from the start, any violation of Lorentz-invariance within the particles. On the other hand we shall take care to formulate the conditions for Lorentz-invariance within the general framework.

Part I is concerned with the general formulation of the non-local theory to be studied, with the conservation of the total charge and with general conditions for invariance pertaining, for example, to both Lorentz- and gauge-invariance. The former is treated more in detail.

Part II is concerned with the special case of quantum electrodynamics where gauge-invariance will be treated in detail. The convergence of the theory for a specified form factor will be the subject of a special paper by O'Raifeartaigh.

([5]) Compare the critical survey by P. S. Farago and L. Jánossy: *Nuovo Cimento*, **5**, 1411 (1957).

1. – Hamiltonian.

The starting point of the non-local theory we wish to discuss is the Schrödinger equation for the state vector in *interaction-representation*

$$i\frac{\partial \Psi(t)}{\partial t} = H(t)\Psi(t)\,, \qquad H = \int \mathscr{H}\,\mathrm{d}^3x\,. \tag{1}$$

H is the interaction Hamiltonian. For simplicity we consider the interaction of a spinor-field $\psi(x)$ and a scalar real field $\varphi(x)$, where ψ and φ are operators in interaction representation. We assume them to fulfil the same commutation relations

$$\{\psi(x), \bar{\psi}(y)\} = -iS(x-y) \tag{2a}$$

$$[\varphi(x), \varphi(y)] = \quad iD(x-y) \tag{2b}$$

and to satisfy the same free wave equations as in local theory. We choose interaction representation because a modification of H, like in the extended source model, seems to offer the easiest possibility for convergence. The corresponding field equations in Heisenberg picture would be extremely complicated. We generalize the local Hamiltonian by the introduction of a form factor, so that (6)

$$H(t) = g\int_{t=x_0} \mathrm{d}^3x \int \mathrm{d}^4(x'x''x''')\,\bar{\psi}(x')\,F(x-x',\, x-x'',\, x-x''')\,\psi(x'')\varphi(x''')\,. \tag{3}$$

We have chosen F so that invariance against space-time translations is preserved, but otherwise we shall not yet specify F further, except for the conditions (4), (4′) below. We leave it in general even open whether F is a c-number or q-number, nor do we demand relativistic invariance of F. For specified theorems F is assumed to commute with $\bar{\psi}$, ψ, φ, (it may still be a q-number in the space of the γ's) but in these cases the assumption is always mentioned explicitly. None of the arguments of this paper are changed if some operator like γ stand between $\bar{\psi}$ and ψ or if φ is a vector ($=A_\mu$) or if any derivative operators stand before φ. The limiting case of the local theory is given by $F = \delta^4(x-x')\,\delta^4(x-x'')\,\delta^4(x-x''')$. There is one normalization demand we have to make on F, namely,

$$\int F(x-x',\, x-x'',\, x-x''')\,\mathrm{d}^4x'''\,\mathrm{d}^4x = \delta^4(x'-x''). \tag{4}$$

(6) If F is a q-number we reserve the right to choose the position of F.

The meaning of this condition can best be seen after Fourier transformation: Let $f(p, q, k)$ be the Fourier-transform of F, (p, q, k) corresponding to $x - x'$, ..., $x - x'''$, then (4) means $f(p, p, 0) = 1$. This means that no form factor occurs when there is no genuine interaction (no emission of a virtual φ-particle k). In addition we demand H to be hermitian, which puts a certain further restriction on F:

$$F(x', x'', x''') = \gamma^4 F^\dagger(x'', x', x''')\gamma_4 . \tag{4'}$$

The Hamiltonian of the free fields H_0 is assumed to be the same as in local theory

$$H_0 = \int \overline{\psi}(\gamma_i \partial_i + m)\psi \, \mathrm{d}^3 x + H_\varphi , \tag{5}$$

where H_φ refers to the φ-field depending on its spin, etc.

2. – The charge integral.

Even at this general stage it can be shown that an integral exists describing the total charge and this total charge Q is identical with the expression of the local theory, *viz.*

$$Q(t) = \int \mathrm{d}^3 y \, \overline{\psi}(y)\gamma_4 \psi(y) .$$

Since ψ satisfies the Dirac-equation (interaction representation) $\partial Q/\partial t = 0$. We now show that

$$[QH] = 0 . \tag{6}$$

The only specification we make here is that F shall commute with $\overline{\psi}$, ψ and φ. It may still be a q-number in the space of the γ's. Applying (2a) we find

$$[QH] = -ig \int \{\overline{\psi}(x') F(x - x', x - x'', x - x''') S(x'' - y)\gamma_4 \psi(y) - \tag{6'}$$
$$- \overline{\psi}(y)\gamma_4 S(y - x') F(x - x', x - x'', x - x''')\psi(x'')\} \varphi(x''') \, \mathrm{d}^3 x \, \mathrm{d}^3 y \, \mathrm{d}^4 x' \ldots x''' .$$

It is well known that

$$-i \int S(x'' - y)\gamma_4 \psi(y) \, \mathrm{d}^3 y = \psi(x'') , \tag{7}$$

because S satisfies the Dirac equation (with x'' as variable) and for $x_0'' = y_0$, $S(x'' - y) = i\gamma_4 \delta^3(x'' - y)$; thus the left hand side of (7) agrees with $\psi(x'')$ at $x_0'' = y_0$, and since it satisfies the Dirac equation, it must be equal to $\psi(x'')$ at all times. Similarly

$$-i\int \overline{\psi}(y)\gamma_1 S(y - x')\, \mathrm{d}^3 y = \overline{\psi}(x') .$$

The bracket $\{\}$ in (6′) vanishes therefore after integration $\int \mathrm{d}^3 y$.

The fact that Q is an integral distinguishes our theory from previous non-local theories where the total charge is a much more complicated expression. We shall see in Part II, on the other hand, that this does not mean that the current vector j_μ is equally simple. In fact this will not be the case, but $\int j_0 \, \mathrm{d}^3 x$ will reduce to Q.

3. – Invariance, general.

We now discuss the question in what sense the wave equation and the ensuing theory is invariant against various transformations. The most important transformations to be discussed are the Lorentz-transformation and the gauge transformation in the case of electrodynamics. We shall see that, if (1) is invariant against some such transformation, this does not necessarily mean that, for example, also the S-matrix is invariant. We first discuss a very general type of transformation which can be specified later to include both Lorentz- and gauge transformations.

Suppose that H depends on a certain variable (or variables) α and let therefore Ψ also depend on α. Thus

$$i\dot{\Psi}(t, \alpha) = H(t, \alpha)\Psi(t, \alpha) \tag{8}$$

Consider now an infinitesimal transformation $\alpha \to \alpha + \delta\alpha$ where $\delta\alpha$ (but not necessarily α) is assumed to be a c-number.

We show that then a transformed $\Psi(t, \alpha + \delta\alpha) = \Psi'(t, \alpha)$ *always* exists such that (8) is invariant, *viz.*,

$$i\dot{\Psi}'(t, \alpha) = H'(t, \alpha)\Psi'(t, \alpha) , \qquad H'(t, \alpha) \equiv H(t, \alpha + \delta\alpha) . \tag{8′}$$

Writing

$$H(t, \alpha + \delta\alpha) = H(t, \alpha) + \frac{\partial H}{\partial \alpha}\delta\alpha ,$$

and

$$\Psi(t, \alpha) = \Psi(t, \alpha) - iK(t, \alpha)\Psi(t, \alpha)\delta\alpha \equiv \Psi(t, \alpha) + \frac{\partial \Psi}{\partial \alpha}\delta\alpha ,$$

(which defines K) we find that (8′) is valid together with (8), if

$$i\frac{\partial}{\partial t}K(t,\alpha) = i\frac{\partial H}{\partial \alpha} + [H, K]\,. \tag{9}$$

or

$$\left[i\frac{\partial}{\partial t} - H,\ i\frac{\partial}{\partial \alpha} - K\right] = 0\,.$$

The question is whether (9) can be solved for K. That this is the case can be seen by expansion of K according to the coupling constant contained in H

$$K(t,\alpha) = \sum_{j=1}^{\infty} K^{(j)}(t,\alpha)$$

and from (9)

$$\left\{\begin{array}{l} i\dfrac{\partial}{\partial t}K^{(1)}(t,\alpha) = i\dfrac{\partial}{\partial \alpha}H(t,\alpha)\,, \\ \quad\cdots\cdots\cdots\cdots\cdots\cdots \\ i\dfrac{\partial}{\partial t}K^{(j)}(t,\alpha) = [H(t,\alpha), K^{(j-1)}(t,\alpha)]\,. \end{array}\right. \tag{10}$$

These are differential equations for $K^{(j)}(t,\alpha)$ which can be solved successively.

Let us assume that H is switched off at $t=-\infty$, then the solution of (10) is

$$K^{(1)}(t,\alpha) = \int_{\infty}^{t} \mathrm{d}t'\ \frac{\partial H(t',\alpha)}{\partial \alpha}\,,$$

$$K^{2}(t,\alpha) = i\int_{\infty}^{t}\mathrm{d}t_1\int_{\infty}^{t_1}\mathrm{d}t_2\left[\frac{\partial H(t_2,\alpha)}{\partial \alpha}\,,\ H(t_1,\alpha)\right],$$

etc. This can also be written in closed form with help of $S(t,\alpha)$ defined below (11):

$$K(t) = S(t)\int_{-\infty}^{t}\mathrm{d}t'\,S^{-1}(t')\,\frac{\partial H(t',\alpha)}{\partial \alpha}\,S(t')\,S^{-1}(t)\,.$$

Thus for *any transformation* $\alpha \to \alpha+\delta\alpha$ *and for any Hamiltonian* $H(t,\alpha)$, a *corresponding transformation of the state vector exists*, such that the *wave equation* (1) is *invariant*. This does not mean, however, that quantities like the

S-matrix are also invariant. Further conditions are required for that purpose. Let us define the S-matrix, as usual, by

$$\left\{ \begin{array}{l} \Psi(t, \alpha) = S(t, \alpha)\, \Psi(-\infty, \alpha) \\ \qquad S \equiv S(\infty, \alpha)\ . \end{array} \right. \tag{11}$$

The relation $i(\partial\Psi/\partial\alpha) = K\Psi$ now becomes

$$i\,\frac{\partial S(t)}{\partial\alpha}\,\Psi(-\infty) + i\,S(t, \alpha)\,\frac{\partial}{\partial\alpha}\,\Psi(-\infty) = K(t, \alpha)\,S(t, \alpha)\,\Psi(-\infty)\ .$$

We may suppose that the initial state $\Psi(-\infty, \alpha)$ is invariant $(\partial/\partial\alpha)\Psi(-\infty,\alpha) = 0$. Then

$$i\,\frac{\partial S(t, \alpha)}{\partial\alpha} = K(t, \alpha)\,S(t, \alpha)\ , \tag{12}$$

$S \equiv S(\infty, \alpha)$ will therefore be invariant if

$$K(\infty, \alpha) = 0 \tag{13}$$

or by (9)

$$\int_{-\infty}^{\infty} \mathrm{d}t \left(\frac{\partial H(t, \alpha)}{\partial\alpha} - i[H, K] \right) = 0\ . \tag{13'}$$

Thus the invariance of the wave equation is not enough to garantee the invariance of the S-matrix (which depends on the elements of Ψ and not on $|\Psi|^2$), a point which seems to have been overlooked in most discussions concerning invariance. We shall see, that (13) or (13') is fulfilled in the local theory for both Lorentz-invariance and gauge invariance, but that (13) is a very restrictive condition in our non-local theory that is not easily satisfied.

4. – Conditions for Lorentz-invariance.

We now consider more in detail the conditions for Lorentz-invariance. For this purpose we first try to generalize (1) into what is a specialization of the Tomonaga equation. Consider a plane in space-time defined by

$$n_\mu x_\mu + \tau = 0\ ,$$

where n_μ is a fixed time-like 4-vector $n_\mu^2 = -1$, with $n_0 > 0$. Further define

$$H(\tau, n) = \int \mathrm{d}^4x\, \delta(nx + \tau)\mathscr{H}(x) .$$

We then demand

$$i\frac{\partial}{\partial\tau}\Psi(\tau, n) = H(\tau, n)\Psi(\tau, n) . \tag{14}$$

If $n = (0, 0, 0, i)$, $\tau = x_0 = t$ and (14) goes over into (1). For a given n_μ, the equation (14) can always be set up. Consider now an infinitesimal Lorentz-transformation

$$\left\{\begin{array}{l} x_\mu \to x_\mu + \delta\omega_{\mu\nu}x_\nu = (\delta_{\mu\nu} + \delta\omega_{\mu\nu})x_\nu \equiv x'_\mu , \\ n_\mu \to n_\mu + \delta\omega_{\mu\nu}n_\nu = (\delta_{\mu\nu} + \delta\omega_{\mu\nu})n_\nu \equiv n'_\mu . \\ \qquad\qquad \delta\omega_{\mu\nu} = -\delta\omega_{\nu\mu} . \end{array}\right. \tag{15}$$

(The last equation guarantees $n'^2_\mu = -1$). By this transformation the state vector will suffer a transformation

$$\Psi(\tau, n') = \Psi(\tau, n) + \frac{\partial\Psi}{\partial n_\lambda}\delta\omega_{\lambda\nu}n_\nu . \tag{15'}$$

Let us write this in the form

$$i\frac{\delta\Psi}{\delta\omega_{\lambda\nu}} = \frac{\partial\Psi}{\partial n_\lambda}n_\nu - \frac{\partial\Psi}{\partial n_\nu}n_\lambda = -iM_{\lambda\nu}\Psi(\tau, n) , \qquad M_{\lambda\nu} = -M_{\nu\lambda} . \tag{16}$$

We can write (16) as

$$i\left(n_\nu\frac{\partial}{\partial n_\lambda} - n_\lambda\frac{\partial}{\partial n_\nu} - M_{\lambda\nu}\right)\Psi = 0 . \tag{16'}$$

This condition is compatible with (14), if and only if the integrability condition

$$\left[i\left(n_\nu\frac{\partial}{\partial n_\lambda} - n_\lambda\frac{\partial}{\partial n_\nu}\right) - M_{\lambda\nu}\,,\; i\frac{\partial}{\partial\tau} - H\right] = 0 , \tag{17}$$

is fulfilled. In this case (14) is also valid in another Lorentz system *viz.*

$$i\frac{\partial}{\partial\tau}\Psi(\tau, n') = H(\tau, n')\Psi(\tau, n') . \tag{18}$$

(17) is the analogue of the well known integrability condition of the Tomonaga equation

$$(17') \qquad \left[i \frac{\delta}{\delta\sigma(x')} - \mathscr{H}(x', \sigma),\ i \frac{\delta}{\delta\sigma(x'')} - \mathscr{H}(x'', \sigma) \right] = 0 . \quad (x' - x'')^2 > 0 .$$

As in the general case of Section 3 one can easily see, that (17) in contrast to (17') can always be solved, *i.e.* $M_{\lambda\nu}$ can be found which satisfies (17).

Thus it can be stated, that an equation of the form (14) exists in any Lorentz-system. During a Lorentz transformation Ψ transforms according to (15'), (16), and $M_{\lambda\nu}$ can be determined, for example explicitly, as in Section 3, by expansion (see below). In this sense the theory is Lorentz invariant.

It is remarkable that this kind of Lorentz invariance is quite independent of the special form of H. We have nowhere used any particular properties of H, and the question of whether « H is an interaction belonging to a Lorentz invariant theory » or not does not arise.

This does not mean, however, that the S-matrix is Lorentz invariant. In the preceeding section it was shown quite generally that the S-matrix is only invariant if $K(t = \infty, \alpha) = 0$. In the case of Lorentz invariance this condition now becomes

$$(19) \qquad M_{\lambda\nu}(\tau = \infty, n) = 0 ,$$

τ taking the place of t, and n that of the parameter α. (19) is a condition that is not always satisfied, and if we demand this (which we shall *not* do in the following) it represents a demand on H. To see what (19) means we obtain $M_{\lambda\nu}$ from (17) by expansion. From (17) (or (14) and (18)) it follows that

$$(20) \qquad \begin{cases} i \dfrac{\partial}{\partial\tau} M_{\lambda\nu} = m_{\lambda\nu} + [H, M_{\lambda\nu}] , \\ m_{\lambda\nu} = i \left(n_\nu \dfrac{\partial}{\partial n_\lambda} - n_\lambda \dfrac{\partial}{\partial n_\nu} \right) H(\tau, n) . \end{cases}$$

Hence, if $M_{\lambda\nu}$ is expanded according to the coupling constant ($m_{\mu\nu}$ is of first order)

$$M^{(1)}_{\lambda\nu} = -i \int_{-\infty}^{\tau} m_{\lambda\nu} \, \mathrm{d}\tau' ,$$

$$M^{(2)}_{\lambda\nu} = -\int_{-\infty}^{\tau} \mathrm{d}\tau' \int_{-\infty}^{\tau'} \mathrm{d}\tau'' \, [H(\tau'), m_{\lambda\nu}(\tau'')] .$$

The general term is:

$$(20') \qquad M_{\lambda\nu}^{(k)} = -i^k \int_{-\infty}^{\tau} \mathrm{d}t_1 \int_{-\infty}^{\tau_1} \mathrm{d}t_2 \ldots \int_{-\infty}^{\tau_{k-1}} \mathrm{d}\tau_k \cdot$$

$$\cdot \left[\left[\ldots \left[m_{\lambda\nu}(\tau_k, n), H(\tau_{k-1}, n) \right], H(\tau_{k-2}, n) \right] \ldots, H(\tau_1, n) \right] .$$

The condition for the Lorentz invariance of the S-matrix is therefore (up to the 2nd order)

$$(21) \qquad M_{\lambda\nu}^{(2)}(\infty) = -i \int_{-\infty}^{\infty} \mathrm{d}\tau' \int_{-\infty}^{\tau'} \mathrm{d}\tau'' \left[H(\tau', n), \left(n_\nu \frac{\partial}{\partial n_\lambda} - n_\nu \frac{\partial}{\partial n_\nu} \right) H(\tau'', n) \right] = 0 .$$

We have put $H(-\infty, n) = 0$ which we may well do, if we imagine the interaction to be switched off at $\tau = -\infty$. Now

$$\int_{-\infty}^{\tau'} \mathrm{d}\tau'' n_\nu \frac{\partial}{\partial n_\lambda} H(\tau'', n) = \int \mathrm{d}^4x \int_{-\infty}^{\tau'} n_\nu x_\lambda \delta'(nx + \tau'') \mathscr{H}(x) \, \mathrm{d}\tau'' =$$

$$= \int \mathrm{d}^4x \, n_\nu x_\lambda \delta(nx + \tau') \mathscr{H}(x) .$$

(21) contains the commutator

$$(22) \qquad \int \mathrm{d}^4x \, \mathrm{d}^4y \, \delta(nx + \tau') \, \delta(ny + \tau') [\mathscr{H}(x), \mathscr{H}(y)] \qquad \text{or} \qquad [\mathscr{H}(x), \mathscr{H}(y)]_{nx = ny} .$$

$n(x - y) = 0$ means that x and y lie on a space-like surface, or that $(x - y)^2 > 0$. Thus it is sufficient for (21) to hold if $[\mathscr{H}(x), \mathscr{H}(y)] = 0$ for $(x - y)^2 > 0$, a well known condition, which is fulfilled in the local theory but not necessarily here. This also applies to higher orders.

The necessary conditions for the S-matrix to be Lorentz invariant up to the second order is, however

$$\int_{-\infty}^{\infty} \mathrm{d}\tau' \int \mathrm{d}^4x \mathrm{d}^4y \, [\mathscr{H}(x), \mathscr{H}(y)] \, (n_\nu x_\lambda - n_\lambda x_\nu) \, \delta(nx + \tau') \, \delta(ny + \tau') =$$

$$= \int \mathrm{d}^4x \, \mathrm{d}^4y \, [\mathscr{H}(x), \mathscr{H}(y)] \, (n_\nu x_\lambda - n_\lambda x_\nu) \, \delta(n(x - y)) = 0 .$$

which may be less restrictive than the vanishing of $[\mathscr{H}(x), \mathscr{H}(y)]$.

* * *

This work was begun at the Lorentz-Institut, Leiden, and two of us (E.A. and W.H.) would like to express their thanks for the hospitality offered by this University. Two of us (E.A. and Y.T.) wish to express their gratitude to the Swiss National Fonds for financial aid which enabled them to work repeatedly in Zürich.

RIASSUNTO (*)

Si sviluppa (e si formula nella rappresentazione delle interazioni) una teoria non-locale del campo allo scopo di ottenere una teoria convergente. Si conosce almeno un tipo speciale di fattore di forma per cui questa teoria *converge uniformemente*, ma in questo scritto e nel seguente il fattore di forma non è specificato (può anche essere un numero q). Si giudica che la convergenza debba aver la precedenza sull'esatta invarianza di Lorentz, perchè lo stato attuale delle conoscenze non esclude necessariamente una violazione della invarianza di Lorentz *nell'interno della sorgente*. Si dimostra che la carica totale è la stessa che nella teoria locale ed è conservata, purchè almeno il fattore di forma commuti con gli operatori di campo. L'invarianza verso gruppi di trasformazioni viene discussa sia in generale sia per il caso speciale delle trasformazioni di Lorentz. Si dimostra che l'equazione di Schrödinger può sempre scriversi in forma invariante, ma che questo non implica l'invarianza della matrice S. Si deducono le condizioni per l'invarianza della matrice S. La teoria contiene la teoria locale come caso speciale.

(*) *Traduzione a cura della Redazione.*

Photostar Production between 500 and 1100 MeV.

C. Castagnoli (*) and M. Muchnik

Istituto Nazionale di Fisica Nucleare - Sezione di Roma
Istituto di Fisica dell'Università - Roma

G. Ghigo

Laboratori Nazionali del C.N.R.N. - Frascati

R. Rinzivillo

Istituto di Fisica Superiore dell'Università - Napoli
Istituto Nazionale di Fisica Nucleare - Sottosezione di Napoli

(ricevuto il 25 Gennaio 1960)

Summary. — Experimental results are reported on the photoproduction of stars in photographic emulsions exposed to a high energy bremsstrahlung beam of maximum energies between 500 and 1100 MeV. The cross-sections, per number of equivalent quanta and per photon are calculated. The results are compared with those which can be derived using experimental values of the cross-sections for single and multiple pion photoproduction. Good agreement is found.

---

1. – An interesting feature of the interaction of photons with atomic nuclei is the photodisintegration of the nucleus, or production of photostars. This process has been studied so far, up to 500 MeV, by Miller [1], Kikuchi [2], George [3], and Peterson and Roos [4]. We have extended this investigation up to 1100 MeV at the Frascati electronsynchrotron.

(*) Now at the Istituto di Fisica dell'Università - Parma.

(1) R. D. Miller: *Phys. Rev.*, **82**, 260 (1951).
(2) S. Kikucki: *Phys. Rev.*, **86**, 41 (1952).
(3) E. P. George: *Proc. Phys. Soc.* (*London*), A **69**, 110 (1956).
(4) V. Z. Peterson and C. E. Roos: *Phys. Rev.*, **105**, 1620 (1957).

2. – The experimental arrangement is shown in Fig. 1. The γ-ray beam goes through a collimator 18 mm in diameter, a broom magnet, the shielding, the emulsion, and the monitor. The latter one was a quantameter of the Wilson type, for which we have used the constant $4.82 \cdot 10^{18}$ MeV/coulomb, a theoretical value agreed upon with Cornell (5).

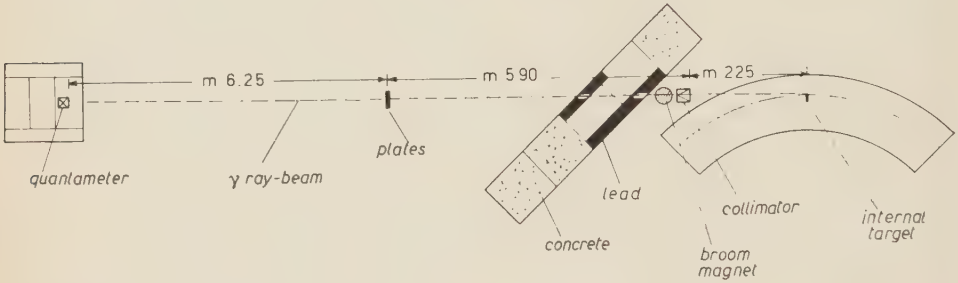

Fig. 1.

Fourteen 200 and 400 μm Ilford G-5 plates were exposed at normal incidence, one by one to the single energies. Each plate was coupled to a Ferrania « N » X-ray film, which was later used to determine exactly the zone to be scanned on the nuclear plate, and to give a point by point dosimetry. The beam diameter at the point where the plates were exposed was 5 cm.

The plates were scanned with either a 55×6 or a 50×8 optics, over a strip diametrical to the beam, partly in Naples and partly in Rome; the results have been mutually controlled. Scanning speed was about 0.3 cm^2/day $\times$ scanner. Efficiencies have been determined with the double scanning method. On the basis of this determination, an efficiency of $(90 \pm 5)\%$ has been attributed on the average to the experimental data.

3. – The cross-section per equivalent quantum and per emulsion nucleus, assuming an axially symmetric beam, is given by

$$\sigma_Q = \frac{N_s}{ND} = \frac{2\pi \int_0^{r_0} p(r) r \, dr}{N 2\pi A \int_0^{r_0} y(r) r \, dr}, \tag{1}$$

where N_s is the total number of stars in the plate; D the total dose in equivalent quanta; N the number of nuclei per cm^2 (hydrogen excluded); r the distance from the beam axis; r_0 the beam cross-section radius on the plate;

(5) R. R. Wilson: *Nucl. Instr.*, **1**, 101 (1957).

$\varrho(r)$ the star density (in cm^{-2}); $y(r)$ the dosimetric co-ordinate ($1 - y(r) > 0$ for $0 \leqslant r \leqslant r_0$), and A a constant depending only on the exposure parameters. Defining $R = n(r)/y(r)$, with $n(r) = \varrho(r) \times s$ being the number of stars found within a small fixed area s, then one expects R to be constant. Therefore

$$\sigma_Q = \frac{R}{NAs}, \tag{2}$$

where A is determined by integration of $y(r)$ at each energy, and the mean value of $n(r)/y(r)$ over the plate is taken for R. The fact that R is indeed approximately constant, for each energy, supports the assumption, implicit in our method of treating the data, that the ratio of high to low energy photons is roughly constant over the beam cross-section.

Three methods have been used to determine a possible neutron contamination of the beam: 1) a further exposure with a lucite absorber in front of the collimator so as to greatly enhance the number of neutrons in the beam; 2) the analysis of the stars so as to establish the percentages due to light or to heavy nuclei; 3) the study of the distribution of single prong stars as a function of the radial distance from the beam axis and a study of their forward-backward ratio. The conclusion is that the contribution of the neutrons is negligible. Equally negligible is the contribution of the radioactive contamination of the emulsion and of the cosmic rays, as seen from the scanning of unexposed areas.

To compare our results with those of previous authors, Fig. 2 shows σ_Q for production of 3 or more prong photostars, plotted against maximum bremsstrahlung energy on a semilog diagram. Monitor calibration uncertainties and possible differences in scanning criteria may account for the unsatisfactory agreement at 500 MeV with the results of PETERSON and ROOS. As it is seen σ_Q increases monotonically, as it should, since it includes the effects of all quanta in the beam, which increase in number with increasing energy for a given value of Q. The errors on the individual points are not only statistical, but comprise the uncertainties on the efficiencies. On the other hand, errors due to the measurement of the dose, to the determination of the maximum energy, and so on, have not been taken into account.

Our points—with the possible exception at 1 100 MeV—seem to lie on a straight line, as shown in Fig. 2. The cross-section σ_k per photon of a given energy when the bremsstrahlung spectrum is of the form [6] $f(k) = Q/k$ is given by

$$\sigma_k = \frac{\mathrm{d}\sigma_Q}{\mathrm{d}(\ln E_\gamma^{\max})}. \tag{3}$$

(6) G. DIAMBRINI, A. S. FIGUERA, B. RISPOLI and A. SERRA: private communication.

Hence, in our case, σ_k is directly given by the slope of the straight line in Fig. 2. However, to obtain the correct value of σ_k one has to consider the contribution of the 1 and 2 prong stars. An analysis of the 2 prong events shows that the

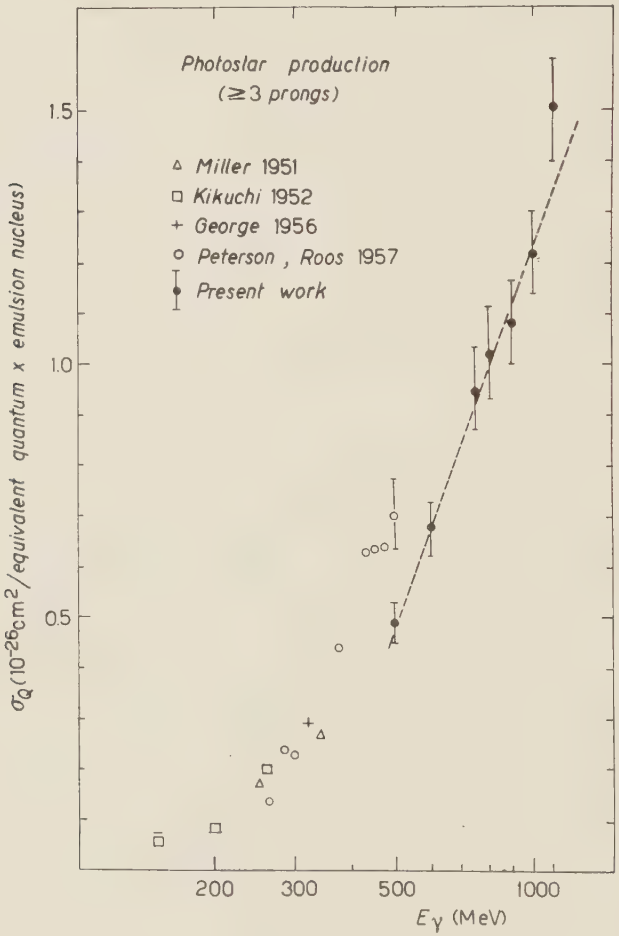

Fig. 2.

number of these to be attributed to scattering of a single track is negligible: over a carefully examined sample, we found 90% of sure stars, 9% of « probable » stars [4], and 1% of « probable » scatterings. The experimentally determined percentage of 2 prong stars is, according to our data, 35% of the 3 or more prong stars, at all energies.

As for the one prong stars, let us define the cross-section σ_{Q1} per equivalent quantum and per emulsion nucleus for production of 1 prong stars. A somewhat difficult experimental determination of σ_{Q1} has been carried out at various

energies. Within the experimental errors σ_{Q1} turns out to be practically independent of energy. If it were exactly so, then equation (3) would show the corresponding cross-section per quantum to be zero: $\sigma_{Q1} = 0$. In that case all the—rather frequent—one prong stars ought to be attributed to the giant resonance and quasi-deuteron low-energy processes. Our experimental errors allow the possibility for some increase of σ_{Q1} with energy, but the estimated contribution to the total cross-section per quantum is in any case less than some 10%. We will ignore this supposed contribution in the final calculation.

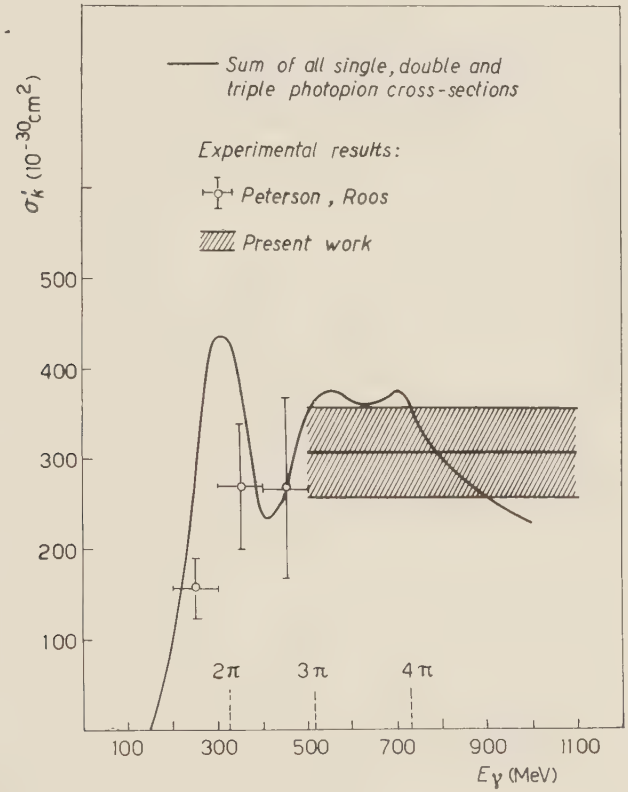

Fig. 3.

Our data then show that σ_k should be constant over the energy interval considered, and for the production of 1 or more prong photostars is equal to $\sigma_k = (146 \pm 22) \cdot 10^{-28}$ cm^2/nucleus. For the interpretation of this result, it is convenient to express it per nucleon rather than per nucleus. In this way one obtains

(4) $$\sigma'_k = (306 \pm 60) \cdot 10^{-30} \text{ cm}^2/\text{nucleon} \qquad 500 \leqslant k \leqslant 1100 \text{ MeV}.$$

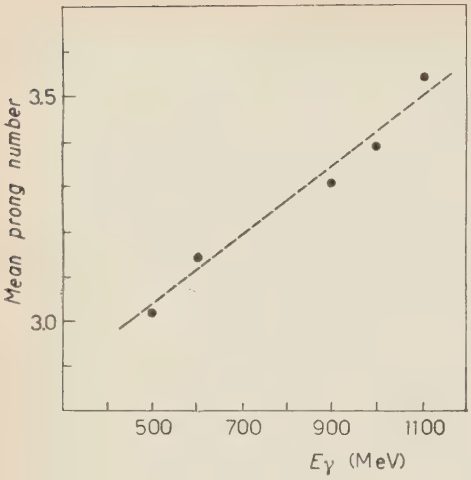

Fig. 4.

Fig. 3 shows our result, as a straight line, and those of previous authors at lower energies. The error band shown is limited by the maximum and minimum slopes of the straight lines which can be fitted within the experimental errors in Fig. 2. Multiple photopion thresholds are also indicated.

Fig. 4 shows the mean number of prongs as a function of peak bremsstrahlung energy. It is seen that this number increases steadily with energy.

4. – WILSON (7) suggested that the photostar production process at hig energies consists of the photoproduction of pions on the nucleon, and the subsequent absorption of these pions by the nucleus. An optical model calculation for σ_k' as a function of the mean cross-section for photoproduction of charged and neutral pions in hydrogen has been carried out by REFF (8), with the absorption mean free path λ for pions in nuclear matter as a parameter. An upper limit to σ_k' is obviously obtained by putting $\lambda = 0$, which is equivalent to assume that all pions are reabsorbed, and by neglecting the effects of the binding of the nucleons in the nucleus.

We have calculated σ_k' using the experimental values of the photoproduction cross-sections known up to now, and using, for the single pion photoproduction the data of BERNARDINI (9), while for the double and triple photoproduction we have used to the data of SELLEN *et al.* (10). The resulting curve is shown in Fig. 3. As it is seen the experimental values of σ_k' are in good agreement with the curve. It is to be noted that the agreement gets better if, as PETERSON suggested (11), one takes into account the motion of the nucleons within the emulsion nuclei, thus smoothing out the curve. It is to be equally noted that the experimental value of σ_k' is slightly higher than this theoretical prediction, which constitutes, as said before, the limiting case of the model.

(7) R. R. WILSON: *Phys. Rev.*, **86**, 125 (1952).
(8) I. REFF: *Phys. Rev.*, **91**, 150 (1953).
(9) G. BERNARDINI: *Kiev Conference* (1959).
(10) J. M. SELLEN, G. COCCONI, V. T. COCCONI and E. L. HART: *Phys. Rev.*, **113**, 1323 (1959).
(11) V. Z. PETERSON: private communication.

However, the rather large cross-section, especially at high energies (1000 ÷ 1100 MeV) could be an indication of higher multiplicities in the pion production contributing to the photostar process. This last point would find support in the steady rise of the mean prong number with increasing energy, as shown in Fig. 4.

* * *

Thanks are due to Prof. G. CORTINI for his continuous help throughout this work; to Dr. V. Z. PETERSON for some fruitful discussion and private communications on the work done at Cal Tech by PETERSON and ROOS up to 1150 MeV (to be published); to the Frascati electron-synchrotron staff for providing all exposure facilities; to the scanning team, and in particular to Dr. A. CELANO for her disinterested contributions.

RIASSUNTO

Si presentano i risultati ottenuti sulla fotoproduzione di stelle in emulsioni nucleari irraggiate con raggi γ di bremsstrahlung di energia massima compresa tra 500 e 1100 MeV. Vengono calcolate le sezioni d'urto per quanto equivalente e per fotone. I risultati vengono confrontati con quelli di precedenti autori ad energie inferiori e con quelli deducibili dai valori noti per fotoproduzione singola o multipla di π, e si trova un buon accordo.

IL NUOVO CIMENTO Vol. XVI, N. 4 16 Maggio 1960

One-Particle Singularities of Green's Functions in Quantum Field Theory - II.

W. Zimmermann

Institut für theoretische Physik der Universität - Hamburg
CERN - Geneva

(ricevuto il 27 Gennaio 1960)

Summary. — The time ordered Green's functions are expanded with respect to the singularities arising from intermediate one-particle states.

Introduction.

In a preceding paper (1) the one-particle singularities of Green's functions in quantum field theory have been investigated. It has been shown

i) that the Fourier transform $\tau(p_1, ..., p_n)$ of the τ-function $\langle TA(x_1)...A(x_n)\rangle_0$ has a pole along

$$q^2 = -m^2$$

for any $q = p_{\alpha_1}+...+p_{\alpha_r}$ if m is a discrete mass of the system;

ii) that the residuum of this pole is a product of two τ-functions.

The results will be applied here in order to expand the τ-functions with respect to the singularities

$$(q_1^2 + m^2 - i\varepsilon)^{-1} ... (q_l^2 + m^2 - i\varepsilon)^{-1} \qquad \varepsilon \to +0,$$

where q_i denote arbitrary partial sums of the momenta $p_1, ..., p_n$. The residua of these singularities will turn out to be either zero or products of $r-1$ factors. So the expansion expresses the complete structure of the one-particle singularities of an arbitrary τ-function.

(1) W. Zimmermann: *Nuovo Cimento*, **13**, 503 (1959), in the following quoted as I.

In Section 1 the general assumptions and results of I are summarized so far as needed in this paper. For a model of one scalar field and one discrete mass the expansion of $\tau(p_1, ..., p_n)$ with respect to the one-particle singularities is derived in Section 2. Examples for $n = 3$, 4 and 5 are given in Section 3. In Section 4 is demonstrated how to generalize to the case of several masses, including bound states: the τ-functions corresponding to various two-particle scattering processes are considered for the model of a neutral and a charged scalar field having one stable bound state of charge two.

We finally mention two possible applications to the S-matrix theory not being considered in this paper. The first application refers to the physical domain of the S-matrix elements. The one-particle structure of $\tau(p_1, ..., p_n)$ leads to certain relations among S-matrix elements first found by M. FIERZ [2] as a characteristic property of causal S-matrices. For details we refer to [2] and to the investigations by V. GLASER [3].

The second application concerns the unphysical domain of S-matrix elements. In the two-particle scattering amplitude, for instance, no one-particle singularity occurs so long as the momenta are real four vectors (physical domain). By analytical continuation into the unphysical domain, however, one-particle poles should be reached. A report on this program has been given by CHEW and LOW [4]. Further references are contained in that paper.

1. – General results of part I.

In this section we repeat some of the definitions and results given in I so far as necessary for the investigations that follow.

We consider the model of one scalar field $A(x)$ with one discrete mass m. The field operator is assumed to be invariant, causal, complete, etc. Asymptotic field operators $B^{\text{out}}_{\text{in}}(x; \xi_1 ... \xi_{r-1})$ are defined by

$$(1) \qquad B^{\text{out}}_{\text{in}}(x; \xi_1 ... \xi_{r-1}) = B(x; \xi_1 ... \xi_{r-1}) + \int dx' \, \Delta^{\text{Adv}}_{\text{Ret}}(m, x - x') j(x'; \xi_1 ... \xi_{r-1}),$$

with

$$B(x; \xi_1 ... \xi_{r-1}) = TA(x_1) ... A(x_r), \qquad r \geqslant 1$$

$$j(x; \xi_1 ... \xi_{r-1}) = (\Box_x - m^2) B(x; \xi_1 ... \xi_{r-1}),$$

$$x = \frac{1}{r}(x_1 + ... + x_r),$$

$$\xi_i = x_i - x_{i+1}; \qquad i = 1, ..., r-1.$$

---

[2] M. FIERZ: *Helv. Phys. Acta.* **23**, 731 (1950).

[3] V. GLASER: private communication.

[4] G. F. CHEW and F. E. LOW: *Phys. Rev.*, **113**, 1640 (1959).

For the Fourier transform of $B^{\text{out}}_{\text{in}}$ we introduce the notation

$$\delta(q^2+m^2)\,\tilde{B}_{\substack{\text{out}\\\text{in}}}(q;\,\xi_1 \dots \xi_{r-1}) = \frac{1}{(2\pi)^{\frac{5}{2}}}\int \mathrm{d}x\, \exp\,[-iqx]\, B_{\substack{\text{out}\\\text{in}}}(x;\,\xi_1 \dots \xi_{r-1})\,.$$

Investigating the one-particle singularities of the τ-function [5]

$$\delta(p_1+\dots+p_n)\,\tau_n(p_1 \dots p_n) = \tag{2}$$
$$= \frac{1}{(2\pi)^{5n/2}}\int \mathrm{d}x_1 \dots \int \mathrm{d}x_n\, \exp\,[-i(p_1x_1+\dots+p_nx_n)]\,\langle TA(x_1)\dots A(x_n)\rangle_0\,,$$

we obtained in I the following results:

i) for $q = p_1+\dots+p_r$ the relation

$$\tau(p_1,\dots,p_n) = \lim_{\varepsilon\to+0}\frac{\{(q^2+m^2)\,\tau(p_1,\dots,p_n)\}}{q^2+m^2-i\varepsilon}\,, \tag{3}$$

holds. Due to the (assumed) existence of the asymptotic operators (1) the residuum $(q^2+m^2)\,\tau(p_1,\dots,p_n)$ is finite [6] for $q^2=-m^2$ as follows from (see I, eq. (33)):

$$\int \mathrm{d}x\, \exp\,[-iqx]\, K_x\langle TA(x_1)\dots A(x_n)\rangle_0\,|_{q^2=-m^2} = \tag{4}$$
$$= i(2\pi)^{\frac{3}{2}}\{\langle \tilde{B}_{\text{out}}(q;\,\xi_1\dots\xi_{r-1})\,TA(x_{r+1})\dots A(x_n)\rangle_0 +$$
$$+ \langle TA(x_{r+1})\dots A(x_n)\,\tilde{B}_{\text{in}}(q;\,\xi_1\dots\xi_{r-1})\rangle_0\}\,.$$

ii) In case of $2\leqslant r\leqslant n-2$ this leads to the product relation [7,8] (see I, eq. (35)):

$$(q^2+m^2)\,\tau_n(p_1,\dots,p_n)|_{q^2=-m^2} = \tag{5}$$
$$= 2\pi i\{(q^2+m^2)\,\tau_{r+1}(p_1,\dots,p_r,-q)\}\,\{(q^2+m^2)\,\tau_{n-r+1}(p_{r+1},\dots,p_n,q)\}\,.$$

(5) $\langle\,\rangle_0$ denotes the vacuum expectation value.

(6) By finite we mean that $(q^2+m^2)\tau_n(p_1\dots p_n)$ is a well defined « distribution » in the remaining variables when q^2 is set equal to $-m^2$.

(7) Provided that $A(x)$ is properly normalized.

(8) In the derivation of (5) causality has been used, for instance, in order to justify that

$$\int \mathrm{d}x \int \mathrm{d}z\, \exp\,[-i(px+qz)]\, K_xK_y\, TA(x_1)\dots A(x_r)\,A(z) =$$
$$= \int \mathrm{d}z \int \mathrm{d}x\, \exp\,[-i(px+qz)]\, K_xK_y\, TA(x_1)\dots A(x_r)\,A(z)$$

for $\qquad x=\frac{1}{r}(x_1+\dots+x_r), \qquad p^2=q^2=-m^2\,.$

In general one has for any partial sum

$$q = p_{\alpha_1} + \ldots + p_{\alpha_r}$$

of the basic momenta $p_1, \ldots, p_n$ the two relations

$$\tau_n(p_1, \ldots, p_n) = \lim_{\varepsilon \to +0} \frac{\{(q^2 + m^2)\, \tau_n(p_1, \ldots, p_n)\}}{q^2 + m^2 - i\varepsilon}\,, \tag{6}$$

$$(q^2 + m^2)\, \tau_n(p_1, \ldots, p_n) = 2\pi i \,\{(q^2 + m^2)\, \tau_{r+1}(p_{\alpha_1} \ldots p_{\alpha_r}, -q)\} \cdot \cdot \{(q^2 + m)\, \tau_{n-r+1}(p_{\alpha_{r+1}} \ldots p_{\alpha_n}, q)\} \qquad \text{if } 2 \leqslant r \leqslant n-2\,. \tag{7}$$

2. – Expansion of τ-functions with respect to one-particle singularities.

Relation (7) indicates a certain product structure of τ_n which we now study in more detail. We first remove from τ_n all the singularities $\delta(p_{\alpha_1} + \ldots + p_{\alpha_r})$ and $(p_i^2 + m^2 - i\varepsilon)^{-1}$ by forming [9]

$$\eta_n'(p_1, \ldots, p_n) = (p_1^2 + m^2) \ldots (p_n^2 + m^2)\, \eta_n(p_1, \ldots, p_n) \qquad p_1 + \ldots + p_n = 0\,, \tag{8}$$

where η_n is defined [10] recursively by eq. (I.14). As is well known, these functions η_n' give the S-matrix elements when all p_i are taken on the energy shell.

In terms of η_n' the two basic relations (6) and (7) are

$$\eta_n'(p_1, \ldots, p_n) = \lim_{\varepsilon \to +0} \frac{\{(q^2 + m^2)\, \tau(p_1, \ldots, p_n)\}}{q^2 + m^2 - i\varepsilon}\,, \tag{9}$$

$$(q^2 + m^2)\, \eta_n'(p_1, \ldots, p_n) = 2\pi i\, \eta_{r+1}'(p_{\alpha_1} \ldots p_{\alpha_r}, -q)\, \eta_{n-r+1}'(p_{\alpha_{r+1}} \ldots p_{\alpha_n}, q) \tag{10}$$

for

$$q = p_{\alpha_1} + \ldots + p_{\alpha_r}\,, \qquad 2 \leqslant r \leqslant n-2\,,$$

if $q^2 = -m^2$.

All possible momentum squares q^2 are obtained by forming

$$q^2_{\alpha_1 \ldots \alpha_r} = \Big(\sum_{\nu=1}^{r} p_{\alpha_\nu}\Big)^2\,, \qquad 1 \leqslant \alpha_i \leqslant n-1\,, \quad 2 \leqslant r \leqslant n-2\,,$$

[9] The τ-function can be reobtained from η' by the formula (see I, eq. (26))

$$\eta_n(p_1 \ldots p_n) = \lim_{\varepsilon \to +0} \frac{\eta_n'(p_1 \ldots p_n)}{(p_1^2 + m^2 - i\varepsilon) \ldots (p_n^2 + m^2 - i\varepsilon)}\,.$$

[10] In perturbation theory η_n represents all those contributions to τ_n which come from simply connected Feynman graphs.

for any partial sum $q_{\alpha_1 \ldots \alpha_r}$ of the $n-1$ independent four vectors $p_1, \ldots, p_{n-1}$. Accordingly we write η_n' as a function [11] of $p_1^2, \ldots, p_n^2$ and all $q^2_{\alpha_1 \ldots \alpha_r}$

$$\eta_n' = \eta_n'(p_1^2, \ldots, p_n^2, q_{12}^2, \ldots, q_{ij}^2, \ldots, q_{ijk}^2, \ldots) .$$

We consider η_n' as defined only for those values of p_i^2, $q^2_{(\alpha)}$ which can be obtained by inserting *real* four vectors for p_i. Then only $\binom{n}{2}$ of the coordinates p_i^2, q^2 are independent.

From the relations (9), (10) we know that η_n' can have poles when one of the variables $q^2_{(\alpha)}$ is on the mass shell $q^2_{(\alpha)} = m^2$. η_n' will further have multiple poles of the form

$$(q^2_{(\beta_1)} + m^2 - i\varepsilon)^{-1} \ldots (q^2_{(\beta_\tau)} + m^2 - i\varepsilon)^{-1} , \qquad \varepsilon \to +0 ,$$

when the squares of the τ momenta

$$\begin{aligned} q_{(\beta_1)} &= q_{\beta_{11}\beta_{12}} \ldots = p_{\beta_{11}} + p_{\beta_{12}} + \ldots \\ q_{(\beta_2)} &= q_{\beta_{21}\beta_{22}} \ldots = p_{\beta_{21}} + p_{\beta_{22}} + \ldots \\ &\ldots\ldots\ldots\ldots \\ q_{(\beta_\tau)} &= q_{\beta_{\tau 1}\beta_{\tau 2}} \ldots = p_{\beta_{\tau 1}} + p_{\beta_{\tau 2}} + \ldots \end{aligned}$$

are on the mass shell. One would expect that η_n' can be expanded with respect to these singularities

$$\eta_n' = \lambda_n + \sum_{\tau} \sum_{(\beta_1)\ldots(\beta_\tau)} \frac{\lambda_{n;(\beta_1)\ldots(\beta_\tau)}}{(q^2_{(\beta_1)} + m^2 - i\varepsilon) \ldots (q^2_{(\beta_\tau)} + m^2 - i\varepsilon)} , \qquad \varepsilon \to +0 . \tag{11}$$

where

a) the coefficients $\lambda_{n;(\beta_1)\ldots(\beta_\tau)}$ do not depend on the variables $q^2_{(\beta_1)}, \ldots, q^2_{(\beta_\tau)}$ appearing in the denominator;

b) λ_n as well as $\lambda_{n;(\beta_1)\ldots(\beta_\tau)}$ are regular when one or more of the variables are on the mass shell.

We now want to prove the possibility of the expansion (11) and to determine the coefficients. That will be done in two steps. We first *define* functions λ_n and study their properties. We then express η_n' in terms of the λ-functions, which automatically leads to the desired expansion.

[11] As an invariant function without singularities $\delta(p_{\alpha_1} + \ldots + p_{\alpha_r})$ the function η_n' depends only on the squares p_i^2 and the products $p_i p_j$ of $n-1$ independent four vectors.

We start defining λ_n by

$$\lambda_n = \eta'_n + \sum_\tau (-1)^\tau \sum_{(\beta_1)\dots(\beta_\tau)} \frac{\eta_{n;(\beta_1)\dots(\beta_\tau)}}{(q^2_{(\beta_1)} + m^2 - i\varepsilon \ \dots \ (q^2_{(\beta_\tau)} + m^2 - i\varepsilon)}\,, \qquad \varepsilon \to +0\,, \tag{12}$$

Here $\eta'_{n;(\alpha_1)\dots(\alpha_\sigma)}$ denotes

$$\eta'_{n;(\alpha_1)\dots(\alpha_\sigma)} = (q^2_{(\alpha_1)} + m^2) \dots (q^2_{(\alpha_\sigma)} + m^2)\, \eta\,|_{q^2_{(\alpha_1)} = \dots = q^2_{(\alpha_\sigma)} = -m^2} \tag{13}$$

for

$$q^2_{(\alpha_1)} = \dots = q^2_{(\alpha_\sigma)} = -m^2\,.$$

$\eta'_{n;(\alpha_1)\dots(\alpha_\sigma)}$ is a function of the p_i^2 and of the $q^2_{(\alpha)}$, except for $q^2_{(\alpha_1)}, \dots, q^2_{(\alpha_\sigma)}$. Sometimes it is more convenient to write $\eta'_{n;(\alpha_1)\dots(\alpha_\sigma)}$ as a function

$$\eta'_{n;(\alpha_1)\dots(\alpha_\sigma)} = \eta'_{n;(\alpha_1)\dots(\alpha_\sigma)}(p_1, \dots, p_n)$$

of the n four-vectors p_i restricted by

$$p_1 + \dots + p_n = 0\,,$$
$$(p_{\alpha_{i1}} + p_{\alpha_{i2}} + \dots)^2 = -m^2\,, \qquad i = 1, \dots, \sigma.$$

It is easy to see that λ_n is regular when one or several of the variables are on the mass shell. We consider for instance the dependence on $q^2_{(\alpha)}$ and show that λ_n has no singularities $P(q^2_{(\alpha)}+m^2)^{-2}$ of $\delta(q^2_{(\alpha)}+m^2)$. We have [12]

$$\lambda_n = \eta'_n + \sum_\tau (-1)^\tau \sum_{(\beta_1)\dots(\beta_\tau)} \frac{\eta'_{n;(\beta_1)\dots(\beta_\tau)}}{(q^2_{(\beta_1)} + m^2 - i\varepsilon) \dots (q^2_{(\beta_\tau)} + m^2 - i\varepsilon)} =$$
$$= \eta'_n - \frac{\eta'_{n;(\alpha)}}{q^2_{(\alpha)} + m^2 - i\varepsilon} + \sum_\tau (-1)^\tau \sum'_{(\beta_1)\dots(\beta_\tau)} \frac{\eta'_{n;(\beta_1)\dots(\beta_\tau)}}{(q^2_{(\beta_1)} + m^2 - i\varepsilon) \dots (q^2_{(\beta_\tau)} + m^2 - i\varepsilon)} -$$
$$- \sum_\tau (-1^\tau) \sum'_{(\beta_1)\dots(\beta_\tau)} \frac{\eta'_{n;(\alpha)(\beta_1)\dots(\beta_\tau)}}{(q^2_{(\alpha)} + m^2 - i\varepsilon)(q^2_{(\beta_1)} + m^2 - i\varepsilon) \dots (q^2_{(\beta_\tau)} + m^2 - i\varepsilon)}\,,$$

where the sum $\sum'$ is taken over all $(\beta_1), \dots, (\beta_\tau)$ which are different from (α). Using relation (9), we obtain

$$\lambda_n = \frac{(q^2_{(\alpha)} + m^2)\eta'_n - \eta'_{n;\alpha}}{q^2_{(\alpha)} + m^2 - i\varepsilon} +$$
$$+ \sum_\tau (-1)^\tau \sum'_{(\beta_1)\dots(\beta_\tau)} \frac{(q^2_{(\alpha)} + m^2)\eta'_{n;(\beta_1)\dots\beta_\tau)} - \eta'_{n;(\alpha)(\beta_1)\dots(\beta_\tau)}}{(q^2_{(\alpha)} + m^2 - i\varepsilon)(q^2_{(\beta_1)} + m^2 - i\varepsilon) \dots (q^2_{(\beta_\tau)} + m^2 - i\varepsilon)}\,. \tag{14}$$

[12] In all following formulae the limit $\varepsilon \to +0$ has to be taken.

This relation shows that λ_n has no singularities of the form $\delta(q^2_{(\alpha)}+m^2)$ because

$$(q^2_{(\alpha)}+m^2)\eta'_n=\eta'_{n;(\alpha)}\,,\qquad (q^2_{(\alpha)}+m^2)\eta'_{n;(\beta_1)\dots(\beta_\tau)}=\eta'_{n;(\alpha)(\beta_1)\dots(\beta_\tau)}\,.\qquad \text{for } q^2_{(\alpha)}=-m^2\,.$$

There are also no poles $P(q^2_{(\alpha)}+m^2)^{-1}$, because

$$(q^2_{(\alpha)}+m^2)\lambda_n|_{q^2_{(\alpha)}=-m^2}=0$$

follows from (14).

We can show further that λ_n is finite ([13]) for $q^2_{(\alpha)}=-m^2$ if we assume that the derivative

$$\frac{\partial}{\partial q^2_{(\alpha)}}\{(q^2_{(\alpha)}+m^2)\eta'_n\}|_{q^2_{(\alpha)}=-m^2}$$

is continuous at $q^2_{(\alpha)}=-m^2$. Then it follows from (14)

$$\lambda_n|_{q^2_{(\alpha)}=-m^2}=F+\sum_\tau(-1)^\tau\sum'_{(\beta_1)\dots(\beta_\tau)}\frac{F_{(\beta_1)\dots(\beta_\tau)}}{(q^2_{(\beta_1)}+m^2-i\varepsilon)\dots(q^2_{(\beta_\tau)}+m^2-i\varepsilon)}\,,$$

with

$$F=\frac{\partial}{\partial q^2_{(\alpha)}}\{(q^2_{(\alpha)}+m^2)\eta'_n\}|_{q^2_{(\alpha)}=-m^2}\,,$$

$$F_{(\beta_1)\dots(\beta_\tau)}=(q^2_{(\beta_1)}+m^2)\dots(q^2_{(\beta_\tau)}+m^2)F|_{q^2_{(\beta_1)}=\dots=q^2_{(\beta_\tau)}=-m^2}\,.$$

The right hand side of (12) can be simplified considerably by using the product relation (10). Thus we obtain

$$\eta'_{n;(\alpha_1\dots\alpha_r)}(p_1,\dots,p_n)=2\pi i\,\eta'_{r+1}(p_{\alpha_1},\dots,p_{\alpha_r},-q_{\alpha_1\dots\alpha_r})\cdot \tag{15}$$

$$\cdot\eta'_{n-r+1}(p_{\alpha_{r+1}}\dots p_{\alpha_{n-1}}p_n q_{\alpha_1\dots\alpha_r})\qquad (q^2_{\alpha_1\dots\alpha_r}=-m^2)$$

i.e. $\eta'_{n;(\alpha_1\dots\alpha_r)}$ is a product of two η'-functions with $r+1$ and $n-r+1$ variables. The first factor depends only on the variables $q^2_{\beta_1\dots\beta_s}$ (except $q^2_{\alpha_1\dots\alpha_r}$) with each β_μ being one of the indices $(\alpha_1,\dots,\alpha_r)$. The second factor depends only on the variables $q^2_{\beta_1\dots\beta_s}$ and $(q_{\beta_1\dots\beta_s}+p_n)^2$ (except $(q_{\alpha_{r+1}\dots\alpha_{n-1}}+p_n)^2$) with each β_i

([13]) *I.e.* λ_n is a defined « distribution » in the remaining variables when $q^2_{(\alpha)}=-m^2$.

being one of the indices $(\alpha_{r+1}, \ldots, \alpha_{n-1})$. Hence the function $\eta'_{n;(\alpha_1 \ldots \alpha_r)}$ depends only on those variables [14] $q^2_{\beta_1 \ldots \beta_s}$ belonging to one of the three groups:

i) $q_{\beta_1 \ldots \beta_s}$ is a partial sum of $q_{\alpha_1 \ldots \alpha_r}$, *i.e.* p_{β_i} occurs in $(p_{\alpha_1}, \ldots, p_{\alpha_r})$ and $s < r$;

ii) the partial sums $q_{\alpha_1 \ldots \alpha_r}$ and $q_{\beta_1 \ldots \beta_s}$ have no common summand, *i.e.* $\alpha_\nu \neq \beta_\mu$ for any ν, μ;

iii) $q_{\alpha_1 \ldots \alpha_r}$ is a partial sum of $q_{\beta_1 \ldots \beta_s}$.

As a consequence of this result

$$\eta'_{n;(\alpha_1 \ldots \alpha_r)(\beta_1 \ldots \beta_s)} = (q^2_{\beta_1 \ldots \beta_s} + m^2)\, \eta'_{n;(\alpha_1 \ldots \alpha_r)} \big|_{q^2_{\beta_1 \ldots \beta_s} = -m^2}$$

vanishes identically when $q_{\beta_1 \ldots \beta_s}$ does not satisfy one of the conditions i), ii) or iii). In any other case, however, $q^2_{\beta_1 \ldots \beta_s}$ appears as co-ordinate in one of the factors of $\eta'_{n;(\alpha_1 \ldots \alpha_r)}$: Hence the product relation can be applied again and leads to a product of three η'-functions for $\eta'_{n;(\alpha_1 \ldots \alpha_r)(\beta_1 \ldots \beta_s)}$.

We now want to determine $\eta'_{n;(\alpha_1) \ldots (\alpha_\sigma)}$ for an arbitrary set of momenta $q_{(\alpha_1)}, \ldots, q_{(\alpha_\sigma)}$. We call $q_{(\alpha_1)}, \ldots, q_{(\alpha_\sigma)}$ a normal system when between any two $q_{(\alpha_i)}$, $q_{(\alpha_j)}$ one of the three relations i), ii) or iii) holds. Repeated application of the product relation (10) leads to the result that $\eta'_{n;(\alpha_1) \ldots (\alpha_\sigma)}$ is a product of $\sigma+1$ η'-functions when the $q_{(\alpha_1)}, \ldots, q_{(\alpha_\sigma)}$ form a normal system. When the $q_{(\alpha_1)}, \ldots, q_{(\alpha_\sigma)}$ do not form a normal system, however, $\eta'_{n;(\alpha_1) \ldots (\alpha_\sigma)}$ vanishes identically. For formulating precisely the product structure of an arbitrary $\eta_{n;(\alpha_1) \ldots (\alpha_\sigma)}$ it is convenient to use some combinatorial tools which we introduce now. To an arbitrary normal system $q_{(\alpha_1)}, \ldots, q_{(\alpha_\sigma)}$ we attribute a Feynman graph of the following type:

a) the graph has n external lines, corresponding to the basic momenta $p_1, \ldots, p_n$;

b) the graph has σ internal lines, corresponding to the partial sums $q_{(\alpha_i)}$;

c) the graph is simply connected and has no closed loops. The number of vertices is $\sigma+1$.

---

[14] In general these variables are not independent from each other. As the first factor of $\eta'_{n;(\alpha_1 \ldots \alpha_r)}$ depends on $\binom{r+1}{2} - 1$ and the second factor on $\binom{n-r+1}{2} - 1$ independent variables only $\binom{r+1}{2} + \binom{n-r+1}{2} - 2$ among the $q^2_{\beta_1 \ldots \beta_s}$ are independent.

Given an arbitrary normal system $q_{(\varkappa_1)}, \ldots, q_{(\varkappa_\sigma)}$ we define the corresponding graph by the following construction. We start drawing the external line p_n which leads to a vertex denoted by V_0. Let $q_{(\beta_1)}, \ldots, q_{(\beta_\tau)}$ denote the maximal elements within the system $q_{(\alpha_1)}, \ldots, q_{(\alpha_\sigma)}$; by maximal elements we mean those $q_{(\varkappa_i)}$ which are *not* partial sums of any other $q_{(\varkappa_j)}$ of the system. Let further $p_{b_1}, \ldots, p_{b_t}$ denote all basic momenta $(1 \leqslant b_i \leqslant n-1)$ which do not occur in any one of the maximal $q_{(\beta_i)}$. Then we draw from the vertex V_0 the internal lines $q_{(\beta_1)}, \ldots, q_{(\beta_\tau)}$ and the external lines $p_{b_1}, \ldots, p_{b_t}$.

We proceed constructing the graph as follows. Each internal line $q_{(\beta_i)}$ connects V_0 with another vertex V_{0i}. Let $q_{(\beta_{i1})}, q_{(\beta_{i2})}, \ldots$ denote all maximal elements among the partial sums of $q_{(\beta_i)}$. Let further $p_{b_{i1}}, p_{b_{i2}}, \ldots$ denote all momenta occurring in the sum $q_{(\beta_i)}$ but not occurring in any $q_{(\beta_{ij})}$. Then we draw from the vertex V_{0i} the internal lines $q_{(\beta_{i1})}, q_{(\beta_{i2})}, \ldots$ and the external lines $p_{b_{i1}}, p_{b_{i2}} \ldots$.

Proceeding in this way until any p_i is used up we finally obtain a Feynman graph of the described type. Apparently there is a one-to-one correspondence between the normal systems of partial sums from $n-1$ vectors and the Feynman graphs satisfying *a*), *b*) and *c*).

In terms of the defined graphs it is now easy to formulate the explicit product form of $\eta'_{n;(\alpha_1)\ldots(\alpha_\sigma)}$ when $q_{(\alpha_1)}, \ldots, q_{(\alpha_\sigma)}$ is an arbitrary system. It is

$$\eta'_{n;(\alpha_1)\ldots(\alpha_\tau)}(p_1, \ldots, p_n) = (2\pi i)^\tau \prod_{\nu=1}^{\tau+1} \eta_{n_\nu}(u_{\nu 1} u_{\nu 2} \ldots u_{\nu n_\nu})\big|_{q^2_{(\alpha_1)} = \ldots = q^2_{(\alpha_\tau)} = -m^2} \tag{16}$$

where each factor $\eta_{n\nu}$ corresponds to a vertex V_ν of the graph corresponding to $q_{(\alpha_1)}, \ldots, q_{(\alpha_\sigma)}$: n_ν is the number of lines joining at V_ν. The variables $u_{\nu 1}, \ldots, u_{\nu n_\nu}$ denote (up to a sign) the momenta attributed to the lines joining at V_ν. The sign of the $u_{\nu i}$ has to be taken appropriately so that $\sum_{i=1}^{n} u_{\nu i} = 0$: all external and internal $u_{\nu i}$ get a positive sign, except that internal $u_{\nu j}$ which contains the other internal $u_{\nu i}$ as partial sums. Finally all squares $q^2_{(\varkappa_i)}$ of internal momenta are set equal to $-m^2$.

Inserting this result into the definition of λ_n we obtain

$$\lambda_n = \eta'_n - \sum_G (-1)^\tau (2\pi i)^{\tau-1} \lim_{\varepsilon \to +0} \frac{\eta'_{n_1} \ldots \eta'_{n_\tau}}{(q^2_{(\beta_1)} + m^2 - i\varepsilon) \ldots (q^2_{(\beta_{\tau-1})} + m^2 - i\varepsilon)}, \tag{17}$$

$$(q^2_{(\beta_1)}, \ldots, q^2_{(\beta_{\tau-1})} \text{ are set equal to } -m^2 \text{ in } \eta'_{n_1}, \ldots, \eta'_{n_\tau}).$$

The sum $\sum_G$ is taken over all Feynman graphs satisfying *a*), *b*) and *c*). The product is constructed along the rules given to eq. (16). In addition we have to any internal line $q_{(\varkappa_i)}$ a Feynman propagator $(q^2_{(\varkappa_i)} + m^2 - i\varepsilon)^{-1}$ in (17).

Finally we will show that η'_n can be expanded in the form ([15])

$$\eta'_n = \lambda_n + \sum_G (2\pi i)^{\tau-1} \lim_{\varepsilon\to+0} \frac{\lambda_{n_1} \dots \lambda_{n\tau}}{(q^2_{(\beta_1)} + m^2 - i\varepsilon) \dots (q^2_{(\beta_{\tau-1})} + m^2 - i\varepsilon)}, \tag{18}$$

$$(q^2_{(\beta_1)}, \dots, q^2_{(\beta_{\tau-1})} \text{ are set equal to } -m^2 \text{ in } \eta'_{n_1}, \dots, \eta'_{n_\tau}).$$

when λ_n is given by (17). For the proof we assume that relation (18) is valid for all $n \leqslant m-1$ and derive (18) for $n = m$. Relation (17) gives

$$\eta'_m = \lambda_m + \sum_G (-1)^\tau (2\pi i)^{\tau-1} \lim_{\varepsilon\to+0} \frac{\eta'_{n_1} \dots \eta'_{n\tau}}{(q^2_{(\alpha_1)} + m^2 - i\varepsilon) \dots (q^2_{(\alpha_{\sigma-1})} + m^2 - i\varepsilon)}.$$

As $n_\lambda \leqslant m-1$ we may use relation (18) in order to express η'_{n_λ} by the λ-functions. We obtain the double sum

$$\eta'_m = \lambda_m + \sum_G (-1)^\tau \sum_{G' \supset G} (2\pi i)^{\sigma-1} \lim_{\varepsilon\to+0} \frac{\lambda_{n_1} \dots \lambda_{n\sigma}}{(q^2_{(\alpha_1)} + m^2 - i\varepsilon) \dots (q^2_{(\alpha_{\sigma-1})} + m^2 - i\varepsilon)},$$

where the summand corresponds to the graph G'. The sum $\sum_{G' \supset G}$ is taken over all graphs G' which can be obtained from G by inserting vertex parts. Collecting all terms of the double sum with the same denominator we get

$$\eta'_m = \lambda_m + \sum_G C_G (2\pi i)^{\sigma-1} \lim_{\varepsilon\to+0} \frac{\lambda_{n_1} \dots \lambda_{n\sigma}}{(q^2_{(\alpha_1)} + m^2 - i\varepsilon) \dots (q^2_{(\alpha_{\sigma-1})} + m^2 - i\varepsilon)},$$

where the multiplicity c_G is

$$c_G = (-1)^\tau + (-1)^{\tau-1} c_{G1} + (-1)^{\tau-2} c_{G2} + \dots + (-1)^2 c_{G,\tau-2}.$$

Here c_{Gi} denotes the number of all graphs with $\tau - i$ vertices from which G can be obtained by inserting vertex parts. It is

$$c_{Gi} = \binom{n-1}{i}$$

hence $c_G = 1$ for any graph G.

Relation (18) represents the desired expansion (11). We have seen that (18) is an identity when only λ_n is defined by (12). We finally have to check whether the coefficients of (18) satisfy the conditions *a*), *b*) which we have demanded in the beginning of this section. Condition *a*) is fulfilled because all $q^2_{(\alpha_i)}$ are set equal to $-m^2$ in the coefficient

$$\lambda_{n;(\alpha_1)\dots(\alpha_{\sigma-1})} = (2\pi i)^{\sigma-1} \lambda_{n_1} \dots \lambda_{n_\sigma}.$$

([15]) The notation in (18) is the same as in (16), (17).

That λ_n satisfies *b*) was already shown. Then *b*) is also true for the coefficients $\lambda_{n;(\alpha_1)\ldots(\alpha_{\sigma-1})}$ as they are either products of λ-functions or vanish identically.

3. – Examples.

For illustrating the general investigations of the last section let us consider the one-particle structure of η'-functions depending on 3, 4 and 5 variables. The η-functions are defined by (see I, eq. (14))

$$
(19)\qquad \begin{cases} \eta(x_1x_2x_3) = \langle TA(x_1)\,A(x_2)\,A(x_3)\rangle_0\,, \\ \eta(x_1x_2x_3x_4) = \langle TA(x_1)\,A(x_2)A(x_3)A(x_4)\rangle_0 - \langle TA(x_1)A(x_2)\rangle_0\langle TA(x_3)A(x_4)\rangle_0 - \\ \qquad\qquad - \text{perm. terms}\,, \\ \eta(x_1\ldots x_5) = \langle TA(x_1)\ldots A(x_5)\rangle_0 - \langle TA(x_1)\,A(x_2)\,A(x_3)\rangle_0\langle TA(x_4)\,A(x_5)\rangle_0 - \\ \qquad\qquad - \text{perm. terms}\,. \end{cases}
$$

Apart from a δ-function the Fourier transforms depend only on the squares and inner products of the independent variables:

$$
(20)\qquad \delta(p_1+p_2+p_3)\,\eta_3(p_1^2,\,p_2^2,\,p_1p_2) = \\ = \frac{1}{(2\pi)^{15/2}}\int \mathrm{d}x_1\,\mathrm{d}x_2\,\mathrm{d}x_3\,\exp\left[-i(p_1x_1+p_2x_2+p_3x_3)\right]\eta(x_1x_2x_3)\,,
$$

(corresponding for η_4, η_5). The variables p_i^2, $q_{(ij)}^2$ used in the last section will here be denoted by

$$
\begin{aligned} n=3:\quad & p_1^2,\ p_2^2,\ p_3^2, \\ n=4:\quad & p_1^2,\ p_2^2,\ p_3^2,\ p_4^2, \\ & q_{12}^2,\ q_{23}^2,\ q_{13}^2\,. \qquad\qquad q_{ij}=p_i+p_j, \\ n=5:\quad & p_1^2,\ p_2^2,\ p_3^2,\ p_4^2,\ p_5^2, \\ & q_{12}^2,\ q_{13}^2,\ q_{14}^2,\ q_{23}^2,\ q_{24}^2,\ q_{34}^2, \qquad\qquad q_{ijk}=p_i+p_j+p_k\,, \\ & q_{15}^2=q_{234}^2,\ q_{25}^2=q_{341}^2,\ q_{35}^2=q_{124}^2,\ q_{51}^2=q_{123}^2\,. \end{aligned}
$$

In these variables we write the functions η_3', η_4' and η_5' (which are defined by eq. (8))

$$
(21)\qquad \begin{cases} \eta_3'(p_1^2p_2^2p_3^2) = (p_1^2+m^2)(p_2^2+m^2)(p_3^2+m^2)\,\eta_3(p_1^2,\,p_2^2\,,\,p_1p_2)\,, \\ \eta_4'(p_1^2p_2^2p_3^2p_4^2q_{12}^2q_{13}^2q_{23}^2) = (p_1^2+m^2)\ldots(p_4^2+m^2)\,\eta_4(p_1^2,\ldots,p_1p_2\ldots)\,, \\ \eta_5'(p_1^2\ldots p_5^2q_{12}^2\ldots q_{45}^2) = (p_1^2+m^2)\ldots(p_5^2+m^2)\,\eta_5(p_1^2,\ldots,p_1p_2\ldots)\,, \end{cases}
$$

According to (12), (17) we define λ-functions by

$$\lambda_3(p_1^2 p_2^2 p_3^2) = \eta_3'(p_1^2 p_2^2 p_3^2)\,, \tag{22a}$$

$$\begin{aligned}\lambda_4(p_1^2 \dots p_4^2 q_{12}^2 q_{13}^2 q_{23}^2) = \eta_4'(p_1^2 \dots p_4^2 q_{12}^2 q_{13}^2 q_{23}^2) - \\ - \lim_{\varepsilon\to+0} 2\pi i \frac{\eta_3'(p_1^2,\, p_2^2,\, -m^2)\,\eta_3'(-m^2,\, p_3^2,\, p_4^2)}{q_{12}^2 + m^2 - i\varepsilon} - \\ - \lim_{\varepsilon\to+0} 2\pi i \frac{\eta_3'(p_1^2,\, p_3^2,\, -m^2)\,\eta_3'(-m^2,\, p_2^2,\, p_4^2)}{q_{12}^2 + m^2 - i\varepsilon} - \\ - \lim_{\varepsilon\to+0} 2\pi i \frac{\eta_3'(p_2^2,\, p_3^2,\, -m^2)\,\eta_3'(-m^2,\, p_1^2,\, p_4^2)}{q_{23}^2 + m^2 - i\varepsilon}\,,\end{aligned} \tag{22b}$$

$$\begin{aligned}\lambda_5(p_1^2 \dots p_5^2 q_{12}^2 \dots q_{45}^2) = \eta_5'(p_1^2 \dots p_5^2 q_{12}^2 \dots q_{45}^2) - \\ - \lim_{\varepsilon\to+0} 2\pi i \frac{\eta_3'(p_1^2,\, p_2^2,\, -m^2)\,\eta_4'(-m^2,\, p_3^2 p_4^2 p_5^2 q_{45}^2 q_{35}^2 q_{34}^2)}{q_{12}^2 + m^2 - i\varepsilon} - \text{perm. terms} + \\ + \lim_{\varepsilon\to+0} (2\pi i)^2 \frac{2\eta_3'(p_1^2,\, p_2^2,\, -m^2)\,\eta_3'(-m^2,\, p_3^2,\, -m^2)\,\eta_3'(-m^2,\, p_4^2,\, p_5^2)}{(q_{12}^2 + m^2 - i\varepsilon)(q_{45}^2 + m^2 - i\varepsilon)} + \text{perm. terms}\,.\end{aligned} \tag{22c}$$

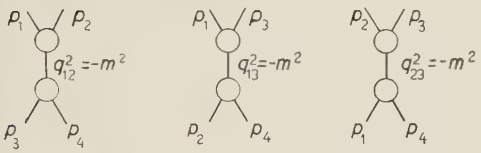

Fig. 1. - Graphs corresponding to eq. (22*b*) and (23*b*).

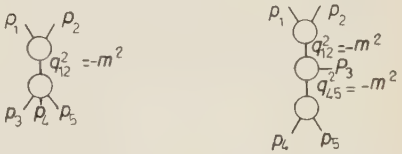

Fig. 2. – Graphs corresponding to eq. (22*c*) and (23*c*).

(The corresponding graphs are drawn in Fig. 1, 2.) These λ-functions do not have singularities at $q_{(\alpha)}^2 = -m^2$ any more. η_3', η_4', η_5' can be re-expressed in terms of the λ-function (eq. (18))

$$\eta_3'(p_1^2 p_2^2 p_3^2) = \lambda_3(p_1^2 p_2^2 p_3^2)\,, \tag{23a}$$

$$\begin{aligned}\eta_4'(p_1^2 \dots p_4^2 q_{12}^2 q_{13}^2 q_{23}^2) = \lambda_4(p_1^2 \dots p_4^2 q_{12}^2 q_{13}^2 q_{23}^2) + \\ + \lim_{\varepsilon\to+0} 2\pi i \frac{\lambda_3(p_1^2,\, p_2^2,\, -m^2)\,\lambda_3(-m^2,\, p_3^2,\, p_4^2)}{q_{12}^2 + m^2 - i\varepsilon} + \\ + \lim_{\varepsilon\to+0} 2\pi i \frac{\lambda_3(p_1^2,\, p_3^2,\, -m^2)\,\lambda_3(-m^2,\, p_2^2,\, p_4^2)}{q_{13}^2 + m^2 - i\varepsilon} + \\ + \lim_{\varepsilon\to+0} 2\pi i \frac{\lambda_3(p_2^2,\, p_3^2,\, -m^2)\,\lambda_3(-m^2,\, p_1^2,\, p_4^2)}{q_{23}^2 + m^2 - i\varepsilon}\,,\end{aligned} \tag{23b}$$

$$(23c)\quad \eta_5'(p_1^2 \dots p_5^2 q_{12}^2 \dots q_{45}^2) = \lambda_5(p_1^2 \dots p_5^2 q_{12}^2 \dots q_{45}^2) +$$

$$+ \lim_{\varepsilon \to +0} 2\pi i \, \frac{\lambda_3(p_1^2, p_2^2, -m^2)\, \lambda_4(-m^2, p_3^2 p_4^2 p_5^2 q_{45}^2 q_{35}^2 q_{34}^2)}{q_{12}^2 + m^2 - i\varepsilon} + \text{perm. terms} +$$

$$+ \lim_{\varepsilon \to +0} (2\pi i)^2 \, \frac{\lambda_3(p_1^2, p_2^2, -m^2)\, \lambda_3(-m^2, p_3^2, -m^2)\, \lambda_3(-m^2, p_4^2, p_5^2)}{(q_{12}^2 + m^2 - i\varepsilon)(q_{45}^2 + m^2 - i\varepsilon)} + \text{perm. terms.}$$

These formulae represent the expansions of η_3', η_4', η_5' with respect to all singularities of the form $P(q_{ij}^2 + m^2)^{-1}$, $\delta(p_{ij}^2 + m^2)$ and products thereof.

4. – Extension to several fields and particles.

The investigations of the preceding sections can easily be extended to models with several fields and particles (including stable bound states). As an example we discuss here the one-particle structure of some Green's functions associated with various two-particle scattering processes. We consider the model of a charged scalar field $\psi(x)$ interacting with a neutral scalar field $A(x)$. The field operators are as usual assumed to be invariant, causal, complete, etc. We further demand that the system have the discrete (non-vanishing) mass values $\varkappa$, m amd M corresponding to the charge values 0, 1 and 2. The corresponding particles are called « meson », « nucleon » and « deuteron ». All particles are assumed to be spinless.

We consider the three τ-functions

$$\tau^{\mathrm{I}} = \langle T\psi(x)\, \overline{\psi}(y)\, A(z_1) A(z_2)\rangle_0 ,$$

$$\tau^{\mathrm{II}} = \langle T\psi(x_1)\, \psi(x_2)\, \overline{\psi}(y_1) \overline{\psi}(y_2)\rangle_0 ,$$

$$\tau^{\mathrm{III}} = \langle T\psi(x_1)\, \psi(x_2) A(y)\, \bar{B}(z)\rangle_0 ,$$

with the deuteron field operator $B(x)$ defined by

$$B(x) = \lim_{\xi \to 0} (2\pi)^{\frac{3}{2}} \frac{T\psi(x+\xi)\, \psi(x-\xi)}{(\Omega,\ T\psi(\xi)\, \psi(-\xi)\Phi)} ,$$

where Φ is the deuteron state at rest. We split off the vacuum singularities by forming

$$(24a)\quad \eta^{\mathrm{I}}(x; y; z_1 z_2) = \langle T\psi(x)\, \overline{\psi}(y)\, A(z_1) A(z_2)\rangle_0 - \langle T\psi(x)\, \overline{\psi}(y)\rangle_0 \langle TA(z_1) A(z_2)\rangle_0 ,$$

$$(24b)\quad \eta^{\mathrm{II}}(x_1 x_2; y_1 y_2) = \langle T\psi(x_1)\, \psi(x_2)\, \overline{\psi}(y_1)\, \overline{\psi}(y_2)\rangle_0 -$$

$$- \langle T\psi(x_1)\, \overline{\psi}(y_1)\rangle_0 \langle T\psi(x_2)\, \overline{\psi}(y_2)\rangle_0 - \langle T\psi(x_1)\, \overline{\psi}(y_2)\rangle_0 \langle T\psi(x_2)\, \overline{\psi}(y_1)\rangle_0 ,$$

$$(24c)\quad \eta^{\mathrm{III}}(x_1 x_2; y; z) = \langle T\psi(x_1)\, \psi(x_2) A(y)\, \bar{B}(z)\rangle_0 ,$$

$$\delta(p_1 + p_2 + p_3 + p_4)\, \eta_4^{(0)}(p_1 p_2 p_3 p_4) =$$

$$= \frac{1}{(2\pi)^{10}} \int \mathrm{d}x_1\, \mathrm{d}x_2\, \mathrm{d}x_3\, \mathrm{d}x_4 \exp\left[-i(p_1 x_1 + \dots p_4 x_4)\right] \eta^{(0)}(x_1 x_2 x_3 x_4) .$$

We further remove all one-particle singularities in p_1^2, p_2^2, p_3^2, p_4^2 by applying the corresponding Klein-Gordon operators

$$(25)\quad \begin{cases} \eta_1'^{\mathrm{I}}(p;q;k_1k_2) = (p^2+m^2)(q^2+m^2)(k_1^2-\varkappa^2)(k_2^2+\varkappa^2)\,\eta_4^{\mathrm{I}}(p;q;k_1k_2)\,, \\ \eta_4'^{\mathrm{II}}(p_1p_2;q_1q_2) = (p_1^2+m^2)(p_2^2+m^2)(q_1^2+m^2)(q_2^2+m^2)\,\eta_4^{\mathrm{II}}(p_1p_2;q_1q_2)\,, \\ \eta_1'^{\mathrm{III}}(p_1p_2;k;q) = (p_1^2+m^2)(p_2^2+m^2)(k^2+k^2)(q^2+M^2)\,\eta_1^{\mathrm{III}}(p_1p_2;k;q)\,. \end{cases}$$

The remaining one-particle singularities of these functions can now be studied in a manner analogous to that of Section 2. We obtain the relations

$$(26a)\quad \eta_4'^{\mathrm{I}}(p;q;k_1k_2) = \lambda_4^{\mathrm{I}}(p;q;k_1k_2) + \lim_{\varepsilon\to+0} 2\pi i\,\frac{\lambda_3^{NNM}(p^2;-m^2;k_1^2)\,\lambda_3^{NNM}(-m^2;q^2;k_2^2)}{(p+k_1)^2+m^2-i\varepsilon} + \lim_{\varepsilon\to+0} 2\pi i\,\frac{\lambda_3^{NNM}(p^2;-m^2;k_2^2)\,\lambda_3^{NNM}(-m^2;q^2;k_1^2)}{(p+k_2)^2+m^2-i\varepsilon} + \lim_{\varepsilon\to+0} 2\pi i\,\frac{\lambda_3^{N\bar{N}M}(p^2;q^2;-\varkappa^2)\,\lambda_3^{MMM}(k_1^2,k_2^2,-\varkappa^2)}{(p+q)^2+\varkappa^2-i\varepsilon}\,,$$

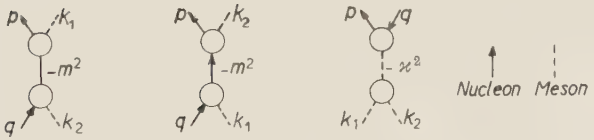

Fig. 3. – Graphs corresponding to eq. (26*a*).

$$(26b)\quad \eta_4'^{\mathrm{II}}(p_1p_2;q_1q_2) = \lambda_4^{\mathrm{II}}(p_1p_2;q_1q_2) + \lim_{\varepsilon\to+0} 2\pi i\,\frac{\lambda_3^{\bar{N}\bar{N}D}(p_1^2p_2^2;-M^2)\,\lambda_3^{N\bar{N}D}(q_1^2q_2^2,-M^2)}{(p_1+p_2)^2+M^2-i\varepsilon} + \lim_{\varepsilon\to+0} 2\pi i\,\frac{\lambda_3^{N\bar{N}M}(p_1^2,q_1^2;-\varkappa^2)\lambda_3^{N\bar{N}M}(p_2^2,q_2^2;-\varkappa^2)}{(p_1+q_1)^2+\varkappa^2-i\varepsilon} + \lim_{\varepsilon\to+0} 2\pi i\,\frac{\lambda_3^{N\bar{N}M}(p_2^2,q_1^2;-\varkappa^2)\lambda_3^{NNM}(p_1^2,q_2^2;-\varkappa^2)}{(p_2+q_1)^2+\varkappa^2-i\varepsilon}\,,$$

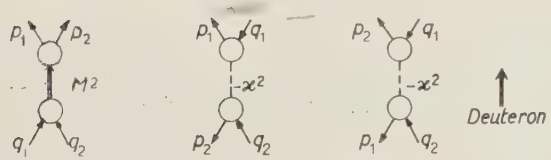

Fig. 4. – Graphs corresponding to eq. (26*b*).

$$(26c)\qquad \eta_4'^{\mathrm{III}}(p_1p_2;\,k;\,q)=\lambda_4^{\mathrm{III}}(p_1p_2;\,q)+$$

$$+\lim_{\varepsilon\to+0}2\pi i\,\frac{\lambda_3^{N\bar{N}D}(p_1^2,\,p_2^2;\,-M^2)\,\lambda_3^{D\bar{D}M}(-M^2;\,q^2;\,k^2)}{(p_1+p_2)^2+M^2-i\varepsilon}+$$

$$+\lim_{\varepsilon\to+0}2\pi i\,\frac{\lambda_3^{\bar{N}NM}(p_1^2,\,-m^2;\,k^2)\,\lambda_3^{N\bar{N}\bar{D}}(-m^2,\,p_2^2;\,q^2)}{(p_1+k)^2+m^2-i\varepsilon}+$$

$$+\lim_{\varepsilon\to+0}2\pi i\,\frac{\lambda_3^{\bar{N}NM}(p_2^2,\,-m^2;\,k^2)\,\lambda_3^{N\bar{N}\bar{D}}(-m^2,\,p_1^2;\,q^2)}{(p_2+k)^2+m^2-i\varepsilon}\,.$$

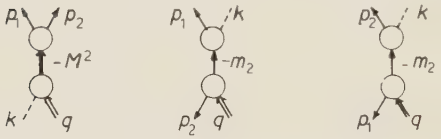

Fig. 5. – Graphs corresponding to eq. (26c).

Here λ_4 and the residua do not contain any one-particle singularities. The factors of the residua are identical with the so-called vertex functions:

$$\lambda_3^{ijk}(p_1^2p_2^2p_3^2)=(p_1^2+m_i^2)(p_2^2+m_j^2)(p_3^2+m_k^2)\,\eta_3^{ijk}(p_1^2p_2^2p_3^2)\,,$$

$$(27)\qquad \delta(p_1+p_2+p_3)\,\eta_3^{ijk}(p_1^2p_2^2p_3^2)=$$

$$=\frac{1}{(2\pi)^{15/2}}\int \mathrm{d}x_1\,\mathrm{d}x_2\,\mathrm{d}x_3\,\exp\left[-i(p_1x_1+\ldots+p_3x_3)\right]\langle TA_i(x_1)\,A_j(x_2)\,A_k(x_3)\rangle_0\,,$$

where $i,\,j,\,k=N,\,\bar{N},\,M,\,D,\,\bar{D}$

$$A_N(x)=\psi(x)\,,\qquad A_{\bar{N}}(x)=\bar{\psi}(x)\,,\qquad A_M(x)=A(x)\,,$$

$$A_D(x)=B(x)\,,\qquad A_{\bar{D}}(x)=\bar{B}(x)\,,$$

$$m_N=m_{\bar{N}}=m\,,\qquad m_M=k\,,\qquad m_D=m_{\bar{D}}=M\,.$$

* * *

I am grateful to Professors M. Fierz, V. Glaser, H. Joos and many other physicists for helpful discussions.

RIASSUNTO (*)

Le funzioni di Green ordinate temporalmente vengono sviluppate per le singolarità che nascono da stati intermedi ad una particella.

(*) *Traduzione a cura della Redazione.*

IL NUOVO CIMENTO Vol. XVI, N. 4 16 Maggio 1960

The Axial Vector Current in Beta Decay (*).

M. Gell-Mann (**)

Collège de France and Ecole Normale Supérieure - Paris (***)

M. Lévy

Faculte des Sciences, Orsay, and Ecole Normale Supérieure - Paris (*)

(ricevuto il 19 Febbraio 1960)

Summary. — In order to derive in a convincing manner the formula of Goldberger and Treiman for the rate of charged pion decay, we consider the possibility that the divergence of the axial vector current in β-decay may be proportional to the pion field. Three models of the pion-nucleon interaction (and the weak current) are presented that have the required property. The first, using gradient coupling, has the advantage that it is easily generalized to strange particles, but the disadvantages of being unrenormalizable and of bringing in the vector and axial vector currents in an unsymmetrical way. The second model, using a strong interaction proposed by Schwinger and a weak current proposed by Polkinghorne, is renormalizable and symmetrical between V and A, but it involves postulating a new particle and is hard to extend to strange particles. The third model resembles the second one except that it is not necessary to introduce a new particle. (Renormalizability in the usual sense is then lost, however). Further research along these lines is suggested, including consideration of the possibility that the pion decay rate may be plausibly obtained under less stringent conditions.

(*) Supported in part by the Alfred P. Sloan Foundation and by the United States Air Force through the European Office, Air Research and Development Command.

(**) National Science Foundation Senior Postdoctoral Fellow.

(***) Permanent address: California Institute of Technology, Pasadena, Cal.

(*) Postal address: Laboratoire de Physique Théorique et Hautes Energies, B.P. 12, Orsay (Seine et Oise).

1. – Introduction.

The decay of the muon is the only process known experimentally in which the weak interactions can apparently be studied without complications due to the strong interactions. The electromagnetic corrections, moreover, are finite and have been calculated [1]. All evidence so far supports the correctness of the following Lagrangian for the interaction:

$$(1) \qquad \mathscr{L}(\mu \text{ decay}) = 2^{-\frac{1}{2}} G_\mu [\bar{\nu}\gamma_\alpha(1+\gamma_5)e][\bar{\nu}'\gamma_\alpha(1+\gamma_5)\mu]^+ + \text{Herm. conj.}$$

(The two neutrinos involved have been denoted by different symbols ν and ν' because we are not certain that they are identical, although they are both massless and they exhibit the same helicity). The value of the constant G_μ can be determined from the rate of decay of the muon according to the formula:

$$(2) \qquad \Gamma_\mu = (192\pi^3)^{-1} G_\mu^2 m_\mu^5 (0.995\,6)\,,$$

which is well known, perhaps with the exception of the final factor, which gives the electromagnetic correction computed in Ref. [1]. If we take [2] the muon lifetime Γ_μ^{-1} to be $2.208 \pm 0.003 \cdot 10^{-6}$ s and the mass m_μ to be 106.65 ± 0.01 MeV, then we get for the dimensionless quantity $G_\mu m_p^2$ the value:

$$G_\mu m_p^2 = 1.204 \pm 0.001 \cdot 10^{-5}\,,$$

where m_p is the proton mass and our units are such that $\hbar = c = 1$.

Now let us turn to those leptonic weak processes in which baryons and mesons are involved (bringing in the strong interactions), but in which there is no change of strangeness ($\Delta S = 0$). Experimentally, we deal with nuclear β decay (including K capture and inverse β decay), muon capture by nuclei, and the decay of the charged pion. It appears that all these processes can be described by an interaction Lagrangian of the form:

$$(3) \qquad \mathscr{L}_{\text{int.}} = 2^{-\frac{1}{2}} G[V_\alpha + P_\alpha][\bar{\nu}\gamma_\alpha(1+\gamma_5)e + \bar{\nu}'\gamma_\alpha(1+\gamma_5)\mu]^+ + \text{Herm. conj.}\,,$$

where V_α and P_α are vector and pseudovector currents which can transform neutron into proton. As has, of course, been remarked [3,4], the experiments

---

(1) S. M. BERMAN: *Phys. Rev.*, **112**, 267 (1958).
(2) Private communication from V. L. TELEGDI on the work of the Chicago group.
(3) R. P. FEYNMAN and M. GELL-MANN: *Phys. Rev.*, **109**, 193 (1958).
(4) E. C. G. SUDARSHAN and R. E. MARSHAK: *Phys. Rev.*, **109**, 1860 (1958).

suggest that $G(V_\alpha + P_\alpha)$ is very much like $G_\mu \bar{p}\gamma_\alpha(1+\gamma_5)n$, so that the weak interactions are essentially «universal» in their strength and form for the pairs νe, ν′μ, and pn. However, $G(V_\alpha + P_\alpha)$ need not be precisely of the form indicated; there may, for example, be other terms. It is with just this question of the structure of the currents, especially of P_α, that we are concerned here.

For the sake of definiteness, let us agree that the coefficient of $\bar{p}\gamma_\alpha n$ in V_α is unity—that is our definition of G. We also assume that the coefficient of $\bar{p}\gamma_\alpha\gamma_5 n$ in P_α is unity.

Because of the presence of strong interactions, we do not necessarily observe G directly. In the β decay of the neutron, for example, we can measure the matrix elements of GV_α and GP_α between free nucleon states with very little momentum transfer ($\lesssim 1$ MeV). In this limit we have:

$$G\langle p|V_\alpha|n\rangle \to G_V \bar{u}_f \tau_+ \gamma_\alpha u_i , \tag{4a}$$

$$G\langle p|P_\alpha|n\rangle \to -G_A \bar{u}_f \tau_+ \gamma_\alpha \gamma_5 u_i , \tag{4b}$$

where G_V and G_A are the conventional Fermi and Gamow-Teller coupling constants of nuclear β decay and u_i and u_f are the initial and final free nucleon spinors.

It is well known that the experimental value of G_V is remarkably close to that of G_μ and an explanation ([3]) of this fact has been offered based on two theoretical hypotheses:

a) Exact «universality» of strength: $G = G_\mu$.

b) The conserved vector current theory ([3,5]) of V_α, which gives $G_V = G$ (apart from electromagnetic corrections) as a consequence of the vanishing of the divergence $\partial_\alpha V_\alpha$.

So far the best evidence for this point of view is the *ft* value of the decay of ^{14}O, which is predicted to be $3\,001 \pm 6$ on the basis of *a*) and *b*) and the value of G_μ quoted above, while the experimental result ([6]) is $3\,088 \pm 56$. The theoretical prediction is subject to error only from the experimental muon lifetime and mass and from electromagnetic corrections to the decay of ^{14}O.

There is, of course, some discrepancy between theory and experiment, which is made worse if we accept Berman's estimate ([1]) of the electromagnetic corrections, which reduces the predicted *ft* value to 2917. If we take seriously

---

([5]) S. S. Gershtein and J. B. Zeldovich: *Žurn. Éksp. Teor. Fiz.*, **29**, 698 (1955) (translation: *Sov. Phys. Journ. Exp. Theor. Phys.*, **2**, 576 (1957)).

([6]) D. A. Bromley, E. Almquist, H. E. Gove, A. E. Litherland, E. B. Paul and A. J. Ferguson: *Phys. Rev.*, **105**, 957 (1957).

this number, the experimental value, and the conserved vector current hypothesis, we obtain $G/G_\mu = 0.97 \pm 0.01$ rather than unity (*).

Other tests of the theory have been proposed ([3-7]) but not yet carried out. For the time being, let us suppose it to be correct and go on to inquire about the form of the pseudovector current P_α.

At one time it was suggested ([3]) that here too the renormalization factor might be unity. Some effort was put into a search for theories in which that would be true. Certain authors tried to find theories in which P_α would be divergenceless, by analogy with the vector case. The following points are now clear in connection with this type of investigation:

A) Experimentally ([8]) the quantity $-G_A/G_V$ is 1.25 ± 0.06, so that the axial vector renormalization factor is not unity, although it is not very far away.

B) The divergence $\partial_\alpha P_\alpha$ of the axial vector current cannot in any case be zero, because that would make the rate of decay of the charged pion vanish ([9]).

C) If, in some particular theoretical model, there is a limit in which $\partial_\alpha P_\alpha$ is zero, it is a delicate limit in which, for example, the nucleon mass or the pion mass vanishes; and the question of whether in this limit $-G_A/G$ is really unity must be carefully investigated for each model ([10]).

D) No one has found a theory in which a reasonable calculation of $-G_A/G$ can be made with present methods.

(*) *Note added in proof.* – Should this discrepancy be real, it would probably indicate a total or partial failure of the conserved vector current idea. It might also mean, however, that the current is conserved but with $G/G_\mu < 1$. Such a situation is consistent with universality if we consider the vector current for $\Delta S = 0$ and $\Delta S = 1$ together to be something like:

$$GV_\alpha + GV_\alpha^{(\Delta S=1)} = G_\mu \bar{p}\gamma_\alpha(n + \varepsilon\Lambda)(1+\varepsilon^2)^{-\frac{1}{2}} + \dots,$$

and likewise for the axial vector current. If $(1+\varepsilon^2)^{-\frac{1}{2}} = 0.97$, then $\varepsilon^2 = .06$, which is of the right order of magnitude for explaining the low rate of β decay of the Λ particle. There is, of course, a renormalization factor for that decay, so we cannot be sure that the low rate really fits in with such a picture.

([7]) M. GELL-MANN: *Phys. Rev.*, **111**, 362 (1958).

([8]) M. T. BURGY, V. E. KROHN, T. B. NOVEY, G. R. RINGO and V. L. TELEGDI: *Phys. Rev.*, **110**, 1214 (1958). See also C. S. WU: *Rev. Mod. Phys.*, **31**, 783 (1959).

([9]) J. C. TAYLOR: *Phys. Rev.*, **110**, 1216 (1958); M. L. GOLDBERGER and S. B. TREIMAN: *Phys. Rev.*, **110**, 1478 (1958).

([10]) R. J. BLIN-STOYLE: *Nuovo Cimento*, **10**, 132 (1958); S. OKUBO: *Nuovo Cimento*, **13**, 292 (1959).

Despite the lack of success of the program just discussed, it has turned up at least three models in which $\partial_\alpha P_\alpha$, instead of vanishing, is proportional to a component of the pion field. This relation is interesting, not because it explains why $-G_A/G$ is fairly close to one, but because it gives a relation between the value of $-G_A$ and the rate of decay of the charged pion.

The connection of the formula

$$\partial_\alpha P_\alpha = \frac{ia}{\sqrt{2}}\pi^- \tag{5}$$

with the rate of pion decay was discovered originally (*) for a particular model, in which the pion-nucleon strong interaction has the gradient form.

Our work on this model is an extension of that of NORTON and WATSON [11] and J. C. TAYLOR [12].

The formula relating $-G_A$ to the charged pion decay amplitude is essentially the one proposed by GOLDBERGER and TREIMAN [13], which gives remarkable agreement with experiment. We shall derive, in any theory for which eq. (5) is valid, an exact formula for pion decay, to which the equation of Goldberger and Treiman is a very plausible approximation.

We shall then investigate three models of strong and weak couplings of nucleons and pions that yield eq. (5). All of these models present some difficulties, however. None is a really convincing theory. We must therefore come back to the question of whether eq. (5) is really necessary in order to derive the result of GOLDBERGER and TREIMAN in a convincing manner.

2. – The rate of charged pion decay.

Suppose we have a theory of the strong interactions and a definition of the axial vector current such that eq. (5) holds. Then the matrix element of P_α for negative pion decay may be written:

$$\langle 0 | P_\alpha(x) | \pi^- \rangle = -\frac{a}{\sqrt{2}} \frac{q_\alpha}{m_\pi^2} \langle 0 | \pi^-(x) | \pi^- \rangle , \tag{6}$$

where q_α is the four-momentum of the pion, since, on taking the divergence of both sides, we get back just eq. (5) between the pion state and the vacuum. Note $q^2 = -m_\pi^2$.

(*) By R. P. FEYNMAN, with some assistance from one of us (M. G.-M.).

[11] R. E. NORTON and W. K. R. WATSON: *Phys. Rev.*, **110**, 996 (1958).

[12] J. C. TAYLOR: quoted in ref. [17]. See also R. F. STREATER and J. C. TAYLOR: *Nucl. Phys.*, **7**, 276 (1958).

[13] M. L. GOLDBERGER and S. B. TREIMAN: *Phys. Rev.*, **110**, 1178 (1958). A recent criticism of their paper has been given by R. F. SAWYER: *Phys. Rev.*, **116**, 231 (1959); like us, SAWYER seeks a better derivation of their result.

The pion field operator $\pi^-(x)$ may be written as the product of a field renormalization factor, conventionally called $\sqrt{Z_3}$, and the renormalized operator $\pi_r^-(x)$, for which the matrix element between the pion state and the vacuum is just the same as that of a free field between a free particle state and the free vacuum. So we have for the matrix element of P_α in pion decay the following formula in terms of a $\sqrt{Z_3}$:

$$\langle 0 | P_\alpha(x) | \pi^- \rangle = -\frac{a\sqrt{Z_3}}{\sqrt{2}} \frac{q_\alpha}{m_\pi^2} \langle 0 | \pi_r^-(x) | \pi^- \quad . \tag{7}$$

Now we may also evaluate $-G_A/G$ in terms of $a\sqrt{Z_3}$. We take the divergence of both sides of eq. (4*b*) in the limit of very small momentum transfer k (final momentum minus initial momentum) and we have:

$$G\langle p | \partial_\alpha P_\alpha | n \rangle \to -G_A(-ik_\alpha)\bar{u}_f \tau_+ \gamma_\alpha \gamma_5 u_i = 2m(-G_A)\bar{u}_f \tau_+ \gamma_5 u_i \,, \tag{8}$$

where m is the nucleon mass. If we are to apply eq. (5) we must calculate $\langle p | \pi^- | n \rangle$ in the limit of zero momentum transfer. Now in the neighborhood of $k^2 = -m_\pi^2$, we know this matrix element to be expressible in terms of the renormalized coupling constant g_1 as follows:

$$\langle p | \pi^- | n \rangle \approx \sqrt{Z_3}(k^2 + m_\pi^2)^{-1} i\sqrt{2}\, g_1 \bar{u}_f \tau_+ \gamma_5 u_i \,. \tag{9}$$

To make this formula correct at all values of k^2, we must simply replace the free propagator $(k^2 + m_\pi^2)^{-1}$ of the meson by the exact renormalized propagator, which we may call $(k^2 + m_\pi^2)^{-1} d_\pi(k^2)$, and the free vertex $\tau_+ \gamma_5$ by the exact renormalized vertex, which we may call $\tau_+ \gamma_5 F_\pi(k^2)$. The « form factors » $d_\pi(k^2)$ and $F_\pi(k^2)$ are both unity at $k^2 = -m_\pi^2$. We have, then, as $k^2 \to 0$, the result:

$$\langle p | \partial_\alpha P_\alpha | n \rangle \to \frac{ia}{\sqrt{2}} \frac{\sqrt{Z_3}}{m_\pi^2} d_\pi(0) F_\pi(0)\, i\sqrt{2}\, g_1 \bar{u}_f \tau_+ \gamma_5 u_i \,. \tag{10}$$

Comparing this equation with eq. (8), we find:

$$a\sqrt{Z_3} = -\frac{2m}{g_1} m_\pi^2 \left(-\frac{G_A}{G}\right) \frac{1}{d_\pi(0)\, F_\pi(0)} \,. \tag{11}$$

The unknown quantity in our formula (7) for the pion decay matrix element is now evaluated and we may calculate the rate of the process $\pi^- \to \mu^- + \bar{\nu}$,

which gives essentially the reciprocal lifetime of the charged pion:

$$\Gamma_\pi = \left(16\pi^2 \frac{g_1^2}{4\pi}\right)^{-1} (G_A m^2)^2 m_\pi \frac{m_\mu^2}{m^2}\left(1 - \frac{m_\mu^2}{m_\pi^2}\right)^2 [d_\pi(0) F_\pi(0)]^{-2} . \tag{12}$$

Except for the final factor, this is the same as the formula given by GOLDBERGER and TREIMAN [13]. Their derivation, based on the conventional pseudoscalar theory of the strong interactions and the conventional definition $\bar{p}\gamma_\alpha\gamma_5 n$ of the current P_α, involves several violent approximations which are not really justified. The formula, however, is in excellent agreement with experiment. The measurements [14] give:

$$\frac{\Gamma_\pi}{m_\pi} = (1.84 \pm 0.04)\cdot 10^{-16} , \tag{13}$$

while eq. (12) yields:

$$\frac{\Gamma_\pi}{m_\pi} = [d_\pi(0) F_\pi(0)]^{-2} \{(1.56 \pm 0.2)\cdot 10^{-16}\} , \tag{14}$$

with $g_1^2/4\pi = 15 \pm 2$.

In the work of GOLDBERGER and TREIMAN, it was very mysterious that the agreement of the figures should be so close. If, however, eq. (12) is derived, as above, from a theory in which eq. (5) holds, then the discrepancy is to be attributed solely to the form factor $[d_\pi(0) F_\pi(0)]^{-2}$, which we know equals unity when the argument is $-m_\pi^2$. We would not be surprised if at zero the departure from unity amounts to only twenty percent or so.

We must be careful not to exaggerate the advantage of models in which eq. (5) holds. It can be shown (*) that in *any* theory that predicts a non-vanishing rate of pion decay we can obtain an *exact* equation analogous to (12), with the form factor $d_\pi(0)F_\pi(0)$ replaced by a general «form factor» $\varphi(0)$, where φ, like $d_\pi F_\pi$, equals unity at the value $-m_\pi^2$ of its argument. The difference between one theory and another lies merely in the question of whether this general «form factor» φ is likely to be slowly varying. If the theory is such that eq. (5) is valid, so that $\varphi = d_\pi F_\pi$, then it is not unreasonable that φ be slowly varying. In the conventional theory, where φ is something much more complicated, the conclusion is much less plausible. In any case, we cannot exclude the possibility that the formula of Goldberger and Treiman

---

(14) As listed by K. M. CROWE: *Nuovo Cimento*, **5**, 541 (1957).

(*) See forthcoming article by BERNSTEIN, FUBINI, GELL-MANN and THIRRING.

is approximately valid even in the conventional theory, for which they tried to derive it.

In the subsequent sections, we shall study models in which eq. (5) actually holds, but we must bear in mind the question of whether such an assumption is really necessary in order to explain what seems to be an experimental fact, that $\varphi(0)$ is close to unity.

In order to study the models conveniently, and in order to show the relation between the vector and the pseudovector currents, let us now review some formalism.

3. – The divergence of a current and gauge transformations [15].

Let us consider a theory of the strong interactions derivable from a Lagrangian density $\mathscr{L}$ expressed in terms of field components ψ_i and their first spatial derivatives $\partial_\alpha \psi_i$. Then the equations of motion of Lagrange are (*):

$$\frac{\delta \mathscr{L}}{\delta \psi_i} = \partial_\alpha \frac{\delta \mathscr{L}}{\delta(\partial_\alpha \psi_i)} \,. \tag{15}$$

Suppose we now subject each field component $\psi_i(x)$ to an infinitesimal local gauge transformation:

$$\psi_i(x) \to \psi_i(x) + \Lambda(x) F_i[\psi_1(x), \psi_2(x), \ldots] \,. \tag{16}$$

with a gauge function Λ. Then we may examine the variation of $\mathscr{L}$ under this change and we find, always to first order-:

$$\delta \mathscr{L} = \frac{\delta \mathscr{L}}{\delta \Lambda} \Lambda + \frac{\delta \mathscr{L}}{\delta \partial_\alpha \Lambda} \partial_\alpha \Lambda \,, \tag{17}$$

where

$$\frac{\delta \mathscr{L}}{\delta \Lambda} = \frac{\delta \mathscr{L}}{\delta \psi_i} F_i + \frac{\delta \mathscr{L}}{\delta \partial_\alpha \psi_i} \partial_\alpha F_i \,, \tag{18}$$

and

$$\frac{\delta \mathscr{L}}{\delta_\alpha \partial \Lambda} = \frac{\delta \mathscr{L}}{\delta \partial_\alpha \psi_i} F_i \,. \tag{19}$$

---

[15] Our point of view in this section has much in common with that of S. GLASHOW: *Nucl. Phys.*, **10**, 107 (1959), as well as that of S. BLUDMAN: *Nuovo Cimento*, **9**, 433 (1958). See, also, the earlier work of J. SCHWINGER: ref. [16].

(*) Our discussion is classical. We ignore certain complications that may arise in quantum mechanics from the non-commutation of boson fields and their canonical momenta, making necessary a careful ordering of the operators.

Using (8), (11) and (12), we see immediately that we have Lagrange's equation for $\Lambda(x)$:

$$\frac{\delta \mathscr{L}}{\delta \Lambda} = \partial_\alpha \frac{\delta \mathscr{L}}{\delta \partial_\alpha \Lambda} . \tag{20}$$

Now suppose that under a particular transformation with infinitesimal gauge function Λ taken *independent of co-ordinates*, the Lagrangian $\mathscr{L}$ is *invariant*. Then $\delta \mathscr{L}/\delta \Lambda$ vanishes and thus:

$$\partial_\alpha \frac{\delta \mathscr{L}}{\delta \partial_\alpha \Lambda} = 0 . \tag{21}$$

We may then identify $\delta \mathscr{L}/\delta \partial_\alpha \Lambda$ as the current which is conserved as a result of the invariance of the theory under the gauge transformation with constant Λ.

Consider, for example, the conservation of baryons. Let each baryon field acquire a factor $(1 + i\Lambda_1(x))$, while the meson fields are left unchanged. The baryon current $\propto \delta \mathscr{L}/\delta \partial_\alpha \Lambda_1$ is then conserved.

For conservation of charge, we let each field acquire a factor $(1 + iQ\Lambda_2(x))$, where Q is the charge destroyed by the field. The Lagrangian is chosen invariant under this for constant Λ_2. The electric current $\propto \delta \mathscr{L}/\delta \partial_\alpha \Lambda_2$ is then conserved.

We note that we are working only with the Lagrangian of the strong interactions; that is to say, we are ignoring all higher effects of the electromagnetic field. We are therefore not concerned, at the moment, with the more general gauge transformation that includes photons and that also leaves the electric current exactly conserved.

For conservation of isotopic spin, we consider rotations in isotopic space with an isotopic vector gauge function $\boldsymbol{u}$. For example, for the nucleon field $N(x)$ and the pion field $\boldsymbol{\pi}(x)$, we have:

$$\begin{cases} N \to (1 + i\boldsymbol{\tau}\cdot\boldsymbol{u})N , \\ \boldsymbol{\pi} \to \boldsymbol{\pi} - 2\boldsymbol{u}\times\boldsymbol{\pi} . \end{cases} \tag{22}$$

With the Lagrangian invariant under these rotations for $\boldsymbol{u}$ constant, we have conservation of the isotopic spin current $\propto \delta \mathscr{L}/\delta \partial_\alpha \boldsymbol{u}$.

In the conserved vector current theory of the weak couplings, $V_\alpha(x)$ is simply the + component of an isotopic vector current $\boldsymbol{V}_\alpha(x)$ which is equal to the isotopic spin current:

$$\boldsymbol{V}(x) = i\frac{\delta \mathscr{L}}{\delta \partial_\alpha \boldsymbol{u}} = \bar{N}\boldsymbol{\tau}\gamma_\alpha N + 2i\boldsymbol{\pi}\times\partial_\alpha\boldsymbol{\pi} + \ldots , \tag{23}$$

where the terms we have written explicitly come from the free Lagrangian of N and $\boldsymbol{\pi}$.

Now for the axial vector weak current $P_\alpha(x)$ it is reasonable to suppose that it too is the – component of an isotopic vector $\boldsymbol{P}_\alpha(x)$ which can be generated from $\mathscr{L}$ by a gauge transformation with a gauge function $\boldsymbol{v}(x)$ that is a pseudoscalar in space and an isotopic vector:

$$\boldsymbol{P}_\alpha(x) = i\frac{\delta\mathscr{L}}{\delta\partial_\alpha\boldsymbol{v}}. \tag{24}$$

We are not, however, free to suppose that this current is divergenceless, *i.e.* that the Lagrangian is invariant under our gauge transformation with constant $\boldsymbol{v}$. Thus in place of the conservation law (14) we must use the more general formula (13), which gives us for the divergence of the pseudoscalar current the result:

$$\partial_\alpha\boldsymbol{P}_\alpha = i\frac{\delta\mathscr{L}}{\delta\boldsymbol{v}}. \tag{25}$$

Let us take as an example the conventional pseudoscalar theory of nucleons and pions with Lagrangian density:

$$\mathscr{L}_{ps} = -\bar{N}(\gamma\partial + m_0 - ig_0\boldsymbol{\tau}\cdot\boldsymbol{\pi}\gamma_5)N - \frac{\mu_0^2\pi^2}{2} - \frac{(\partial\boldsymbol{\pi})^2}{2} - \lambda_0(\pi^2)^2. \tag{26}$$

If we wish to have for our axial vector current P_α just the simple form $\bar{N}\boldsymbol{\tau}\gamma_\alpha\gamma_5 N$, then we take for our gauge transformation the following:

$$N \to (1 + i\boldsymbol{\tau}\cdot\boldsymbol{v}\gamma_5)N,$$

$$\boldsymbol{\pi} \to \boldsymbol{\pi}.$$

We then obtain for $\partial_\alpha\boldsymbol{P}_\alpha$ the result:

$$\frac{i\delta\mathscr{L}_{ps}}{\delta\boldsymbol{v}} = 2m_0\bar{N}\boldsymbol{\tau}\gamma_5 N - 2ig_0\boldsymbol{\pi}\bar{N}N.$$

If the gauge transformation is chosen instead to be this one:

$$N \to (1 + i\boldsymbol{\tau}\cdot\boldsymbol{v}\gamma_5)N,$$

$$\boldsymbol{\pi} \to \boldsymbol{\pi} + \frac{2m_0}{g_0}\boldsymbol{v},$$

then P_α is $\bar{N}\boldsymbol{\tau}\gamma_\alpha\gamma_5 N - (2im_0/g_0)\,\partial_\alpha\boldsymbol{\pi}$ and its divergence is:

$$i\,\frac{\delta\mathscr{L}_{ps}}{\delta\boldsymbol{v}} = -2ig_0\boldsymbol{\pi}\bar{N}N - \frac{2m_0}{g_0}\,\mu_0^2 i\boldsymbol{\pi} - \frac{8\lambda_0 m_0}{g_0}\,i\pi^2\boldsymbol{\pi}\,.$$

In neither of these two cases does the divergence seem to have any simple properties. If, however, we change the theory of the strong interactions, we may find a gauge transformation that yields an axial vector current with a simple divergence; in fact we may find a current for which

$$\partial_\alpha \boldsymbol{P}_\alpha = ia\boldsymbol{\pi}\,,$$

giving eq. (5) and implying eq. (12) that explains the pion lifetime.

Evidently what we require is a Lagrangian for which there is a gauge transformation with pseudoscalar gauge vector $\boldsymbol{v}$ such that:

$$\frac{\delta\mathscr{L}}{\delta\boldsymbol{v}} = a\boldsymbol{\pi}\,. \tag{28}$$

For constant $\boldsymbol{v}$, then, the Lagrangian must be nearly invariant, with the gauge transformation adding only the term $a\,\boldsymbol{\pi}\cdot\boldsymbol{v}$.

Let us now examine the models so far discovered in which that happens.

4. – The gradient coupling model.

The first model to be found makes use of the gradient coupling theory. If we treat just nucleons and pions for simplicity, the Lagrangian is:

$$\mathscr{L}_1 = -\bar{N}(\gamma\,\partial + m_0 + if_0\boldsymbol{\tau}\cdot\partial_\alpha\boldsymbol{\pi}\gamma_\alpha\gamma_5)N - \frac{(\partial\boldsymbol{\pi})^2}{2} - \frac{\mu_0^2\pi^2}{2}\,. \tag{29}$$

Except for the last term it is invariant under the gauge transformation:

$$\begin{cases} N \to N\,, \\ \boldsymbol{\pi} \to \boldsymbol{\pi} + f_0^{-1}\boldsymbol{v}\,, \end{cases} \tag{30}$$

when $\boldsymbol{v}$ is constant and the last term gives just $a\boldsymbol{\pi}\cdot\boldsymbol{v}$ with:

$$a = -\frac{\mu_0^2}{f_0}\,. \tag{31}$$

The current $\boldsymbol{P}_\alpha$ is, of course, given by:

$$\boldsymbol{P}_\lambda = i\frac{\delta\mathscr{L}_1}{\delta\partial_\lambda\boldsymbol{v}} = \bar{N}\boldsymbol{\tau}\gamma_\alpha\gamma_5 N - \frac{i}{f_0}\partial_\alpha\boldsymbol{\pi}\,. \tag{32}$$

Comparing eq. (31) with eq. (11) we find:

$$-\frac{G_A}{G} = \frac{\mu_0^2}{m_\pi^2}\frac{\sqrt{Z_3}f_1}{f_0}\,d_\pi(0)\,F_\pi(0)\,, \tag{33}$$

where $f_1 = g_1/2m$ is the renormalized version of f_0. This relation can, of course, be proved directly for the gradient coupling theory with the axial vector current given in (32). In fact, there are two independent relations in the theory:

$$-\frac{G_A}{G} = \frac{f_1}{f_0\sqrt{Z_3}}\,F_\pi(0)\,, \tag{34}$$

and

$$\frac{Z_3\mu_0^2}{m_\pi^2}\,d_\pi(0) = 1\,, \tag{35}$$

the product of which gives eq. (33). Both are easy to prove. The first follows from the similarity of the weak pseudovector current and the source of the pion field. (The term in $\partial_\lambda\boldsymbol{\pi}$ in the weak current contributes nothing at zero energy.) The second relation obtains because at zero momentum the correction to the free meson propagator vanishes, since the source of the field is the divergence of $\bar{N}\boldsymbol{\tau}\gamma_\alpha\gamma_5 N$.

The gradient coupling model has two weak points. First, as is well known, there are violent divergences in every term of the perturbation expansion. If these were to be expressed as renormalizations, it would require the renormalization of an infinite number of parameters. Of course, we could simply introduce a cut-off, but then all quantities of physical interest would depend strongly on the cut-off (at least in the perturbation expansion) and the formal manipulations of the theory, such as we have carried out above, are not obviously meaningful.

The second point, which might not be serious, is that in our introduction of the weak currents by the gauge transformations (22) and (30), there is no similarity whatever between the gauges that generate the vector and the pseudovector currents. In the transformations (30) the term $\gamma_\lambda\gamma_5$ in the weak current for the nucleons is generated from the *coupling term* of the Lagrangian (29), while the corresponding vector term γ_α is, of course, generated from the free Lagrangian.

Yet we have evidence that the weak interactions are symmetrical between V and A, particularly their apparent equality of strength and the fact that for the leptons, which have no strong couplings, the weak coupling is just $\gamma_\alpha(1+\gamma_5)$.

5. – The σ model.

We have another example of a theory in which eq. (5) holds, if we take a Lagrangian for the strong interactions that is essentially one proposed by SCHWINGER ([16]) and then for the axial vector current the form suggested by POLKINGHORNE ([17]).

Again, for simplicity, we restrict ourselves to nucleons and pions only, except that we introduce (following SCHWINGER) a new scalar meson σ, with isotopic spin zero. It has strong interactions, and thus might easily have escaped observation if it is much heavier than π, so that it would disintegrate immediately into two pions. It would appear experimentally as a resonant state of two pions with $J=0$, $I=0$.

We take for our Lagrangian the following one, which leads to a renormalizable theory of the strong interactions:

$$\mathscr{L}_2 = -\bar{N}[\gamma\partial + m_0 - g_0(\sigma + i\boldsymbol{\tau}\cdot\boldsymbol{\pi}\gamma_5)]N - \frac{(\partial\boldsymbol{\pi})^2}{2} - \frac{(\partial\sigma)^2}{2} - \frac{\mu_0^2\pi^2}{2} - \left(\mu_0^2 + \frac{2\lambda_0}{f_0^2}\right)\frac{\sigma^2}{2} - \lambda_0\left[(\pi^2+\sigma^2)^2 - \frac{2}{f_0}\sigma(\sigma^2+\pi^2)\right], \tag{36}$$

where $f_0 = g_0/2m_0$.

We have the usual pseudoscalar theory of the pion, with the σ added in a rather symmetrical way. The nature of the symmetry is made much clearer if we perform a translation of the field variable σ and re-express the Lagrangian in terms of the variable:

$$\sigma' \equiv \sigma - \frac{1}{2f_0}. \tag{37}$$

We have:

$$\mathscr{L}_2 = -\bar{N}[\gamma\partial - g_0(\sigma' + i\boldsymbol{\tau}\cdot\boldsymbol{\pi}\gamma_5)]N - \frac{(\partial\boldsymbol{\pi})^2}{2} - \frac{(\partial\sigma')^2}{2} - \frac{\mu_0^2}{2}(\pi^2+\sigma'^2) - \lambda_0\left[\pi^2 + \sigma'^2 - \frac{1}{4f_0^2}\right]^2 - \frac{\mu_0^2}{2f_0}\sigma', \tag{38}$$

([16]) J. SCHWINGER: *Ann. Phys.*, **2**, 407 (1957).
([17]) J. C. POLKINGHORNE: *Nuovo Cimento*, **8**, 179, 781 (1958).

apart from an additive constant. It is evident at once that only the last term breaks the symmetry under the gauge transformation:

$$\text{(39)} \qquad \begin{cases} N \to (1 + i\boldsymbol{\tau}\cdot\boldsymbol{v}\gamma_5)N\,, \\ \boldsymbol{\pi} \to \boldsymbol{\pi} - 2\boldsymbol{v}\sigma'\,, \\ \sigma' \to \sigma' + 2\,\boldsymbol{v}\cdot\boldsymbol{\pi}\,, \end{cases}$$

with $\boldsymbol{v}$ constant. It is easy to see also that if the last term were absent the symmetry (39) would prevent the nucleon having any mass.

We now construct the pseudovector weak current from the same gauge transformation. We find:

$$\text{(40)} \qquad \frac{i\,\delta\mathscr{L}_2}{\delta\boldsymbol{v}} = -\,i\,\frac{\mu_0^2}{f_0}\boldsymbol{\pi},$$

so that eq. (27) holds with $a = -\mu_0^2/f_0$ as for the gradient coupling model. The current $\boldsymbol{P}_\alpha$ comes out:

$$\text{(41)} \qquad \boldsymbol{P}_\alpha = \bar{N}\boldsymbol{\tau}\gamma_\alpha\gamma_5 N + 2i(\sigma'\,\partial_\alpha\boldsymbol{\pi} - \boldsymbol{\pi}\partial_\alpha\sigma') = \\ = \bar{N}\boldsymbol{\tau}\gamma_\alpha\gamma_5 N + 2i(\sigma\,\partial_\alpha\boldsymbol{\pi} - \boldsymbol{\pi}\,\partial_\alpha\sigma) - \frac{i}{f_0}\,\partial_\alpha\boldsymbol{\pi}\,.$$

This time the gauge transformation that yields the axial vector current is closely related to the one (eq. (22)) that gives the vector current. Together, in fact, they form the generators of the rotation group in a four-dimensional Euclidean space. It is evident that, apart from the last term, the Lagrangian of eq. (38) is invariant under these four-dimensional rotations when the functions $\boldsymbol{u}$ and $\boldsymbol{v}$ are constant. The last term breaks the four-dimensional symmetry, but leaves the three-dimensional symmetry unchanged.

We may, if we like, consider a rotation in four dimensions that is a product of the rotations (22) and (39) with $\boldsymbol{u} = \boldsymbol{v} = \boldsymbol{w}$. We have:

$$\text{(42)} \qquad \begin{cases} N \to [1 + i\boldsymbol{\tau}\cdot\boldsymbol{w}(1 + \gamma_5)]N\,, \\ \boldsymbol{\pi} \to \boldsymbol{\pi} - 2\,\boldsymbol{w}\sigma' - 2\boldsymbol{w}\times\boldsymbol{\pi}\,, \\ \sigma' \to \sigma' + 2\boldsymbol{w}\cdot\boldsymbol{\pi}\,. \end{cases}$$

It is this rotation that generates the complete weak current $\boldsymbol{P}_\alpha + \boldsymbol{V}_\alpha$.

We see that if the mesons are taken out of the theory, then the transformation (42) works only on the free nucleon Lagrangian and we generate a weak current equal to $\bar{N}\tau_\alpha(1+\gamma_5)N$, which resembles the lepton weak current. Thus

the lack of symmetry between V and A mentioned in connection with the gradient coupling theory is not present here.

We don't have the divergence difficulty either—the present model is fully renormalizable. Moreover, the various matrix elements of the weak current seem to come out finite as well; even the renormalization factor $-G_A/G$ is finite (*).

Note that since $a = -\mu_0^2/f_0$ in both theories, eq. (33) is valid for both. (At first sight, it may look as if the individual theorems (34) and (35) also hold in the σ model, but in fact they don't work in perturbation theory.)

In view of eq. (33), which expresses $-G_A/G$ in terms of several divergent quantities, it may appear rather remarkable that it is finite. In particular, the reader may wonder what cancels the quadratic divergences of $\mu_0^2 - m_\pi^2$. The answer is that f_1/f_0 is the product of g_1/g_0 and m_0/m_1 and that in the σ model the quantity m_0/m_1 possesses quadratic divergences, even in second order. They come from « tadpole » diagrams in which a σ meson, emitted by the nucleon, turns into a nucleon and antinucleon that eat each other. It is the scalar, $I = 0$ quality of σ that makes such diagrams possible.

The σ model, although it has some agreable features that we have mentioned, is quite artificial. A new particle is postulated, for which there is no experimental evidence. It is true that if σ had a high enough mass it would not be easily detectable and that the theory allows for different π and σ masses, but we know of no theoretical reason for the mass of σ to come out very high.

The fact that the σ coupling is responsible for the nucleon mass is a curious property of the model. Unless we can explain all masses, or at least all baryon masses, in a similar way, it is not very satisfactory.

In any case, we are faced with the problem of extending our invariance under the v transformation to the strange particles. If we want to preserve the relation (27), we must add no new terms that violate the invariance for constant v.

Unfortunately the invariant coupling of π and σ', which we have used for the nucleon and which gives the nucleon mechanical mass through the coupling to σ', cannot be applied to an isotopic singlet or triplet like the Λ and Σ. We may, of course, make use of global symmetry ([18]) or a restricted version of it in which Λ and Σ are degenerate, so that they can be treated as a pair of doublets. But then all our theorems are approximate, violated by the mechanism that splits Λ and Σ; and the idea that the splitting interactions are « medium strong » and not very important has not received much experimental support.

(*) J. Bernstein, M. Gell-Mann and L. Michel: *Nuovo Cimento*, **16**, 560 (1960).

([18]) M. Gell-Mann: *Phys. Rev.*, **106**, 1296 (1957) and J. Schwinger: ref. ([16]).

6. – The non-linear model.

Let us consider the possibility of modifying the σ model by making the σ field a function of the π field rather than the field of a new particle. We want, however, to preserve the invariance (in eq. (38)) of the strong interaction Lagrangian $\mathscr{L}_2$ (except for the term $-(\mu_0^2/2f_0)\sigma'$) under four-dimensional rotations among π_x, π_y, π_z and σ'. Thus the only condition we can apply to $\boldsymbol{\pi}$ and σ' is the condition:

$$\boldsymbol{\pi}^2 + \sigma'^2 = C^2 , \tag{43}$$

where C is a constant. If we define g_0 to be positive, then we must take the negative square root for σ':

$$\sigma' = -\sqrt{C^2 - \boldsymbol{\pi}^2} ,$$

in order to have a positive mass term for the nucleon. If, when g_0 tends to zero, this mass term is to be simply m_0, then C^2 must be $1/4f_0^2$ so that $g_0\sqrt{C^2} = m_0$. We have, then,

$$\sigma' = -\sqrt{\frac{1}{4f_0^2} - \boldsymbol{\pi}^2} = -\frac{1}{2f_0}\sqrt{1 - 4f_0^2\boldsymbol{\pi}^2} . \tag{44}$$

Instead of the Lagrangian $\mathscr{L}_2$, we have:

$$\mathscr{L}_3 = \left\{ -\bar{N}[\gamma\,\partial - g_0(\sigma' + i\boldsymbol{\tau}\cdot\boldsymbol{\pi}\gamma_5)]\,N - \frac{(\partial\boldsymbol{\pi})^2}{2} - \frac{(\partial\sigma')^2}{2} - \frac{\mu_0^2}{2f_0}\sigma' \right\} \tag{45}$$

$$\sigma' = -\frac{1}{2f_0}\sqrt{1 - 4f_0^2\boldsymbol{\pi}^2} ,$$

to within a constant.

This Lagrangian can also be derived by another, slightly more general, method. We can modify the usual pseudoscalar coupling theory by changing every constant into an arbitrary function of π^2:

$$\mathscr{L}_3' = -\bar{N}\gamma\,\partial N - m_0(\pi^2)\bar{N}N + ig_0(\pi^2)\bar{N}\gamma_5\boldsymbol{\tau}\cdot\boldsymbol{\pi}N - \mu_0^2(\pi^2)\frac{\pi^2}{2} - \frac{1}{2}F_{ij}(\pi^2)\,\partial_\mu\pi_i\,\partial_\mu\pi_j ,$$

with

$$F_{ij}(\pi^2) = f_1(\pi^2)\,\delta_{ij} + f_2(\pi^2)\,\pi_i\pi_j .$$

This general expression contains five different *functions* of π^2 instead of only

one as in the previous derivation (*i.e.* $\sigma'(\pi^2)$). We now require that equations of motion have as a consequence eq. (27), and that $\mathscr{L}_3'$ tend to the usual pseudoscalar coupling theory when $g_0 \to 0$. It then follows that the five arbitrary functions are determined uniquely by these requirements and that the corresponding Lagrangian coincides with $\mathscr{L}_3$ to within a constant.

The new Lagrangian represents a theory of the strong interactions of nucleons and pions different from both the gradient coupling and the pseudoscalar coupling theories. We may re-express it as follows:

$$(46) \quad \mathscr{L}_3 = -\bar{N}[\gamma\partial + m_0\sqrt{1-4f_0^2\pi^2} - ig_0\boldsymbol{\tau}\cdot\boldsymbol{\pi}\gamma_5]N - \\ - \frac{(\partial\boldsymbol{\pi})^2}{2} - \frac{2f_0^2[\boldsymbol{\pi}\cdot\partial_\alpha\boldsymbol{\pi}]^2}{1-4f_0^2\pi^2} + \frac{\mu_0^2}{4f_0^2}(\sqrt{1-4f_0^2\pi^2}-1),$$

again to within a constant. Expanding the Lagrangian to first order in the coupling constant, we have just the pseudoscalar coupling theory, but the remaining orders modify the interaction and destroy its renormalizability in perturbation theory (*).

It is conceivable that the theory may somehow be renormalizable anyway. Suppose we consider the Lagrangian $\mathscr{L}_2$, which is certainly renormalizable, and express all the various amplitudes as functional integrals over classical field variables $\boldsymbol{\pi}$ and σ'. The results of the new theory are obtained from those of the σ theory simply by incorporating in the functional integrals a δ-function of $\sigma' + \sqrt{1/4f_0^2 - \pi^2}$. It is hard to see how this restriction of the integrations can really render the theory *more* singular.

We may think of the restriction $\pi^2 + \sigma'^2 = 1/4f_0^2$ as resulting simply from a choice of the parameter λ_0 in the Lagrangian $\mathscr{L}_2$ of the σ model. If we take $\lambda_0 \to +\infty$, then that corresponds, at least classically, to an infinitely steep potential well for the quantity $\pi^2 + \sigma'^2 - (1/4f_0^2)$, confining it to the value zero.

It should be noted that in the non-linear theory the higher order corrections to the pseudoscalar coupling Lagrangian are perhaps such as to improve agreement with experiment. We know that in the pseudoscalar theory in second order the scattering length for zero-momentum, zero-energy pions on nucleons is $-g^2/m$, while experimentally the low energy S-wave π-N scattering amplitude without charge exchange is very small. We can see, though, that in the Lagrangian $\mathscr{L}_3$ the second order term $2m_0f_0^2\bar{N}N\pi^2$ just cancels out the second order effect of the first order coupling. It seems that the cancellation of obnoxious terms like g^2/m, g^4/m, etc., occurs to all orders.

(*) J. Bernstein, M. Gell-Mann and L. Michel: *Nuovo Cimento*, **16**, 560 (1960).

There is perhaps some hope, then, that the non-linear Lagrangian might lead to a small S-wave π-$\mathcal{N}$ scattering amplitude without charge exchange in perturbation theory. The lowest order S-wave amplitude with charge exchange is in any case of the right order of magnitude, as in the pseudoscalar and gradient coupling theories.

The other new term that appears in second order is $-2f_0^2(\boldsymbol{\pi}\cdot\hat{\partial}_\alpha\boldsymbol{\pi}^2) - -(\mu_0^2/2)f_0^2(\pi^2)^2$, which describes π-π scattering with an unrenormalized amplitude of the order of $\mu_0^2 f_0^2$; it is interesting that CHEW and MANDELSTAM have considered π-π scattering with a renormalized amplitude of the order of $m_\pi^2 f_1^2$.

In the non-linear model, the construction of the weak currents by gauge transformations from the strong coupling Lagrangian goes through much as in the σ model. The important features are that the vector current is still divergenceless, the divergence of the pseudovector current is still proportional to the π field, and the gauge group is essentially the same as before.

It should be added that the π field used here is not of the usual type, since $|\boldsymbol{\pi}|<\frac{1}{2}f_0$. We can transform, however, to a more normal pion field $\tilde{\boldsymbol{\pi}}$ by a simple substitution such as $\boldsymbol{\pi} = \tilde{\boldsymbol{\pi}}(1+f_0^2\tilde{\boldsymbol{\pi}}^2)^{-1}$. Of course $\partial_\alpha \boldsymbol{P}_\alpha$ is still proportional to $\boldsymbol{\pi}$, not to $\tilde{\boldsymbol{\pi}}$. See BERNSTEIN, FUBINI, GELL-MANN and THIRRING (loc. cit.).

This third model belongs to a class of theories recently discussed by GÜRSEY [19], who has particularly emphasized the four-dimensional rotations, although he has not considered isotopic rotations that are functions of space and time.

7. – Symmetry operators of the models.

The symmetry properties of the models can best be exhibited in terms of the operators that generate the gauge transformations which, in turn, generate the weak current $\boldsymbol{P}_\alpha+\boldsymbol{V}_\alpha$. Let us consider the truncated version of each theory in which the term in the Lagrangian proportional to a is suppressed so that the weak current is exactly conserved. We may then construct the constant operator $\boldsymbol{R}$, proportional to $\int \mathrm{d}^3x(P_4+V_4)$, which generates the gauge transformations of the theory with infinitesimal gauge function $\boldsymbol{w}$:

$$(47)\qquad \left\{\begin{array}{l} \psi_i(x) \to (1-i\boldsymbol{R}\cdot\boldsymbol{w}(x))\,\psi_i(x)(1+i\boldsymbol{R}\cdot\boldsymbol{w}(x)) \\ \qquad\quad \to \psi_i(x) - i\boldsymbol{w}(x)\cdot[\boldsymbol{R},\,\psi_i(x)]\,, \end{array}\right.$$

[19] F. GÜRSEY: *Nuovo Cimento*, **16**, 230 (1960).

where ψ_i represents any of the field components. The operator $\boldsymbol{R}$ for the weak current is analogous to the electric charge operator Q for the electromagnetic current. We may, of course, separate the parts of $\boldsymbol{R}$ that correspond to the vector and the pseudovector currents. As long as we stick to the conserved vector current theory (and to our choice of scale for the gauge function), then the first part of $\boldsymbol{R}$ is simply twice the isotopic spin $\boldsymbol{I}$. Let us write:

$$\boldsymbol{R} = 2\boldsymbol{I} + 2\boldsymbol{D}\,, \tag{48}$$

where $2\boldsymbol{D}$ generates the pseudovector gauge transformations.

In the first model, it is easy to see from eq. (30), that $\boldsymbol{D}$ is a translation operator, so that we have the commutation rules:

$$[D_i, D_j] = 0\,, \tag{49}$$

as well as the rules

$$\begin{cases} [I_i, I_j] = i e_{ijk} I_k\,, \\ [I_i, D_j] = i e_{ijk} D_k\,, \end{cases} \tag{50}$$

that follow from $\boldsymbol{I}$ being the isotopic spin and $\boldsymbol{D}$ an isotopic vector. Here e_{ijk} is, of course the Kronecker antisymmetric tensor). The total operator $\boldsymbol{R}$ then has the commutation rules:

$$[R_i, R_j] = 4 i e_{jik}(I_k + 2D_k) \tag{51}$$

that exhibit the asymmetry between V and A characteristic of the gradient coupling model (*).

In the second and third models, the operator $\boldsymbol{D}$ is not a translation operator; in place of (4*a*) we have the commutation rules:

$$[D_i, D_j] = i e_{ijk} I_k\,, \tag{52}$$

which give for $\boldsymbol{R}$ the very simple rules:

$$[R_i, R_j] = 8 i e_{ijk}(I_k + D_k) = 4 i e_{ijk} R_k\,. \tag{53}$$

(*) Of course, what really counts is the nature of the commutation relations for the *complete* operators that generate the sum of the $\Delta S = 0$ and $\Delta S = 1$ currents.

In other words, $\boldsymbol{R}$ is just four times an angular momentum:

$$\boldsymbol{R} = 4\,\boldsymbol{I}_A \,. \tag{54}$$

But in the same way we can show that $2\boldsymbol{I} - 2\boldsymbol{D}$ is four times an angular momentum $\boldsymbol{I}_B$ and furthermore that $\boldsymbol{I}_A$ and $\boldsymbol{I}_B$ commute. Thus the isotopic spin $\boldsymbol{I}$ can be written as the sum of two commuting angular momenta:

$$\boldsymbol{I} = \boldsymbol{I}_A + \boldsymbol{I}_B \,. \tag{55}$$

and the weak current is just proportional to the current of the « spin » $\boldsymbol{I}_A$. We have just demonstrated the well-known property of the group of rotations in a four-dimensional Euclidean space ([20]), that it can be generated by two commuting angular momenta.

In our second and third models, we have assigned quantum numbers as follows:

$$\left\{ \begin{array}{ll} N_L & (\tfrac{1}{2},\, 0)\,, \\ N_R & (0,\, \tfrac{1}{2})\,, \\ (\pi,\, \sigma') & (\tfrac{1}{2},\, \tfrac{1}{2})\,, \end{array} \right. \tag{56}$$

where we use the notation of Gürsey ([19]), in which $N_L \propto (1+\gamma_5)N$ and $N_R \propto (1-\gamma_5)N$ and the quantum numbers are written in the form (I_A, I_B).

8. – Conclusions.

We have found three models of the strong and weak interactions of nucleons and pions in which the divergence of the axial vector weak current is proprotional to the pion field, and we have shown that this property can explain the decay rate of the charged pion.

The gradient coupling model is highly divergent without a cut-off and the weak interaction is introduced in a way that is unsymmetrical between V and A. However, to extend this model to the $\Delta S = 0$ weak interactions of strange particles is very easy. As long as the source of the pion field is the divergence of a pseudovector, we can always find an axial vector current with the right property.

([20]) A. PAIS: *Proc. Nat. Acad. Sci.*, **40**, 835 (1954).

The σ model is renormalizable and even the matrix elements of the weak coupling seem to be finite. Moreover, the four-dimensional invariance (broken only by one term which is responsible for the nucleon mass and for the non vanishing divergence of the axial vector current) gives complete symmetry between V and A. However the model involves the introduction of a new particle. It also presents difficulties when we try to extend it to the strange particles, because the high symmetry of the coupling to π and σ', while easy to arrange for a fermion of isotopic spin $\frac{1}{2}$ like the nucleon, is hard to imitate Λ or Σ or K, unless, of course, we do it approximately, making use of something like global symmetry.

The non linear model does not appear renormalizable although it might be so in some unusual sense. It avoids, however, the introduction of a new particle, while retaining the symmetry properties of the σ model. The difficulty of extension to the strange particles is of course the same for both models.

Since all the models seem to have some unpleasant features, we should certainly reconsider whether the formula of Goldberger and Treiman can be plausibly derived without such a stringent condition as eq. (5).

To the extent that one tries to retain eq. (5) or something like it, one might pursue further research along several lines: trying to include the strange particles; trying to renormalize the third model; exploring the connection of our gauge transformations with possible intermediate fields for the weak interactions; seeking to describe the $\Delta S = 1$ weak interactions as well as those with $\Delta S = 0$; and looking for parallels between the weak interactions of leptons and those of baryons and mesons.

In closing, let us emphasize that we wish this work to be considered as a highly tentative effort. We have after all, explained only one experimental number, the charged pion lifetime. We do not want to give the impression that the whole theory of strong and weak interactions should be based on this one number, like a pyramid balanced on one point. We do hope, however, that if this type of investigation is pursued further, it may lead to other predictions or to correlations of experimental data.

* * *

One of us (M. Gell-Mann) would like to thank Prof. Abdus Salam for his hospitality at Imperial College, London, and for many valuable conversations. He is grateful to Prof. R. P. Feynman and Drs. E. R. Norton and W. K. R. Watson for the discussions of the gradient coupling model that initiated this work. He is also indebted to Dr. J. Bernstein for discussions of gauge invariance.

RIASSUNTO (*)

Allo scopo di dedurre in maniera convincente la formula di Goldberger e Treiman per il tasso di decadimento dei pioni carichi, prendiamo in considerazione la possibilità che la divergenza della corrente vettoriale assiale nel decadimento β sia proporzionale al campo del pione. Si presentano tre modelli della interazione pione-nucleone (e della corrente debole) che hanno la proprietà richiesta. Il primo, che si serve dell'accoppiamento di gradiente, ha il vantaggio di poter essere facilmente generalizzato alle particelle strane, ma gli svantaggi di non essere rinormalizzabile e di introdurre le correnti vettoriale e vettoriale assiale in modo asimmetrico. Il secondo modello, che usa un'interazione forte proposta da SCHWINGER ed una corrente debole proposta da POLKINHORNE, è rinormalizzabile e simmetrico fra V ed A, ma comporta la postulazione di una nuova particella ed è difficilmente estensibile alle particelle strane. Il terzo modello è simile al secondo salvo che non è necessario introdurre una nuova particella. (Si perde, tuttavia, la rinormalizzazione nel senso usuale.) Si suggerisce una ulteriore ricerca su queste linee, compresa la considerazione della possibilità che il tasso di decadimento del pione possa ottenersi in modo plausibile con condizioni meno restrittive.

(*) *Traduzione a cura della Redazione.*

Compton Effect on the Bound Electrons.

D. Brini, E. Fuschini, N. T. Grimellini and D. S. R. Murty (*)

Istituto di Fisica dell'Università - Bologna
Istituto Nazionale di Fisica Nucleare - Sezione di Bologna

(ricevuto il 24 Febbraio 1960)

Summary. — The behaviour of the Compton differential cross section on the K-electrons of Pb was measured, using γ-rays of 664 keV energy. The investigated angles cover the $(10 \div 85)^\circ$ range. The behaviour, roughly, is not very different from the behaviour corresponding to free electrons. The more significant aspect is the indication of a cross section for the bound electrons greater than the cross section for free electrons.

1. – Introduction.

One of the important problems in the experimental study of the γ-rays elastic scattering is the separation of the elastic contribution from the inelastic (Compton) one. This problem is of considerable importance for small scattering angles ([1-3]) because the determination of the elastic scattering cross-section is, in these regions, usually carried out by subtracting the inelastic contribution, calculated using the Klein-Nishina formula, from the observed total scattering cross-section. Now, though these estimates could be reasonable for high energies ($\geqslant 1$ MeV) and light elements, it may happen that they are not so, when the electrons responsible for the scattering, are bound with binding energies which cannot be neglected with respect to the energy of the incident gamma. The inelastic scattering, in this case, may happen to have different cross-section from the corresponding one in the free electron case.

(*) Now at the Physics Department, Science College, Saifabad Hyderabad.
([1]) A. Storruste: *Proc. Roy. Soc.*, A **63**, 1197 (1950).
([2]) A. Storruste and O. P. Tjom: *Nucl. Phys.*, **6**, 151 (1958).
([3]) W. L. Davey: *Proc. Phys. Soc.*, A **66**, 1059 (1953).

Moreover, the problem has also some importance for the large scattering angles [4] because it seems that the predominating contribution to the scattering in this region is attributed to the electrons of the K-shell rather than to the others.

Several theoretical works exist in the literature on this subject [5-10] but unfortunately, the predictions made in these papers, supported by few experimental data, are very often in disagreement with one another, for different approximations, introduced in the development of the calculations.

The interest in the experimental study of the γ-ray inelastic scattering on bound electrons is twofold: firstly it may provide a possibility of carrying out more accurate determinations of the elastic scattering cross-section; secondly it seems possible to shed some light on the validity of the approximations introduced in the different theoretical works.

In addition, a better knowledge of this phenomenon provides the possibility of performing more correct calculations in projecting biological shielding against γ-radiations, especially if the diffusion from bound electrons plays, as it seems, an important role.

In the present paper we report the results of an experiment on the anelastic scattering of the 0.664 MeV γ-rays of ^{137}Cs on the strongly bound electrons of the K-shell of Pb.

2. – Experimental arrangement.

The selection of the inelastic scattering events on bound electrons was made by putting in coincidence the scattered γ-ray with the X-ray emitted by the atom after the emission of the electron; the energy of the X-photon is about equal to the binding energy.

In our experiment we chose a lead scatterer, because the K-electrons of lead are bound with 88 keV binding energy, and a source ^{137}Cs emitting γ-rays of 0.664 MeV energy. The essential of the scattering equipment is sketched in Fig. 1: the detectors are NaI(Tl) scintillators mounted on 6282 Dumont photomultipliers. The counter (1) (dimensions of scintillator 2 in. $\times\frac{1}{2}$ in.) detects the X-photons, which are isotropically emitted, and the counter (2) (dimensions of scintillator 1 in. $\times$ 1 in.) detects the Compton scattered photons. The

(4) J. RANDLES: *Proc. Phys. Soc.*, A **70**, 337 (1957).
(5) W. HEISENBERG: *Phys. Zeits.*, **32**, 737 (1931).
(6) L. BEWILOGUA: *Phys. Zeits.*, **32**, 740 (1931).
(7) W. FRANZ: *Zeits. Phys.*, **90**, 9, 635 (1934).
(8) A. T. NELMS: N.B.R. Circ 524 (1953).
(9) G. R. WHITE: N.B.R. Report 2763 (1953).
(10) C. M. DAVISSON: *Beta and Gamma Ray Spectroscopy* (Amsterdam, 1955).

detector (2) can be rotated in such a way as to collect the diffused γ-rays throughout the angles between 10° and 90°.

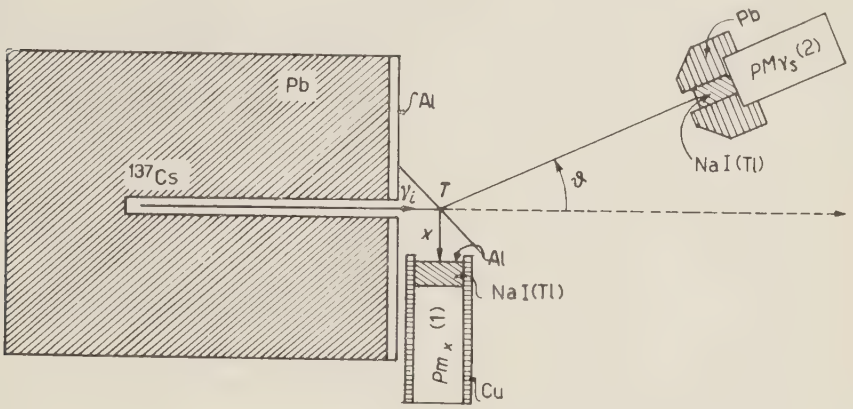

Fig. 1.

Counter (1) is placed outside the direct beam at a distance from its centre of 4.2 cm, and it is shielded by about 1 cm of Cu against X-photons coming from the lead of the collimation system. Counter (2) is shielded and collimated with lead to reduce the background and it is placed at a distance of 23.5 cm from the centre of the target. The target is a lead disk of 6.4 cm in diameter and 92.8 mg/cm² in thickness and was chosen to provide the maximum efficiency taking into account the self absorption of X-photons and the secondary diffusions of the scattered γ-rays.

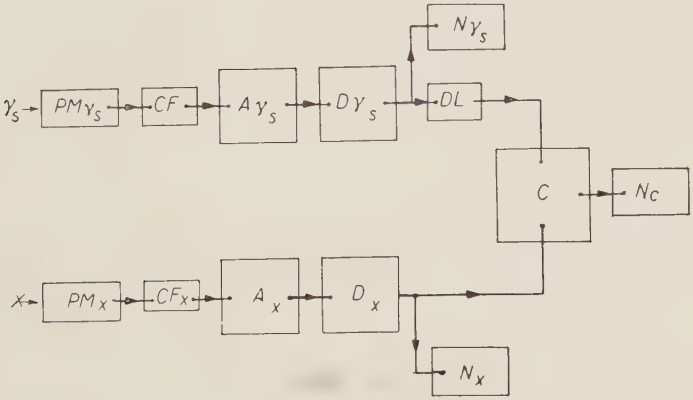

Fig. 2.

A block diagram of the electronic equipment is shown in Fig. 2. The two signals, indicated by X and γ_s are sent into two amplifiers A_X and A_{γ_s} and

afterwards into two integral discriminators D_X and D_{γ_s}. A delay line DL is inserted for counting the random events. The coincidence circuit C has a resolving time $\tau = 3 \cdot 10^{-7}$ s. The numerators N_X and N_{γ_s} count the single pulses of the two channels; they serve for controlling the stability of the equipment and to provide useful information about the normal Compton effect.

The measurements at every scattering angle, were carried out in the following order:

a) measurements with target and undelayed coincidence
b) » » » » delayed »
c) » without » » undelayed »
d) » » » » delayed »

The frequency of the seeked events is then given by

$$\nu_k = (a - b) - (c - d) .$$

3. – Experimental results.

Three series of measurements, corresponding to three different experimental conditions were performed. In the first series the bias of the X af γ_s channels were put at values corresponding to energies of 40 keV and 130 keV respectively. In the second series we set the bias in the X channel at a value corresponding to an energy of 60 keV and 70 keV. Evidently, the three different series correspond to three different efficiencies of the apparatus.

Measurements were performed at the following scattering angles: 10°, 17°.5, 25°, 35°, 50°, 65°, 85°; the angular uncertainty was about $\pm 5°$ estimated taking into account the possible scattering from the collimator of the diffused γ-rays.

The experimental results showed that the angular distribution has identical behaviour in the three series of measurements. For this reason we have averaged the values obtained, after a suitable normalization on the value at 50° of the third series.

TABLE I.

θ_{lab}	10°	17°.5	25°	35°	50°	65°	85°
ν_k (counts/min)	5.72 ± 0.92	5.15 ± 0.54	4.20 ± 0.38	2.33 ± 0.38	3.82 ± 0.42	2.14 ± 0.38	2.12 ± 0.19

The result is tabulated in Table I and plotted in Fig. 3. Table II shows the frequencies of the Compton scattered photons averaged on the three measurements and normalized on the third series.

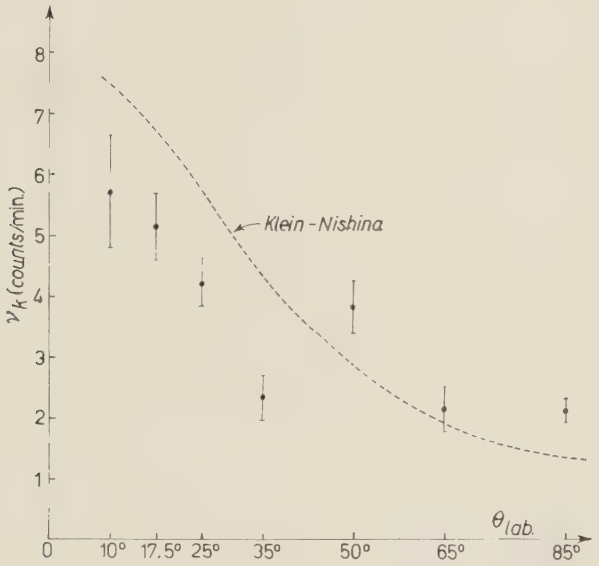

Fig. 3.

TABLE II.

θ_{lab}	10°	17°.5	25°	35°	50°	65°	85°
ν	1332±212	1040±147	836±120	708±147	477±57	312±21	189±71

4. – Discussion.

The behaviour of the coincidence frequency as a function of the scattering angles (Table I) is plotted in Fig. 3. The dashed line represents the behaviour of the Compton scattering cross-section calculated by the usual Klein-Nishina formula for 0.664 MeV energy.

As one can see, the experimental points show a slight indication of a certain smearing out in comparison with the free electron case.

We think that more significant indications can be desumed from the experimental data by comparing the cross-section of the investigated effect with the cross-section of the inelastic scattering from all the atomic electrons. For this purpose it is necessary to estimate the detection efficiency of the counting

apparatus. An overestimated approximation can be made using the following assumptions and data:

a) the average thickness of the target, crossed by isotropically emitted X-rays is:

$$s_m = s/\cos 45^\circ \simeq 65 \text{ mg/cm}^2 ;$$

b) the absorption coefficient in Pb, for X-rays coming from the electronic transitions MK, LK and ML in lead, which correspond to the energies:

$$E_1 = 88 \text{ keV} , \quad E_2 = 73 \text{ keV} , \quad E_3 = 15 \text{ keV} ,$$

respectively, are [11]

$$\mu_1 = 7.6 \text{ cm}^2/\text{g} , \quad \mu_2 = 2.1 \text{ cm}^2/\text{g} , \quad \mu_3 = 80 \text{ cm}^2/\text{g} ,$$

as a consequence, the transmission coefficients due to self absorption, result to be

$$\varepsilon_1 \simeq 0.61 , \quad \varepsilon_2 \simeq 0.87 , \quad \varepsilon_3 \simeq 0.006 .$$

One can see that the ML line is completely absorbed; therefore only the 88 keV and 73 keV lines remain;

c) the relative intensity of the two lines are given by [12]

$$I_{r1} = 0.25 , \quad I_{r2} = 0.75 ;$$

d) the fluorescence yield in lead is assumed to be [13]:

$$R \sim 94.8 \% ;$$

e) the interposed materials between the target and the X-rays detector correspond to a thickness of about 0.30 g/cm^3 of Al, whose absorption coefficients for the energies E_1 and E_2 are [11]:

$$\mu_{1\text{Al}} \simeq 0.18 \text{ cm}^2/\text{g} , \quad \mu_{2\text{Al}} \simeq 0.22 \text{ cm}^2/\text{g} .$$

This leads to the following transmission coefficients

$$\varepsilon_{1\text{Al}} \simeq 0.948 , \quad \varepsilon_{2\text{Al}} \simeq 0.938 ;$$

(11) R. D. Evans: *The Atomic Nuclei* (New York, 1955), p. 715.
(12) A. H. Compton and K. Allison: *X-Rays in Theory and Experiment.*
(13) F. Suzor and C. Charpak: *Journ. Phys. et Rad.*, **20**, 462 (1959).

f) the detection efficiency of the NaI(Tl) crystal for X-rays is about 100% for both energies;

g) the fraction of solid angle covered by the counter (1) is:

$$f = \Omega/4\pi \simeq 7 \cdot 10^{-2} ;$$

h) the electronic equipment efficiency is assumed equal to one.

From these positions the overall detecting efficiency results to be

$$\eta = \eta\,(88\ \text{keV}) + \eta\,(73\ \text{keV}) \leqslant 5 \cdot 10^{-2} .$$

Assuming this upper limit of the efficiency one can compare the scattering cross-section on the K-electrons with the cross-section relative to free electrons.

For this purpose we observe that the frequency of the events due to scattered γ-rays (Table II) may be expressed by:

$$\nu(\theta) = \alpha[(Z - Z_k)\sigma(\theta) + Z_k\sigma_k(\theta)] , \tag{1}$$

where Z is the atomic number of the element on which the inelastic scattering takes place, Z_k the number of electrons in the K-shell, σ and σ_k the cross sections for scattering on free and bound electrons respectively; α is a coefficient of proportionality depending upon the geometry and efficiency of the counter (2).

On the other hand, the frequency of the events corresponding to the coincidences may be expressed in the following form:

$$\nu_k(\theta) = \alpha\varepsilon\sigma_k(\theta)Z_k , \tag{2}$$

where every symbol has a meaning already defined. From equations (1) and (2) we can derive

$$\frac{\sigma_k(\theta)}{\sigma(\theta)} \gtrsim \frac{Z - Z_k}{Z_k[\eta R(\theta) - 1]} , \tag{3}$$

where $R(\theta)$ is the experimental value of the ratio ν_k/ν relative to every scattering angle.

Using the data of Tables I and II with $Z_k = 2$ we obtained the ratios tabulated in Table III and plotted in Fig. 4.

TABLE III.

θ_{lab}	10°	17°.5	25°	35°	50°	65°	85°
$\sigma_k(\theta)/\sigma(\theta)$	3.76 ± 1.02	4.40 ± 0.75	4.47 ± 0.91	2.75 ± 0.67	7.62 ± 1.52	6.35 ± 1.27	14.9 ± 6.27

Fig. 4 shows clearly enough a contribution of the strongly bounded K-electrons, to the Compton effect, greater than that of the other electrons. If we take into account also the contribution of the elastic scattering this effect would be emphasized. Table III, moreover, shows that the effect is more evident for large scattering angles.

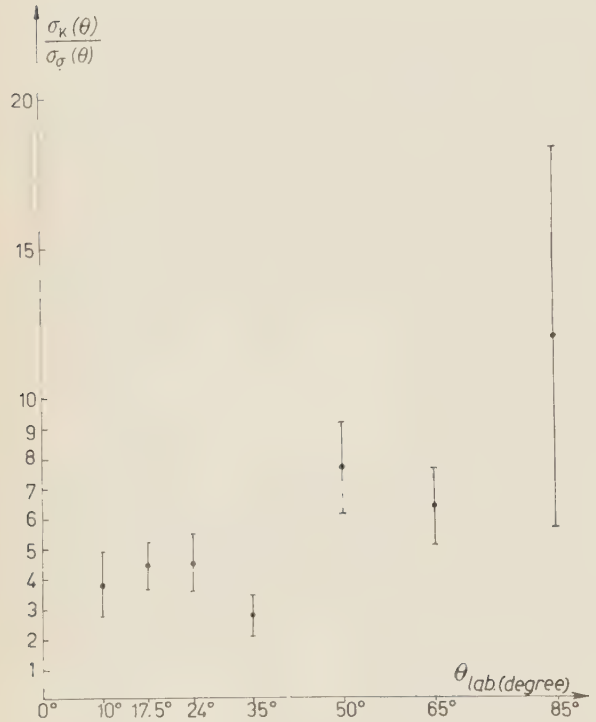

Fig. 4.

These results are supported by Randles' calculations ([4]), which confirm that the overall contribution of the K-electrons of heavy elements to the Compton effect amounts to about 80% of the total for large scattering angles and for γ energies < 1 MeV. From the Randles' point of view the ratio $\sigma_k(\theta)/\sigma(\theta)$ should have a value of the order of hundred. This value is, certainly overestimated, otherwise, as a consequence, we would expect an increasing in the overall diffused intensity of some orders of magnitude: this is not experimentally observed. Assuming, instead, an averaged ratio over all scattering angles $\sigma_k(\theta)/\sigma(\theta) \simeq 10$, one obtains, for Pb, a rise of the total diffused intensity of the order of some units per cent. Indeed examining the differences between the total absorption coefficients of Pb, measured and calculated, as given by WHITE ([14]), one can see that these differences are not equal to zero, and they increase when the energy of the incident gammas decreases.

Let us assume that this difference is due to the Compton effect on bound electrons and that it essentially depends on the ratio of binding energy with respect to the energy of the incident gammas. Fig. 5 shows the behaviour of

$$R = \frac{\mu_{\text{tot}}\,(\text{measured}) - \mu_{\text{tot}}\,(\text{calculated})}{\mu_{\text{Compton}}\,(\text{calculated})}\,,$$

([14]) G. WHITE GRODSTEIN: *X-Ray Attenuation Coefficients from* 10 keV *to* 100 MeV, N.B.S. circular, 583 (1957).

versus $\sqrt[3]{B_k}(h\nu/B_k)$, for Pb, Sn, Cu, Al, where $[\mu_{tot}\,(\text{measured}) - \mu_{tot}\,(\text{calculated})]$ is taken from White's ([14]) data and $[\mu_{Compton}\,(\text{calculated})]$ is calculated using the Klein-Nishina formula.

The choice of the parameter $\sqrt[3]{B_k}(h\nu/B_k)$ is suggested by the dependence of the total cross-section for photoelectric effect on the gamma incident energy $h\nu$ and on the K-electrons binding energy B_k ([15]). As it appears from Fig. 5, $\sqrt{B_k}(h\nu/B_k)$ seems to be a good parameter for the description of this phenomenon. Thus one can conclude that these results are in reasonable agreement with our assertion concerning the existence of an unnegligible contribution of the bound electrons to Compton scattering. This contribution works in the sense of an increase in the effective absorption, due to Compton effect, in comparison with that calculated; it rises with the binding energy of electrons (*i.e.* with Z) and decreases with increasing $h\nu$.

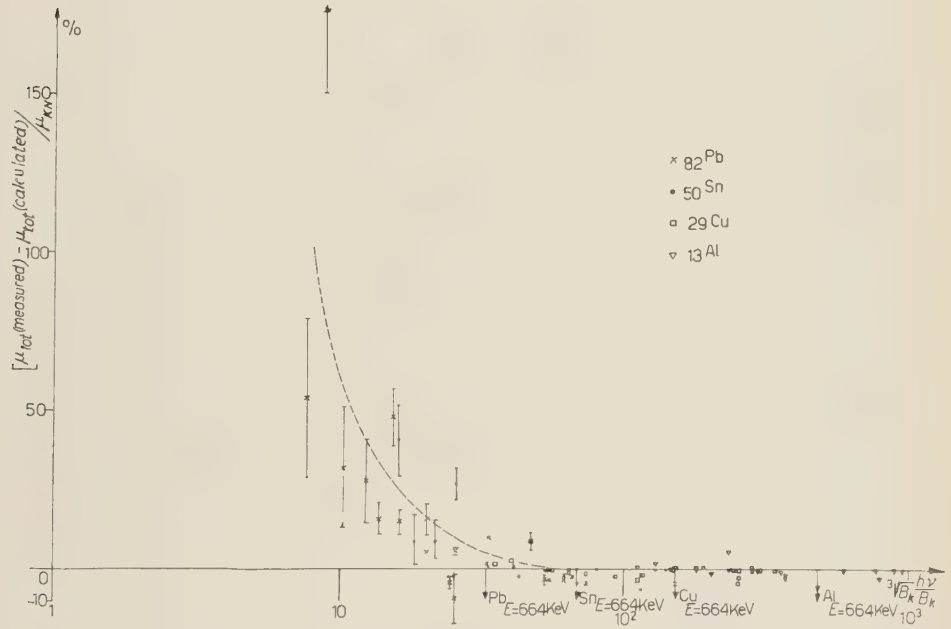

Fig. 5.

It is to be noticed that we used in our considerations, for the elastic scattering and photoelectric effect, the data reported by White. Since the data on the elastic scattering are overestimated, our quoted differences result to be lower limits. However, it is inessential, for our present considerations, to use

([15]) W. Heitler: *The Quantum Theory of Radiation* (1954), p. 207.

either the theory of Franz ([16]) or that of Brown and Mayer ([17]) on the elastic scattering of γ-rays.

For the reasons hitherto explained it seem to us that calculation of the incoherent scattering functions $S(q, z)$ ([11]) assuming the Thomas-Fermi model could lead to incorrect results. However, the indications provided by this experiment require more rigorous investigation from the theoretical point of view and more complete and systematic measurements which we are planning at present

* * *

The authors wish to thank Professors G. Puppi and P. Bassi for their many helpful discussions, and Mr. Fantazzi for his help in maintening the electronic equipment.

([16]) W. Franz: *Zeits. Phys.*, **98**, 314 (1936).

([17]) G. E. Brown and D. F. Mayers: *Proc. Roy. Soc.*, A **234**, 387 (1956); A **242**, 89 (1957).

RIASSUNTO

È stato misurato l'andamento della sezione d'urto differenziale per effetto Compton su elettroni K del Pb, usando raggi γ di energia 664 keV. Gli angoli investigati vanne da 10° a 85°. L'andamento, non si discosta molto da quello relativo agli elettroni liberi. L'aspetto più significativo dell'esperimento è l'indicazione di una maggior seziono d'urto per gli elettroni legati che per gli elettroni liberi.

IL NUOVO CIMENTO Vol. XVI, N. 4 16 Maggio 1960

The Problem of the Σ^-/Σ^+ Ratio in K^--p Interaction in Relation to the Hypothesis of Restricted Symmetry.

M. L. Gupta

Dept. of Mathematics, Imperial College - London

(ricevuto il 24 Febbraio 1960)

Summary — The problem of the Σ^-/Σ^- ratio has been discussed in the T^{-1} matrix formalism of Matthews and Salam (*). Global symmetry being found to be incompatible with the Σ^-/Σ^+ ratio even at threshold on the basis of new experimental data (Alvarez, Kiev Conference), consideration has been given to the restricted symmetry principle for explaining the behaviour of this quantity with energy. It has been found that restricted symmetry is quite compatible with the experimental data on hyperon production ratios in the K^--meson-proton interaction. The difference in the phase-shifts in the scattering of the systems πY and πZ in states of « restricted symmetry isotopic spin » $\frac{1}{2}$ and $\frac{3}{2}$ is found to be $-60°$ or $120°$, where Y and Z represent the two doublets formed out of Λ and Σ states as first proposed by Gell-Mann (3). It has also been indicated that the conclusions about the restricted symmetry principle reached by d'Espagnat and Prentki (8) on the basis of old experimental data are reversed when the new experimental values are substituted in place of the old ones, and the principle therefore remains quite a useful one for the interpretation of K^--meson-proton interaction phenomena.

1. – Introduction.

It has been recognized for a long time (1) that the K^--p interactions provide a fairly good test for the symmetries in pion-baryon interactions. The importance of the problem of the Σ^-/Σ^+ ratio in this connection was stressed by

(*) P. T. Matthews and A. Salam: *Nuovo Cimento*, **13**, 381 (1959).
(1) D. Amati and B. Vitale: *Nuovo Cimento*, **9**, 895 (1958).

SALAM (2) at the Kiev conference in relation to the hypothesis of global symmetry of the pion-baryon interaction put forward by GELL-MANN (3) and SCHWINGER (4) two years ago. It was shown by him that if the elements of the T^{-1} matrix for the K^--p interaction, pertaining to pion-hyperon processes are taken from the pion-nucleon scattering, the results obtained for the Σ^-/Σ^+ ratio are quite incompatible with the experimental behaviour of this quantity. Calculation with the new experimental data (5) presented at the conference only alters this position with regard to global symmetry for the worse, in that the Σ^-/Σ^+ ratio obtained at threshold now is found to be only 1:1 (as against the experimental value of 2.18:1), in the most favourable case, whereas with the use of old experimental data, an agreement between the theoretical and experimental values was found at least at threshold (2).

2. – Application of restricted symmetry.

The next step in understanding the behaviour of the Σ^-/Σ^+ ratio with energy is to use the less restrictive principle, that of restricted symmetry, by which we mean the equality, in the absence of K interactions of only the $\pi\Lambda$, $\pi\Sigma$ coupling constants, with no reference to the pion-nucleon coupling. The Σ and Λ states being arranged in two doublets of isotopic spin, $i = \frac{1}{2}$ defined by,

$$y = \begin{pmatrix} \Sigma^+ \\ Y^0 \end{pmatrix}, \qquad z = \begin{pmatrix} Z^0 \\ \Sigma^- \end{pmatrix},$$

with

$$Y^0 = \frac{\Lambda - \Sigma^0}{\sqrt{2}}, \qquad Z^0 = \frac{\Lambda + \Sigma^0}{\sqrt{2}},$$

the amplitudes of scattering in the states of isotopic spin 0 and 1 of the systems $\Sigma\pi$ and $\Lambda\pi$ can be expressed with the aid of the amplitudes of scattering $T'_{\frac{1}{2}}$ and $T'_{\frac{3}{2}}$ of the systems $Y\pi$ and $Z\pi$ ($i = \frac{1}{2}$ and $\frac{3}{2}$), defined by,

$$\langle \tfrac{1}{2} | T' | \tfrac{1}{2} \rangle = T'_{\frac{1}{2}}, \qquad \langle \tfrac{3}{2} | T' | \tfrac{3}{2} \rangle = T'_{\frac{3}{2}}, \tag{2.3}$$

with the orthogonality relation,

$$\tfrac{1}{2} | T' | \tfrac{3}{2} \rangle = 0$$

(2) *Lecture at the International Conference on High Energy Physics at Kiev* (July 1959).
(3) M. GELL-MANN: *Phys. Rev.*, **106**, 1297 (1957).
(4) J. SCHWINGER: *Ann. Phys.*, **2**, 407 (1957).
(5) L. W. ALVAREZ *et al.*: *Kiev Conference* (July 1959).

We have then, ($|\Sigma\pi\rangle_1$ meaning state of $\Sigma\pi$ with isotopic-spin 1, etc.)

$$(2.4)\qquad \begin{cases} \langle\Sigma\pi|\,T'\,|\Sigma\pi\rangle_0 = T'_{\frac{1}{2}}, \qquad \langle\Sigma\pi|\,T'\,|\Sigma\pi\rangle_1 = \frac{2}{3}\,T'_{\frac{1}{2}} + \frac{1}{3}\,T'_{\frac{3}{2}}, \\ \langle\Lambda\pi|\,T'\,|\Lambda\pi\rangle_1 = \frac{1}{3}\,T'_{\frac{1}{2}} + \frac{2}{3}\,T'_{\frac{3}{2}}; \\ \langle\Sigma\pi\,|\,T'\,|\Lambda\pi\rangle_1 \quad \langle\Lambda\pi\,|\,T'\,|\Sigma\pi\rangle_1 = \dfrac{\sqrt{2}}{3}\,T'_{\frac{3}{2}} - \dfrac{\sqrt{2}}{3}\,T'_{\frac{1}{2}}, \end{cases}$$

as obtained by Amati and Vitale [1] and similar relations for the elements of the T'^{-1} matrix. Thus,

$$(2.5)\qquad \langle\Sigma\pi|\,T'^{-1}\,|\Sigma\pi\rangle = \tfrac{2}{3}T'^{-1}_{\frac{1}{2}} + \tfrac{1}{3}T'^{-1}_{\frac{3}{2}} = \tfrac{2}{3}k\,\mathrm{ctg}\,\alpha_{\frac{1}{2}} + \tfrac{1}{3}k\,\mathrm{ctg}\,\alpha_{\frac{3}{2}} - ik =$$

$$= (\tfrac{2}{3}\alpha_1 + \tfrac{1}{3}\alpha_3) - ik \qquad \text{putting } k\,\mathrm{ctg}\,a_{\frac{1}{2}} = \alpha_1;\ k\,\mathrm{ctg}\,\alpha_{\frac{3}{2}} = \alpha_3.$$

where $\alpha_{\frac{3}{2}}$ and $\alpha_{\frac{1}{2}}$ are the phase-shifts for πY and πZ scattering in states of isotopic spin $i = \frac{3}{2}$ and $\frac{1}{2}$ respectively in the absence of K interactions. The same form of relations (2.4) is true for the elements of the R and R^{-1} matrices defined in the next section.

The elements of the T^{-1} matrix for the K^--p interaction pertaining to pion-hyperon processes having thus been expressed on the basis of the hypothesis of restricted symmetry, in terms of the two phase-shifts $\alpha_{\frac{1}{2}}$ and $\alpha_{\frac{3}{2}}$, the solution of the problem of the Σ^-/Λ^+ ratio consists of finding whether any real values of $\alpha_{\frac{1}{2}}$ and $\alpha_{\frac{3}{2}}$ exist which may give results for the Σ^-/Σ^+ ratio consistent with its experimental behaviour and with the other hyperon production ratios. The existence or non-existence of such values of $\alpha_{\frac{3}{2}}$ and $\alpha_{\frac{1}{2}}$ compatible with the experimental values of the Σ and Λ production ratios and phases, would constitute a proof for or gaainst the hypothesis of restricted symmetry.

3. – The T^{-1} matrix formalism for K^--p interaction.

We will analyse the problem of the Σ^-/Σ^+ ratio in the T^{-1} matrix formalism presented by Salam [2] at the Kiev Conference. The T^{-1} matrix is given by

$$T^{-1} = R^{-1} - ic\,,$$

R being the reaction matrix, real and symmetric (invariant with respect to time-reversal) and $c_{ij} = k_i\delta_{ij}$. For the s wave K^--p interaction, it consists of nine real parameters and may be written in two parts for the isotopic spin 0

and 1 channels. Thus,

$$T_0^{-1} = \begin{vmatrix} a_0 - ik_K & h_0 \\ h_0 & b_0 - ik_\Lambda \end{vmatrix}, \tag{3.1}$$

$$T_1^{-1} = \begin{vmatrix} a_1 - ik_K & h_1 & g_1 \\ h_1 & b_1 - ik_\Sigma & f_1 \\ g_1 & f_1 & c_1 - ik_\Lambda \end{vmatrix}. \tag{3.2}$$

For the isotopic spin zero case, the rows and columns of the matrix refer to K^--p and $\pi\Sigma$ channels while for the second case of isotopic spin one, they refer to K^--p, $\pi\Sigma$ and $\pi\Lambda$ channels.

The matrix elements of the T matrix can be obtained from the above and will satisfy necessarily the relations arising from the unitarity of the s matrix. The relationship between the T matrix and s matrix is expressed by,

$$S_{fi} = \delta_{fi} + 2i\sqrt{k_f}\, T_{fi} \sqrt{k_i}\,. \tag{3.3}$$

The cross-section for any process is given by,

$$\sigma_{fi} = 4\pi \frac{k_f}{k_i} |T_{fi}|^2\,. \tag{3.4}$$

In (3.3) and (3.4) the symbols have their usual meanings.

The elements T_{011} and T_{012} for elastic scattering and production respectively in isotopic spin 0 state are given by,

$$T_{011} = \frac{1}{[a_0 - h_0^2/(b_0 - ik\varepsilon)] - ik_k} = \frac{1}{z_0 - ik_k}\,. \tag{3.5}$$

where z_0 is the inverse of the complex scattering length introduced by Dalitz ([6]). Writing $z_0 = x_0 - iy_0$, we have,

$$x_0 = a_0 - \frac{h_0^2 b_0}{b_2^2 + k_\Sigma^2}, \qquad y_0 = \frac{h_0^2 k_\Sigma}{b_0^2 + k_\Sigma^2}\,. \tag{3.6}$$

Thus

$$T_{011} = \frac{1}{x_0 - i(y_0 + k_K)} = |T_{011}| \exp[i\theta_0]\,; \tag{3.7}$$

([6]) R. H. Dalitz: *CERN Report* (1958).

where

$$\text{tg}\,\theta_0 = \frac{y_0 + k_K}{x_0}, \tag{3.8}$$

$$T_{012} = \frac{-h_0}{(b_0 - ik_\Sigma)} |T_{011}| \exp[i\theta_0] = \sqrt{y_0/k_\Sigma}\, |T_{011}| \exp[i(\theta_0 + \varphi_0)], \tag{3.9}$$

where

$$\varphi_0 = k_\Sigma / b_0 . \tag{3.10}$$

Similarly the elements T_{1ij} of the T matrix for $I = 1$ case are given by

$$T_{1ij} = \frac{A_{ij}}{A_{11}} \frac{A_{11}}{\Delta} = \frac{|A_{ij}|}{|A_{11}|} \cdot |T_{111}| \exp[i(\theta_1 + \psi_{ij} - \psi_{11})], \tag{3.11}$$

where Δ is the determinant of the matrix T_1^{-1}, and ψ_{ij} are the phases of the complex numbers A_{ij} which are the co-factors of the elements a_{ij} in the determinanant of the matrix T_1^{-1}; also

$$\text{tg}\,\theta_1 = \frac{y_1 + k_K}{x_1}, \tag{3.12}$$

where $x_1 - iy_1 = z_1$ is the inverse of the complex scattering length for $I = 1$.

The angles ψ_{11} and ψ_{12} are given respectively by,

$$\text{tg}\,\psi_{11} = \frac{-k_\Sigma c_1 - k_\Lambda b_1}{b_1 c_1 - f_1^2 - k_\Lambda k_\Sigma}, \qquad \text{tg}\,\psi_{12} = \frac{h_1 k_\Lambda}{f_1 g_1 - h_1 c_1} . \tag{3.13}$$

4. – The new experimental data.

The new experimental results for the hyperon production ratios are (ALVAREZ: Kiev Conference, July, 1959):

$$\Sigma^- : \Sigma^+ : \Sigma^0 : \Lambda = 45 : 21 : 27 : 7 \quad \text{at threshold} . \tag{4.1}$$

Sigma production isotopic spin amplitudes,

$$\frac{T_1(\Sigma)}{T_0(\Sigma)} = r \exp[i\varphi] \qquad \text{where} \qquad |\varphi| = 62^\circ \pm 4^\circ . \tag{4.2}$$

Ratio of absorption in $I=0$ to $I=1$ states,

$$\frac{\sigma_{I=0}}{\sigma_{I=1}} = \frac{11.0 \pm 7.2}{17.4 \pm 7.7}. \tag{4.3}$$

The behaviour of the Σ^-/Σ^+ ratio is characterized by the fact that starting with a value 2.18:1 at threshold it rapidly drops to 1:1 at $k_K \approx .5\, m_{\pi c}$, and then remains in the neighbourhood of this value at higher energies.

5. – Relationships between the parameters of the T^{-1} matrix.

The T^{-1} matrix contains nine real parameters. These have been reduced to seven by expressing the elements pertaining to pion-hyperon processes in terms of the parameters α_1 and α_3. In order that all these parameters may be determined we must have seven relations between them. Four of these are provided by the Dalitz solutions giving the complex scattering lengths for $I=0$ and $I=1$. These utilize the information about the ratio of absorption in $I=0$ and $I=1$ state and other experimental data for elastic charge exchange and reaction cross-sections. We may get two more independent relations from the hyperon production ratios, one from the Σ^-/Σ^+ ratio, and the other from the ratio $\sigma(\Lambda)/\sigma_{I=1}(\Sigma)$. Thus in principle it is possible to find a relationship between α_1 and α_3 compatible with all the experimental data, provided restricted symmetry (equality of the interaction of Y and Z doublets or the Λ and Σ multiplets with the π field) is a valid concept and it is not too drastic an approximation to take the elements of the T^{-1} matrix corresponding to π-hyperon processes from the corresponding matrix for πY, πZ scattering in which the K interactions are switched off, *i.e.* to neglect the interaction of the K for the elements b_0, b_1, f_1 and c_1 of the T^{-1} matrix. Knowing the values of the Dalitz parameters there are thus two relationships to be fulfilled by the parameters α_1 and α_3, one arising from the Σ^-/Σ^+ ratio, and the other from the ratio $\sigma(\Lambda)/\sigma_{I=1}(\Sigma)$.

The Σ^-/Σ^+ the ratio is given by the expression,

$$\frac{\sigma(\Sigma^-)}{\sigma(\Sigma^+)} = \frac{\frac{1}{6}\sigma_{I=0} + \frac{1}{4}\sigma_{I=1}(\Sigma) + \sqrt{\sigma_{I=0}\sigma_{I=1}(\Sigma)}}{\frac{1}{6}\sigma_{I=0} + \frac{1}{4}\sigma_{I=1}(\Sigma) - \sqrt{\sigma_{I=0}\sigma_{I=1}(\Sigma)}}, \tag{5.1}$$

where $\chi =$ phase of $T_0(\Sigma)/T_1(\Sigma)$ or T_{012}/T_{112}.

Now we know from experiment the difference of phase of the Σ production amplitudes in $I=0$ and $I=1$ state, *i.e.* the phase difference between the elements T_{012} and $T_{1,12}$. The phase of T_{012} is $(\theta_0+\varphi_0)$, while that of $T_{1,12}$ is $(\theta_1+\psi_{12}-\psi_{11})$.

Thus $(\theta_1+\psi_{12}-\psi_{11})-(\theta_0+\varphi_0)=\gamma=\pm(62\pm4)^\circ$ (at threshold)or $(\psi_{12}-\psi_{11}-\varphi_0)=(\pm62\pm4)^\circ+\theta_0-\theta_1$.

Since ψ_{12}, ψ_{11} and φ_0 are independent of k_K (cf. (3.13) and (3.10)), they are nearly constant angles. Hence it follows that the angle on the right is also nearly constant with energy. Thus the relationship arising out of the behaviour of the Σ^-/Σ^+ ratio is that,

$$(5.2)\qquad (\psi_{12}-\psi_{11}-\varphi_0)=(\gamma+\theta_0-\theta_1)=\alpha \text{ (say) be nearly constant}$$

The other relationship coming from the ratio $\sigma(\Lambda)/\sigma_{I=1}(\Sigma)$ may be derived as follows.

From experiment,

$$\frac{\sigma(\Lambda)}{\sigma_{I=1}(\Sigma)}=\frac{\sigma(\Lambda)}{\sigma(\Sigma^+)+\sigma(\Sigma^-)-2\sigma(\Sigma^0)}=\frac{7}{12}\,.$$

From theory (cf. (3.4))

$$(5.3)\qquad \begin{cases} \dfrac{\sigma(\Lambda)}{\sigma_{I=1}(\Sigma)}=\dfrac{k_\Lambda\,|\,T_1(\Lambda)\,|^2}{k_\Sigma\,|\,T_1(\Sigma)\,|^2}=\dfrac{k_\Lambda}{k_\Sigma}\dfrac{\{(h_1f_1-g_1b_1)^2+g_1^2k_\Sigma^2\}}{\{(f_1g_1-h_1c_1)^2+h_1^2k_\Lambda^2\}} \\ \text{or} \\ \dfrac{7}{12}\cdot\dfrac{k_\Sigma}{k_\Lambda}=p \text{ (say)}=\dfrac{\{f_1^2-2f_1b_1x+b_1^2x^2+x^2k_\Sigma^2\}}{f_1^2x^2-2f_1xc_1+c_1^2+k_\Lambda^2}\,, \end{cases}$$

where $x=g_1/h_1$.

This relationship thus expresses the ratio of the parameters g_1/h_1 of the T^{-1} matrix (the elements corresponding to Λ and Σ production) in terms of b_1, c_1 and f_1 and hence in terms of α_1 and α_3 (cf. (2.5)). We have now to determine whether any real values of the parameters α_1 and α_3 exist compatibly with these two relations, which would thus provide a test for the validity of the principle of restricted symmetry in the presence of K interactions. To this end, we now derive the condition for the existence of real values of α_1 and α_3, based on the above two relationships and hence compatible with them. We shall call it the compatibility condition.

6. – The compatibility condition.

In the analysis that follows, we shall neglect the mass difference between the Λ and Σ particles in keeping with the principle of restricted symmetry.

The first relationship gives,

$$(6.1)\qquad \mathrm{tg}\,(\psi_{12}-\psi_{11}-\varphi_0)=\mathrm{tg}\,(\gamma+\theta_0-\theta_1)=\mathrm{tg}\,\alpha=m \text{ (say)}\,.$$

The values of b_0, b_1, c_1, f_1 of the T^{-1} matrix in terms of α_1 and α_3 are (cf. (2.4), (2.5))

$$(6.2)\quad b_0 = \alpha_1, \qquad b_1 = \frac{2\alpha_1}{3} + \frac{\alpha_3}{3}, \qquad c_1 = \frac{2\alpha_3}{3} + \frac{\alpha_1}{3}, \qquad f_1 = \frac{\sqrt{2}}{3}\alpha_3 - \frac{\sqrt{2}}{3}\alpha_1,$$

where

$$(6.3)\quad \alpha_1 = k \operatorname{ctg} \alpha_{\frac{1}{2}} : \operatorname{tg} \alpha_{\frac{1}{2}} = \frac{k}{\alpha_1},$$

$$(6.4)\quad \alpha_3 = k \operatorname{ctg} \alpha_{\frac{3}{2}} : \operatorname{tg} \alpha_{\frac{3}{2}} = \frac{k}{\alpha_3}.$$

Now $\operatorname{tg} \varphi_0 = k_\Sigma / b_0 = k_\Sigma / \alpha_1$ (from (3.10) and (6.2))
Hence

$$(6.5)\quad \varphi_0 = \alpha_{\frac{1}{2}} \qquad \text{or} \qquad (\alpha_{\frac{1}{2}} + \pi)$$

also

$$\operatorname{tg} \psi_{11} = \frac{-k_\Sigma(b_1 + c_1)}{b_1 c_1 - f_1^2 - k_\Sigma^2} \qquad \text{(cfr. (3.13))}$$

$$= \frac{-k_\Sigma(\alpha_1 + \alpha_3)}{\alpha_1\alpha_3 - k_\Sigma^2} = -\operatorname{tg}(\alpha_{\frac{1}{2}} + \alpha_{\frac{3}{2}}).$$

Hence

$$(6.6)\quad \psi_{11} = -(\alpha_{\frac{1}{2}} + \alpha_{\frac{3}{2}}) \qquad \text{or} \qquad -(\alpha_{\frac{1}{2}} + \alpha_{\frac{3}{2}}) + \pi.$$

Again from(3.13)

$$\operatorname{tg} \psi_{12} = \frac{h_1 k_\Sigma}{f_1 b_1 - h_1 c_1} = \frac{k_\Sigma}{f_1 x - c_1},$$

where $g_1/h_1 = x$.

Now the value of x is given by the second relation, equation (5.3), and is found to be

$$(6.7)\quad x = \frac{-(2f_1b_1 - 2pf_1c_1) \pm \sqrt{4p(b_1c_1 - f_1^2)^2 + 4p(k_\Sigma^2 c_1^2 + b_1^2 k_\Sigma^2 + k_\Sigma^4) - 4p^2 f_1^2 k_\Sigma^2 - 4k_\Sigma^2 f_1^2}}{2(pf_1^2 - b_1^2 - k_\Sigma^2)}.$$

In the above expressions $p = 1/1.71 = k_\Sigma/k_\Lambda = .41$, which is the exact value of this quantity. On making the approximation $k_\Sigma = k_\Lambda$, $p \approx .6$ which is much different from its true value. It is a much better approximation, and it leads to a great simplification to choose $p = .5$.

Expressing b_1, c_1 and f_1 in terms of α_1 and α_3 and making the above approximation, we find

$$(6.8)\quad x = \frac{-\sqrt{\frac{2}{3}}(\alpha_3 - \alpha_1)\alpha_1 \pm \sqrt{2}(\alpha_1\alpha_3 + k_\Sigma^2)}{-\frac{2}{3}(\alpha_1^2 + 2\alpha_1\alpha_3 + 3k_\Sigma^2)}.$$

Case 1. Taking the positive sign first in the numerator, we have,

$$x = -\frac{\sqrt{2}}{2} = -.7 .$$

Thus one of the values of x is independent of α_1 and α_3 and is nearly constant $\approx -.7$.

Using this value of x in the expression of tg ψ_{12}, we have,

$$\text{tg } \psi_{12} = \frac{k_\Sigma}{f_1 x - c_1} = \frac{k_\Sigma}{(\sqrt{2}/3)(\alpha_3 - \alpha_1)(-\sqrt{2}/2) - (2\alpha_3/3 + \alpha_1/3)} = \frac{k_\Sigma}{-\alpha_3} .$$

Hence

$$\psi_{12} = -\alpha_{\frac{3}{2}} \qquad \text{or} \qquad -\alpha_{\frac{3}{2}} + \pi ,$$

$$(6.9) \qquad (\psi_{12} - \psi_{11} - \varphi_0) = (-\alpha_{\frac{3}{2}} + n_1\pi) + (\alpha_{\frac{1}{2}} + \alpha_{\frac{3}{2}} - n_2\pi) - \alpha_{\frac{1}{2}} - n_3\pi = 0 \quad \text{or} \quad \pi$$

(where n_1, n_2, n_3 are each equal to zero or π) or

$$(6.10) \qquad (\gamma + \theta_0 - \theta_1) = 0 \qquad \text{or} \qquad \pi ,$$

which is the first compatibility condition. The principle of restricted symmetry would be valid if the angle $(\gamma + \theta_0 - \theta_1)$ satisfied this condition, although we do not expect it, since that would imply that any values of the phase shifts $\alpha_{\frac{1}{2}}$ and $\alpha_{\frac{3}{2}}$ are consistent with the Σ^-/Σ^+ ratio and the other hyperon production ratios. It is actually found on substituting the values of θ_0 and θ_1 obtained from the Dalitz and Tuan's solutions $a^\pm$ and $b^\pm$ that the value of γ obtained from this condition is very different from the experimental value of $(62 \pm 4)^\circ$ at threshold. Hence the value of x chosen is quite incompatible with the behaviour of the Σ^-/Σ^+ ratio. We shall therefore discard it.

Case 2. We now choose the negative sign in the expression of x. Thus, from (6.8)

$$x = \frac{(-\sqrt{2}/3)(\alpha_3 - \alpha_1)\alpha_1 - \sqrt{2}(\alpha_1\alpha_3 + k_\Sigma^2)}{-\frac{2}{3}(\alpha_1^2 + 2\alpha_1\alpha_3 + 3k_\Sigma^2)} = \frac{(4\alpha_1\alpha_3 - \alpha_1^2 + 3k_\Sigma^2)}{\sqrt{2}(\alpha_1^2 + 2\alpha_1\alpha_3 + 3k_\Sigma^2)},$$

which gives

$$(6.11) \qquad \text{tg } \psi_{12}\left(= \frac{k_\Sigma}{f_1 x - c_1}\right) = \frac{k_\Sigma(\alpha_1^2 + 2\alpha_1\alpha_3 + 3k_\Sigma^2)}{(-3\alpha_1^2\alpha_3 - k_\Sigma^2\alpha_3 - 2k_\Sigma^2\alpha_1)} .$$

Hence

$$(\psi_{12} - \psi_{11} - \varphi_0) = \psi_{12} + (\alpha_{\frac{1}{2}} + \alpha_{\frac{3}{2}}) + n_1\pi - (\alpha_{\frac{1}{2}} + n_2\pi)$$

where n_1 and n_2 have values 0 or 1.

$$= (\psi_{12} + \alpha_{\frac{3}{2}}) + n_1\pi - n_2\pi$$

or

$$\text{tg}\,(\psi_{12} - \psi_{11} - \varphi_0) = \text{tg}\,(\psi_{12} + \alpha_{\frac{3}{2}})\,. \tag{6.12}$$

From the value of $\text{tg}\,\psi_{12}$ given above (equation (6.11)) and of $\text{tg}\,\alpha_{\frac{3}{2}} = k/\alpha_3$ we find,

$$\text{tg}\,(\psi_{12} + \alpha_{\frac{3}{2}}) = \frac{2\,\text{tg}\,\beta}{3 + \text{tg}^2\,\beta}\,, \tag{6.13}$$

where

$$\beta = (\alpha_{\frac{3}{2}} - \alpha_{\frac{1}{2}})\,. \tag{6.14}$$

Thus

$$\frac{2\,\text{tg}\,\beta}{3 + \text{tg}^2\,\beta} = \text{tg}\,(\psi_{12} - \psi_{11} - \varphi_0) = \text{tg}\,(\gamma + \theta_0 - \theta_1) = m \text{ say}\,,$$

$$m\,\text{tg}^2\,\beta - 2\,\text{tg}\,\beta + 3m = 0 \qquad \text{or} \qquad \text{tg}\,\beta = \frac{2 \pm \sqrt{4 - 12m^2}}{2m}\,. \tag{6.15}$$

In order that β may be a real angle,

$$12m^2 \leqslant 4 \qquad \text{or} \qquad |m| \leqslant \frac{1}{\sqrt{3}}\,, \tag{6.16}$$

which is the second compatibility condition.

7. – Comparison with experiment.

i) *Case of Dalitz* $b^{\pm}$ *solution.* The compatibility condition gives, $|\text{tg}\,(\gamma + \theta_0 - \theta_1)| \leqslant 1/\sqrt{3}$. The values of θ_0 and θ_1 are given by the Dalitz solution. Taking the $b^{\pm}$ solution (corresponding to the absorption ratio in $I = 0$ to $I = 1 \approx 4$), which are, $A_0 = \pm\,2.01 + 1.27i$; $A_1 = \pm\,.37 + .32i$, we find, $\theta_0 \approx +\,32^\circ$ or $(\pi - 32^\circ)$; $\theta_1 \approx 41^\circ$ or $(\pi - 41^\circ)$: $(\theta_0 - \theta_1) = \pm\,9^\circ$. Hence $\alpha = (\gamma + \theta_0 - \theta_1) = \pm\,62^\circ \pm 9^\circ \pm 4^\circ = \pm\,71^\circ \pm 4^\circ$ or $\pm\,53^\circ \pm 4^\circ$.

It is seen that the angle α does not satisfy the compatibility condition. Thus the usefulness of restricted symmetry is excluded on the basis of the $b^{\pm}$ solutions.

ii) *The solutions $a^\pm$ of Dalitz.* We now consider the solutions $a^\pm$ of Dalitz. These are $A_0 = \mp .03 + 1.02i$, $A_1 = \pm 1.47 + .25i$ which give, $\theta_0 = 9°41'$ or $(\pi - 91°41')$, $\theta_1 = 9°41'$ or $(\pi - 9°41')$; $(\theta_0 - \theta_1) = \pm 82°$.

Hence $\alpha = ((\pm 62 \pm 4) \pm 82)° = (\pm 20 \pm 4)°$ or $\pm (144 \pm 4)°$.

Now the compatibility condition requires $|\alpha| \leqslant 30°$ or $\geqslant 150°$. It is seen that the first value of α ($(\pm 20 \pm 4)°$) clearly satisfies this condition, while the second value $\pm 148°$ which is very close to 150° must also be regarded as satisfying it in view of the approximations we have made. The results obtained on the basis of restricted symmetry utilizing the $a^\pm$ solutions are therefore quite compatible with the experimental data at threshold.

Since α is nearly a constant angle, one of the above two values of α satisfying the compatibility condition, must give the correct behaviour of the Σ^-/Σ^+ ratio even at a higher energy (assuming the validity of the zero range approximation). This value may easily be found when we remember that γ has to be $\approx 90°$ around $k_K = .5\, m_\pi c$ (cf. 5.1)).

Now at $k_K = .5\, m_\pi c$, $\theta_0 = 91°45'$ or $(\pi - 91°45')$; $\theta_1 = 34°47'$ or $(\pi - 34°47')$ $(\theta_0 - \theta_1) = \pm 57°$.

It is seen that if α is taken to be $\pm 148°$, then $\gamma \pm 91°$. Hence it follows that restricted symmetry is quite compatible with the observed behaviour of the Σ^-/Σ^+ ratio and other hyperon production ratios.

Knowing the value of α, which gives agreement with experiment, we may now find the value of β, the difference of the phase-shifts in πY or πZ scatterings in states of restricted symmetry i-spin, $i = \frac{1}{2}$ and $\frac{3}{2}$.

From (6.15) we have, $\operatorname{tg} \beta = 2/2m$ for $\alpha = 150°$.

$$= \frac{1}{-.58} = -1.7 .$$

Hence $\beta = -60°$ or $+120°$.

Since we are free to choose any signs and magnitudes for the angles $\alpha_{\frac{1}{2}}$ and $\alpha_{\frac{3}{2}}$ consistent with the above values of β, it is clear that many solutions compatible with the principle of restricted symmetry are possible for the problem of the Σ^-/Σ^+ ratio.

After the foregoing conclusions had been reached, we received the preprint of a paper by B. D'ESPAGNAT and J. PRENTKI (7), « Incompatibility between the hypothesis of restricted symmetry and some experimental results » in which the authors using old experimental data and a slightly different formalism had reached quite an opposite conclusion that restricted symmetry was not compatible with experiment and was therefore not a useful concept.

(7) B. D'ESPAGNAT and J. PRENTKI: preprint.

It is however found that the use of new experimental data changes the situation completely, leading even in their formalism to essentially the same compatibility condition as (6.16) and the same value of β as obtained above; and hence to the same conclusions about restricted symmetry. The treatment of the problem of the Σ^-/Σ^+ ratio given in the present paper is analogous to their method II, « the comparison of T^{-1} », and follows in some ways their presentation. It is found that no solutions are possible on the basis of their method I, « the comparison of T's » since the use of this method does not reproduce the qualitative features of the phenomena. It is proposed to discuss this point in a separate note.

* * *

The author feels deeply thankful to Prof. A. Salam for his suggesting the problem and for guidance and encouragement.

RIASSUNTO (*)

Il problema del rapporto Σ^-/Σ^+ è stato discusso nel formalismo della matrice T^{-1} di Matthews e Salam (*). Essendosi riscontrato, sulla base di nuovi dati sperimentali (Alvarez, Congresso di Kiev) che la simmetria globale è incompatibile col rapporto Σ^-/Σ^+ anche alla soglia, si è preso in considerazione il principio della simmetria ristretta per spiegare il comportamento di questa quantità al variare dell'energia. Si è trovato che la simmetria ristretta è perfettamente compatibile con i dati sperimentali sui rapporti di produzione degli iperoni nella interazione fra mesone K^- e protone. Si è trovato che la differenza nello spostamento di fase, nello scattering dei sistemi πY e πZ in stati di « spin isotopico a simmetria ristretta » $\frac{1}{2}$ e $\frac{3}{2}$, è -60° o 120°, in cui Y e Z rappresentano i due doppietti generati dagli stati Λ e Σ, come ha proposto per primo Gell-Mann (3). Si è anche indicato che le conclusioni sul principio di simmetria ristretta a cui giungono d'Espagnat e Prentki (8) sulla base dei vecchi dati sperimentali vengono rovesciate quando si sostituiscono i nuovi valori sperimentali al posto dei vecchi, ed il principio conserva tutta la sua utilità per l'interpretazione dei fenomeni di interazione fra K^- e protoni.

(*) *Traduzione a cura della Redazione.*

An Investigation of the Stability of Nucleons.

G. K. Backenstoss, H. Frauenfelder (*) (**), B. D. Hyams, L. J. Koester jr. (*) and P. C. Marin (**)

CERN - Geneva

(ricevuto il 26 Febbraio 1960)

Summary. — A search has been made for relativistic charged particles emitted by the decay of nucleons. No such events were detected, and according to postulates made about the decay mode, lower limits may be set on the nucleon lifetime. These vary between $1.5 \cdot 10^{26}$ and $2.8 \cdot 10^{26}$ years for nucleons in many-particle nuclei and between $2.2 \cdot 10^{24}$ and $4.7 \cdot 10^{24}$ years for protons in hydrogen.

1. – Introduction.

Some of the well-known conservation laws, *e.g.* for energy, momentum, and parity, are clearly connected to symmetry principles. The meaning of some other empirically observed conservation laws is much less well understood [1,2].

One of the laws, which may be the result of some deeper but not yet well understood symmetry, is the conservation of baryons. This is a generalization of the law of conservation of nucleons, first expressed by Stueckelberg [3], and later used by Wigner to explain the stability of matter [4]. The degree

(*) On sabbatical leave from the University of Illinois, Urbana, Ill., U.S.A.

(**) John Simon Guggenheim Fellow.

(***) On leave of absence from C.N.R.S., France.

(1) G. C. Wick: *Ann. Rev. Nucl. Sci.*, **8**, 1 (1958).

(2) G. Feinberg and M. Goldhaber: *Proc. Natl. Acad. Sci. U. S.*, **45**, 1301 (1959).

(3) E. C. G. Stueckelberg: *Helv. Phys. Acta*, **11**, 317 (1938).

(4) E. P. Wigner: *Proc. Am. Phil. Soc.*, **93**, 521 (1949); *Proc. Natl. Acad. Sci. U. S.*, **38**, 449 (1952).

to which this law holds is usually expressed by a limit on the lifetime of nucleons. An obvious lower limit results from the fact that non-radioactive elements must have been stable at least during the age of the universe. A much better limit was obtained experimentally by REINES, COWAN and GOLDHABER ([5,6]). Looking for possible proton decays in a large scintillation counter, they found for the free proton $\tau > 10^{21}$ years and for bound protons $\tau > 4 \cdot 10^{23}$ years. The stability of certain heavy nuclei against fission yields a limit of $\tau > 2 \cdot 10^{23}$ years for bound nucleons decaying by *any* mode ([7]).

In this paper, we report a reinvestigation of the limit to the stability of nucleons, which was stimulated by a speculation of YAMAGUCHI ([8]). The present experiments result in a lower limit to the lifetime of nucleons a few orders of magnitude longer than that of previous work.

2. – Method.

The interpretation of this experiment is based on the assumption that while charge, energy, momentum and angular momentum may be conserved, a proton or neutron may decay into lighter particles. Possible decays might include

(A) $$\mathrm{p} \rightarrow \mathrm{e}^+ + \mathrm{e}^+ + \mathrm{e}^-$$

or

(B) $$\mathcal{N} \rightarrow \pi^+ + \pi^- + \nu$$

with a total energy release of the rest energy of the nucleon.

This experiment sought to detect relativistic charged particles emerging from such decay processes in matter beneath an array of counters. The background due to natural radioactivity was eliminated by demanding an energy release of at least 5.0 MeV in one counter, and in addition a relativistic particle in another counter. The background due to cosmic rays was reduced by demanding that the relativistic particle travel upwards, and by running the whole experiment at 800 meters below rock.

([5]) F. REINES, C. L. COWAN jr. and M. GOLDHABER: *Phys. Rev.*, **96**, 1157 (1954).
([6]) F. REINES, C. L. COWAN jr. and H. W. KRUSE: *Phys. Rev.*, **109**, 609 (1957).
([7]) G. N. FLEROV, D. S. KLOCHOV, V. S. SKOBKIN and V. V. TERENTIEV: *Sov. Phys. Dokl.*, **3**, 78 (1958).
([8]) Y. YAMAGUCHI: *Progr. Theor. Phys.* (*Kyoto*), **22**, 373 (1959), and *Progr. Theor. Phys. Suppl.*, (1959) to be published.

3. – Apparatus.

The counter array used is drawn to scale in Fig. 1. The upper counter was a Čerenkov detector consisting of a sealed plexiglas box, 50 litres in volume, with 1 cm walls, filled with paraffin oil. It was viewed from above by four photomultiplier tubes, with their outputs in parallel, referred to henceforth as counter (1/4). It was viewed from below by four tubes, with their outputs in parallel, referred to as counter (5/8).

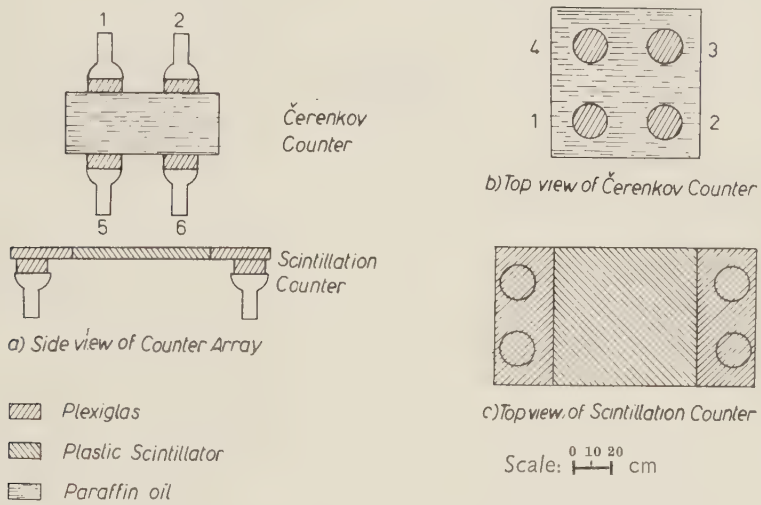

Fig. 1. – Counter arrangement.

The entire Čerenkov counter array could be rotated about a horizontal axis. Except for the surfaces in optical contact with the active area of the photomultipliers the top and bottom surfaces were painted black. The sides of the box were wrapped with aluminum foil.

The lower counter consisted of a scintillating plastic sheet, 4 cm thick, viewed by four photomultipliers, with outputs in parallel, coupled to it with plexiglas light guides. The mean pulse amplitude from cosmic rays traversing it at normal incidence at different positions along the plastic scintillator sheet were observed to differ by less than $\pm 10\%$ anywhere over its surface. All twelve photomultipliers used were 5 in. diameter 10 stage Dumont type 6364 tubes. The separate pulses from the tenth dynodes of the scintillation counters, counter (1/4), and counter (5/8) were delayed with respect to one another, added, displayed on a type 517A oscilloscope and photographed. The oscillo-

scope time base was triggered by pulses from the scintillation counter photomultiplier tube anodes.

The apparatus was run at 400 m above sea level (at Geneva) and below about 800 m of rock of density 2.8 g/cm³, in the Lötschberg tunnel (Kandersteg).

4. – Measurements.

The voltages on all 12 photomultipliers were adjusted to give the same output from cosmic ray particles at sea level. The sensitivity of each tube was thereafter measured and if necessary adjusted with the aid of a ^{60}Co source.

The scintillation counter bias curve was measured regularly with sources of about 1 mC of ^{60}Co and RdTh placed at a fixed distance of about 1 m from it. Its counting rates above ground and under rock are shown in Fig. 2.

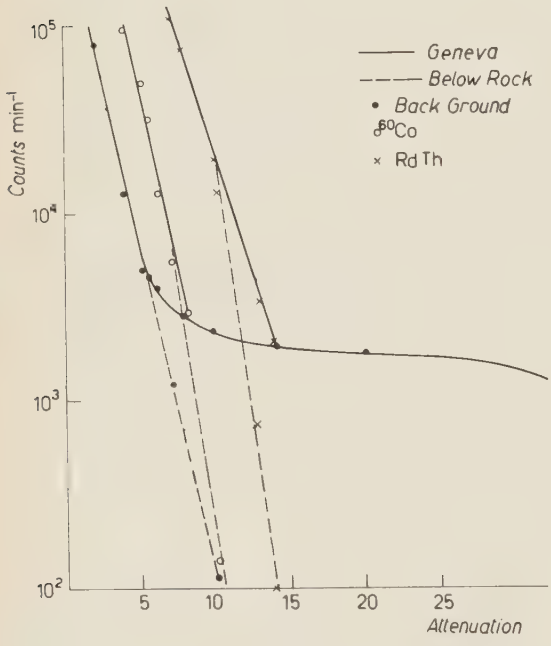

Fig. 2. – Counting rates of the scintillation counter *vs.* attenuation.

Above ground. – At 400 m above sea level the following information was obtained about the counter performance. By coincidence measurements with auxiliary counters, the efficiency of counter (5/8) was shown to be greater than 95% for recording cosmic ray particles traversing its full thickness.

The oscilloscope was thereafter triggered by scintillation counter pulses greater than 5 MeV and the oscilloscope traces showed 600 counts per minute in (5/8), the « upward » looking counter. Thirty percent of these counts were accompanied by measurable pulses from counter (1/4). The ratio of the mean amplitude of (5/8) to (1/4) pulses was 11 to 1, and in only 1% of the events was this ratio less than 3 to 1. When the Čerenkov counter was rotated through 180°, the performance was the same but with the roles of counter (1/4) and (5/8) interchanged. From this the Čerenkov counter is seen to be efficient and highly directional.

About 1 trace per minute showed a larger pulse in the downward « looking » counter than in the upward « looking » counter. This is compatible with the calculated flux from upward moving cosmic ray particles such as decay electrons from μ-mesons, electrons scattered through large angles, and particles from nuclear interactions. From this observed rate it was calculated that below 800 m of rock not more than one upward moving particle would be observed in 60 days.

Below rock. – Below rock, the oscillograph sweep was initiated by pulses in the scintillation counter corresponding to more than 5 MeV energy release. The scintillator counting rate was around 80 per day, and on the oscillograph trace (of which a typical specimen is shown in Fig. 3) 16 events per day showed pulses from the upward looking counter. This rate agrees well with the determination of the flux of cosmic ray particles by other workers (9).

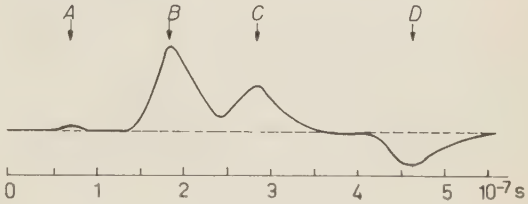

Fig. 3. – Oscilloscope trace of a downward moving particle. *A*) pulse of (1/4); *B*) pulse of scintillation counter; *C*) pulse of (5/8); *D*) reflection of *B*) which was introduced to identify it.

In addition to other checks to ensure that the Čerenkov counters were operating efficiently, they were rotated through 180° for some of the runs without changing any electrical connections. Thus the counter which was normally used to « look » for upward going particles was observed to be recording cosmic ray particles efficiently.

From the observed size of the signals from cosmic ray particles at sea level, it was possible to calculate the minimum energy necessary for incident upward moving particles to give a detectable signal in the counter array. This minimum energy was found to be 20 MeV, 80 MeV, and 100 MeV for electrons, μ-mesons and π-mesons, respectively.

Data were recorded for runs of 82 hours over a 90 cm layer of water (Run I), 78 hours over a 5 cm layer of lead (Run II), and 105 hours over a rock floor (Run III). During the 265 hours of running, 199 pulses were observed from the upward « looking » Čerenkov counter, and 70 pulses were observed from the downward « looking » counter. Each of these 70 pulses was accompanied by a pulse at least twice as large in the other Čerenkov counter.

Thus in all the running time under rock, no event was observed compatible with the traversal of the apparatus by an upward moving particle.

(9) P. H. Barrett, L. M. Bollinger, G. Cocconi, Y. Eisenberg and K. Greisen: *Rev. Mod. Phys.*, **24**, 133 (1952).

5. – Conclusions.

To derive a lower limit for the nucleon lifetime from this experiment, it was necessary to make some assumptions about the decay mode. We assumed arbitrarily that a proton or neutron decays with a lifetime τ, and gives one charged decay product or one photon. We assumed a kinetic energy of 250 MeV to be available to one particle, thereby including a large variety of conceivable decay modes. The charged decay products were assumed to be either positrons, μ-mesons or π-mesons. Then knowing the range of the charged products and the pair production cross-section for the photons, and correcting for radiation loss and nuclear interactions, we calculated the expected upward flux through the counter system. Since no particles were observed, we assumed that the mean number of particles arriving in a time equal to that taken by the experiment was one in order to obtain a lower limit on the lifetime. The limits on the lifetimes obtained for the different assumed decay modes vary by up to a factor of 2. In the text the limits relevant for the decay with the emission of a positron are quoted. Table I summarizes the limits for all the decay modes considered.

TABLE I.

Assumed decay product	Lifetime limit in years for		
	Protons in Hydrogen Run I	Protons in Lead Run II	Nucleons in Nuclei Run III
μ mesons	$4.2 \cdot 10^{24}$ years	$4.3 \cdot 10^{25}$ years	$2.8 \cdot 10^{26}$ years
π-mesons	2.9 »	3.4 »	1.8 »
Positrons	4.7 »	3.6 »	1.8 »
Photons	2.2 »	3.6 »	1.5 »

From the run above water (Run I), we found a lifetime of $4.7 \cdot 10^{24}$ years for the decay of protons in hydrogen, for example by the process

(A) $$p \rightarrow e^+ + e^- + e^+ .$$

The capture process

(C) $$p + e^- + e^+ \rightarrow e^- ,$$

has a lifetime proportional to Z^{-3} per proton in the nucleus ([8]). In order to get a good limit on this reaction, the counters were run over lead (Run II). The limit we found for the lifetime per proton in lead was $3.6 \cdot 10^{25}$ years.

The lifetime for process (C) can be calculated on the basis of CPT invariance and a four-fermion interaction for an assumed lifetime for process (A). The lifetime calculated thus for process (C) with the experimental limit for process (A) obtained from Run I is much longer than the direct experimental limit obtained from Run II. In the spirit of this investigation, however, all conservation laws are suspect.

Finally, assuming that nucleons in nuclei decay with the same lifetime as free nucleons, and combining the above data with those from the runs over a rock floor (Run III), we find a lifetime $\tau \geqslant 1.8 \cdot 10^{26}$ years.

* * *

We should like to express our thanks to the Bern-Lötschberg-Simplon Railway administration and personnel for their most generous and willing help in making this experiment feasible.

We are indebted to the Swiss Federal Railways for making available to us a motor alternator set.

Two of us (H.F. and L.J.K.) are grateful to the Ford Foundation for financial support.

Finally, we wish to acknowledge with appreciation Professor G. BERNARDINI's critical reading of the manuscript, the interest of Professor C. J. BAKKER in this experiment and the hospitality of the CERN laboratory.

RIASSUNTO (*)

Si è eseguita una ricerca delle particelle relativistiche cariche emesse dal decadimento dei nucleoni. Non sono stati individuati eventi del genere, e secondo i postulati assunti sul modo di decadimento, si possono porre limiti inferiori alle vite medie dei nucleoni. Queste variano fra $1.5 \cdot 10^{26}$ e $2.8 \cdot 10^{26}$ anni per nucleoni in nuclei a più particelle e fra $2.2 \cdot 10^{24}$ e $4.7 \cdot 10^{24}$ anni per i protoni nell'idrogeno.

(*) *Traduzione a cura della Redazione.*

LETTERE ALLA REDAZIONE

(La responsabilità scientifica degli scritti inseriti in questa rubrica è completamente lasciata dalla Direzione del periodico ai singoli autori)

A Note on a Possible Classification of Strangeness-2 Mesons.

G. Białkowski and A. Jurewicz

Institute for Theoretical Physics, Warsaw University - Warsaw

(ricevuto il 5 Gennaio 1960)

Recently the existence of two new unstable particles with the mass of about 1400 m_e has been reported [1] on the basis of recent and previous observations as well. These are called $D^{\pm}$ particles and supposed to be heavy mesons of strangeness ± 2 and charge $\pm e$ respectively. In connection to the above interpretation of the experimental data we would like to give some speculations on possible classifications and interactions of D particles.

At first let us investigate some existing classifications schemes from the point of view of the possibility of including $D^{\pm}$ particles into them.

In the d'Espagnat-Prentki theory [2] an introduction of mesons of strangeness 2 leads to $U=\pm 2$. It has been shown by Racah [3] that such values for U lead to ambiguities. According to the «isoparity» formula $p=i^U$ we must assume that φ_D is an isopseudoscalar, if D is an isosinglet (in agreement with Yamanouchi's suggestions). Now, two invariant interaction Hamiltonians can be formed:

$$\tilde{\psi}_N^{*T}\psi_\Xi\varphi_D^* \qquad \text{and} \qquad \tilde{\psi}_N^{*T}\psi_\Xi\varphi_D\,.$$

The former requires φ_D to transform under the gauge transformation with the factor $\exp[-2i\alpha]$, whereas the latter with $\exp[+2i\alpha]$. Thus these two interaction terms cannot occur simultaneously and we must reject one of them. No rule for cancelling one of the above terms is included in the theory. In such a case we may reject some of the originally proposed interaction terms as well.

In another scheme proposed by Tiomno [4] there are many possibilities of introducing new mesons (not only $D^{\pm}$ particles). One of them consists in attributing the symbol $(0;+1,+1)$ to D^+ and $(0;-,1-1)$ to D^-, where the bracket has the meaning $(I_3;J_3,J_3')$. There are still three other available possibilities (all of them as well as the previous ones belong to the representation $I=0$, $J=1$, $J'=1$ in Tiomno's notation), namely $(0;1,-1)$, $(0;-1,1)$ and $(0;0,0)$. The last may correspond to an as yet undiscovered meson, say D^0. The others two are unknown charged particles of strangeness 0. However, in order to intro-

(1) T. Yamanouchi (*preprint*); see also: T. Yamanouchi and M. F. Kaplon: *Phys. Rev. Lett.*, **3**, 283 (1959).

(2) B. d'Espagnat and J. Prentki: *Nucl. Phys.*, **1**, 33 (1956).

(3) G. Racah: *Nucl. Phys.*, **1**, 302 (1956).

(4) J. Tiomno: *Nuovo Cimento*, **6**, 69 (1957).

duce $D^{\pm}$ particles we must reject the limiting condition $|Y| \leqslant 1$, originally proposed by TIOMNO (condition $|Q| \leqslant 1$ still remains valid). In such a situation the possibility of introducing in the theory new representations increases, if we do not confine ourselves to the condition $|Y| \leqslant 2$.

The situation is not clear in the case of the scheme proposed by PAIS [5], since the knowledge of the only isotopic quantities conserved in the interactions, namely I, I_3, K, K_3, gives no information about strangeness, which is rather a phenomenological quantity here. On the other hand no prescription is proposed how to introduce in the theory a new field, in particular how to introduce in an only way the field of new particles of given strangeness and charge. Notice that for mesons of strangeness ± 2 and charges $\pm e$ respectively we have but a condition $I_3 + K_3 = 0$. The situation that is spoken about is caused by the fact, that Pais' scheme deals with an isotructure only, whereas in the case of D particles the structure is as yet unknown and we would like to gain an idea of it basing on the strangeness structure.

Finally let us consider the classification scheme given by SALAM and POLKINGHORNE [6]. In this case we have the possibility of introducing one new kind of baryons connected with the (0, 1) representation, and two new meson fields connected with the (0, 0) (possibly $\pi^{0\prime}$ field) and (0, 1) representations. The last one, which was previously ascribed to the τ-meson, forms a strangeness triplet; according to the formulae

$$S = 2I_3^{(2)} - N \quad \text{and} \quad (Q/e) = I_3^{(1)} + I_3^{(2)},$$

we have one particle with $S = +2$, $Q = +e$ (D^+), one with $S = -2$, $Q = -e$ (D^-), and one with $S = 0$, $Q = 0$ (hypothetic D^0 particle). This seems to be the most natural way of introducing D particles in the theory, but its value strongly depends on the existence of D^0. Then we shall give some considerations concerning D particles and their interactions according to the Salam-Polkinghorne scheme. If the D^0 particle does not exist these considerations would be of little value.

In the Salam-Polkinghorne formalism we have only two three-field interactions with respect to the full four-dimensional rotational group in isospace. They are

$$\bar{N}_\alpha D_{\alpha\beta} N_\beta + \text{h.c.} \quad \text{and} \quad K^*_\alpha D_{\alpha\beta} K_\beta + \text{h.c.},$$

since $D_{\alpha\beta}$ is a skewsymmetrical isotensor of second rank. N_α and K_α denote the quadruplets ($\mathcal{N}$, Ξ) and (K, K) respectively.

The former term contains following components

$$\bar{\Xi}^- \mathrm{n} \mathrm{D}^{+*}, \quad \bar{\Xi}^0 \mathrm{p} \mathrm{D}^{+*}, \quad \bar{\Xi}^- \Xi^- \mathrm{D}^{0*}, \quad \bar{\mathrm{p}} \mathrm{p} \mathrm{D}^{0*},$$

$$\bar{\Xi}^- \mathrm{n} \mathrm{D}^-, \quad \bar{\Xi}^0 \mathrm{p} \mathrm{D}^-, \quad \bar{\Xi}^0 \Xi^0 \mathrm{D}^{0*}, \quad \bar{\mathrm{n}} \mathrm{n} \mathrm{D}^{0*},$$

and their hermitian conjugates, where Ξ, n, p, D stand for operators of corresponding fields. Similar expressions for the interaction of D particles with K-mesons could be written.

On the basis of the above formulae one can say that D particles are produced in the following reactions

$$\pi^- + \mathrm{p} \to \Xi^- + \mathrm{D}^+,$$

$$\pi^- + \mathrm{p} \to \mathrm{n} + \mathrm{D}^0,$$

$$\pi^+ + \mathrm{n} \to \mathrm{p} + \mathrm{D}^0,$$

$$\mathrm{K}^- + \mathrm{p} \to \mathrm{K}^+ + \mathrm{D}^- + \mathrm{n}.$$

As far as decays of $D^{\pm}$ particles are concerned we note the strange fact that till now no decay of $D^{\pm}$ into charged K-meson and neutral pion was observed.

Decays of D^0 might form a different class of reactions, because of zero strange-

[5] A. PAIS: *Phys. Rev.*, **112**, 624 (1958).
[6] A. SALAM and J. C. POLKINGHORNE: *Nuovo Cimento*, **2**, 685 (1655).

ness of the neutral D. For example reactions

$$D^0 \to \pi^+ + \pi^-,$$

$$D^0 \to \pi^0 + \pi^0,$$

should conserve $I^{(1)}$, $I_3^{(1)}$ and $I_3^{(2)}$ (*i.e.* isospin, its third component and strangeness) and then could be considered as fast reactions. The only non-conserving quantity is $I^{(2)}$. If we believe that violation of symmetries causes a reaction to go slowlier, then the D^0 possible decays mentioned above proceed slowlier than the ordinary fast reactions, but faster than the ordinary slow reactions such as *e.g.* K decays. The possible decay $D^0 \to \pi^+ + \pi^-$ might serve to detect the D^0 particle.

* * *

The authors are indebted to Dr. R. SOSNOWSKI for valuable discussions and information about the Dubna event (see [1]).

Low-Energy Photoproduction of Neutral Mesons from Complex Nuclei (*).

R. A. Schrack (**)

National Bureau of Standards - Washington, D. C.
University of Maryland - College Park, Md.

S. Penner and J. E. Leiss

National Bureau of Standards - Washington, D. C.

(ricevuto l'11 Gennaio 1960)

Angular distribution measurements have been made of neutral meson photoproduction from several elements using 170 MeV bremsstrahlung from the National Bureau of Standards synchrotron. The two photons from the pion decay were detected in coincidence by two scintillation counter telescopes placed symmetrically about the X-ray beam. Each telescope subtended approximately 26 degrees at the target. The mean correlation angle between the counter telescopes was 120°.

Angular distributions were measured by rotating the plane of the counters about an axis perpendicular the X-ray beam. The angular resolution of such a detection system is essentially geometrical having a width at half height of $\pm 6.5°$ for the plane of the counters near 90° to the X-ray beam, becoming progressively worse as the plane of the counters approaches the forward or backward directions. Accurate determination of the angular-energy resolution function requires extensive computer calculations which have not yet been completed.

The angular distributions $\sigma_{\text{obs.}}(\theta)$, measured for the elements carbon, aluminum, copper, cadmium, and lead are shown in Fig. 1. The solid curves $(\overline{F^2_{\text{Born}} \sin^2 \theta})$ shown with the data points are based on Born approximation predictions of the angular distributions [1], assuming neutral pion production is equal from neutrons and protons. The nuclear shapes used are those for the charge distribution obtained from electron scattering experiments [2]. The predicted angular distributions shown are averaged over the bremsstrahlung spectrum, the neutral pion production cross section, and the relative efficiency

(*) Supported in part by U. S. Atomic Energy Commission Division of Research.

(**) Based in part on work for a Ph. D. Thesis, University of Maryland.

(1) J. E. Leiss and R. A. Schrack: *Rev. Mod. Phys.*, **30**, 456 (1958).

(2) R. Hofstadter: *Ann. Rev. Nucl. Sci.*, **7**, 231 (1957).

of the counters as a function of decay photon correlation angle in the center-of-mass system.

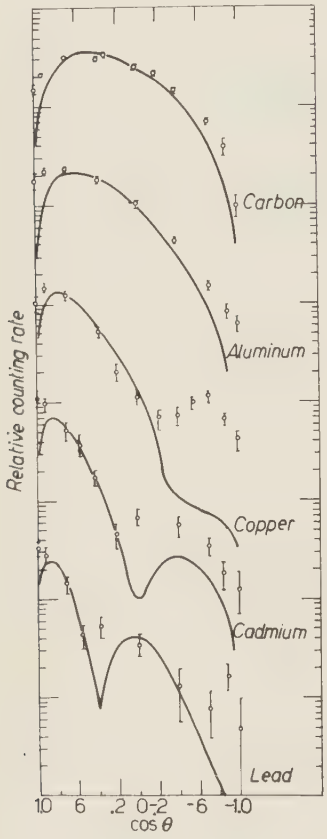

Fig. 1. – Angular distributions of neutral meson production for C, Al, Cu, Cd and Pb. Points are data of this experiment. Errors shown are statistical only. The solid curves are based on Born approximation predictions using the same half-density nuclear radii as determined from electron scattering. Successive curves are shifted vertically one decade for illustrative purposes.

Although these predicted distributions are not exact in that they neither take into account the angular resolution of the counters nor the transformation to the laboratory system, it is possibile to draw some preliminary conclusions:

1) at the photon energies used in this experiment, the photoproduction of neutral mesons occurs primarily by the coherent process;

2) the first peak in the angular distribution is fit fairly well by a Born approximation prediction using nuclear matter distributions having a half density radius the same as that of the charge distributions determined from electron scattering experiments;

3) the secondary maxima of the angular distributions do not agree with Born approximate predictions. The lighter the element the greater the discrepancy. This result is to be expected due to the interaction of the outgoing mesons with the recoil nucleus, and is qualitatively in agreement with the observations of RAINWATER [3] in meson-scattering experiments;

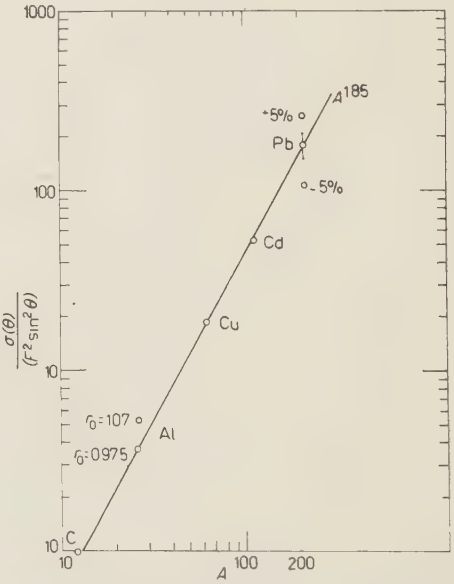

Fig. 2. – Observed cross section for neutral meson production divided by predicted form factor. The two points shown for Al illustrate the effect of changing the radius parameter r_0 for that element.

[3] W. F. BAKER, J. RAINWATER and R. E. WILLIAMS: *Phys. Rev.*, **112**, 1763 (1958).

4) in a Born approximate description of the coherent production process $\sigma \propto A^2 F^2 \sin^2\theta$. As shown in Fig. 1 the ratios $\sigma_{\text{obs.}}(\theta)/(\overline{F^2_{\text{Born}} \sin^2\theta})$ are roughly independent of θ for the first fall-off. Fig. 2 shows the proportionality of this ratio to A. A good fit to this curve is given by $\sigma_{\text{obs.}}(\theta)/(\overline{F^2_{\text{Born}} \sin^2\theta}) \propto A^{1.85}$. This demonstrates that nuclear absorption of the outgoing meson is not a large effect.

The points in Fig. 2 at lead marked $\pm 5\%$ indicate the effect of changing the half-density radius by $\pm 5\%$ from the value given by electron scattering experiments. For changes in radius greater than this, no sensible fit to the angular distribution in lead can be made. The average half-density radius given by electron scattering experiments and used here is $R = r_0 \cdot A^{\frac{1}{3}} \cdot 10^{-13}$ cm where $r_0 = 1.07$ for most elements. For aluminum a value of $r_0 = 0.975$ gives a better fit and is in good agreement with electron scattering results for neighboring elements. The experimental results at higher energies obtained at MIT [4] show many features in excellent agreement with the results reported here.

Complete analysis of these experimental data is in process. A comparison of this data with a theory which includes the effects of meson-nucleus interactions will provide an accurate measure of nuclear density distributions. This more complete theory does not exist at the present time.

[4] G. DAVIDSON: Ph. D. Thesis MIT (Sept. 1959), unpublished.

IL NUOVO CIMENTO Vol. XVI, N. 4 16 Maggio 1960

Mean Free Path of Primary Cosmic Rays in the Atmosphere (*).

R. W. Williams (**)

Physics Department, University of Washington - Seattle, Wash.

(ricevuto il 15 Febbraio 1960)

The interaction (or collision) mean free path of high-energy cosmic rays in the atmosphere is a quantity which is frequently needed in analyses of cosmic-ray intensities; it is also directly related to the fundamental question of the inelasticity of high-energy collisions. In this note we present cross section calculations which relate the mean free path to measured or extrapolated quantities. Recent information on nuclear densities of light nuclei and on elementary cross sections at high energy leads to a rather definite value for the mean free path of nucleons of less than 100 GeV. This quantity is not directly measurable in the cosmic radiation, and in the past it has often been allowed a wide latitude (for example, in the recent analysis of Subramanian and Verma [1]).

It is straightforward to calculate for high energies the interaction cross section of a nucleus of known density distribution [2], in terms of the effective nucleon-nucleon cross section $\bar{\sigma}$. The results are sensitive to the choice of $\bar{\sigma}$, and to a lesser extent to the treatment of the finite range of interaction; these matters are discussed in ref. [2]. For our present purpose it is clear that the elementary act of interest is the production of particles (mainly pions); that enough momentum will be transferred to eliminate Pauli-principle worries; and therefore that $\bar{\sigma}$ must be identified with the inelastic nucleon-nucleon cross section, preferably an average of $(\sigma_{pp})_i$ and $(\sigma_{np})_i$: Fig. 1 shows the (pp) inelastic cross section as measured with proton-synchrotron beams, and a related cosmic-ray measurement. Several measurements cluster around 27 mb in the $(1 \div 3)$ GeV region; emulsion measurements from the Bevatron [3] and from Dubna [4] show little change to 9 GeV; and the interaction cross section in the cosmic-ray beam (in iron) by Brenner and Wil-

(*) Supported by U. S. Office of Naval Research.

(**) On leave of absence from Massachusetts Institute of Technology.

(1) A. Subramanian and S. D. Verma *Nuovo Cimento*, **13**, 572 (1959).

(2) R. W. Williams: *Phys. Rev.*, **98**, 1387 (1955).

(3) R. M. Kalbach, J. J. Lord and C. H. Tsao: *Phys. Rev.*, **113**, 325 (1959); M. Blue and J. J. Lord: to be published.

(4) N. P. Bogachev, S. A. Bonjatov, Ju. P. Merekov and V. M. Siderov: *Dokl. Akad. Nauk. SSSR*, **121**, 617 (1958). A slightly higher value (25 mb) is quoted in the proceedings of the 1958 Geneva Conference.

LIAMS (5) indicates a mean value of the elementary cross section at about 50 GeV nearly equal to the lower-energy results. a calculation with experiment was done by CRONIN, COOL and ABASHIAN (7), who found that an r.m.s. range of 0.78 fermi

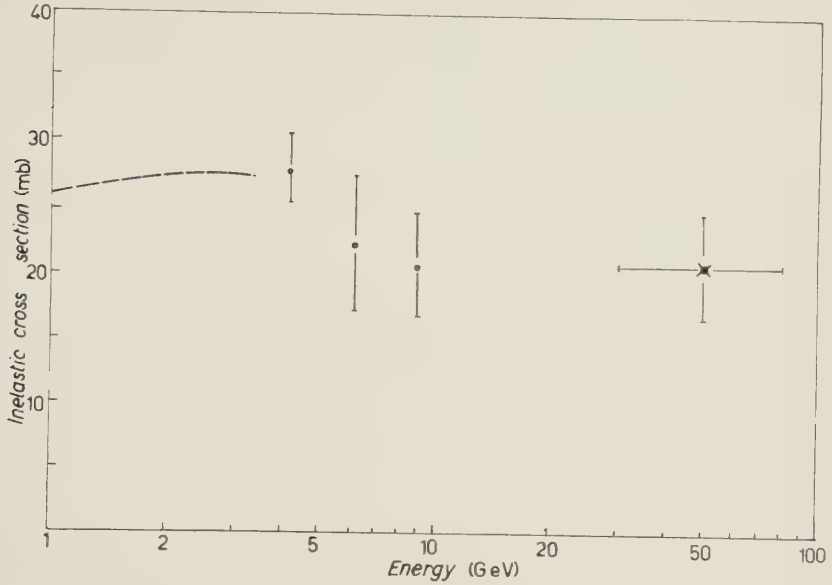

Fig. 1. – Cross section for particle production in p-p collisions. The curve at low energies is an average of several determinations. The 50 GeV point is an indirect cosmic-ray measurement.

The charge density distributions in ^{14}N and ^{16}O nuclei have recently been determined with considerable precision (6). The electron-scattering results agree very well with the form of distribution expected from the shell model with oscillator wave functions:

$$(1) \qquad \varrho \sim \left[1 + \alpha\left(\frac{r}{a}\right)^2\right] \exp\left[-\frac{r^2}{a^2}\right].$$

The empirical values found for the parameters were; N, $\alpha = 1.667$, $a = 1.667$ fermi; O, $\alpha = 1.60$, $a = 1.82$ fermi (1 fermi = $= 10^{-13}$ cm). To calculate the interaction cross section we need the nuclear matter density, folded with a function which describes the finite range of the interaction (2). An accurate comparison of such gave good agreement with the observed cross sections. We used the same r.m.s. range (in a gaussian range function for convenience) to fold into eq. (1). In a typical case it raised the cross section, over that calculated from (1), by $2\frac{1}{2}\%$.

The results, for the interaction cross section of N and O, are given in Fig. 2. As a check, one can compare with a recent high-energy experiment on ^{12}C in which the inelastic cross section for 4.5 GeV neutrons was obtained (8). ATKINSON *et al.* found $\sigma_i = (218 \pm 8)$ mb, whereas for $\bar{\sigma} = 27$ mb our N cross section, scaled down by an approximate scaling law, gives 209 mb.

The interaction mean free path in air (including a small contribution from

(5) A. E. BRENNER and R. W. WILLIAMS: *Phys. Rev.*, **106**, 1020 (1957).

(6) U. MEYER-BERKHOUT, K. W. FORD and A. E. S. GREEN: *Ann. of Phys.*, **8**, 119 (1959).

(7) J. CRONIN, R. COOL and A. ABACHIAN: *Phys. Rev.*, **107**, 1121 (1957).

(8) J. ATKINSON, W. HESS, V. PEREZ-MENDEZ and R. WALLACE: *Phys. Rev. Lett.*, **2**, 168 (1959).

argon) is also shown in Fig. 2. If we take 25 mb for $\bar{\sigma}$ near 10 GeV, $\lambda \sim 106$ g cm^{-2}. It can scarcely be less than 90 g cm^{-2} in the region below 100 GeV, if the data of Fig. 1 are to be believed. In their analysis of the pion intensity in the atmosphere, SUBRAMANIAN and VERMA [1] usually assumed; it seems certain that a value much above 100 g cm^{-2} would come into conflict with the evidence for elasticity, and a new look at the entire problem would be necessary. (The energy retention after an average air-nucleus collision would be <0.5 with $\lambda = 90$ g cm^{-2}).

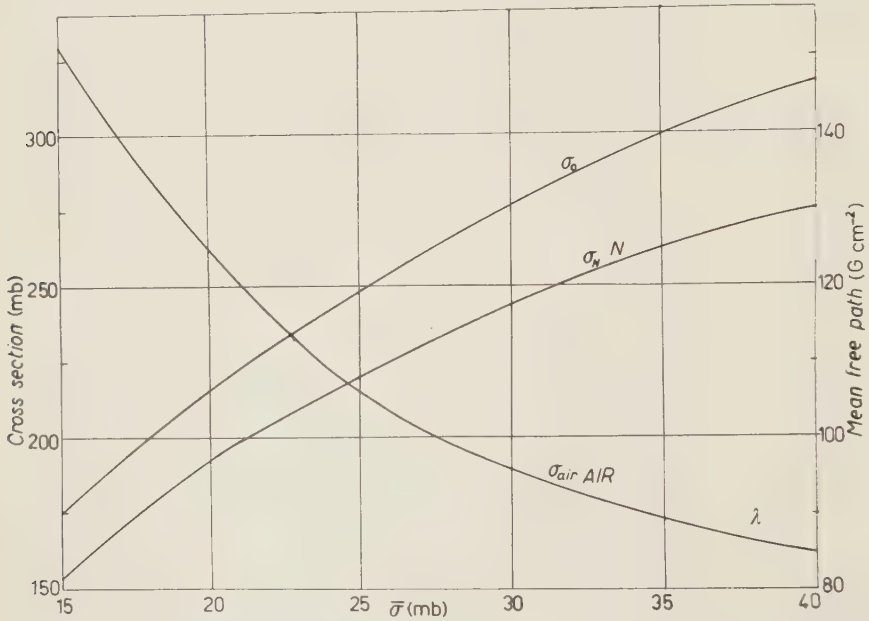

Fig. 2. – Calculated interaction mean free path of nucleons in air as a function of elementary nucleon-nucleon cross section. Also shown are the cross sections of nitrogen and oxygen nuclei.

point out that a λ of 70 g cm^{-2} would lead to better agreement among their calculated quantities, but this value is surely ruled out by experiment, at least over a good part of their energy domain.

The observed attenuation length of primary protons and other high-energy ($\gtrsim 10$ GeV) cosmic-ray nucleons is ~ 125 g cm^{-2}. The difference between this number and λ is generally attributed to the incompleteness of energy degradation in a collision — the « partial elasticity » — and there is independent evidence for some elasticity (*e.g.*, direct measurement at 6 GeV [3]; charge-to-neutral ratio at higher energies). Even our minimum value of 90 g cm^{-2} for λ already indicates less elasticity than is

In summary, the interaction mean free path is constrained to a value near 100 g cm^{-2}, the uncertainty in this value being perhaps 10% in the $(1 \div 10)$ GeV region, somewhat more in the $(10 \div 100)$ GeV region.

An interesting consequence of this long collision path is the penetration of cosmic-ray primaries to mountain altitudes. If the cross sections do not rise dramatically above 100 GeV, the attenuation of the primary proton beam, near the vertical, would be only about 10^{-3} at a depth of 700 g cm^{-2}. With the usual primary proton spectrum this leads to a mountain-altitude intensity of primaries, uncluttered by secondary-interaction products, of ~ 0.02 m^{-2} s^{-1} sr^{-1} with energies $E > 100$ GeV.

On the Cosmic Ray Storms of July 1959.

D. Cattani and M. Galli

Istituto di Fisica dell'Università - Bologna

(ricevuto il 1° Marzo 1960)

A very important group of events interesting solar activity and related geophysical phenomena occurred between the 10th and the 20th of July 1959.

In that period two cosmic ray scintillator monitors were operating in Bologna; we shall give here their characteristics.

Both were placed in this Institute (geomagnetic latitude: 44.5° N, altitude: 50 m above s.l.) in the same thermostatized room under 450 g cm^{-2} of concrete.

In one of them the scintillator is made of toluene with terfenile and POPOP, it is in a cilindrical container coated with white enamel; it is 10 cm thick and has 0.8 m^2 of sensible area. In the other one the scintillator is of polystyrene with terfenile and POPOP, it is 10 cm thick and has 0.5 m^2 of sensitive area.

For each of them, a photomultiplier EMI 6099 has been used with the same type of electronic circuits.

The pulse spectrum has a plateau corresponding to the particles which can traverse the whole layer of scintillator losing the minimum energy. In that plateau a variation of 0.1% of the counting rate corresponds to 1% of the discrimination voltage.

Only the pulses higher than the ones corresponding to the plateau are counted.

The first monitor gives about 200 000 count/h and the second one gives about 300 000 count/h.

In Fig. 1 hourly pressure corrected intensities of the single monitors and their sum are plotted.

At the bottom of the figure, are indicated solar flares with their duration and importance, the radio burst associated to the flares, the SSC, three-hourly values of *Kp* indexes and an Aurora [1,2].

Fifteen-minute pressure corrected intensity for the three decreases of July 11, 15, 17 is plotted in Figs. 2, 3, 4; the counting rate is about 130 000 count/15 min.

The correlation between class 3$^+$ flares associated with radioburst and Forbush decreases is very striking.

A peculiar feature is shown by the July 15 decrease (Fig. 3); after the SSC of 0802 UT there is a small decrease lasting a little longer than an hour, afterwards there are strong fluctuations

---

[1] *Solar Geophysical Data*, Part B, C.R.P.L. Boulder (Colorado) Aug. 1959.

[2] *Preliminary Report Solar Activity* TR 411 and supplement Report, High altitude Observatory, Boulder, Colorado, 1959 (Unpublished).

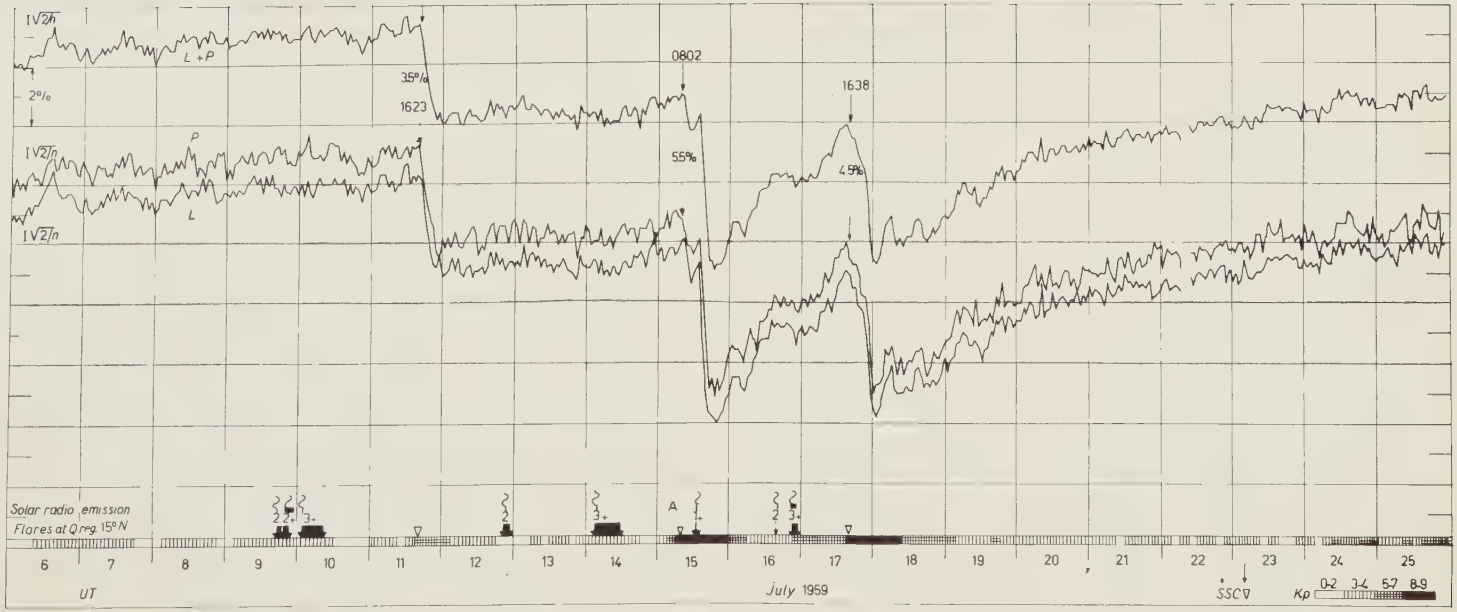

Fig. 1. – Hourly relative counting rate, (centered at the end of each interval) of scintillation monitors and related solar and geophysical phenomena between July 6 and July 25, 1959. L, P: Liquid and Plastic scintillator recording; L + P: Sum of L and P recordings; A: Aurora; S.S.C.: Sudden Storm Commencement.

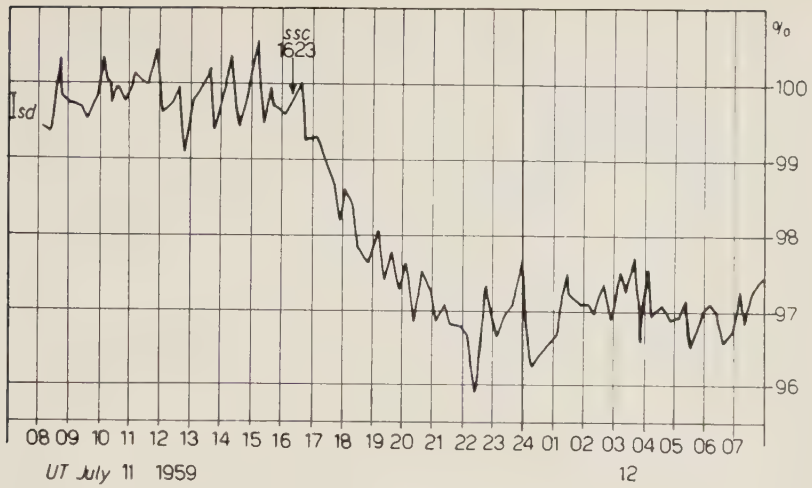

Fig. 2. – Fifteen-minute interval details of Fig. 1 for the Cosmic Ray decrease of July 11, 1959; counting rates are centered at the center of each interval.

with an increasing tendency. At about 1430 UT there is a new decrease occurring in a period not longer than 15 min, it is about one half of the whole decrease and it is the most rapid so far recorded with our devices. From data so far collected it appears that inside an interval not longer than 15 min it is simul-

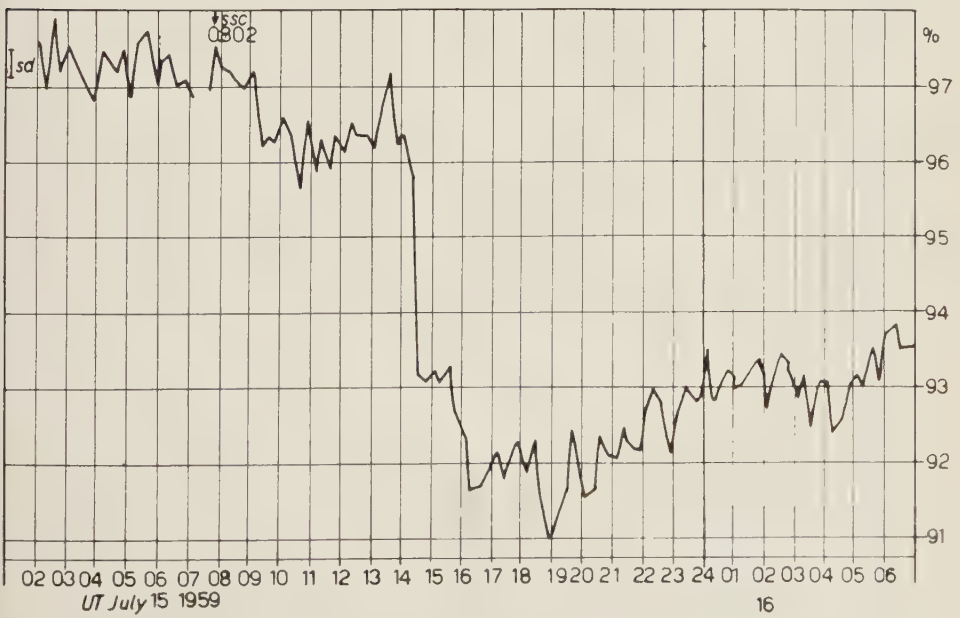

Fig. 3. – Fifteen-minute interval details of Fig. 1 for the Cosmic Ray decrease of July 15, 1959; counting rates are centered at the center of each interval.

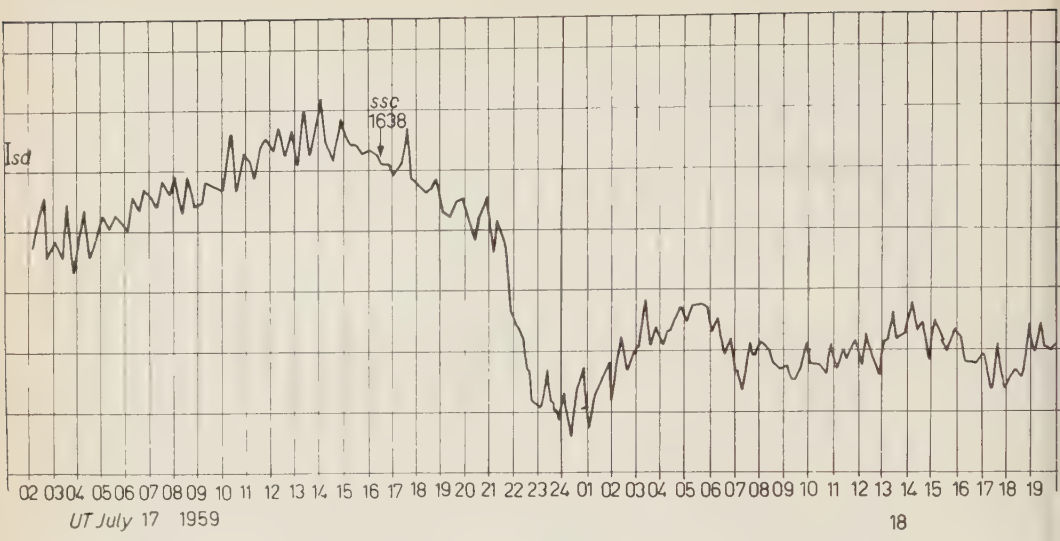

Fig. 4. – Fifteen-minute interval details of Fig. 1 of the Cosmic Ray decrease of July 17, 1959; counting rates are centered at the center of each interval.

taneous with a 3% decrease of the neutron intensity occurred at Deep River, Canada (see Fig. 5).

The same decrease is also simultaneous in an interval shorter than an hour with its correspondent recorded at Hobart.

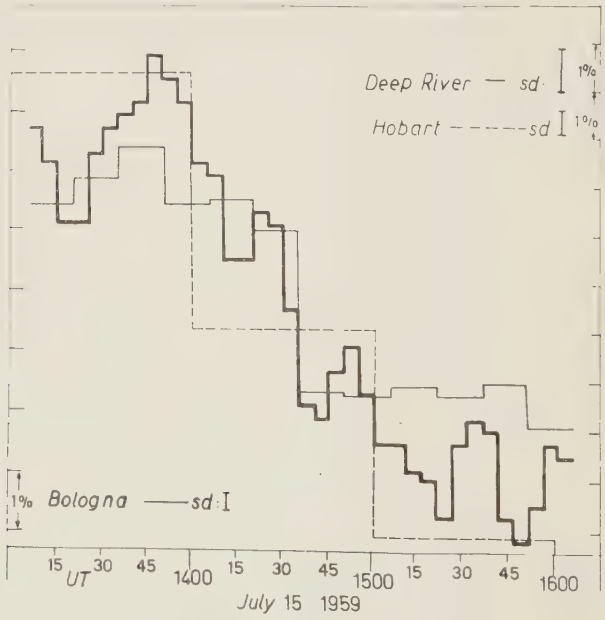

Fig. 5. – Comparison between scintillation monitor counting rate at Bologna and neutron monitor counting rate at Deep River and at Hobart during the main decrease of the July 15, 1959 Cosmic Ray Storm. Deep River five-minutes data are smoothed with a running mean over fifteen minutes.

It would be very interesting to know if this decrease is world-wide simultaneous in a period shorter than 15 min.

The pick immediately before 1500 UT (see Fig. 1) might be interpreted as a superposition of a Forbush decrease with an enhanced diurnal oscillation in agreement with what has been pointed out elsewhere [3].

Decreases of July 11 and 17 (see Figs. 2 and 4) are instead much slower, although they are world-wide; it is difficult to see any simultaneity in an interval shorter than one or two hours.

* * *

We wish to thank the Hobart and Deep River Cosmic Ray Groups for using their data.

[3] D. CATTANI, and M. GALLI: paper presented at the C. R. Moscow meeting July 6-11; 1959.

IL NUOVO CIMENTO Vol. XVI, N. 4 16 Maggio 1960

Determination of K^--n P-Wave Phase Shifts from K^--d Reactions (*).

T. B. Day, L. S. Rodberg, G. A. Snow and J. Sucher
University of Maryland - College Park, Md.

(ricevuto il 25 Marzo 1960)

There seems to be definite evidence for P-wave scattering in the K^+-neutron system from the charge-exchange scattering data at energies of about 200 MeV ([1,2]). Thus, while the isotopic spin $T=1$ scattering can be well represented by S-wave scattering alone in this energy region ([3]), the $T=0$ scattering requires both S- and P-wave phase shifts. K^+-deuteron scattering experiments are currently being performed at Berkeley ([4]). It is the purpose of this letter to discuss the extent to which such experiments can determine the P-wave phase shifts.

We have evaluated the K^+-deuteron differential cross sections for the charge exchange and non-charge exchange (elastic plus break-up) processes at an incident momentum of 520 MeV/c (kinetic energy = 224 MeV). The impulse and closure approximations have been used throughout ([5]). The incident energy is sufficiently high that these approximations are expected to be reliable, but it is not so high that many partial waves will contribute to the elementary K-nucleon cross sections. We are principally interested in the differential cross sections at angles for which the K-nucleon interaction dominates over Coulomb and many-body effects ([6]). The Coulomb scattering corrections are quite small ($\sim 10\%$) for laboratory scattering angles greater than 30° (the Coulomb correction factor for the charge exchange

(*) This research was supported in part by the United States Air Force through the Air Force Office of Scientific Research of the Air Research and Development Command and in part by the U.S. Atomic Energy Commission.

(1) D. Keefe, A. Kernan, A. Montwil, M. Grilli, C. Guerriero and F. A. Salandin: *Nuovo Cimento*, **12**, 241 (1959); E. Helmy, O. R. Price, D. H. Stork and H. K. Ticho: *Proc. of the Ninth Annual Conference on High-Energy Physics* (Kiev, 1959, unpublished); L. Alvarez: *Report, l.c.*, p. 16.

(2) L. S. Rodberg and R. M. Thaler: *Phys. Rev. Lett.*, **4**, 372 (1960).

(3) T. F. Kycia, L. T. Kerth and R. G. Baender: *University of California Radiation Laboratory Report* UCRL-8753 (unpublished).

(4) G. Goldhaber: private communication.

(5) E. M. Ferreira: *Phys. Rev.*, **115**, 1727 (1959).

(6) At smaller angles ($\theta_{lab} < 30°$) where many-body effects become important, the approximations used here are expected to be only qualitatively correct (see S. Fernbach, T. A. Green and K. M. Watson: *Phys. Rev.*, **84**, 1084 (1951)).

cross section (Fig. 1) is negligible at this energy). The interference term between the neutron and proton amplitudes, which depends on the deuteron wave function, falls rapidly with angle and is also negligible at the larger angles of interest.

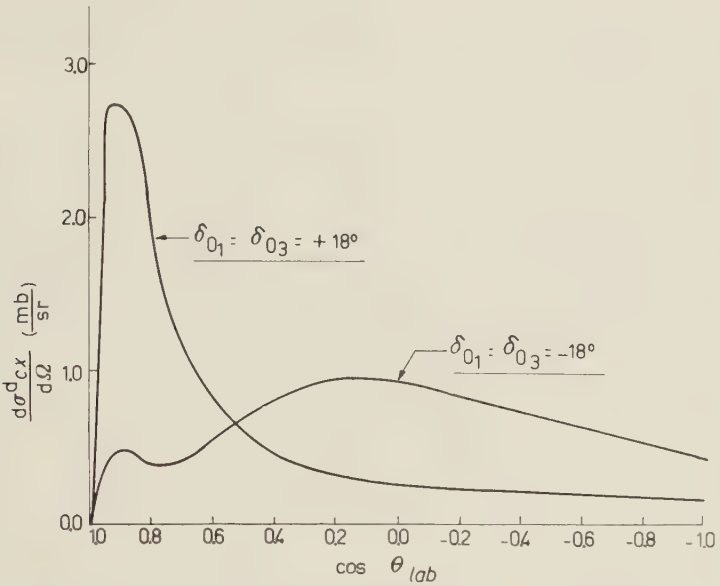

Fig. 1. – K^+-deuteron charge exchange scattering differential cross section (mb/ster) *vs.* cos θ_{lab} of the K^0 in the laboratory, for incident K^+ laboratory momentum of 520 MeV/c. Case no. 1, *i.e.* $\delta_{01} = \delta_{03} = \pm 18°$; $\delta_0 = +7°$; $\delta_1 = -34°$. (Coulomb effects are ignored).

(At $\theta_{lab}=30°$ it is down to 15% of its value at $\theta_{lab}=0°$.) Then the non-exchange cross section reduces simply to the sum of the free neutron and proton scattering cross sections:

$$\frac{d\sigma^d_{ncx}}{d\Omega} = \frac{d\sigma^n_{el}}{d\Omega} + \frac{d\sigma^p_{el}}{d\Omega} . \tag{1}$$

Likewise, the K^+-d charge exchange cross section differs from the corresponding K^+-neutron cross section mainly in the forward direction, where the Pauli principle restricts the possible final states of the two outgoing protons. Since the K^+-d cross section is, according to our assumptions, so closely related to the K^+-nucleon cross sections, it is advantageous to consider the K^+-d cross section in the K^+-nucleon c.m. system. In this system we have (for K^+-nucleon c.m. angles, $\theta_{c.m.} > 48°$, corresponding to $\theta_{lab} > 30°$)

$$\begin{cases} \dfrac{d\sigma^n_{el}}{d\Omega} = \dfrac{1}{4}|\eta_1 + \eta_0 + (2\eta_{03} + \eta_{01})\cos\theta_{c.m.}|^2 + \dfrac{1}{4}|\eta_{03} - \eta_{01}|^2 \sin^2\theta_{c.m.} , \\ \dfrac{d\sigma^p_{el}}{d\Omega} = |\eta_1|^2 , \\ \dfrac{d\sigma^n_{ex}}{d\Omega} = \dfrac{1}{4}|\eta_1 - \eta_0 - (2\eta_{03} + \eta_{01})\cos\theta_{c.m.}|^2 + \dfrac{1}{4}|\eta_{03} - \eta_{01}|^2 \sin^2\theta_{c.m.} , \end{cases} \tag{2}$$

where $\eta_\alpha = (1/k_{\text{c.m.}}) \exp[i\delta_\alpha] \sin\delta_\alpha$ with $\alpha = T$ for S-wave, and $\alpha = (T, 2j)$ for P-wave.

At this energy the K^+-proton scattering data [3] give an S-wave phase shift $\delta_1 = -34°$. A recent analysis of K^+ scattering in emulsion by RODBERG and THALER [2] gives for the S-wave, $T = 0$, K^+-nucleon scattering length, the value $a_0 = (-0.080 \pm 0.068)$ fermi. Their analysis, using only the totali nelastic and total charge exchange cross sections, does not determine the individual P-wave phase shifts, but rather the weighted average

$$\mu_0 = \tfrac{1}{3}\sin^2\delta_{01} + \tfrac{2}{3}\sin^2\delta_{03} \equiv \sin^2\delta_{0p}\,. \tag{3}$$

They fit the values of δ_{0p} with a zero effective range formula, $k^3_{\text{c.m.}} \cot\delta_{0p} = -(\bar{a}_{0p})^{-3}$ and find $|\bar{a}_{0p}| = (0.44 \pm 0.03)$ fermi.

To exhibit the dependence of the charge exchange and non-charge exchange cross sections on the P-wave phase shifts, the results for four representative combinations of δ_{01} and δ_{03} are presented here. These four cases, with values of the

TABLE I. – *Results of impulse and closure approximations calculation for the* K^+-d *reactions at a* K^+*-laboratory momentum of* 520 MeV/c. *The S-wave phase shifts were taken as* $\delta_0 = +7°$, $\delta_1 = -34°$.

	Case no. 1	Case no. 2	Case no. 3	Case no. 4
				$\sin 2\delta_{01} = -2\sin 2\delta_{03}$
	$\delta_{01} = \delta_{03}$ $\delta_{01} = \pm 18°$	$\delta_{01} = 0$ $\delta_{03} = \pm 22°$	$\delta_{03} = 0$ $\delta_{01} = \pm 32°$	$\delta_{03} = \pm 12°$ $\delta_{01} = \mp 26°$
$\dfrac{d\sigma^d_{cx}(58°)}{d\Omega}$	0.63 mb/sr	0.85 mb/sr	1.1 mb/sr	1.3 mb/sr
$\dfrac{d\sigma^d_{cx}(37°)/d\Omega}{d\sigma^d_{cx}(90°)/d\Omega}$	7.3 ($\delta_{01} = +$) 0.44 ($\delta_{01} = -$)	7.9 ($\delta_{03} = +$) 0.38 ($\delta_{03} = -$)	4.7 ($\delta_{01} = +$) 0.89 ($\delta_{01} = -$)	2.2 ($\pm$)
$\dfrac{d\sigma^d_{cx}(26°)/d\Omega}{d\sigma^d_{cx}(90°)/d\Omega}$	10.4 ($\delta_{01} = +$) 0.52 ($\delta_{01} = -$)	10.1 ($\delta_{03} = +$) 0.17 ($\delta_{03} = -$)	5.2 ($\delta_{01} = +$) 0.51 ($\delta_{01} = -$)	1.8 ($\pm$)
$\dfrac{d\sigma^d_{ncx}(58°)}{d\Omega}$	2.4 mb/sr	2.7 mb/sr	2.9 mb/sr	3.0 mb/sr
$\dfrac{d\sigma^d_{ncx}(37°)/d\Omega}{d\sigma^d_{ncx}(90°)/d\Omega}$	2.4 ($\delta_{01} = +$) 5.4 ($\delta_{01} = -$)	2.7 ($\delta_{03} = +$) 5.1 ($\delta_{03} = -$)	3.0 ($\delta_{01} = +$) 4.6 ($\delta_{01} = -$)	3.7 ($\pm$)
$\dfrac{d\sigma^d_{ncx}(26°)/d\Omega}{d\sigma^d_{ncx}(90°)/d\Omega}$	3.0 ($\delta_{01} = +$) 8.4 ($\delta_{01} = -$)	3.2 ($\delta_{03} = +$) 7.4 ($\delta_{03} = -$)	3.6 ($\delta_{01} = +$) 6.3 ($\delta_{01} = -$)	4.5 ($\pm$)

phase shifts chosen to give $|\bar{a}_{0p}| = 0.44$ fermi, are

$$(4)\quad \begin{cases} \text{Case 1:} & \delta_{01} = \delta_{03} = \pm 18^\circ, \\ \text{Case 2:} & \delta_{01} = 0, \quad \delta_{03} = \pm 22^\circ, \\ \text{Case 3:} & \delta_{03} = 0, \quad \delta_{01} = \pm 32^\circ, \\ \text{Case 4:} & \sin 2\delta_{01} = -2 \sin 2\delta_{03}, \quad \delta_{03} = \pm 12^\circ, \quad \delta_{01} = \mp 26^\circ. \end{cases}$$

Case 1 gives no spin-flip while case 4 gives maximum spin-flip. The results for the differential cross sections, with Coulomb and many-body effects included [5], are summarized in Table I.

The differential charge exchange cross section is sensitive to the choice of phase shifts. For a K-nucleon c.m. angle of 90° ($\theta_{lab} = 58^\circ$) the non-spin-flip contribution to the cross section vanishes, and the differential cross section depends (for given S-wave phase shifts) only on the spin-flip combination of P-wave phase shifts, $\sin^2(\delta_{03} - \delta_{01})$. Thus a measurement of the differential cross section at this angle will yield the magnitude of the difference between the P-wave phase shifts. Table I shows that the charge exchange cross section at this angle varies by a factor of two over the range of possible values for this difference.

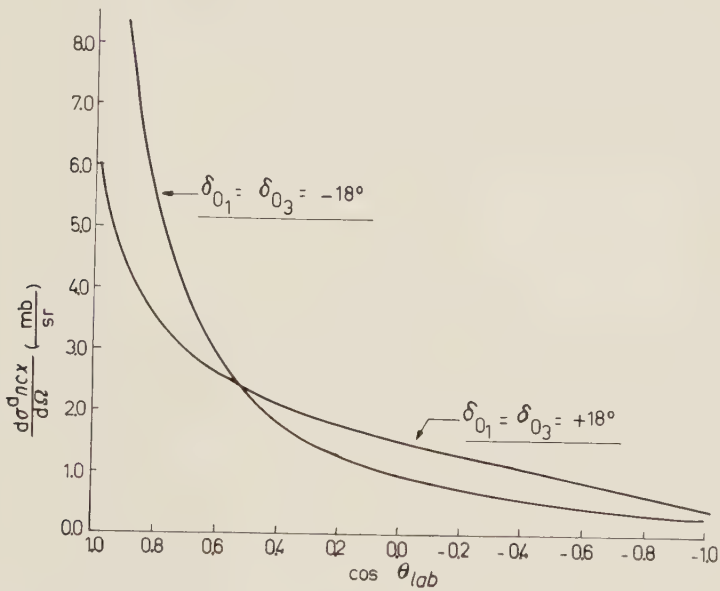

Fig. 2. – K+-deuteron non-charge-exchange scattering differential cross section *vs.* cos θ_{lab} of the K+ in the laboratory, for incident K+ laboratory momentum of 520 MeV/c. Case no. 1, *i.e.* $\delta_{01} = \delta_{03} = \pm 18°$; $\delta_0 = +7°$; $\delta_1 = -34°$. (Coulomb and many-body effects are included).

The shapes of the cross sections are sensitive to the sign of the P-wave phase shifts. This dependence is illustrated in Figs. 1 and 2, where the cross sections for case 1 are presented. Case 1 has the largest dependence upon the sign of the phase shifts, since the non-spin-flip amplitude, which interferes with the S-wave ampli-

tude, is largest for this case (for fixed $\bar{a}_{0p}$). In Table I we give the ratios of the differential cross sections for a laboratory angle of 37° to that at 90°, and for 26° to that at 90°. (The latter ratio, while significantly larger than the former, is not as reliable [6].) These ratios are sensitive to the sign of the P-wave phase shifts for the first three cases. For case 4, the differential cross sections are independent of the sign of these phase shifts. The shape of the non-exchange cross section is not as sensitive to the sign as is the charge exchange cross section, since it contains a large incoherent contribution from the proton (only the neutron cross section contains a P-wave amplitude).

We conclude from these results that a measurement, to an accuracy of $\sim 10\%$, of the differential cross section for charge exchange scattering of K^+-mesons by deuterons can distinguish between the cases discussed here. A measurement at a K-nucleon c.m. angle of 90° can determine the magnitude of these phase shifts, and a measurement of the forward or backward peaking in the K-nucleon system (achieved, for example, by measuring the ratio of the cross sections near 20°, 40° and 90° in the laboratory, at 520 MeV/c) can determine the sign of the P-wave phase shifts (except near case 4). Finally, a measurement of the same ratio for the non-exchange cross section can provide a check on the sign of the P-wave phase shifts.

Evidence for Two Pion-Pion Resonances.

F. Selleri

CERN - Geneva

(ricevuto il 30 Marzo 1960)

Recent experimental results on the detailed behaviour of the total $\pi^{\pm}$-p cross-section ($\sigma^{\pm}$) with energy have appeared [1]. In this note we want to point out that a careful analysis of the existing experimental information on high energy $\pi^{\pm}$-p scattering suggests the existence of two pion-pion resonances in the isotopic spin states $I=1$ and $I=2$. First of all we will discuss the 0.9 GeV maximum in σ^{-}. We will see that the only explanation of it, which does not contradict any existing experimental fact is in terms of a strong pion-pion interaction in the $I=1$ state, in full agreement with current theoretical ideas [2]. Noting furthermore the striking similarity between this maximum and the one in σ^{+} at 1.3 GeV, we will deduce that also a $I=2$ π-π resonance should exist.

1. – Maximum in σ^{-} at 0.9 GeV.

Elastic and inelastic cross-sections for π^{-}-p scattering both show a maximum at 0.9 GeV [3]. Our discussion will be concerned only with the inelastic part. In view of the experimental angular distributions [4] it seems reasonable to believe that the hump in the elastic part is nothing but diffraction scattering. Whether it is so or not, is, however, unimportant for our interpretation of the inelastic part. The latter is $\sim 85\%$ composed of single pion production [3-5] and we will therefore discuss this process only.

The idea that the 0.9 GeV maximum in σ^{-} is due to the π-π interaction is an old one, and was first suggested by Piccioni. Dyson [6] noted that a $I=0$ reso-

---

[1] T. J. Devlin *et al.*: *Phys. Rev. Lett.*, **4**, 242 (1960).

[2] G. F. Chew and S. Mandelstam: UCRL-8728; W. R. Frazer and J. R. Fulco: *Phys. Rev. Lett.*, **2**, 365 (1959); *Phys. Rev.* **117**, 1609 (1960).

[3] R. R. Crittenden *et al.*: *Phys. Rev. Lett.*, **2**, 121 (1959).

[4] A. R. Erwin and J. K. Kopp: *Phys. Rev.*, **109**, 1364 (1958).

[5] V. Alles-Borelli *et al.*: *Nuovo Cimento*, **14**, 211 (1959).

[6] F. J. Dyson: *Phys. Rev.*, **99**, 1037 (1955).

nance for the π-π system would have had no effect at all on π^+-p scattering while it could have strongly enhanced the π^--p total cross-section. TAKEDA (7) remarked that also a $I=1$ resonance could have explained the 0.9 GeV hump. Indeed it would have scarcely influenced the behaviour of σ^+.

The simple model in which the incoming meson hits a meson of the cloud and shakes it off without any further interaction (see Fig. 1) led to definite predictions both on the branching ratios for single pion production and on the qualitative behaviour for the spectra of the final state particles (for example a maximum in the c.m. energetic spectrum of the nucleons, corresponding to the formation of the pion-pion isobar, was expected). More detailed experimental analysis (8) completely disproved these predictions, while on the other hand it fully confirmed the predictions of the Lindenbaum-Sternheimer isobar model (9). This seemed to rule out a strong contribution of pion-pion interaction to single pion production. In favour of this explanation there remained the fact that the radius of the nucleon considered as an absorbing sphere was found to be of the same order as the Compton wave length of the π-meson (4). Let us see now how a careful analysis of experiments leads to the conclusion that the π-π interaction must be responsible for the 0.9 GeV maximum. The known features about π^--p scattering at these energies are:

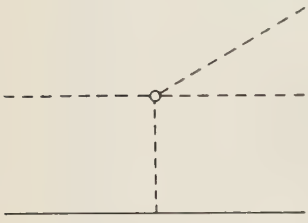

Fig. 1.

i) the isobar model predicts energetic spectra in good agreement with the experimental ones, especially for the reaction

(1) $$\pi^- + p \to n + \pi^+ + \pi^- \quad (5);$$

ii) evidence of a contribution from the diagram of Fig. 1 to the process

(2) $$\pi^- + p \to p + \pi^0 + \pi^-$$

has been found (10-11);

iii) at 1 GeV reaction (2) has a cross-section of ~ 7 mb. In it the diagram of Fig. 1 plays an important role (11). Roughly speaking one can say that its contribution is surely more than 50% at this energy;

iv) at the same energy no evidence at all in favour of this diagram is found in the case of reaction (1) (12).

It is easy to see that the idea that only π-π interaction contributes to pion production does not contradict the fact that the 3.3 isobar model seems to explain

---

(7) G. TAKEDA: *Phys. Rev.*, **100**, 440 (1955).
(8) *E.g.*, see ref. (5).
(9) R. B. STERNHEIMER and S. J. LINDENBAUM: *Phys. Rev.*, **109**, 1723 (1958).
(10) F. BONSIGNORI and F. SELLERI: *Nuovo Cimento*, **15**, 465 (1960).
(11) I. DERADO: *Nuovo Cimento*, **15**, 853 (1960).
(12) I. DERADO: private communication.

experimental facts. Indeed let us suppose that the primary interaction has taken place in the cloud. The wave length of the final state pions is much bigger than that of the incoming one because there has been a loss of energy in the production of one pion and because the energy is now divided among three particles. It happens that the relative energy of each pion and the nucleon is in the range where the 3.3 resonance dominates. Furthermore the dimensions of the wave packets of the pions are such that they partially overlap the nucleon core immediately after having been produced. Thus a secondary interaction between the pions and the nucleon is to be expected and it is not surprising that the 3.3 isobar model gives a good description of the experimental data. If this idea works, however, we do not expect the 3.3 final state interaction always to be present. From the above picture it follows indeed that the two pions have a certain probability of interacting, but also a certain probability of not having any further interaction with the nucleon, the latter being greater when the strength of the pion-nucleon interaction is smaller. Thus we expect that of the two reactions (1) and (2) the second would be more suitable for the observation of the simple Dyson-Takeda π-π interaction (*i.e.* a π-π interaction without final state interaction) owing to the fact that in the final state of the first reaction the π^--n system is in the pure isotopic spin $\frac{3}{2}$ and thus has a much bigger probability of interacting. All this is in full qualitative agreement with points ii)-iv).

Let us now refer to Fig. 1 and discuss the probability of having the incoming and virtual mesons in different isotopic spin states, starting from the initial $\pi^{\pm}$-p systems. As has been shown in [10] the cross-section predicted by this diagram is

$$\frac{\partial^2\sigma}{\partial\Delta^2\,\partial w^2} = \alpha\sigma_{\pi\pi}(w)\,F(w^2,\Delta^2)\,, \tag{3}$$

where Δ is the 4-momentum transfer to the nucleon, w is the total energy of the two π's in their c.m.s., $\alpha=2$ (1) if in the lower vertex a charged (uncharged) pion is emitted, $\sigma_{\pi\pi}$ is the total π-π cross-section, $F(w^2,\Delta^2)$ is a function independent of the charge states of the pions. The various π-π cross-sections for « physical » processes can be written in terms of cross-sections for pure isotopic spin states in the following way

$$\sigma(\pi^+ + \pi^+ \to \pi^+ + \pi^+) = \sigma_2\,, \tag{4}$$

$$\sigma(\pi^{\pm} + \pi^0 \to \pi^{\pm} + \pi^0) = \frac{1}{4}\sigma_2 + \frac{1}{4}\sigma_1 + \frac{1}{2}\sqrt{\sigma_2\sigma_1}\cos\theta_{21}\,, \tag{5}$$

$$\sigma(\pi^- + \pi^+ \to \pi^- + \pi^+) = \frac{1}{36}\sigma_2 + \frac{1}{4}\sigma_1 + \frac{1}{9}\sigma_0 + \frac{1}{6}\sqrt{\sigma_2\sigma_1}\cos\theta_{21} + \tag{6}$$

$$+ \frac{1}{9}\sqrt{\sigma_2\sigma_0}\cos\theta_{20} + \frac{1}{3}\sqrt{\sigma_1\sigma_0}\cos\theta_{10}\,,$$

$$\sigma(\pi^- + \pi^+ \to \pi^0 + \pi^0) = \frac{1}{9}\sigma_2 + \frac{1}{9}\sigma_0 - \frac{2}{9}\sqrt{\sigma_2\sigma_0}\cos\theta_{20}\,, \tag{7}$$

where σ_a is the cross-section for the $I=a$ state and θ_{ab} is the phase difference between the amplitudes for $I=a$ and $I=b$ states. The θ's are chosen so as to satisfy $\theta_{21}+\theta_{20}+\theta_{10}=0$. In the following Table the values of the cross-sections for single pion production as obtained from (3)-(7) are given, in the extreme case where

only one isotopic spin state is important. The quantity

$$J_I = \int \sigma_I(w)\, F(\Delta^2, w^2)\, \mathrm{d}\Delta^2\, \mathrm{d}w^2 ,$$

is taken as the unit.

TABLE I.

	J_I as unit		
	only $I=0$	only $I=1$	only $I=2$
$\sigma(p^+ \to n^{++})$	0	0	2
$\sigma(p^+ \to p^{+0})$	0	$\frac{1}{4}$	$\frac{1}{4}$
$\sigma(p^- \to n^{+-})$	$\frac{2}{9}$	$\frac{1}{2}$	$\frac{1}{18}$
$\sigma(p^- \to p^{-0})$	0	$\frac{1}{4}$	$\frac{1}{4}$
$\sigma(p^- \to n^{00})$	$\frac{2}{9}$	0	$\frac{2}{9}$

As is easily seen from the preceding Table if we want a big effect on σ^- only we are forced to take the π-π interaction in the $I=1$ state, the possibility of it being in $I=0$ being ruled out by the fact that point ii) could not have have been observed in reaction (2). In this case, however, an effect is expected also on σ^+. This could be in agreement with the fact that a smaller hump in σ^+ seems to exist at 0.9 GeV [1]. We note that if the existence of this hump should be confirmed it would constitute strong additional evidence in favour of π-π interaction in the sense that it would exclude the cause of the 0.9 GeV hump in σ^- to be in the $I=\frac{1}{2}$ state of the pion-nucleon system. Thus the idea that the inelastic channel for π^--p scattering goes mainly through the diagram of Fig. 1 followed by a possible final state interaction is in qualitative agreement with all the experimental data listed above. We will now see that such an agreement cannot be given by other possible explanations.

One can imagine that the pion production goes through different channels one of which given by Fig. 1 (the inclusion of the latter is necessary to get agreement with point ii)), and that the validity of the isobar model is determined not by final state interaction effects, but by the contribution of other channels. Once one has given up the possibility of the final state interaction to explain points iii) and iv) one is obliged to assume that the π-π interaction is much stronger in the state $I=2$ than in the other states (see Table I). We can say that if the diagram of Fig. 1 could act alone at 1 GeV it would give a cross-section of at least 4 mb for the reaction (2). But then its contribution to the reaction

$$\pi^+ + p \to \pi^+ + \pi^+ + n ,$$

should be about 32 mb (see Table I) which is surely in disagreement with the total σ^+ of 28 mb. Thus it is not possible to assume that the part of the inelastic channel going through the diagram of Fig. 1 is determined by a strong $I=2$ π-π interaction. The state $I=0$ is excluded because it could not affect reaction (2). There

remains only $I=1$. But in this state as follows from Table I, the π-π interaction should give a double contribution to reaction (1), in disagreement with point iv). Thus the «many channels» model always contradicts the experimental facts.

2. – Maximum in σ^+ at 1.3 GeV.

The first experiment evidence shows a striking similarity between this maximum and the one at 0.9 GeV in σ^-. In fact it is essentially composed of inelastic scattering and the elastic differential cross-section shows a forward diffraction-like peak giving 1 fermi for the nucleon radius, that is to say a value very close to the Compton wave-length of the pion ([13]). Also though direct experimental evidence of the π-π interaction is lacking here, let us suppose that this interaction is responsible for this hump. It follows then from Table I that this interaction must be particularly strong in the $I=2$ state.

In order to be able to say something about the energy of this resonance let us again discuss the 0.9 GeV hump in σ^-. One may suspect that the position of the maximum of σ^- is strongly influenced by the position of the π-π resonance. If one assumes that this maximum is attained when the π-π cross-section has its maximum average value one gets the result that the position of the $T=1$ π-π resonance must be 4.8μ (μ=meson mass) in full agreement with the values deduced from the structure of the nucleon ([14]) and from the spectra of the nucleons in π production ([11]). Thus one is tempted to do the same for the 1.3 GeV σ^+ bump, the result being

$$w^{\text{res}} = 6.4\mu \, .$$

If such a resonance exists it could not have any direct effect either on pion-nucleon and nucleon-nucleon elastic scattering, or on the electro-magnetic structure of the nucleon, in the sense that a nucleon cannot undergo a virtual emission of a system with $I=2$. However the following experimentally detectable effects are to be expected:

1) no hump corresponding to the one at 1.3 GeV in π^+-p scattering should be found in the cross-section for double photoproduction;

2) an experiment on single pion production in pion-nucleon collision around 1.3 GeV analysed as is done in ([10]), should give a strong evidence of π-π interaction for the events

$$\pi^+ + \mathrm{p} \to \mathrm{n} + \pi^+ + \pi^+ .$$

due to the fact that kinematic and isotopic-spin considerations in this case exclude the possibility that the final state interaction is important.

Furthermore the branching ratio $R=\sigma(\mathrm{p}^+ \to \mathrm{n}^{++})/\sigma(\mathrm{p}^+ \to \mathrm{p}^{+0})$ is expected to be rather bigger than 1. The simple diagram of Fig. 1 with the π-π interaction in $I=2$ would give $R=8$, but the final state interactions and the still important effect of the $I=1$ resonance could lower it considerably. This prediction is very different from those of the isobar model ($R=\frac{2}{13}$) and of the statistical theory ($R=\frac{2}{3}$).

* * *

The author wishes to thank Drs. B. Vitale and D. Amati for valuable discussions.

([13]) L. O. Roellig and D. A. Glaser: *Phys. Rev.*, **116**, 1001 (1959).
([14]) J. Bowcock, W. N. Cottingham and D. Lurié: *Nuovo Cimento*, to be published.

Evidence for a New 191 min Half-Period Activity in Nb.

M. Bocciolini, G. Di Caporiacco, L. Foà and M. Mandò

Istituto Nazionale di Fisica Nucleare - Sottosezione di Firenze
Istituto di Fisica dell'Università - Arcetri (Firenze)

(ricevuto il 4 Aprile 1960)

A new activity of 191 min half-period has been found when irradiating a Nb with neutrons from the $^3H(d, n)^4He$ sample reaction.

The γ-spectrum in two NaI crystals was analyzed by means of a ten channel amplitude analyzer of the type described by Johnstone [1]; three main peaks are clearly apparent in the spectrum: at 200 keV (which we will call henceforth γ_1), at 495 keV (γ_2) and at about 930 keV (γ_3); the last one was identified, from the half-life, as the expected and well known 934 keV line which follows the decay of 10.15 days ^{92}Nb [2].

The two lines γ_1 and γ_2 have been shown to exhibit, after proper correction of the residual 10.15 days activity due to the Compton continuum from γ_3, the same half-life; our best value is $T_{\frac{1}{2}} = (191 \pm 3)$ min.

The two lines γ_1 and γ_2 have also been shown to be in coincidence and of the same intensity (with an uncertainty of perhaps 10%, due to the various corrections and efficiency factors involved).

A weaker line at 695 keV is also present; in consideration of the poor geometry this can be interpreted as a sum-line and a speedy check which was made with a different geometry supports this view; a small amount of cross-over, however, could not be excluded on the basis of experiment alone, owing to poor statistics.

Measurements were not extended in this run below 30 keV energy so that the Nb-X line has not been studied.

Some measurements with a thin window Geiger-Müller counter did show that some β or electron conversion activity was also present in the sample, but there was only a small component, if any, of this activity with 191 min half-life. The thickness of the counted sample (~ 30 mg/cm^2) does not allow to exclude the presence of β or conversion electrons with energy less than, say, 100 keV.

By comparing the intensities of $\gamma_3 = 934$ keV and γ_2 and assuming, provisionally, that one $\gamma_2 = 495$ keV quantum is emitted per disintegration, by taking into account the time of exposure we deduce that the ratio of the production cross-section for the 191 min activity to the production cross section for the 10.45 days activity is about 0.018.

Since the chemical purity of the

(1) C. W. Johnstone: *Nucleonics*, p. 36 January 1953.

(2) Cfr., *e.g.*, H. I. West jr., L. G. Mann and G. M. Iddings: *Phys. Rev.*, **113**, 881 (1959).

irradiated sample was better than 0.1% (except for a 0.16% Tantalum impurity) the observed yield of the 191 min activity makes extremely unlikely that it may be due to a reaction on the impurities: since no activity of the kind is known among the possible (n, n', γ), (n, 2n), (n, p) and (n, α) products of Nb, we must assign the 191 min activity to an isomeric state and among these a $^{92}Nb^m$ (or $^{93}Nb^m$) appears to be more likely since charged particle products are intrinsically less probable; a surer assignment, however, awaits chemical separation, which was not carried out in the present series of measurements.

If we accept the tentative assignment of the 191 min activity to a $^{92}Nb^m$ excited state and also exclude the not altogether remote possibility that γ_1 and γ_2 are in cascade with a low energy highly converted transition (which could have escaped detection in our apparatus) we can still draw further conclusions. On the basis of the intensity ratio $\gamma_1 : \gamma_2$ and of the comparison of half-life with Weisskopf's extimates, we are led to admit that γ_2 precedes γ_1, and is a $\Delta J = 4$ transition, most probably an $M4$.

An upper limit was estimated for the production a in our experiments of 2.35 MeV isomeric state of 13 h half-life, reported in the literature [3]; it comes out that $\sigma(13\text{ h}) : \sigma(10.15\text{ days}) < < 4 \cdot 10^{-5}$. It must be pointed out, however, that this cannot be taken as sufficient evidence against the existence of this state, the more so in consideration of its high energy.

In our measurements we did not observe the 88 keV isomeric state, whose existence in ^{92}Nb has been established by DUFFIELD and VEGORS [4]; this fact, however, can easily be accounted for if we assume for the 88 keV isomeric state a lower spin than for the ground state, while assuming a higher spin for our isomeric state; the assignment of our 191 min activity to $^{93}Nb^m$ could be assumed as a possible, though less probable, alternative.

Experiments are in progress to improve our knowledge of the new nuclide and definitely settle some of the questions posed by the present results.

* * *

Thanks are due to Prof. PUPPI and Prof. PETRALIA of the University of Bologna for kindly allowing the free use of the accelerator and to Prof. S. FRANCHETTI for encouraging advice.

[3] R. A. JAMES: *Phys. Rev.*, **93**, 288 (1954).

[4] R. B. DUFFIELD and S. H. VEGORS, jr. *Phys. Rev.*, **112**, 1958 (1959).

New Measurements of the Spin-Lattice Relaxation Time in Liquid Helium 3.

G. Careri, I. Modena and M. Santini
Istituto di Fisica dell'Università - Padova

(ricevuto l'11 Aprile 1960)

The spin-lattice relaxation time T_1 in liquid helium 3, has been previously measured by us, and the results published in this Journal (1). Soon afterwards, measurements were published by Garwin and Reich (2) and by Romer (3). These were in strong disagreement with our data and also among themselves. With the aim of understand the reason for this disagreement, we have repeated the measurements with the same technique of the adiabatic fast passage (4), using the larger quantity of ^{3}He now available to this laboratory. The runs were as follows (see Fig. 1):

a) the same small cell (3 mm i.d. size of pyrex) was used as in the previous experiments (1). The new results confirmed the sharp rise found in our previous data, and the extension to 0.85 °K showed the existence of a flat maximum.

b) the same glass was used, but the cell size was made larger (6 mm i.d.), the new results were now closer to those by Garwin and Reich (2);

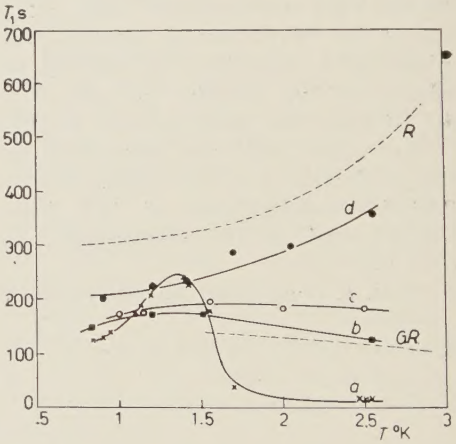

Fig. 1. – The spin-lattice relaxation time T_1 versus temperature, in pure liquid ^{3}He. *GR* data by Garvin and Reich (2) at 2.4 atm. pressure; *R* data by Romer (3) at saturated vapor pressure under different conditions. *a*, *b*, *c*, *d* data of this laboratory reported in the text, at saturated vapor pressure.

c) a larger cell (10 mm i.d.) was used, always of the same glass. T_1 became somewhat larger than in *b*);

(1) G. Careri, I. Modena, M. Santini: *Nuovo Cimento*, **13**, 207 (1959).
(2) R. L. Garwin, H. A. Reich: *Phys. Rev.*, **115**, 1478 (1959).
(3) R. H. Romer: *Phys. Rev.*, **115**, 1415 (1959).
(4) M. Santini: *Nuovo Cimento*, in press.

d) finally the same cell used in *c*) was used again after a long cleaning by hydrogen gas at 150 °C. This procedure is well known in mass-spectrometry, when one wants to eliminate the water and other gases adsorbed on the ion source, since hydrogen takes their place on the surfaces. The T_1 values were then very close to those of ROMER ([3]).

From the above it is obvious that T_1 measurements in a glass cell are affected by the walls, most probably the oxygen adsorbed there acting as a catalyst. It seems also likely that Romer's data are correct because he did not notice any effect when he changed the size of his cell.

However, we want to point out that the wall does not have merely the simple effect of catalyzing the nuclear spin relaxation with a rate controlled by diffusion which is given by ordinary gas kinetic theory. As a matter of fact, the sharp rise of our measurement reported in *a*) is not understandable in terms of the diffusion coefficient D, because D does not show any sharp change at 1.5 °K ([2,5]). As well the decrease of T_1 upon increasing of the pressure found by Garwin and Reich, is not understandable in terms of D, because D is slowly affected by the pressure ([2]) and in the wrong direction. Therefore one must conclude that the walls certainly act as catalyst, but in a rather misterious way which depends on temperature and pressure. This conclusion is of course grounded upon the measurements of D by the spin-echo method, which seem to exclude any spin-diffusion contribution ([2,5]).

* * *

Thanks are due to Dr. W. MCCORMICK for some discussions we had on this subject.

([5]) H. R. HART jr., J. C. WHEATLEY: *Phys. Rev. Lett.*, **4**, 3 (1960).

LIBRI RICEVUTI E RECENSIONI

Libri ricevuti.

F. H. Clauser: *Symposium of Plasma Dynamics.* Addison-Wesley Pub. Inc., Reading, Mass., 1960; pp. IX+369, $ 12.50.

P. Demers: *Photographie Corpusculaire* II. Les Presses Universitaires, Montréal, 1959; pp. 464, senza prezzo.

G. Francis: *Ionization Phenomena in Gases.* Butterworths Scientific Pubblications, London, 1969; pp. VII+300, s. 60.

D. Halliday and R. Resnick: *Physics for Students of Science and Engineering.* John Wiley and Sons, New York, 1960; pp. XIV+1065, $ 6.00.

K. Mendelssohn: *Cryophysics.* Interscience Publishers Inc., New York, pagine VIII+183, $ 4.50 (cloth) 2.50 (paper).

E. M. Pugh and E. W. Pugh: *Principles of Eletricity and Magnetism.* Addison Wesley Pub. Co. Inc., Reading, Mass., 1960; pp. VII+430, $ 8.75.

J. R. Reitz and F. J. Milford: *Foundations of Electromagnetic Theory.* Addison Wesley Pub. Co. Inc., Reading, Mass., 1960; pp. XI+387, $ 8.75.

A. S. Bishop: *Vers la maitrise de la fusion thermonucléaire.* Dunod, Paris, 1960; pp. VI-199; N.F. 39.

J. G. Wilson and S. A. Wouthuysen: *Progress in Elementary Particle and Cosmic Ray Physics.* North Holland Pb. Co., Amsterdam, 1960, pp. XII-461; Fior. 45.

Recensioni.

Bibliography of the Stable Isotopes of Oxigen (^{17}O *and* ^{18}O), compilata da D. Samuel e F. Steckel, Pergamon Press, 1959, pp. 224.

La bibliografia è frutto del lavoro dei ricercatori di Rehovoth, che, oltre allo studio degli isotopi, si dedicano da alcuni anni alla preparazione in larga scala di acqua arricchita in ^{18}O e ^{17}O.

La bibliografia è accuratissima e completa fino al 1957 e potrà essere di grande utilità agli specialisti. Essa è composta di un indice per autori e di un dettagliato indice per materie. Sarebbe augurabile che molte di tali opere fossero a disposizione dei ricercatori sperimentali in un'epoca in cui la superspecializzazione e l'elefantiasi delle pubblicazioni scientifiche rendono estremente difficile la ricerca bibliografica.

G. Boato

Direttore responsabile: G. POLVANI

Tipografia Compositori - Bologna

Questo Fascicolo è stato licenziato dai torchi il 14-VI-1960